



HAL
open science

Probing the gluon Transverse Momentum-Dependent distributions inside the proton through quarkonium-pair production at the LHC

Florent Scarpa

► **To cite this version:**

Florent Scarpa. Probing the gluon Transverse Momentum-Dependent distributions inside the proton through quarkonium-pair production at the LHC. High Energy Physics - Phenomenology [hep-ph]. Université Paris-Saclay; Rijksuniversiteit te Groningen (Groningen, Nederland), 2020. English. NNT : 2020UPASS104 . tel-02923644

HAL Id: tel-02923644

<https://theses.hal.science/tel-02923644>

Submitted on 27 Aug 2020

HAL is a multi-disciplinary open access archive for the deposit and dissemination of scientific research documents, whether they are published or not. The documents may come from teaching and research institutions in France or abroad, or from public or private research centers.

L'archive ouverte pluridisciplinaire **HAL**, est destinée au dépôt et à la diffusion de documents scientifiques de niveau recherche, publiés ou non, émanant des établissements d'enseignement et de recherche français ou étrangers, des laboratoires publics ou privés.

Probing the gluon Transverse Momentum-Dependent distributions inside the proton through quarkonium-pair production at the LHC

**Thèse de doctorat de l'Université Paris-Saclay et de
l'Université de Groningen**

École doctorale n° 576, Particules, Hadrons, Énergie et
Noyau: Instrumentation, Imagerie, Cosmos et Simulation
(PHENIICS)

Spécialité de doctorat: Physique des particules
Unité de recherche: Université Paris-Saclay, CNRS, IJCLab, 91405,
Orsay, France

Référent: : Faculté des sciences d'Orsay

**Thèse présentée et soutenue en visioconférence totale, le 26
juin 2020, par**

Florent SCARPA

Composition du jury:

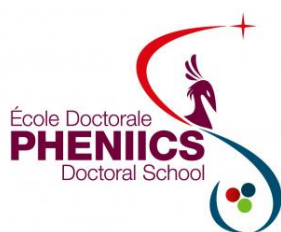
Elisabetta Pallante Professeur, Université de Groningen, Pays-Bas	Présidente
Cédric Lorcé Professeur, École Polytechnique, France	Rapporteur & Examineur
Piet Mulders Professeur, Université Libre d'Amsterdam, Pays-Bas	Rapporteur & Examineur
Bruno Espagnon Professeur des Universités, Université Paris-Saclay, France	Examineur
Cynthia Hadjidakis Chargé de recherche, Université Paris-Saclay, France	Examinatrice
Gerco Onderwater Professeur associé, Université de Groningen, Pays-Bas	Examineur
Robertus Timmermans Professeur, Université de Groningen, Pays-Bas	Examineur
Jean-Philippe Lansberg Chargé de recherche, Université Paris-Saclay, France	Directeur
Daniël Boer Professeur, Université de Groningen, Pays-Bas	Codirecteur

**Probing the gluon Transverse
Momentum-Dependent distributions inside the
proton through quarkonium-pair production at
the LHC**

Florent Scarpa

ISBN: 978-94-034-2789-8 (printed version)
978-94-034-2790-4 (electronic version)

Printed by: IPSKAMP





Probing the gluon Transverse Momentum-Dependent distributions inside the proton through quarkonium-pair production at the LHC

PhD thesis

to obtain the degree of PhD of the
University of Groningen
on the authority of the
Rector Magnificus Prof. C. Wijmenga
and in accordance with
the decision by the College of Deans

and

to obtain the degree of Doctor in Physics, specialty "Particle Physics"
of the University Paris-Saclay

Double PhD degree

This thesis will be defended in public on
Friday 26 June 2020 at 11.00 hours in Groningen, the Netherlands

by

Florent Scarpa

born on 11 March 1993
in Toulouse, France

Supervisors

Prof. D. Boer

Dr. J.-P. Lansberg

Assessment Committee

Prof. B. Espagnon

Prof. C. Lorcé

Prof. P.J.G. Mulders

Prof. R.G.E Timmermans

Composition du jury

Prof. E. Pallante	Président
Prof. C. Lorcé	Rapporteur
Prof. P.J.G. Mulders	Rapporteur
Prof. B. Espagnon	Examineur
Dr. C. Hadjidakis	Examineur
Dr. ir. C.J.G Onderwater	Examineur
Prof. R.G.E Timmermans	Examineur

École doctorale n°576 : particules hadrons énergie et noyau : instrumentation, image, cosmos et simulation (Pheniics)

Spécialité de doctorat : Physique des particules

Unité de recherche : Université Paris-Saclay, CNRS, IJCLab, 91405, Orsay, France

Référent : Faculté des Sciences

Contents

Introduction	1
1 Factorised cross section for proton-proton collisions	7
1.1 Hadronic cross section	7
1.2 The parton correlator	11
1.3 Parton Distribution Functions	16
2 Beyond the collinear approximation: the transverse structure of the proton	23
2.1 Multidimensional correlators and hadron spin	24
2.2 Gluon fusion in proton-proton collisions in the TMD formalism	28
2.3 Evolution in the TMD formalism	33
2.3.1 TMD convolutions in b_T -space	34
2.3.2 The scale dependence of TMDs	35
2.3.3 Organising the perturbative and nonperturbative content of the TMD	36
3 Quarkonium production	39
3.1 Production mechanisms	40
3.2 Explaining inclusive quarkonium production data	45
4 Quarkonia as probes of the gluon TMDs	49
4.1 Processes of interest for the study of the gluon TMDs	50
4.2 J/ψ - and Υ -pair production	54
4.3 Double Parton Scattering and feed-down	58
5 Predictions for Gaussian TMDs in J/ψ-pair production	61
5.1 Hard-scattering coefficients and TMD models	62
5.2 The transverse-momentum spectrum	66

5.3	Azimuthal asymmetries	69
6	Predictions for evolved TMDs in J/ψ- and Υ-pair production	77
6.1	Exploring the nonperturbative component of TMDs with a Gaussian input .	78
6.2	TMD convolutions in the evolution formalism	81
6.3	Improved predictions for the TMD observables	91
6.3.1	The transverse-momentum spectrum in J/ψ -pair production	92
6.3.2	Azimuthal asymmetries	92
7	Polarised quarkonium-pair production	101
7.1	Helicity amplitudes in the high-mass limit	101
7.2	Helicity amplitudes in the threshold limit	107
	Conclusion	111
A	Appendices	115
A	TMD convolutions in b_T -space	115
B	$gg \rightarrow \mathcal{Q}\mathcal{Q}$ hard-scattering coefficients	117
B.1	The full expressions of the $f_{i,n}$ for unpolarised J/ψ -pair production .	117
B.2	The hard-scattering coefficients for polarised J/ψ -pair production in the gluon helicity frame	118
	Lay summary	121
	Samenvatting	125
	Résumé	129
	Acknowledgements	131
	Bibliography	133

Introduction

The invention of bubble and spark chambers led to the discovery in the 1950s and 1960s of a “zoo” of strongly interacting particles, or hadrons. Such large numbers made it difficult to believe all of these particles were elementary bricks of matter. Gell-Mann and Ne’eman sorted them according to their mass and various quantum numbers: electric charge, isospin and strangeness (the latter has been theorised in order to explain the abnormally slow decay of kaons). This classification was called the eightfold way and matched the representation theory of SU(3) [1]. Following this, Gell-Mann and Zweig independently proposed in 1963 that all the hadrons were made up of three flavours of particles called quarks, carrying fractional electric charges. A great success of the eightfold way (and thus of the quark model) was the prediction of the existence, mass and decay products of the Ω^- that was observed in 1964 [2]. Hadrons are divided into two main groups: the mesons, made of a quark-antiquark pair, and the (anti)baryons, made of three (anti)quarks. Let us note that since then, exotic bound states of quarks have been observed, such as tetraquarks and pentaquarks. Struminsky (then a student of Bogolyubov) was the first to suggest in a footnote that the existence of the Ω^- , which was made of three strange quarks with parallel spins and vanishing orbital angular momentum, was violating Pauli’s exclusion principle unless an additional quantum number was added to the quarks [3]. A similar situation was encountered with the Δ^{++} . In 1965, a new SU(3) quantum number (different from SU(3) flavour) was theorised for the quarks in order to explain the existence these baryons by Greenberg on one side [4], and Han and Nambu on the other side [5]. This new charge was later called colour as it could take three forms, namely red, blue and green. Then a Δ^{++} or Ω^- containing a quark of each colour was not violating Pauli’s principle. Greenberg, Han and Nambu also noted that quarks could interact via the exchange of vector gauge bosons, named gluons, and that hadrons and electromagnetism were colour-neutral.

In the beginning, these subhadronic particles were only seen as mathematical artefacts allowing to categorise hadrons according to their characteristics. This was a consequence of the fact that no quark or gluon had ever been observed in isolation in any experiment. There were two main ways to explain such an absence: the first was to consider quarks and gluons to be genuine particles that could be localised and have a definite momentum but were *confined* inside hadrons, while the second was to consider them to not have proper existence as particles and that the strong interaction could not be completely described by quantum field theory. In 1967, the Stanford Linear Accelerator Center (SLAC) started measuring deeply inelastic scatterings: $e + p \rightarrow e + X$. Although large-angle deviations were not expected, they were observed in these reactions. Feynman then came up with the parton model in order to explain hadronic collisions, and in particular deeply inelastic scatterings. The interpretation of the reaction given by this model was that the electron was elastically scattering with one *pointlike*, approximately free, constituent of the proton via the exchange of a virtual photon, such that the inelastic interaction of the electron with the proton is the incoherent sum of all the elastic scatterings between the electron and the constituents. These particles are called partons, are approximated to be massless, and each carries a fraction x of the proton total momentum.

From this picture ensued the prediction of a property of the cross section known as Bjorken scaling, where the structure functions that contain all the information about the proton structure only depend on x , which was initially verified at SLAC. The partons were then identified with the three constituent quarks of the proton. However, in order to reproduce data well, it was necessary to add a sea of $q\bar{q}$ pairs, as well as gluons inside the hadron, in an overall colourless state. The three original quarks are then just valence quarks and the content of the proton as seen by the probe electron varies with the momentum transfer, violating Bjorken scaling. The experimental evidence that partons were confined inside hadrons seemed inconsistent with the fact that the high-energy electron in deeply inelastic scatterings could interact with what appeared to be a freely moving parton.

In 1973 Gell-Mann, Fritzsch and Leutwyler [6], considering colour as the charge associated with the strong interaction, developed Quantum Chromodynamics (QCD) as gauge theory of the strong interaction, with the possibility to use perturbative expansion techniques for the computations of cross sections (provided that the coupling constant is small enough). It is a Yang-Mills, or non-Abelian theory: gluons, the gauge bosons exchanged between coloured particles, carry a colour charge themselves and can directly interact with each other [7]. Gross, Politzer, Wilczek and independently 't Hooft discovered that such a theory presented a characteristic called *asymptotic freedom*: the coupling constant of the strong interaction becomes small and tends toward 0 at large energies.

This discovery (that was rewarded by a Nobel prize in 2004 only) allowed physicists to use perturbative QCD to compute hadronic cross sections, with predictions checked to be correct at the percent level. It is then thought that confinement at low energy also arises from the running of the coupling, that becomes very strong at low energy. In such a case, the energy one needs to transfer to two partons is so important that it becomes large enough to materialise a $q\bar{q}$ pair that forms a meson, leaving us with the original hadron and an extra one instead of free partons. A highly energetic parton will typically fragment into a bunch of other partons before they all eventually hadronise into a group of hadrons (and eventually other particles) roughly collimated inside a cone called a jet. Lattice QCD, a numerical method allowing to gain insight on the nonperturbative regime of QCD, also agrees with the existence of confinement, although there is still no mathematical proof that Yang-Mills theories exhibit a confinement property. The first evidence of the existence of gluons was provided by measuring the decay of Υ mesons (cf. next paragraphs) into three gluons at DESY in 1979 [8]. Their existence was definitely proved by the measurement of three-jet events in the same year: these events were predicted by QCD for configurations where a $q\bar{q}$ pair radiates a hard non-collinear gluon, called gluon Bremsstrahlung [9].

Thanks to deeply-inelastic-scattering measurements, physicists started probing the internal structure of hadrons in terms of their constituent partons. Although such a picture is only tractable at high energy, it still allows one to factorise hadronic cross sections into a partonic-scattering-squared amplitude and Parton Distribution Functions (PDFs) that describe the probability to find a given parton inside the proton with a given momentum fraction at a given scale for the process. This procedure of *factorisation* is central to the computation of hadronic cross sections. Proving factorisation can be highly nontrivial. During the last three decades, physicists have been looking to refine the parton picture by considering partons which do not only carry a fraction of their parent hadron momentum, but also a momentum component that is transverse to it. Since the transverse momentum of a parton must be of the order of the hadron mass, it is generally much smaller than the momentum transfer in the process that scatters particles with large transverse momenta. The intrinsic transverse momentum of initial-state partons can therefore safely be neglected (or integrated over as is the case in DIS). This is however not true when one considers reactions where the overall transverse momentum of the final state remains small. Such events are sensitive to the intrinsic transverse momentum of partons that is of the same magnitude, and can therefore be used to probe the parton dynamics in the transverse plane. One can therefore access the Transverse-Momentum-Dependent PDFs (usually called TMDs) in low-transverse-momentum reactions. In such reactions, the transverse-momentum spectrum of the final state is modified by the influence of the partonic transverse momentum ; azimuthal asymmetries can also

appear in multi-particle final states. TMD factorisation was proved to hold for a handful of processes and permitted to extract several quark TMDs from data. So far, very little is known about the gluon TMDs as one lacks a good probe to measure them at the current hadron colliders. The Electron-Ion Collider (EIC) to be built at the Brookhaven National Laboratory (BNL) would allow us to make great progress in the extraction of TMDs, but the completion of such a project is about ten years away from now.

While the confusion started by the discovery of the particle zoo was steadily making place to a clearer vision of the strong interaction in the 1970s, another series of discoveries paved the way to a new area of hadronic physics. In 1974, two groups at SLAC and BNL simultaneously announced the discovery of a new particle: the J/ψ , whose denomination is a combination of the names given to it by the two collaborations. This was the "November revolution" that started the study of heavy-quark flavours and quarkonium physics. The conclusion that the J/ψ was one of the lowest bound states of a charm-anticharm quark pair, similarly to a positronium formed by a bound e^+e^- pair, had physicists name it and higher spectroscopic states *charmonia*. SLAC was using e^+e^- collisions and observed that the ratio of production of hadrons over $\mu^+\mu^-$ pairs had a clear bump at around 3.1 GeV, meaning a hadron resonance was present. Since the electron-positron pairs primarily interact via the exchange of a virtual photon, the reason for the J/ψ to be the most easily produced charmonium was that it was the lightest charmonium with the same quantum number as the photon, which simply fragmented into a $c\bar{c}$ pair that formed a bound state. The charm flavour was first proposed by Glashow and Bjorken in 1964, but it was also required by the Glashow-Iliopoulos-Maiani (GIM) mechanism (1970) that explains the suppression of Flavour-Changing Neutral Currents (FCNC) in loop diagrams that would violate experimentally observed selection rules. The suppression occurred thanks to a small ratio m_u/m_c multiplying the problematic contributions, the charm quark was therefore expected to be heavy. In addition Kobayashi and Maskawa argued in 1973 that a new doublet of heavy quarks was needed to explain CP -violation in weak decays. One was the bottom quark, discovered in 1977 at Fermilab inside Υ mesons, that are equivalent to J/ψ mesons with b quarks. The other one, the top quark, was only discovered in 1994 due to its uncannily large mass, about 173 GeV, out of reach of colliders until the commissioning of the Tevatron where it was observed. Interestingly, while the top is in majority created through strong interactions, it very quickly decays through the *weak* interaction into a W and a b , in a time much shorter than the typical strong interaction time. For this reason, it does not hadronise, providing an interesting opportunity to study the behaviour of a 'bare' quark.

With the J/ψ and Υ , a large number of new charmonia and bottomonia were regularly detected in the experiments during the 70s and the 80s, as well as open charm

and beauty mesons (mesons containing c and/or b quarks that are not combined with their own antiquark, which therefore carry a nonzero charm or beauty charge). An interesting characteristic of these heavy-quark mesons is that their mass is close to that of their constituent quarks, meaning that the quarks do not have a large relative momentum and are typically nonrelativistic. It is therefore possible to use nonrelativistic potentials to describe with good results the binding between them and the related meson spectroscopy, such as the Cornell potential: the combination of a Coulombic potential at small distance, in accordance with asymptotic freedom in QCD, and a linear potential at large distance describing the effect of confinement. Various mechanisms can be resorted to in order to describe quarkonium production in colliders. So far not all of the numerous production data can be consistently explained, and the contributions of different mechanisms to specific processes are still the subject of debates. Nonetheless, beyond the study of their own production mechanisms, they are already important tools in several fields of high-energy physics: B meson factories were built to study CP -violation in detail, quarkonia are used as probes of the characteristics of the quark-gluon plasma which existence was recently confirmed at the LHC, as well as probes of cold nuclear matter effects. They can also be used to study parton correlations, such as in multiple simultaneous parton scatterings between two protons, or to probe parton distribution functions and their generalised analogues. In particular, quarkonium production can be a way to access the poorly known gluon TMDs in proton collisions at the LHC. At the considered centre-of-mass energies, the gluon density largely surpasses that of all other partons and perturbative QCD can safely be used to describe the partonic subprocess. Since quarkonium production originates in majority from gluon fusion, low-transverse momentum events are sensitive to the intrinsic transverse momentum of the gluons and their measurement could allow to extract the gluon TMDs. This is the subject of this thesis.

In the first chapter of this thesis, we will describe how hadronic cross sections are derived using factorisation. We will define the parton correlator in terms of operators in the parton model and add some necessary corrections. We will also give its parametrisation in terms of PDFs. In the second chapter, we will generalise the parton correlator to include the intrinsic transverse momentum of the parton. We will give the new parametrisation of this multidimensional correlator in terms of TMDs. We will then look at a typical cross section for gluon fusion within the framework of TMD factorisation and the additional observables one can consider in order to access the gluon TMDs. We will finally explain the evolution formalism for TMDs that allows one to account for their scale dependence.

In the third chapter, we will give some details about quarkonium production and the main mechanisms invoked to describe it. We will especially focus on the colour-singlet model and colour-octet mechanism within the framework of the effective theory called

Non-Relativistic QCD to describe the hadronisation of heavy-quark pairs. In the fourth chapter, we will show how quarkonium production, alone or in association with other particles, is a promising tool for the study of the gluon TMDs. We will present the main processes under consideration for such a goal, as well as their advantages and downsides. In particular, we will present J/ψ - and Υ -pair production as very interesting processes for the extraction of the gluon TMDs at the LHC. We will conclude this chapter by talking about contributions from multiple parton scatterings and feed-down that could complicate the extraction of information on the proton structure from these channels.

The fifth chapter describes our predictions for TMD-related observables in double J/ψ production using a Gaussian model for the gluon TMDs. We will show that the specific structure of the partonic scattering amplitude of this processes makes it indeed a powerful tool for the extraction of the TMDs by optimising the magnitude of the observables. The sixth chapter will be dedicated to the inclusion of the TMD evolution formalism in our analysis of J/ψ -pair production in order to make our predictions more realistic and isolate the truly nonperturbative component of the TMDs by evolving them down to their natural scale. It will be showed that in spite of an expected suppression of the TMD observables, the latter should remain sizeable and could be measured with the data already available and to come at the LHC. We add predictions for Υ -pair production that are also quite promising. In the seventh and final chapter of this thesis, we will have a deeper look into the scattering amplitude of J/ψ - and Υ -pair production, including in the polarised case. We will use the helicity formalism, specifically in the high-energy and threshold limits, to understand how the specific characteristics that make these processes so interesting for gluon-TMD study arise.

Chapter 1

Factorised cross section for proton-proton collisions

The complexity and elusiveness of the structure of hadrons stem from the nature of the strong interaction, best described by QCD. The non-Abelian nature of this theory is in majority at the origin of the complications that arise in comparison with QED. A description of hadronic reactions in terms of the degrees of freedom of the theory, namely quarks and gluons, is possible but is only valid for high momentum transfers. For such processes, the running-strong-coupling constant is sufficiently small to apply perturbative-computation techniques, as it tends toward zero at zero distance. This feature is called asymptotic freedom and therefore allows one to describe high-energy processes in terms of interactions between quarks and gluons. On the other hand, at small momentum transfer in the centre of mass of the system, the coupling becomes large and makes the expansion divergent: the quarks and gluons (called partons) do not exist freely and are confined within hadrons. Therefore if one looks for a description of a hadronic reaction, the idea of separating the perturbatively expandable high-energy scattering of partons and the transition from or toward a bound state comes naturally. Such a procedure is referred to as *factorisation* and is central to most high-energy computations of QCD cross sections. Hence, because the partonic sub-process can be evaluated using the theory and provided that factorisation can be established, one can use experiments in order to probe the dynamics of hadronic bound states.

1.1 Hadronic cross section

Describing the inner structure of hadrons at small momentum transfer using quarks and gluons has been the focus of a lot of research in the field of QCD. The cornerstone of this branch is the study of Deeply Inelastic Scattering (DIS) where an electron collides with a proton with large relative momentum, the former probing the content of the latter through electromagnetic interactions with its constituents. The parton model originally proposed by Feynman to give insight about the microscopic behaviour of the strong interaction relied on the separation in time/distance scales of the interactions occurring during the reaction. Indeed, the proton radius being of the order of the femtometer, the

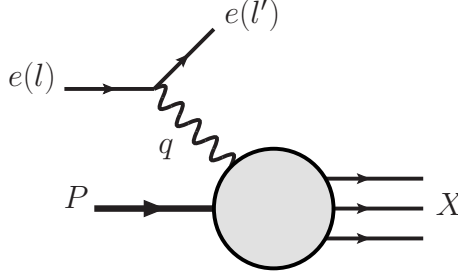


Figure 1.1: DIS amplitude representation at Leading Order (LO) in α . The incident electron e with momentum l scatters on a proton with momentum P , via the exchange of a virtual photon with momentum q . The proton is destroyed into remnants X while the electron is scattered with a momentum l' .

typical scale of interactions (in the proton rest frame) between its constituents is about 1 fm. In a collider like HERA that intensively investigated DIS, the invariant momentum transfer Q was typically of the order of tens of GeV, although measurements ranged from a few to hundreds of GeV. Therefore in the rest frame of the electron-hadron pair, the Lorentz boost applying to the hadron implies a strong time dilation. This makes the interaction scale between partons of the order of 100 fm instead of 1fm in the rest frame of the hadron, while the typical electron scattering scale is $1/Q \sim 10^{-1}$ fm [10]. Hence, the typical interaction time between the electron and a parton (in this case a quark, as gluons do not carry an electric charge) is much shorter than the interaction time between partons. The electron therefore “sees” a frozen picture of the proton in terms of its constituents and only interacts with one of them, while a slow probe would not be able to resolve just one parton. Therefore in the parton model, the momentum exchange between the electron and one of the quarks is realised via the exchange of a virtual photon, its virtuality being $Q^2 = -q^2 > 0$ (see Fig. 1.1). This picture is only valid in a certain area of the phase space accessible at HERA, as we will explain further.

Originally only the scattered electron was detected. Knowing the kinematics of the incident electron and proton, it was already possible to probe the structure of the proton. The cross section is of the form:

$$E' \frac{d\sigma}{d\mathbf{l}'} \simeq \frac{\pi e^4}{2s} \sum_X \delta^{(4)}(p_X - P - q) \left| \langle l' | j_\lambda^{\text{lept}} | l \rangle \frac{1}{q^2} \langle X | j^\lambda | P \rangle \right|^2 \quad (1.1)$$

$$= \frac{2\alpha^2}{sQ^4} L_{\mu\nu} W^{\mu\nu}, \quad (1.2)$$

where one neglects the masses of the proton and the electron in comparison with the electron-proton centre-of-mass energy \sqrt{s} . The matrix element $\langle l' | j_\lambda^{\text{lept}} | l \rangle$ designs

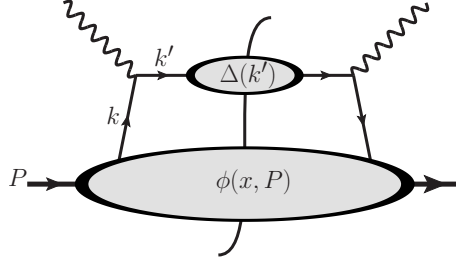


Figure 1.2: Cut-diagram representation of the DIS squared amplitude. The large blob represents the transition between the bound state, that is the proton, to a quasi-free quark that interacts with the virtual photon. The struck quark then eventually fragments and hadronises into other bound states that form the final state X . The vertical line, called final-state cut, represents the final state $|X\rangle$ and implies a sum and integration over all possible out states.

the electromagnetic current between the initial and final states of the electron, while $\langle X|j^\lambda|P\rangle$ is the hadronic current for an initial-state proton and final-state remnants X that are not detected and therefore summed over all possibilities. One calls such a cross section *inclusive*, it is the main type of cross sections that are studied in hadronic reactions as it is often impossible to detect all the particles of a destroyed hadron. The exception is diffractive processes where the proton is not broken. We see in the second line of Eq. (1.2) that the cross section can be expressed as a contraction between a leptonic tensor $L_{\mu\nu}$ and a hadronic tensor $W^{\mu\nu}$. While the leptonic tensor can be perturbatively evaluated using Feynman rules for QED, the situation is more complex for the hadronic one that is intrinsically nonperturbative. Following the idea of factorisation, one can separate the small-scale electron-quark scattering from the long scale initial-state and final-state partonic interactions. The squared amplitude associated with this picture is displayed in Fig. 1.2. It can be written as:

$$W^{\mu\nu} = \sum_j \frac{e_j^2}{4\pi} \int \frac{d^4k}{(2\pi)^4} \text{Tr}(\gamma^\mu \Delta_j(k+q) \gamma^\nu \phi_j(k, P)). \quad (1.3)$$

Eq. (1.3) emphasises the idea of factorisation: the hadronic tensor is the product of gamma matrices emerging from the Feynman rules of QED encoding the interaction vertex between a quark and a photon, with nonperturbative objects ϕ and Δ representing the transition between quasi-free partons and bound states. ϕ is usually called a parton *correlator* while Δ is called a fragmentation correlator. A sum over quark flavours and momenta is also needed as all of them contribute to the cross section. An important approximation that can be made is to consider the momentum component of the parton

that is transverse to its parent hadron momentum to be negligible. Indeed, if one defines a longitudinal axis z as the direction followed by the colliding electron-proton pair, the longitudinal proton momentum P_z is large and in particular much larger than its mass M_p . Therefore the partons inside of this proton must also have momenta that are much larger in the z direction than in the plane transverse to z . Particles in the final state generally acquire large transverse momenta through the hard quark-virtual-photon scattering, where the scattered electron recoils against the quark. Otherwise, the scattered electron would remain close to the beam, undergoing many interactions with proton remnants that would break factorisation. In addition, particles close to the beam are harder to detect, precisely because of their proximity with many other particles. The partonic momenta are approximated as collinear to that of their parent hadron (*i.e.* longitudinal), and each parton carries a fraction of the hadron momentum: $k = xP$ with $0 < x < 1$. The longitudinal momentum fraction x is taken to be between 0 and 1 as it is unlikely that a parton would have a momentum larger than or in the opposite direction of the hadron momentum¹. In this picture, the sum of all partonic momenta must be equal to the hadron momentum: $\sum_i k_i = P$. This simplification is called the *collinear* approximation. It is relevant when one considers one-particle final states like in DIS, as one cannot define a transverse-plane angle that the cross section would depend on. It is also relevant for multi-particle final states where the *total* transverse momentum is much larger than the proton mass. Indeed in that scenario, any effect from the intrinsic partonic transverse momentum is washed out by the perturbatively generated transverse momentum of the final-state particles. Therefore the hadronic tensor will not explicitly depend on the *unintegrated* correlator $\phi(k, P)$ that depends on the four components of k . Instead the hadronic tensor will depend on the integrated correlator $\phi(x, P)$ (hence the use of x instead of k in Fig. 1.1).

The factorisation procedure is similar for other hadronic processes. Each parton entering the high-energy scattering is associated with an object describing the transition between the hadronic bound state and a quasi-free parton. In the case of a proton-proton collision where the hard scattering is initiated by two gluons (sometimes referred to as gluon fusion), the cut-diagram representation of the squared amplitude is shown in Fig. 1.3. The general cross section for this process then reads:

$$\frac{d\sigma}{d\mathcal{R}} = \int \frac{d^4 k_1}{(2\pi)^4} \frac{d^4 k_2}{(2\pi)^4} \delta^4(k_1 + k_2 - q) \text{Tr} \left[\Gamma^{\mu\rho}(k_1, P_1) H_{\rho\sigma}^* \Gamma^{v\sigma}(k_2, P_2) H_{\mu\nu} \right], \quad (1.4)$$

where $d\mathcal{R}$ is an infinitesimal volume of the phase space, and we kept the unintegrated gluon correlators as we will look at them in more details in the following. We thus have a

¹in DIS, one can prove the support properties of PDFs: $q(-x) = -\bar{q}(x)$ where \bar{q} is the distribution of anti-quarks.

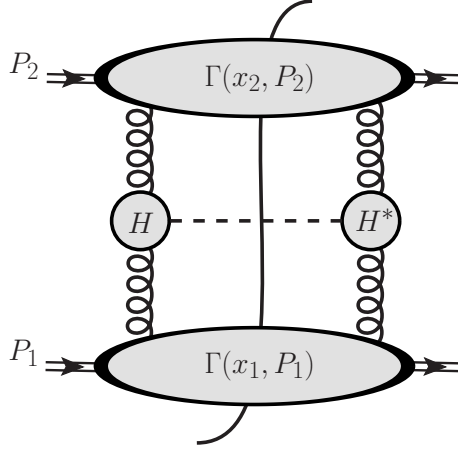


Figure 1.3: pp collision via gluon fusion. The unspecified hard scattering is represented by the H blob (H^* in the conjugate amplitude). The observed final state is also general and is represented by a dashed line.

correlator for each of the gluons entering the hard-scattering. We see that each correlator has two Lorentz indices contracting with the hard-scattering amplitude and its complex conjugate, the factorised formula is therefore valid at the squared amplitude level. Similarly, the factorised expression for DIS (cf. Eq. (1.2)) is provided at the tensor level and describes a squared amplitude. We will now analyse the correlator and try to see how one can extract information about the proton structure from it.

1.2 The parton correlator

Let us get back to the hadronic tensor in the cross section of DIS. This tensor is proportional to a product of local currents $\langle P|j^\mu(0)|X\rangle\langle X|j^\nu(0)|X\rangle$. One can make this product bilocal by translating one of the fields: $\langle P|j^\mu(0)|X\rangle \rightarrow \langle P|j^\mu(\eta)|X\rangle e^{i(k-k')\cdot z}$ with k and k' the quark momenta before and after scattering, and then use the Dirac delta function that ensures momentum conservation $\delta(k+q-k')$ to sum the product over the position interval η . Using the completeness relation over undetected final states: $\sum_X |X\rangle\langle X| = \mathbb{1}$, one finds:

$$\sum_X \delta(k+q-k') \langle P|j^\mu(0)|X\rangle\langle X|j^\nu(0)|X\rangle = \frac{1}{(2\pi)^4} \int d^4z e^{iz\cdot q} \langle P|j^\mu(0)j^\nu(\eta)|P\rangle. \quad (1.5)$$

The interest in re-writing the current product as an integral over the non-locality η (moreover as one matrix element thanks to the completeness relation over unobserved final

states) resides in the use of an Operator Product Expansion (OPE) to select the dominant contributions to the matrix element $\langle P | j^\mu(0) j^\nu(\eta) | P \rangle$ [11, 12]. As opposed to products of electromagnetic and/or weak currents, hadronic currents are expanded in sums of *non-local* operators. It can be showed that the coefficient functions multiplying various operator combinations are proportional to powers of $(M/Q)^{t-2}$, where t is the so-called *twist* of the operator product. Since this ratio is supposedly small at large momentum transfer, one can then select the leading contributions only by realising a twist expansion in order to evaluate the DIS cross section. The cross section and related observables of a QCD can therefore be evaluated through a double expansion in powers of α_s and (M/Q) . However, a rigorous OPE is only applicable to DIS and $e + e -$ annihilation processes. Another technique that is valid under some assumptions and allows one to easily visualise the leading contributions to a hadronic cross section is the diagrammatic approach [13]. In this approach, the quark spinors/gluon polarisation vectors that would connect to the extremities of Feynman diagrams describing the hard-scattering as in a free-field theory are replaced by their correlators, whose operator structure is that of the fields entering the diagrams. For example, one can show that the leading-twist correlator of the quark involved in a DIS with an electron will be of the form:

$$\Phi_{ij}(k; P) = \int \frac{d^4\eta}{(2\pi)^4} e^{ik\cdot\eta} \langle P | \bar{\psi}_j(0) \mathbb{P}_{3^*} \psi_i(\eta) | P \rangle, \quad (1.6)$$

and corresponds to the diagram in Fig. 1.4 where $\psi_i(x)$ is the free quark field with a Dirac index i . The twist-2 correlator “extracts” a quark from the proton bound state to scatter with the virtual photon in the hard-scattering amplitude before “reinserting” it into the proton in the complex conjugate part. Since it is acting on a squared amplitude, it should be labelled a quark-quark correlator to avoid any confusion, but will usually be called quark correlator unless necessary. Since we extract a quark from the proton that is in a colour-triplet state, the remnants naturally are in an anti-triplet state. The sum over remnants states therefore gives an identity operator over the space obeying this configuration, denoted \mathbb{P}_{3^*} . It will be omitted in the following for brevity, as well as the summation over colours in all correlators. The diagrammatic expansion generates the same ordering in powers of (M/Q) as the rigorous OPE when it is applicable; it *de facto* assumes factorisation and can be seen as an improved version of the parton model that only accounts for the leading-twist contribution, while within the expansion, sub-leading contributions can also be taken into account. In a similar way, one can define a gluon correlator as follows:

$$\Gamma^{\mu\nu;\rho\sigma}(k; P) = \int \frac{d^4\eta}{(2\pi)^4} e^{ik\cdot\eta} \langle P | F^{\mu\nu}(0) F^{\rho\sigma}(\eta) | P \rangle. \quad (1.7)$$

The use of F fields rather than A fields will be justified in the following. This correlator expression is similar to that for a quark entering the scattering. The corresponding diagram is therefore equivalent to Fig. 1.4 where the quark lines would be replaced by gluons.

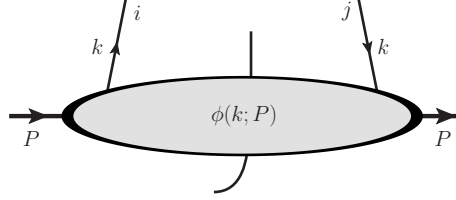


Figure 1.4: Diagrammatic representation of the quark correlator.

This correlator is twist-2 as well, but gluons do not directly couple to the electromagnetic field. Hence the leading contribution from gluons to the hard-scattering is sub-leading in the expansion of the coupling constant α_s when compared to the quark one, as it requires higher-order Feynman diagrams. One may then think that any gluon-related effect can be safely neglected in the description of DIS, but this is incorrect since an expansion does not always converge properly or a process may be gluon-dominated. Let us introduce the quark-gluon-quark correlator:

$$\Phi_{Aij}^\mu(k, k_1; P) = \int \frac{d^4\eta}{(2\pi)^4} \frac{d^4\xi}{(2\pi)^4} e^{ik\cdot\eta} e^{ik_1\cdot(\xi-\eta)} \langle P | \bar{\psi}_j(0) A^\mu(\xi) \psi_i(\eta) | P \rangle. \quad (1.8)$$

which corresponds to the diagram in Fig. 1.5a. The qgq vertex diverges for gluons that are soft or collinear to the quark, as the denominator contains a scalar product of the quark and gluon momenta. Therefore the contribution brought by the quark-gluon-quark correlator is actually leading-twist and cannot be neglected since the sum over undetected gluon momenta also covers the regions where the gluon is soft or collinear. Furthermore, a correlator connecting n gluons to the hard part is a leading contribution as well (cf. Fig. 1.5b), one must therefore sum all diagrams connecting a number of gluons between 0 and ∞ to each side of the squared amplitude. Another way to phrase this is that one cannot differentiate an isolated quark from a quark accompanied by an arbitrary number of soft and/or collinear gluons, and the state is then degenerate. The KLN theorem ensures that all infrared singularities cancel at each order of perturbation theory when all the degenerate states are summed over [14]. While the final states are summed over and hence cancel any infrared divergence, the initial state singles out a quark and the state is degenerate so one needs to sum over all these states. It is practical to use lightcone coordinates to describe the kinematics of hadronic processes at high energies where masses can be neglected. The coordinates are defined such that for a 4-vector x :

$$x^+ = \frac{1}{\sqrt{2}} (x^0 + x^3) \equiv x \cdot n_-, \quad (1.9)$$

$$x^- = \frac{1}{\sqrt{2}} (x^0 - x^3) \equiv x \cdot n_+, \quad (1.10)$$

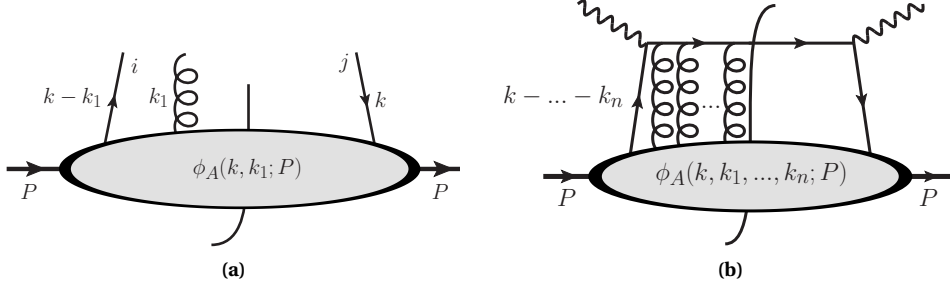


Figure 1.5: (a) Diagrammatic representation of the quark-gluon-quark correlator $\Phi_{Aij}^\mu(k, k_1; P)$. (b) Representation of a correction term to the parton model for DIS with n soft or collinear gluons connecting to the hard-scattering amplitude.

$$x_T = (x^1, x^2), \quad (1.11)$$

with the lightlike vectors n_\pm that can be formed using the Cartesian basis:

$$n_+ = \frac{1}{\sqrt{2}}(\hat{e}_0 + \hat{e}_3), \quad n_- = \frac{1}{\sqrt{2}}(\hat{e}_0 - \hat{e}_3) \quad \Rightarrow \quad n_+^2 = n_-^2 = 0, \quad n_+ \cdot n_- = 1. \quad (1.12)$$

The proton is conventionally chosen to have a large momentum along the n_- direction, which means P^+ is the large component. Logically, the partons coming from the proton also have large “+” momenta such that these will generate the leading terms in the twist expansion. The collinear correlator that will ultimately be relevant for processes like DIS can be written:

$$\phi_{ij}(x, P) = \int dk^- d^2 \mathbf{k}_T \phi_{ij}(k; P) = \int \frac{d\eta^-}{2\pi} e^{ik^+ \eta^-} \langle P | \bar{\psi}_j(0) \psi_i(\eta) | P \rangle \Big|_{\eta^+ = \eta_T = 0}. \quad (1.13)$$

We see that integrating over the small parton momentum components places the field on the lightcone as each integral generates a Dirac delta in position space, so that the separation is restricted to be on the “-” axis. Now if one computes the diagram with n connected gluons, the correlator can be written in the following form:

$$\phi_A(k, k_1, \dots, k_n; P) = \phi(k; P) (-ig)^n \int_{-\infty}^{\eta^-} d^4 \xi_1^- A^+(\xi_1) \dots \int_{\xi_{n-1}}^{\eta^-} d^4 \xi_n^- A^+(\xi_n) \Big|_{\xi^+ = \eta^+ = 0, \xi_T = \eta_T = 0}, \quad (1.14)$$

where $g = \sqrt{\alpha_s}$ is the amplitude-level strong coupling. Therefore one sees from Eq. (1.14) that adding an arbitrary number of gluons fields at leading-twist only multiplies the quark-quark correlator by integrals over paths of the A field. Indeed the gluon fields are classical, or *eikonal* in this contribution, one can therefore decompose a diagram of n

gluons connecting to a quark line into a product of n diagrams where one gluon connects to the quark line. Since products of gluon fields need ordering, one can order them by their position: $\xi_{i-1} < \xi_i < \xi_{i+1}$. One can see that the overall factor multiplying the quark-quark correlator in Eq. (1.14) corresponds to the n^{th} term of the Taylor expansion of an exponential. The consequence is that the sum of all the gluon contributions on one side of the final-state cut can be *exponentiated* into one operator called a Wilson line:

$$\begin{aligned} U_{[\infty,\eta]}^- &= \sum_{n=0}^{\infty} (-ig)^n \int_{\infty}^{\eta^-} d\xi_1^- A^+(\xi_1) \dots \int_{\xi_{n-1}^-}^{\eta^-} d\xi_n^- A^+(\xi_n) \Big|_{\xi_i^+ = \eta^+ = \xi_T = \eta_T = 0} \\ &= \mathcal{P} \exp \left(-ig \int_{\infty}^{\eta} d\xi^- A^+(\xi) \right) \Big|_{\xi_i^+ = \eta^+ = \xi_T = \eta_T = 0}, \end{aligned} \quad (1.15)$$

where \mathcal{P} is the path-ordering operator for the expansion. The new collinear quark correlator encompassing all the considered corrections then reads:

$$\begin{aligned} \phi_{ij}(k; P) &= \int \frac{d\eta^-}{2\pi} e^{ik^+ \eta^-} \langle P | \bar{\psi}_j(0) U_{[0,\infty]}^- \psi_i(\eta) U_{[\infty,\eta]}^- | P \rangle \Big|_{\eta^+ = \eta_T = 0} \\ &= \int \frac{d\eta^-}{2\pi} e^{ik^+ \eta^-} \langle P | \bar{\psi}_j(0) U_{[0,\eta]}^- \psi_i(\eta) | P \rangle \Big|_{\eta^+ = \eta_T = 0}, \end{aligned} \quad (1.16)$$

where we used the causality property of the Wilson lines to combine them into one line that finally connects the two quark fields in position. Connecting the fields in the correlator also has as a consequence to restore its invariance under colour-gauge transformation. Indeed, the correlator definition given in Eq. (1.13) is not gauge invariant and thus not a physical object. This is the reason Wilson lines are also called *gauge links*. Similarly for the gluon correlator, the combination of fields and links $F^{\mu\nu}(0) U_{[0,\eta]} F^{\rho\sigma}(\eta) U'_{[\eta,0]}$ takes into account all leading-twist soft gluons and makes the correlator gauge-invariant. The leading-twist correlator reads:

$$\begin{aligned} \Gamma^{\mu\nu}(x; P) &= \int dk^- n_{-\rho} n_{-\sigma} \Gamma^{\mu\rho;\nu\sigma}(k; P) \\ &= \int \frac{d\eta^-}{2\pi} e^{ik^+ \eta^-} \langle P | F^{\mu+}(0) U_{[0,\eta]} F^{\nu+}(\eta) U'_{[\eta,0]} | P \rangle \Big|_{\eta^+ = \eta_T = 0}. \end{aligned} \quad (1.17)$$

It requires two distinct links in the fundamental representation due to the more complex colour structure of the gluon strength fields F [15]. After this introduction to the operator definition of parton correlators, we are going to look at their parametrisation in terms of PDFs that are the quantities we can study to get information about the structure of the proton.

1.3 Parton Distribution Functions

So far we neglected any effect related to the spin state of the proton on the structure of the parton correlators. Indeed in this thesis, we will focus on the phenomenology of proton collisions made at the LHC, where the beams are unpolarised. Proton spin effects will therefore be irrelevant to us, but we will briefly introduce how correlations between momenta and spins of the proton and partons modify the parametrisation of the correlator. The idea to follow in order to provide a parametrisation for a given correlator is to find the most general form that parametrisation can take while still respecting the symmetries the operator definition must respect, and by retaining only terms that will give a leading contribution to cross sections in the twist expansion (see e.g. [16]). One can then write the correlator as a combination of vectors at hand, namely the lightcone vectors $n_+ \sim P$ and n_- , the proton spin S , γ matrices, as well as scalar quantities. The nature of such scalar quantities will then provide information about the internal structure of the proton. The quark correlator needs to respect hermiticity and P -invariance. One can also get an extra condition from symmetry under time reversal but this can be more subtle to implement as we will briefly see in the next chapter for the TMD case where gluonic poles can generate T -odd contributions. The quark correlator can be parametrised as follows [17]:

$$\Phi(x; P, S) = \frac{1}{2} [f_1(x) \not{n}_+ + g_1(x) S_L \gamma_5 \not{n}_+ + h_1(x) i \sigma_{\mu\nu} \gamma_5 n_+^\mu S_T^\nu]. \quad (1.18)$$

We find at leading twist three terms, each associated with a scalar function, that respectively correspond to an unpolarised, longitudinally polarised or transversely polarised proton. Hermiticity restricts the scalar functions to be real-valued. If one rewrites the correlator in the quark-spin basis, it can be seen that each scalar function identifies with the probability of finding a quark of spin α and momentum fraction x inside a proton of spin S . The scalar functions can therefore be interpreted as distribution functions, which is the reason they are named PDFs. f_1 is the unpolarised quark distribution inside unpolarised protons; g_1 is the longitudinally polarised quark distribution inside longitudinally polarised protons, also called helicity distributions; and h_1 is the transversely polarised quark distribution inside a transversely polarised proton, also called transversity distribution. The subscript 1 means that these are leading-twist distributions, as more would be necessary to parametrise a higher-twist correlator. While f_1 is the only distribution appearing in the correlator of an unpolarised proton, it also contributes alongside g_1 or h_1 in the description of a polarised state. Since the PDFs are the only unknown values in the parametrisation of a correlator entering the cross section of a hadronic process, it is clear that one can extract them from experimental measurements of hadronic cross sections. Moreover one expects the PDFs to be *universal*: since they are describing the internal dynamics of the proton, the distributions extracted should be independent of the considered process. If true, this gives predictive power to QCD by allowing one to use a PDF

extracted from the cross-section measurements of one process to predict cross sections in all other processes where the PDF plays a role. The gluon correlator is parametrised as follows:

$$\Gamma^{\mu\nu}(x; P, S) = \frac{1}{2x} [-g_T^{\mu\nu} f_1^g(x) + i e_T^{\mu\nu} \lambda g_1^g(x)]. \quad (1.19)$$

with λ the nucleon helicity, $g_T^{\mu\nu} = g^{\mu\nu} - P^\mu n^\nu - P^\nu n^\mu$ and $e_T^{\mu\nu} = \epsilon^{\mu\nu\rho\sigma} P_\rho n_\sigma$ where n is any lightlike vector non-orthogonal to P . The gluon distributions are denoted by a superscript g ; we note that there is no equivalent to the quark transversity PDF for gluons.

We need to bring some refinements to the parton model in order to be able to make predictions for QCD-related observables. So far we considered the coupling α_s to be a constant. If one would want to include higher-order corrections in powers of α_s , loop diagrams would contribute from which singularities need to be removed. This is done via the renormalisation procedure in which the bare parameters of the theory are redefined in order to absorb the divergences. However this procedure introduces an arbitrary renormalisation scale usually denoted μ at which the singularities are removed. Since a physical observable cannot depend on an arbitrary parameter, one needs to enforce the independence of observables from variations of μ through Renormalisation Group Equations (RGEs). If one takes a dimensionless variable R that can only depend on the ratio Q/μ , the RGE will read [18]:

$$\mu^2 \frac{d}{d\mu^2} R\left(\frac{Q^2}{\mu^2}, \alpha_s\right) \equiv \left(\mu^2 \frac{\partial}{\partial \mu^2} + \mu^2 \frac{\partial \alpha_s}{\partial \mu^2} \frac{\partial}{\partial \alpha_s} \right) R = 0. \quad (1.20)$$

The consequence is that the explicit variations of R with μ/\mathcal{Q} must be compensated by also varying α_s with μ or Q . This introduces the need of a *running* coupling constant in renormalisable theories. Solving the RGE allows to compute how the coupling varies with the scale, after having measured the coupling at one point (usually at m_Z [19]):

$$\mu^2 \frac{\partial \alpha_s(\mu^2)}{\partial \mu^2} = Q^2 \frac{\partial \alpha_s(Q^2)}{\partial Q^2} = \beta(\alpha_s), \quad \alpha_s(Q^2) = \frac{\alpha_s(\mu^2)}{1 + \alpha_s(\mu^2) b \ln(\mu^2/Q^2)}. \quad (1.21)$$

The β function can be perturbatively evaluated in powers of α_s (provided that both scales are in the perturbative regime), by applying corrections to the QCD bare vertices: $\beta(\alpha_s) = -b \alpha_s^2 (1 + b' \alpha_s + \mathcal{O}(\alpha_s^2))$. The one-loop coefficient is $b = (33 - 2n_f)/12\pi$ with n_f the number of active quark flavours in the considered energy range. The negative sign of the β function in QCD makes α_s tend toward 0 at large energy and is at the origin of asymptotic freedom. On the other side, the running coupling diverges when approaching the Landau pole of QCD $\Lambda \sim 200$ MeV, making perturbative techniques non-applicable below the GeV scale. Another common definition for the running coupling (again at one-loop order

here) uses the Landau pole:

$$\alpha_s(Q^2) = \frac{1}{b \ln\left(\frac{Q^2}{\Lambda^2}\right)}. \quad (1.22)$$

A similar procedure can be applied to the quark masses that are simple parameters of the Lagrangian, in an analogous way to the coupling. One can show that light-quark masses can safely be neglected at large energy scales, while heavy-quark masses must be taken into account in the computations if they are of the same order of magnitude as Q . However, quarks with masses m that are much larger than the considered hard scale decouple from the process as their contribution is suppressed by inverse powers of m and can be neglected as well. The mass also runs with Q , an effect that might need to be taken into account in order to make accurate predictions.

To this point, we also considered PDFs in the collinear approximation which only depend on the momentum fraction x carried by a parton entering a hard scattering. This is in accordance with the picture given by the parton model: partons are point-like particles, the quark scattering with the virtual photon does not undergo any QCD interaction over the short interaction distance $\sim 1/Q$. We already saw that this is not completely true, as one needs to account for soft and collinear gluons coupling to the hard part, but these corrections can be factored out of the latter and simply add a matrix-valued phase factor to the quark correlator that is a Wilson line. Hence a primarily expected feature of the PDFs is the so-called Bjorken scaling, where the PDFs remain independent of the hard scale Q . This scale can be seen as the resolution that the virtual photon of DIS can probe the proton with. However one could imagine a scenario where the quark entering the scattering originates from the splitting of another parton. Such splittings are not soft and can therefore be computed using perturbative techniques, they are called initial-state radiations. One can imagine that a parton entering a specific hard scattering comes from a cascade of initial-state radiations (cf. Fig. 1.6).

The cross section describing a quark emitting a gluon and then entering the hard scattering represented by the blob in Fig. 1.6 can be factorised: it is the product of the probability for the parent quark to emit a gluon with the cross section of the process occurring within the blob. Such a probability, computed for a given (squared) transverse momentum of the gluon, needs to be integrated between a minimal scale $\mu_0^2 \sim \Lambda^2$ and a maximal scale $\mu^2 \leq Q^2$. The probability is proportional to $\alpha_s \ln(\mu^2/\mu_0^2)$. As μ and μ_0 can cover a wide range, the logarithm can be large and make the contribution non-negligible since it appears with the same power as α_s . Within the collinear approximation, it can be shown that for an arbitrary number of initial-state radiations, the main contribution comes from emissions that are strongly ordered in transverse momentum:

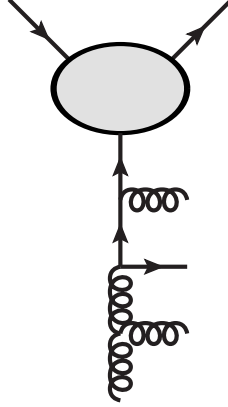


Figure 1.6: Representation of initial-state splittings a parton can undergo before entering a hard scattering. Such diagrams translate into corrections to the PDFs.

$k_{T_1}^2 \ll k_{T_2}^2 \dots \ll k_{T_n}^2$. The parton extracted from the proton is collinear, and its transverse momentum can be neglected as is done in the collinear approximation, while that entering the hard scattering with the probe has a large transverse momentum that is perturbatively generated. The probability for a quark or gluon to come from n previous strongly ordered emissions is proportional to $(\alpha_s \ln(\mu^2/\mu_0^2))^n$. Then all the emissions can be summed and this component can be included in the definition of the PDF, which then acquires a dependence on the scale μ (as well as the correlator it parametrises). By perturbatively computing the splitting functions associated with the various emission scenarios, one can write an integro-differential equation that is the DGLAP equation that allows one to compute how a given PDF varies with the scale μ . [20, 21, 22]. The DGLAP equation explains the violation of Bjorken scaling. The parton model initially makes the approximation that partons do not interact at all with each other; therefore the photon in DIS will always see a point-like quark, independently of the resolution $1/Q$ with which it probes the proton. When taking into account initial-state radiations, the photon now sees a quark dressed with other partons, and this picture is dependent on the resolution achieved, hence the momentum transfer Q . This variation of parton distributions with the scale is called *evolution*. The considered corrections generate UV divergences that are removed through a renormalisation procedure applied to the PDF that introduces a dependence on the renormalisation scale μ , and the DGLAP equation is the RGE of the PDF associated with μ .

The PDFs have been extracted in many processes at different colliders. The main process used first was DIS. The H1 and ZEUS experiments at the HERA electron(positron)-

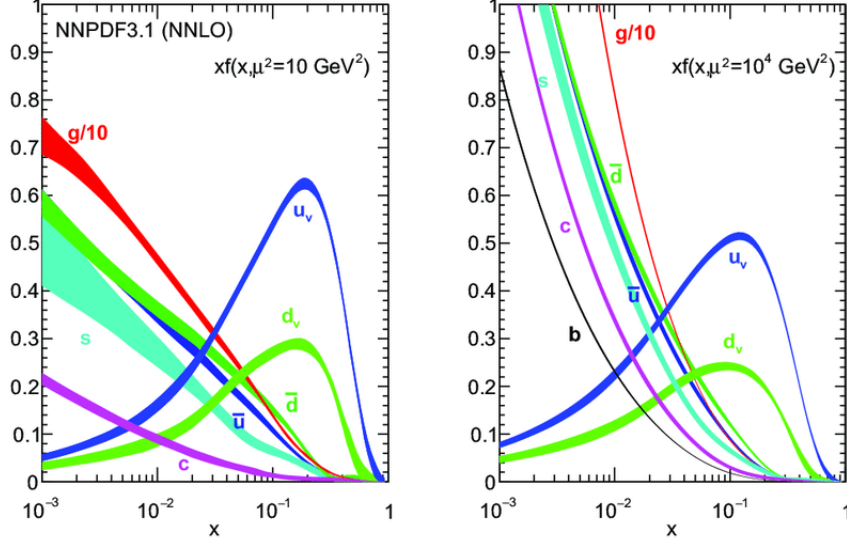


Figure 1.7: Global fit of the different (x -weighted) PDFs inside the proton as functions of $x > 10^{-3}$ for $\mu^2 = 10$ and 10^4 GeV^2 by the NNPDF collaboration [23].

proton accelerator extracted PDFs in a range of $0.045 < Q^2 < 50000$ GeV^2 and $6 \cdot 10^{-7} < x < 0.65$ for neutral currents (γ^* , Z^0) that allow one to extract valence quarks and gluons PDFs, and $200 < Q^2 < 50000$ GeV^2 and $1.3 \cdot 10^{-2} < x < 0.4$ for charged currents (W^\pm) that allow one to separate quark flavours. Fig. 1.7 presents a modern global fit of unpolarised PDFs as functions of x for two different values of $\mu = 3.16$ and 100 GeV [23]. From this figure, it is clearly visible that the parton content of the proton strongly varies with the reference frame it is considered in, hence high-scale probes will encounter a much denser parton sea than low-scale ones. Moreover, gluons quickly become strongly predominant below $x = 10^{-1}$ (the gluon distribution is divided by 10 in both plots for presentation purposes). Therefore, hard scatterings within hadron collisions are very likely to occur within gluon fusion. Even in processes that are primarily quark induced, the gluon distribution might bring a dominant contribution through splittings of gluons into quarks.

In this chapter, we explained how one could provide a description of hadronic reactions, using the parton model that provides a picture of the proton in terms of the degrees of freedom of QCD that are the partons. In this picture where the partons do not interact with each other during the short interaction time with the probe, the latter sees

a “snapshot” of the proton and the associated cross section can be factorised into the product of two objects. The first one is a hard scattering between the probe and a parton computable perturbatively, *i.e.* using an expansion in the coupling constant α_s that is supposedly small. The second one is a correlator that is intrinsically nonperturbative and encodes information about the proton structure in terms of partons. We saw that this correlator could be parametrised in terms of scalar quantities that had a probabilistic interpretation, the PDF that give the probability of finding a specific parton with momentum fraction x . We then saw that some corrections that would be a priori sub-leading in the twist expansion of the correlator actually need to be taken into account. Wilson lines so far only intervene in operator definition of the correlator. Vertex corrections imply the running of the coupling constant with the renormalisation scale as well as the quark masses when the latter cannot be neglected. Initial-state radiations are hard emissions occurring before the scattering with the probe that can be absorbed into the distribution by making it dependent on the scale which it is probed at: this phenomenon is called evolution (fragmentation functions also undergo evolution due to final-state radiations in the case of processes with hadron creation in the final state). We finally saw that PDFs as functions of x were indeed larger at high energies (except for the valence quark ones), with the gluon PDF being highly predominant.

Chapter 2

Beyond the collinear approximation: the transverse structure of the proton

Up to this point, we considered the structure of the proton and its study within the collinear approximation. The intrinsic transverse component of the parton momentum is neglected in the hard scattering when it is much smaller than the detected transverse momentum of the final state, generated via perturbative interactions. The partonic correlator appearing in a cross section within this approximation is integrated over all components of the parton momentum but the longitudinal one. Collinear factorisation theorems are rigorously proven for processes that are inclusive enough like DIS, but also the Drell-Yan process ($q\bar{q} \rightarrow \gamma^* \rightarrow l^+l^-$) and direct photon, W , Z^0 production which allow a valid extraction of PDFs, and many other processes are expected to be factorisable [24, 25]. On the other hand, it is not possible to get any information about the transverse structure of the proton in the collinear regime. One might want to consider processes where the total transverse momentum of the final state is closer to the mass of the proton, and might therefore be sensitive to the intrinsic transverse momentum of the partons. It would then be practical to also use factorisation theorems in order to disentangle the perturbative and nonperturbative components, the latter encoding the extra information on the proton structure that eludes collinear factorisation. Such a procedure is called Transverse Momentum-Dependent factorisation, or TMD factorisation [26, 27, 28]. Many concepts can be seen as extensions of the ones defined within collinear factorisation, but we will also see some fundamental differences between the two regimes. In particular, a parametrisation in terms of universal parton distributions remains possible for most cases. We will start by considering a general picture of parton correlators that are less inclusive than the integrated version intervening in the collinear case. We will then have a more detailed look at the gluon TMD correlator in unpolarised protons and its parametrisations, the relevant gluon distributions remaining poorly known. The following step is to look at the cross section for a gluon-fusion-initiated process in the TMD formalism, the relevant gluon TMD distributions (often simply called TMDs). To continue, we will quickly review what is the status of our knowledge on TMDs, especially the gluon ones, and what are the key processes to their extraction. Although a complete TMD factorisation process has only been demonstrated for a handful of

processes, we will provide arguments in favour of the factorisability of quarkonium production in association with colourless particles as well as quarkonium-pair production. Finally we will explain the formalism of TMD evolution and how it can be implemented in a cross section in order to improve the extraction of the nonperturbative component of distributions.

2.1 Multidimensional correlators and hadron spin

Although we introduced the unintegrated parton correlator in the previous chapter, we will not work with it as processes analysed within the collinear factorisation only probe the one-dimensional correlator $\phi(x, P)$. Even when accounting for the proton spin, the phenomenology of a reaction is not much richer as rotational invariance is enforced. In order to probe the proton structure in more details, one needs to consider less inclusive processes. As already mentioned, processes where the final-state transverse momentum is of the same order as the partonic transverse momentum are sensitive to its effects. Distributions depending on the intrinsic transverse momentum of the parton are called TMDs. A different family of processes of interest in the study of the proton structure are exclusive processes where one measures the momentum shift of the proton denoted Δ . Indeed through Fourier transforms, the Δ -dependence translates into a dependence in the position of partons inside the proton, bringing information that is complementary to those encoded in momentum-dependent correlators. The Δ -dependence is usually divided into its "+" component (via the shift fraction $\xi = -\Delta^+/2P^+$ called skewness) and the transverse component Δ_T , the "-" component being fixed by the on-shell condition of the proton. Distributions encoding the Δ -dependence are called Generalised Parton Distributions, or GPDs. Fig. 2.1 presents some types of correlators and the relations between them, from the most general one on top that the fully unintegrated correlator, to the one-dimensional collinear PDF. Integrating the full correlator over k^- gives a Generalised TMD (GTMD) that still depends both on three-dimensional partonic momenta and proton momentum shifts. Integrating over transverse partonic momenta \mathbf{k}_T will give a GPD, while taking the forward limit $\Delta = 0$ (hence no proton momentum shift) will give a TMD. Naturally, enforcing the forward limit on a GPD or integrating a TMD over \mathbf{k}_T must result in a collinear PDF, although the matching between the two requires specific care [29]. For a more complete review of the proton structure landscape and different types of correlators, we refer to [30]. One can see for example that Fourier-transformed GPDs become functions of the impact parameter of the parton, *i.e.* its position in the transverse plane. One can then define proper impact parameter distributions as Fourier-transformed GPDs with zero skewness.

Since such correlators have more variables, their parametrisation will require more

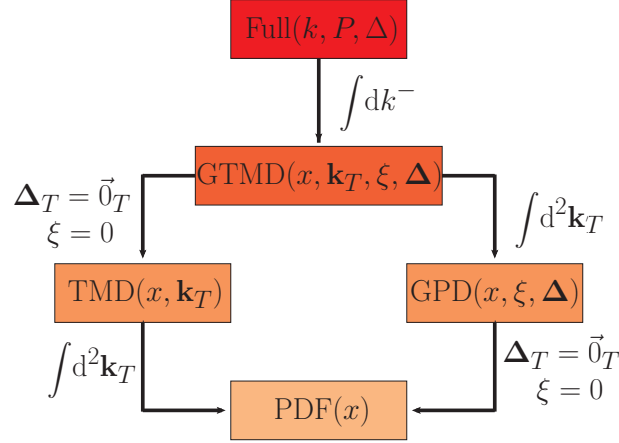


Figure 2.1: Multidimensional parton correlators from the fully unintegrated correlator to the one-dimensional collinear PDF, and the connections between them.

terms to describe all the possible interactions. The TMD correlators for example will contain distributions that encapsulate the correlation between a parton transverse momentum and its spin, or the spin of the proton in the polarised case. We provide in Table 2.1 a classification of the leading-twist TMDs depending on the polarisation of the parton and its parent hadron. We note that all TMDs with a “ \perp ” sign in their name are multiplied by tensors that are functions of the parton transverse momentum in the relevant correlator parametrisation. Therefore their contributions to a cross section where the partonic transverse momentum is neglected will vanish. If one integrates the distributions over \mathbf{k}_T , one should retrieve the collinear distributions from the ones in the diagonal of the table. We note that all TMDs are functions of the magnitude \mathbf{k}_T^2 as the Lorentz structure is contained in the pre-factor they multiply in the correlator parametrisation.

In order to probe the TMD correlator, one can consider a process that is less inclusive than reactions with only one detected particle in the final state. This allows one in particular to define an angle between the two final-state momenta in the transverse plane, making the corresponding cross section sensitive to *azimuthal* asymmetries. One-particle final states may also be subjected to TMD effects on the transverse-momentum spectrum of the detected particle but not to azimuthal asymmetries. Two famous processes used to probe the quark TMDs are Semi-Inclusive DIS (or SIDIS) and the Drell-Yan (DY) process. In such reactions, two particles are detected in the final state. For SIDIS, it is a produced hadron that is detected in addition to the scattered electron, while for DY it is a dilepton. Less inclusive processes logically allow one to probe more complex correlators. In partic-

		Parent hadron polarisation		
		Unpolarised	Longitudinal	Transverse
Parton polarisation	U	$f_1(x, \mathbf{k}_T^2)$ (Number density)		$f_{1T}^\perp(x, \mathbf{k}_T^2)$ (Sivers)
	L		$g_{1L}(x, \mathbf{k}_T^2)$ (Helicity)	$g_{1T}(x, \mathbf{k}_T^2)$ (Worm-gear)
	T	$h_1^\perp(x, \mathbf{k}_T^2)$ (Boer-Mulders)	$h_{1L}^\perp(x, \mathbf{k}_T^2)$ (Worm-gear)	$h_{1T}(x, \mathbf{k}_T^2)$ (Transversity) $h_{1T}^\perp(x, \mathbf{k}_T^2)$ (Pretzelosity)

Table 2.1: Classification of TMDs according to the polarisation of the parton and its parent hadron. Note that gluon distributions are distinguished from quark ones by a g in the superscript.

ular, TMD correlators have a non-trivial structure in terms of Wilson lines. Indeed, in the case of a TMD correlator, it can be shown that transverse gluon fields at lightcone infinity produce a leading-twist contribution to Wilson lines [31]. Therefore the associated Wilson lines will have a component in the transverse coordinates, as can be seen in Fig. 2.2a and are called "staple-like" gauge links. Moreover, depending on the space-time structure of the considered reaction, the transverse part will either be located at plus or minus infinity in the lightcone coordinate. The quark TMD correlators associated with such links are called past- or future- pointing and read:

$$\begin{aligned}
\Phi_{ij}^{[+]}(x, k_T) &= \int \frac{d\eta^- d^2\eta_T}{(2\pi)^3} e^{ik\cdot\eta} \langle P, S | \bar{\psi}_j(0) U_{[0, \infty]}^- U_{[0_T, \infty_T]}^T \times \\
&\quad U_{[\infty_T, \eta_T]}^T U_{[\infty, \eta]}^- \psi_i(\eta) | P, S \rangle \Big|_{\eta^+ = 0}, \\
\Phi_{ij}^{[-]}(x, k_T) &= \int \frac{d\eta^- d^2\eta_T}{(2\pi)^3} e^{ik\cdot\eta} \langle P, S | \bar{\psi}_j(0) U_{[0, -\infty]}^- U_{[0_T, \infty_T]}^T \times \\
&\quad U_{[\infty_T, \eta_T]}^T U_{[-\infty, \eta]}^- \psi_i(\eta) | P, S \rangle \Big|_{\eta^+ = 0}, \tag{2.1}
\end{aligned}$$

A gauge-invariant definition of gluon correlators require two separate gauge links due to the way gluon fields transform under a gauge transformation. They are usually labeled $\Gamma^{[\pm, \pm]\mu\nu}(x, k_T)$. Depending on the considered process, the appropriate gauge links can mix past- and future-pointing links.

Gauge-invariant correlators are remarkable as they allow T-odd distributions to enter

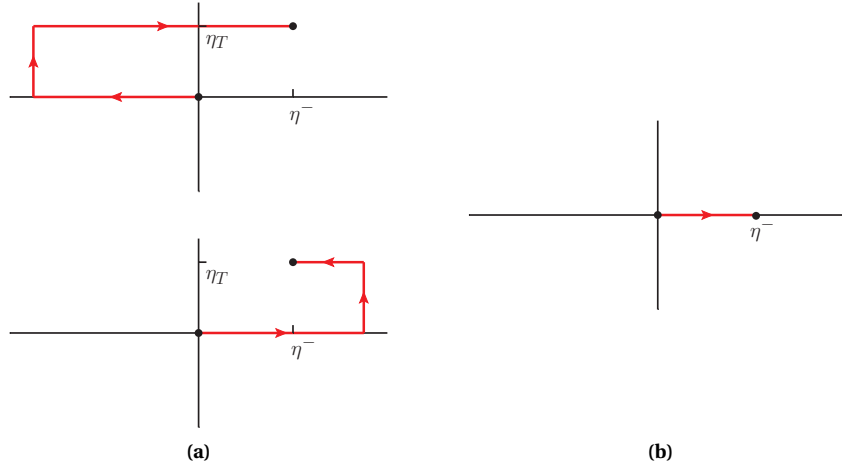


Figure 2.2: (a) Past- and future-pointing staple-like paths for TMD gauge links in the plane of the field nonlocality variable η . (b) In the collinear approximation, the transverse separation disappears, reducing the gauge links to collinear ones that can combine into a one-dimensional path between 0 and η^- .

into their parametrisation [32]. These distributions would vanish if one naively assumed time-reversal invariance before computing the gauge link structure of a reaction. It was then demonstrated [32, 33, 34] that including the proper gauge-link structure allows one to have nonzero T-odd distributions. While in the collinear case, Wilson lines were only necessary to ensure the gauge invariance of the operator definition of the correlator, their presence were thought more as a technicality and had no impact on the phenomenology.

It is generally not the case for TMDs, as was first discovered for T-odd ones (Sivers and Boer-Mulders distributions for the quark). It was realised that the Sivers asymmetry (a left-right asymmetry in the cross section of TMD processes) could actually arise from the corresponding TMD being nonzero. It was also clear that due to the distribution T-oddness, the Sivers function changed sign between the Drell-Yan and SIDIS processes. A consequence is that the corresponding asymmetry also changes sign between the two processes (its magnitude will also change due to the weightings of the different flavours). This discovery has a deep meaning as it proves an impact of a TMD operator nonlocality over physical observables and invalidates the absolute universality of TMDs: the distributions that supposedly characterise the proton internal structure regardless of any external factor can actually vary depending on the way one probes them. It was later found out that T-even distributions could also be non-universal [35]. The TMDs

presented in Table 2.1 can be expanded into a sum of universal TMDs multiplied by process-dependent coefficients.

This entanglement between the definition of the proton constitution and the way one interacts with it is however not fatal to the predictive power of TMD factorisation, as the non-universality is bound to the gauge link structure of the relevant TMDs. Yet, when talking about one of those functions, one should always mention in what physical process they are investigated since they probe different combinations of their universal counterparts. The experimental verification of the sign change of the Sivers function is still ongoing, with encouraging preliminary results [36].

We will now have a look at the parametrisation of the gluon TMD correlator for an unpolarised proton and review the structure of the TMD cross section for a gluon-fusion-induced process. We will in particular describe the observables from which one can extract information about the gluon TMDs.

2.2 Gluon fusion in proton-proton collisions in the TMD formalism

As we can see from Table 2.1, the leading-twist TMD correlator for an unpolarised proton can be parametrised by two functions: the number density function f_1^g that describes unpolarised gluons and survives transverse-momentum integration, and the gluon analogue of the Boer-Mulders function $h_1^{\perp g}$ that corresponds to transversely polarised gluons. While the quark version h_1^\perp is T-odd, $h_1^{\perp g}$ is T-even and thus does not change sign between the different reactions it can be accessed through. The correlator itself can be parametrised as follows:

$$\Gamma_U^{\mu\nu}(x, k_T) = \frac{1}{2x} \left[-g_T^{\mu\nu} f_1^g(x, k_T^2) + \frac{k_T^\mu k_T^\nu - \frac{1}{2} k_T^2 g_T^{\mu\nu}}{M_p^2} h_1^{\perp g}(x, k_T^2) \right], \quad (2.2)$$

where the second term vanishes upon integration over \mathbf{k}_T . We see that the tensors are symmetric under the exchange of the Lorentz indices μ and ν , making the terms invariant by rotation in the transverse plane. This would not be the case for a transversely polarised proton for which distributions can vary with the angle defined by the proton spin and the parton transverse momentum. In order to keep a probability distribution interpretation, it can be showed that the TMDs must respect positivity bounds. In the case of $h_1^{\perp g}$, the bound is [37, 38]:

$$\left| h_1^{\perp g}(x, \mathbf{k}_T^2) \right| \leq \frac{2M_p^2}{\mathbf{k}_T^2} f_1^g(x, \mathbf{k}_T^2). \quad (2.3)$$

We are interested in processes where two initial state gluons scatter at high energies to give a two-particle observed final state: $g(k_1) + g(k_2) \rightarrow X_1(q_1) + X_2(q_2)$. The TMD factorised cross section for such a process reads:

$$\begin{aligned} d\sigma = & \frac{(2\pi)^4}{NS^2} dV \int d^2\mathbf{k}_{1T} \int d^2\mathbf{k}_{2T} \delta^{(2)}(\mathbf{k}_{1T} + \mathbf{k}_{2T} - \mathbf{q}_T) \Gamma^{\rho\mu}(x_1, \mathbf{k}_{1T}) \Gamma^{\sigma\nu}(x_2, \mathbf{k}_{2T}) \\ & \times \left[\frac{1}{(N_c^2 - 1)^2} \sum_F \mathcal{M}_{\mu\nu;F}^{ab}(k_1, k_2; q_1, q_2) \left(\mathcal{M}_{\rho\sigma;F}^{ab} \right)^*(k_1, k_2; q_1, q_2) \right], \end{aligned} \quad (2.4)$$

where N is the symmetry factor ($N = 2$ for two identical particles in the final state), $S = (P_1 + P_2)^2$ is the centre-of mass energy of the colliding protons, dV is the appropriate phase space element of volume. A Dirac delta function ensures the transverse momentum conservation between the gluons and the final state, whose various quantum numbers F are summed over. $\mathcal{M}^{(*)}$ is the partonic scattering amplitude computed using the relevant Feynman diagrams. At leading twist, the gluons going into the hard scattering are collinear to the protons: $k_{1,2T} \sim \Lambda_{\text{QCD}} \ll Q$ where Q is the hard scale of the process. One can therefore expand the partonic amplitude in powers of q_T/Q , where $\mathbf{q}_T = \mathbf{k}_{1T} + \mathbf{k}_{2T} \sim \Lambda_{\text{QCD}}$ is the pair transverse momentum, and taking the leading term amounts to setting the gluon transverse momenta to 0 inside \mathcal{M} . We will see later that one may still use TMD factorisation for $\Lambda_{\text{QCD}} \ll q_T \ll Q$. In the regime $q_T \sim Q$, one needs to match TMD and collinear factorisations using a ‘‘Y-term’’. Matching the two regimes is an active research area, cf. [29, 39, 40, 41]. We have one correlator for each gluon that contracts with the amplitude and its complex conjugate, and each correlator is the sum of two tensors containing one TMD. This results in a sum of different combinations of two gluon TMDs, each associated with a scalar factor that is the contraction of each TMD tensor with the hard-scattering amplitudes. Since one integrates over the unobserved transverse momenta of the gluons, these products of two TMDs are actually convolutions. The cross section can then be rewritten as follows (here for two identical final-state particles):

$$\begin{aligned} \frac{d\sigma}{dQ dY d^2\mathbf{q}_T d\Omega} = & \frac{\sqrt{Q^2 - 4M^2}}{(2\pi)^2 8SQ^2} \times \\ & \left\{ F_1 \mathcal{C}[f_1^g f_1^g] + F_2 \mathcal{C}[w_2 h_1^{\perp g} h_1^{\perp g}] + \cos(2\phi_{\text{CS}}) \left(F_3 \mathcal{C}[w_3 f_1^g h_1^{\perp g}] \right. \right. \\ & \left. \left. + F_3' \mathcal{C}[w_3' h_1^{\perp g} f_1^g] \right) + \cos(4\phi_{\text{CS}}) F_4 \mathcal{C}[w_4 h_1^{\perp g} h_1^{\perp g}] \right\}, \end{aligned} \quad (2.5)$$

where the cross section is expressed in terms of observables: Y is the rapidity of the pair defined in the hadron centre-of-mass frame like \mathbf{q}_T , $d\Omega = d\cos(\theta_{\text{CS}}) d\phi_{\text{CS}}$ is the solid angle element. θ_{CS} and ϕ_{CS} are the Collins-Soper angles [42]. The Collins-Soper frame is the rest frame of the final-state pair, oriented such that the z-axis bisects the proton momenta P_1 and $-P_2$. The angle θ_{CS} is the angle between the final-state pair momentum axis and the z-axis, while ϕ_{CS} is the angle between the plane containing the final-state

pair momenta and the plane containing the proton momenta. The factors F_i multiplying each convolution are called hard-scattering coefficients. While the expression in Eq. (2.5) is universal to all $gg \rightarrow X + Y$ processes, the hard-scattering coefficients are specific to the considered process. Since the latter are computed within the collinear approximation, all the transverse-momentum is contained in the convolutions, that are defined the following way:

$$\mathcal{C}[wfg] = \int d^2 \mathbf{k}_{1T} \int d^2 \mathbf{k}_{2T} \delta^{(2)}(\mathbf{k}_{1T} + \mathbf{k}_{2T} - \mathbf{q}_T) w(\mathbf{k}_{1T}, \mathbf{k}_{2T}) f(x_1, \mathbf{k}_{1T}^2) g(x_2, \mathbf{k}_{2T}^2), \quad (2.6)$$

where $w(\mathbf{k}_{1T}, \mathbf{k}_{2T})$ are generic transverse weights resulting from the contraction of the two correlators and are also general to gluon-fusion processes. They are given by:

$$\begin{aligned} w_2 &= \frac{2(\mathbf{k}_{1T} \cdot \mathbf{k}_{2T})^2 - \mathbf{k}_{1T}^2 \mathbf{k}_{2T}^2}{4M_p^4}, \\ w_3 &= \frac{\mathbf{q}_T^2 \mathbf{k}_{2T}^2 - 2(\mathbf{q}_T \cdot \mathbf{k}_{2T})^2}{2M_p^2 \mathbf{q}_T^2}, \quad w'_3 = \frac{\mathbf{q}_T^2 \mathbf{k}_{1T}^2 - 2(\mathbf{q}_T \cdot \mathbf{k}_{1T})^2}{2M_p^2 \mathbf{q}_T^2}, \\ w_4 &= 2 \left[\frac{\mathbf{k}_{1T} \cdot \mathbf{k}_{2T}}{2M_p^2} - \frac{(\mathbf{k}_{1T} \cdot \mathbf{q}_T)(\mathbf{k}_{2T} \cdot \mathbf{q}_T)}{M_p^2 \mathbf{q}_T^2} \right]^2 - \frac{\mathbf{k}_{1T}^2 \mathbf{k}_{2T}^2}{4M_p^4}. \end{aligned} \quad (2.7)$$

Eq. (2.5) has two terms that contain a convolution of $h_1^{\perp g}(x_1, \mathbf{k}_{1T})$ and $h_1^{\perp g}(x_2, \mathbf{k}_{2T})$ with different transverse weights; one is multiplied by a $\cos(4\phi_{CS})$ factor, while the other is independent of the azimuthal angle. To understand this, it is instructive to look at the correlator and cross section as functions of the helicity of the gluons. A possible choice to define the polarisation vectors of the initial-state gluons is:

$$\begin{aligned} \varepsilon_{\lambda_1}^\mu(\bar{\mathbf{k}}_1) &= \left(0, -\frac{\lambda_1}{\sqrt{2}}, -\frac{i}{\sqrt{2}}, 0 \right) \text{ for } \bar{k}_1^\mu = x_1 \frac{\sqrt{S}}{2} (1, 0, 0, 1), \\ \varepsilon_{\lambda_2}^\mu(\bar{\mathbf{k}}_2) &= \left(0, \frac{\lambda_2}{\sqrt{2}}, -\frac{i}{\sqrt{2}}, 0 \right) \text{ for } \bar{k}_2^\mu = x_2 \frac{\sqrt{S}}{2} (1, 0, 0, -1). \end{aligned} \quad (2.8)$$

The cross section in gluon helicity space reads:

$$\begin{aligned} d\sigma &= \frac{(2\pi)^4}{NS^2} dV \sum_{\lambda_1, \lambda_2; \bar{\lambda}_1, \bar{\lambda}_2} \int d^2 \mathbf{k}_{1T} \int d^2 \mathbf{k}_{2T} \delta^{(2)}(\mathbf{k}_{1T} + \mathbf{k}_{2T} - \mathbf{q}_T) \\ &\quad \times \Gamma^{\bar{\lambda}_1 \lambda_1}(x_1, \mathbf{k}_{1T}) \Gamma^{\bar{\lambda}_2 \lambda_2}(x_2, \mathbf{k}_{2T}) \left[\frac{1}{(N_c^2 - 1)^2} \sum_F \mathcal{M}_{\lambda_1 \lambda_2; F}^{ab} \left(\mathcal{M}_{\bar{\lambda}_1 \bar{\lambda}_2; F}^{ab} \right)^* \right], \end{aligned} \quad (2.9)$$

where the helicity amplitudes and correlators are simply their bare equivalents contracted with the polarisation vectors of a given helicity state:

$$\mathcal{M}_{\lambda_1 \lambda_2} = \varepsilon_{\lambda_1}^\mu(k_1) \varepsilon_{\lambda_2}^\nu(k_2) \mathcal{M}_{\mu\nu}, \quad (2.10)$$

$$\Gamma_{\bar{\lambda}\lambda}(x, \mathbf{k}_T) = \varepsilon_{\bar{\lambda}}^{\mu}(\bar{\mathbf{k}}) (\varepsilon_{\lambda}^{\nu}(\mathbf{k}))^* \Gamma_{\mu\nu}(x, \mathbf{k}_T). \quad (2.11)$$

While the amplitudes are process dependent, the correlators are not and provide some interesting insight on the gluon TMDs in the unpolarised proton. Their expressions are as follows:

$$\Gamma_{U;\bar{\lambda}\lambda}(x, \mathbf{k}_T) = \frac{1}{2x} \left[\delta_{\lambda,\bar{\lambda}} f_1^g(x, \mathbf{k}_T^2) - \frac{k_x^2 - k_y^2 + 2i\lambda n k_x k_y}{2M_p^2} \delta_{\lambda,-\bar{\lambda}} h_1^{\perp g}(x, \mathbf{k}_T^2) \right], \quad (2.12)$$

with $n = -1$ for the first gluon and $+1$ for the second one. From Eq. (2.12), one sees that each term of the correlator corresponds to specific gluon helicity configurations. The first term multiplies the number density distribution f_1^g with a Kronecker symbol $\delta_{\lambda,\bar{\lambda}}$ which enforces that the helicity of the gluon entering the hard-scattering amplitude is equal to that in the complex conjugate. This is always the case in the collinear approximation where no interference with reversed helicity states contribute to the cross section. However one can see that the second term of the gluon TMD correlator that contains $h_1^{\perp g}$ also contains a $\delta_{\lambda,-\bar{\lambda}}$ which flips the helicity of the gluon in the conjugate amplitude. It is then straightforward to see that the hard-scattering coefficients are sums of helicity cross sections containing zero, one or two helicity flips between the amplitude and its conjugate. Hence F_1 corresponds to the sum of helicity cross sections with no flip, F_3 and F_3' are the sums of single-flip contributions and F_2 and F_4 are the sums of the double-flip ones. To understand the reason why double-flip contributions are separated in two terms with a different ϕ_{CS} dependence requires to write them down. One defines the helicity cross section as follows:

$$d\sigma_{\lambda_1\lambda_2;\bar{\lambda}_1\bar{\lambda}_2} = \frac{1}{(N_C^2 - 1)^2} \sum_F \mathcal{M}_{\lambda_1\lambda_2;F}^{ab}(\bar{\mathbf{k}}_1, \bar{\mathbf{k}}_2; q_1, q_2) \left(\mathcal{M}_{\bar{\lambda}_1\bar{\lambda}_2;F}^{ab}(\bar{\mathbf{k}}_1, \bar{\mathbf{k}}_2; q_1, q_2) \right)^*, \quad (2.13)$$

and the hard-scattering coefficients can be expressed as the following sums:

$$\begin{aligned} F_1 &= \sum_{\lambda_1=\pm 1} \sum_{\lambda_2=\pm 1} d\sigma_{\lambda_1,\lambda_2;\lambda_1,\lambda_2}, \\ F_2 &= \sum_{\lambda=\pm 1} d\sigma_{\lambda,\lambda;-\lambda,-\lambda}, \\ F_3 &= \sum_{\lambda_1=\pm 1} \sum_{\lambda_2=\pm 1} d\sigma_{\lambda_1,\lambda_2;-\lambda_1,\lambda_2}, \\ F_3' &= \sum_{\lambda_1=\pm 1} \sum_{\lambda_2=\pm 1} d\sigma_{\lambda_1,\lambda_2;\lambda_1,-\lambda_2}, \\ F_4 &= \sum_{\lambda=\pm 1} d\sigma_{\lambda,-\lambda;-\lambda,\lambda}. \end{aligned} \quad (2.14)$$

Therefore F_2 corresponds to double-flip cross sections for which the two gluons of one amplitude have the same helicity, while F_4 corresponds to double-flip cross sections

with initial-state gluons of opposite helicities. It happens that helicity amplitudes with two gluons that have opposite helicities carry a phase $e^{\pm 2i\phi_{CS}}$ regardless of the considered two-particle final state, while same-gluon-helicity states have no azimuthal phase. Knowing this, it is already obvious that cross sections in F_2 cannot generate a ϕ_{CS} -dependence. While some of the amplitudes in F_1 can have a phase, they will always combine with a complex conjugate that cancels the phase, making the whole cross sections and the hard-scattering factor ϕ_{CS} -independent. One therefore requires a helicity-flip contribution to the cross section in order to generate a possible azimuthal asymmetry. This is what happens with F_3 that combines an amplitude with two opposite-helicity gluons (with a phase) with an amplitude with same-helicity gluons (no phase). In this case, the product of the amplitudes does not cancel the phase out, and one can factor out $e^{2i\phi_{CS}} + e^{-2i\phi_{CS}} \propto \cos(2\phi_{CS})$ from F_3 , as well as F_3' . The situation is similar for F_4 where both amplitudes have a phase, but these generate a constructive interference that leads to a factor $e^{4i\phi_{CS}} + e^{-4i\phi_{CS}} \propto \cos(4\phi_{CS})$ that can be extracted from F_4 , generating an additional azimuthal asymmetry in the TMD cross section. It is then understood that the phase of the amplitudes used in the definition of the F_i coefficients are taken at $\phi_{CS} = 0$, the entire azimuthal dependence being explicitly shown by the cosines in Eq. (2.5).

If one rewrites the hard-scattering coefficients as functions of the linear polarisation amplitudes $\mathcal{M}_{T_1, T_2} = \varepsilon_{T_1}^\mu(\bar{k}_1) \varepsilon_{T_2}^\nu(\bar{k}_2) \mathcal{M}_{\mu\nu}$ with $T_{1,2} = x$ or y such that $\varepsilon_\lambda = \varepsilon_x + i\lambda\varepsilon_y$, they yield the following expressions:

$$\begin{aligned}
F_1 &= |\mathcal{M}_{xx}|^2 + |\mathcal{M}_{xy}|^2 + |\mathcal{M}_{yx}|^2 + |\mathcal{M}_{yy}|^2, \\
F_2 &= \frac{1}{2} |\mathcal{M}_{xx} + \mathcal{M}_{yy}|^2 - \frac{1}{2} |\mathcal{M}_{xy} - \mathcal{M}_{yx}|^2, \\
F_3 &= -|\mathcal{M}_{xx}|^2 - |\mathcal{M}_{xy}|^2 + |\mathcal{M}_{yx}|^2 + |\mathcal{M}_{yy}|^2, \\
F_3' &= -|\mathcal{M}_{xx}|^2 + |\mathcal{M}_{xy}|^2 - |\mathcal{M}_{yx}|^2 + |\mathcal{M}_{yy}|^2, \\
F_4 &= \frac{1}{2} |\mathcal{M}_{xx} - \mathcal{M}_{yy}|^2 - \frac{1}{2} |\mathcal{M}_{xy} + \mathcal{M}_{yx}|^2,
\end{aligned} \tag{2.15}$$

from which one can infer the bound: $F_{2,3,4}^{(\prime)} \leq F_1$. Although one cannot extract one TMD independently of another one in a gluon-fusion process since the two always come together inside a convolution, it is possible to extract TMD convolutions using a model for the TMDs as we will see in the next chapters. The convolutions then give information on the TMDs, although the model-dependence remains. In order to isolate one type of convolution, it is useful to define the observables:

$$\langle \cos(n\phi_{CS}) \rangle = \frac{\int d\phi_{CS} \cos(n\phi_{CS}) d\sigma}{\int d\phi_{CS} d\sigma}. \tag{2.16}$$

When one computes the ϕ_{CS} -integrals for $n = 0, 2, 4$, one gets:

$$\begin{aligned}
n = 0 & : \int_0^{2\pi} d\phi_{\text{CS}} d\sigma = 2\pi A \left(F_1 \mathcal{C}[f_1^g f_1^g] + F_2 \mathcal{C}[w_2 h_1^{\perp g} h_1^{\perp g}] \right), \\
n = 2 & : \int_0^{2\pi} d\phi_{\text{CS}} \cos(2\phi_{\text{CS}}) d\sigma = \pi A \left(F_3 \mathcal{C}[w_3 f_1^g h_1^{\perp g}] + F_3' \mathcal{C}[w_3' h_1^{\perp g} f_1^g] \right), \\
n = 4 & : \int_0^{2\pi} d\phi_{\text{CS}} \cos(4\phi_{\text{CS}}) d\sigma = \pi A F_4 \mathcal{C}[w_4 h_1^{\perp g} h_1^{\perp g}], \tag{2.17}
\end{aligned}$$

where A is a common pre-factor from the expression of the differential cross section under consideration that cancels in the ratio of $\langle \cos(n\phi_{\text{CS}}) \rangle$. The integral selects the contributions associated with one type of ϕ_{CS} -(in)dependence, and the observable $\langle \cos(n\phi_{\text{CS}}) \rangle$ for $n = 2, 4$ becomes:

$$\begin{aligned}
\langle \cos(2\phi_{\text{CS}}) \rangle &= \frac{1}{2} \frac{F_3 \mathcal{C}[w_3 f_1^g h_1^{\perp g}] + F_3' \mathcal{C}[w_3' h_1^{\perp g} f_1^g]}{F_1 \mathcal{C}[f_1^g f_1^g] + F_2 \mathcal{C}[w_2 h_1^{\perp g} h_1^{\perp g}]}, \\
\langle \cos(4\phi_{\text{CS}}) \rangle &= \frac{1}{2} \frac{F_4 \mathcal{C}[w_4 h_1^{\perp g} h_1^{\perp g}]}{F_1 \mathcal{C}[f_1^g f_1^g] + F_2 \mathcal{C}[w_2 h_1^{\perp g} h_1^{\perp g}]}. \tag{2.18}
\end{aligned}$$

Therefore one sees that $\langle \cos(2, 4\phi_{\text{CS}}) \rangle$ corresponds to the relative size of the $\cos(2, 4\phi_{\text{CS}})$ -modulations of the cross section with respect to the azimuthally invariant component, up to a factor $1/2$. On the other hand, when one integrates the cross section over the azimuthal angle, the azimuthal asymmetries vanish and one is left with the transverse-momentum spectrum that is dependent on the two first terms of Eq. (2.5). It is understood that an integral on $\langle \cos(n\phi_{\text{CS}}) \rangle$ corresponds to integrating the numerator and denominator separately.

Similarly to the collinear case, including initial-state radiations inside the TMD definitions is necessary and implies a dependence on the renormalisation scale μ . However, the TMD correlators suffers the presence of extra divergences that need to be removed. This makes the evolution of TMDs fundamentally different from that of PDFs, which is the topic of our next section.

2.3 Evolution in the TMD formalism

It was shown in [43] that distributions unintegrated over all partonic transverse momenta present divergences when the gauge links entering their definition were taken along a lightcone direction. The divergence arises from gluon contributions with infinite negative rapidity, *i.e.* zero “+” momentum. As such, they are different from collinear divergences. A solution to remove these divergences is to set the gauge links slightly off

the lightcone ($n^- \neq 0$), which is equivalent to introducing a cut-off parameter ζ on the gluon rapidity. The value of the cut-off sets the shift of the gauge link: $\zeta^2 = (2P \cdot n)^2 / n^2$ so that gluons with rapidity y_n larger than $\ln n^+ / n^-$ are excluded from the distribution [44]. The TMD therefore undergoes evolution with the rapidity scale ζ .

Implementing evolution in TMDs is more easily done in b_T -space, where convolutions become simple products. We will start by defining TMDs in b_T -space and compute the corresponding convolutions, before giving the evolution equations they follow and the solutions and prescriptions that will be used for phenomenological study.

2.3.1 TMD convolutions in b_T -space

The definition for the Fourier-transformed TMDs over the transverse components are the following:

$$\begin{aligned} \tilde{f}_1^g(x, \mathbf{b}_T^2; \zeta, \mu) &= \int d^2 \mathbf{k}_T e^{-i \mathbf{b}_T \cdot \mathbf{k}_T} f_1^g(x, \mathbf{k}_T^2; \zeta, \mu), \\ \tilde{h}_1^{\perp g}(x, \mathbf{b}_T^2; \zeta, \mu) &= \int d^2 \mathbf{k}_T \frac{(\mathbf{b}_T \cdot \mathbf{k}_T)^2 - \frac{1}{2} \mathbf{b}_T^2 \mathbf{k}_T^2}{\mathbf{b}_T^2 M_p^2} e^{-i \mathbf{b}_T \cdot \mathbf{k}_T} h_1^{\perp g}(x, \mathbf{k}_T^2; \zeta, \mu), \end{aligned} \quad (2.19)$$

Let us note that the quantity $\tilde{h}_1^{\perp g}$ is not exactly the Fourier transform of $h_1^{\perp g}$, as we see a transverse weight included in the integral. The function defined here is actually proportional to the second \mathbf{b}_T^2 -derivative of the Fourier transform of $h_1^{\perp g}$. It is more practical to take this definition as it will actually always be the one appearing inside the convolutions, which simplifies the expressions while still allowing us to connect it to its momentum-space analogue. Computing the various convolutions from Eq. (2.5) with the corresponding TMDs and weights of Eq. (2.7) yields the expressions:

$$\begin{aligned} \mathcal{C}[f_1^g f_1^g] &= \int_0^\infty \frac{db_T}{2\pi} b_T J_0(b_T q_T) \tilde{f}_1^g(x_1, b_T^2; \zeta_1, \mu) \tilde{f}_1^g(x_2, b_T^2; \zeta_2, \mu), \\ \mathcal{C}[w_2 h_1^{\perp g} h_1^{\perp g}] &= \int_0^\infty \frac{db_T}{2\pi} b_T J_0(b_T q_T) \tilde{h}_1^{\perp g}(x_1, b_T^2; \zeta_1, \mu) \tilde{h}_1^{\perp g}(x_2, b_T^2; \zeta_2, \mu), \\ \mathcal{C}[w_3 f_1^g h_1^{\perp g}] &= \int_0^\infty \frac{db_T}{2\pi} b_T J_2(b_T q_T) \tilde{f}_1^g(x_1, b_T^2; \zeta_1, \mu) \tilde{h}_1^{\perp g}(x_2, b_T^2; \zeta_2, \mu), \\ \mathcal{C}[w_4 h_1^{\perp g} h_1^{\perp g}] &= \int_0^\infty \frac{db_T}{2\pi} b_T J_4(b_T q_T) \tilde{h}_1^{\perp g}(x_1, b_T^2; \zeta_1, \mu) \tilde{h}_1^{\perp g}(x_2, b_T^2; \zeta_2, \mu). \end{aligned} \quad (2.20)$$

We omitted the convolution $\mathcal{C}[w_3' h_1^{\perp g} f_1^g]$ as it is equal to $\mathcal{C}[w_3 f_1^g h_1^{\perp g}]$ under an exchange of the gluon momentum fractions. We see that the convolutions take a rather simple form, where the TMDs multiply each other inside the integral, without the presence of transverse weights that are absorbed in the definition of $\tilde{h}_1^{\perp g}$. The angular structure of

the convolutions is only reflected in a $J_n(b_T q_T)$ function that is a Bessel function of the first kind. Convolutions that are not associated with azimuthal modulations contain J_0 , while the $\cos(n\phi_{CS})$ -modulations have convolutions with J_n for $n = 2, 4$. We provide a demonstration of the fourth line of Eq. (2.20) in Appendix B as an example. Let us recall that Fourier-transformed TMDs are not impact-parameter distributions: the argument b_T does not represent the position of the parton in the transverse plane but a separation between the two gluon fields in the operator definition, much like η_T in Section 2.1. Now that we have defined the TMDs and their convolutions in b_T -space, we are going to use their evolution equations to evaluate them at different scales. This will allow us to get rid of possibly large logarithms arising from perturbative corrections and focus on the exclusively nonperturbative component of TMDs.

2.3.2 The scale dependence of TMDs

A correct definition of TMDs that is free of the aforementioned divergences can be found in [45]. In this definition, each TMD entering a two-parton scattering absorbs a square root of a combinations soft factor. One obtains the Collins-Soper-Sterman (CSS) equation by differentiating the soft factors that use Wilson lines of rapidity y_n with respect to y_n :

$$\frac{\partial \ln \tilde{f}(x, b_T; \zeta, \mu)}{\partial \ln \sqrt{\zeta}} = \tilde{K}(b_T; \mu). \quad (2.21)$$

The CSS kernel \tilde{K} can be perturbatively computed at large energy scales, which correspond to small distances b_T . This kernel is universal: it is flavour- and spin-independent for all quarks, and does not depend on the longitudinal momentum fraction x or the considered hadron. It is different for quarks and gluons as it depends on the colour representation of the considered parton. As \tilde{K} varies with the renormalisation scale μ , one can write the RGE:

$$\frac{d\tilde{K}(b_T; \mu)}{d \ln \mu} = -\gamma_K(\alpha_s(\mu)). \quad (2.22)$$

In addition, we write the RGE for the TMD itself:

$$\frac{\partial \ln \tilde{f}(x, b_T; \zeta, \mu)}{\partial \ln \mu} = \gamma(\alpha_s(\mu); \zeta/\mu^2) = \gamma(\alpha_s(\mu); 1) - \frac{1}{2} \gamma_K(\alpha_s(\mu)) \ln \frac{\zeta}{\mu^2}, \quad (2.23)$$

where the second equality can be obtained using the previous equations. One can use these equations to express the Fourier-transformed TMD at one scale set (ζ, μ) as product of its equivalent at a different scale (ζ_0, μ_0) and a Sudakov factor $e^{-1/2 S_A(b_T; \zeta, \zeta_0, \mu)}$ which reads:

$$S_A(b_T; \zeta, \zeta_0, \mu, \mu_0) = 2\tilde{K}(b_T; \mu_0^2) \ln \frac{\zeta}{\zeta_0} + 2 \int_{\mu_0}^{\mu} \frac{d\bar{\mu}}{\bar{\mu}} \left[\gamma_K(\alpha_s(\bar{\mu})) \ln \frac{\zeta}{\bar{\mu}^2} + \gamma(\alpha_s(\bar{\mu})) \right]. \quad (2.24)$$

While the renormalisation scale μ should be set around the hard scale $\mu \sim Q$ in order to avoid large logarithms of μ/Q , the TMDs should be evaluated at their natural scale $\sqrt{\zeta_0} \sim \mu_0 \ll \mu, \zeta$ (one gets $\zeta_1 \zeta_2 \sim Q^4$ from their definition). This allows one to avoid large logarithms of μ/μ_0 and ζ/ζ_0 . We will set the large scales to be the hard scale: $\sqrt{\zeta}, \mu = Q$ while the low scales will be $\sqrt{\zeta_0}, \mu = \mu_b = b_0/b_T$ with $b_0 = 2e^{-\gamma_E}$. The Sudakov factor resums the logarithms and allows one to evolve the TMDs between from one scale to another.

2.3.3 Organising the perturbative and nonperturbative content of the TMD

The TMD scale μ_b should be much smaller than the hard scale Q , but it is also interesting to keep it in the intermediate range where it is also sufficiently larger than the nonperturbative scale Λ . In this area, TMD factorisation remains valid but the scale is still large enough to allow for a perturbative expansion of the Sudakov factor and the TMDs themselves. Computing the leading terms in the α_s -expansion of \tilde{K} , γ and γ_K , one gets at next-to-leading logarithmic accuracy (NLLA):

$$S_A(b_T; \zeta, \mu) = 2 \frac{C_A}{\pi} \int_{\mu_b}^{\mu} \frac{d\bar{\mu}}{\bar{\mu}} \ln \left(\frac{\zeta}{\bar{\mu}^2} \right) \left[\alpha_s(\bar{\mu}^2) + \frac{67 - 3\pi^2 - 20T_f n_f}{9} \frac{\alpha_s^2(\bar{\mu}^2)}{4\pi} \right] + 2 \frac{C_A}{\pi} \int_{\mu_b}^{\mu} \frac{d\bar{\mu}}{\bar{\mu}} \alpha_s(\bar{\mu}^2) \left[-\frac{11 - 2n_f/C_A}{6} \right], \quad (2.25)$$

with $C_A = 3$, $T_f = 1/2$ and n_f the number of active flavours. The unpolarised gluon TMD f_1^g at leading order in α_s is the gluon collinear PDF:

$$\tilde{f}_1^g(x, b_T^2; \zeta, \mu) = f_{g/P}(x; \mu) + \mathcal{O}(\alpha_s) + \mathcal{O}(b_T \Lambda). \quad (2.26)$$

On the other hand, $h_1^{\perp g}$ requires a helicity flip and therefore an additional gluon exchange. Its perturbative expansion will therefore start at $\mathcal{O}(\alpha_s)$ as a sum of splitting functions from both quarks and gluons [46]:

$$\tilde{h}_1^{\perp g}(x, b_T^2; \zeta, \mu) = -\frac{\alpha_s(\mu)}{\pi} \int_x^1 \frac{d\hat{x}}{\hat{x}} \left(\frac{\hat{x}}{x} - 1 \right) \left(C_A f_{g/P}(\hat{x}; \mu) + C_F \sum_{i=q, \bar{q}} f_{i/P}(\hat{x}; \mu) \right) + \mathcal{O}(\alpha_s^2) + \mathcal{O}(b_T \Lambda), \quad (2.27)$$

As said previously, these expressions are only valid within a given range of b_T (or equivalently μ_b): at large b_T , the perturbative expansion in α_s fails while at small b_T , the scale μ_b becomes larger than the hard scale where the evolution should stop. There are many methods to restrict the use of the perturbative expressions to their domain of validity [47].

A common prescription is the following [29]:

$$b_T^*(b_c(b_T)) = \frac{b_c(b_T)}{\sqrt{1 + \left(\frac{b_c(b_T)}{b_{T\max}}\right)^2}} \quad \text{where} \quad b_c(b_T) = \sqrt{b_T^2 + \left(\frac{b_0}{Q}\right)^2}, \quad (2.28)$$

where

$$b_c(b_T) = \sqrt{b_T^2 + \left(\frac{b_0}{Q}\right)^2}. \quad (2.29)$$

$b_c(b_T)$ has a lower bound b_0/Q such that μ_b remains lower than the hard scale Q . Then b_T^* , in addition to inheriting the lower bound of b_c , cannot get larger than a parameter $b_{T\max}$. This parameter roughly sets the limit at which one cannot trust perturbative computations anymore. The value of $b_{T\max}$ can be chosen to optimise fits of TMDs. Fits from Drell-Yan as well as W, Z production use the value $b_{T\max} = 1.5 \text{ GeV}^{-1}$ [48, 49, 50, 47, 51]. Naturally since we limit the range of our expressions to $b_T < b_{T\max}$, one needs to add a component that takes over as the b_T -integrals of TMD convolutions run to infinity. This component is intrinsically nonperturbative and can only be extracted from data. It is usually called a nonperturbative Sudakov factor and encodes the discrepancy between the perturbative expansion of TMDs inside a cross section and their actual value. If one takes all the elements developed in this section to rewrite the TMD convolutions including the nonperturbative Sudakov factor S_{NP} , they read:

$$\begin{aligned} \mathcal{C}[f_1^g f_1^g] &= \int_0^\infty \frac{db_T}{2\pi} b_T J_0(b_T q_T) e^{-S_A(b_T^*; Q^2, Q)} e^{-S_{\text{NP}}(b_c)} \\ &\quad \times \tilde{f}_1^g(x_1, b_T^{*2}; \mu_b^2, \mu_b) \tilde{f}_1^g(x_2, b_T^{*2}; \mu_b^2, \mu_b), \\ \mathcal{C}[w_2 h_1^{\perp g} h_1^{\perp g}] &= \int_0^\infty \frac{db_T}{2\pi} b_T J_0(b_T q_T) e^{-S_A(b_T^*; Q^2, Q)} e^{-S_{\text{NP}}(b_c)} \\ &\quad \times \tilde{h}_1^{\perp g}(x_1, b_T^{*2}; \mu_b^2, \mu_b) \tilde{h}_1^{\perp g}(x_2, b_T^{*2}; \mu_b^2, \mu_b), \\ \mathcal{C}[w_3 f_1^g h_1^{\perp g}] &= \int_0^\infty \frac{db_T}{2\pi} b_T J_2(b_T q_T) e^{-S_A(b_T^*; Q^2, Q)} e^{-S_{\text{NP}}(b_c)} \\ &\quad \times \tilde{f}_1^g(x_1, b_T^{*2}; \mu_b^2, \mu_b) \tilde{h}_1^{\perp g}(x_2, b_T^{*2}; \mu_b^2, \mu_b), \\ \mathcal{C}[w_4 h_1^{\perp g} h_1^{\perp g}] &= \int_0^\infty \frac{db_T}{2\pi} b_T J_4(b_T q_T) e^{-S_A(b_T^*; Q^2, Q)} e^{-S_{\text{NP}}(b_c)} \\ &\quad \times \tilde{h}_1^{\perp g}(x_1, b_T^{*2}; \mu_b^2, \mu_b) \tilde{h}_1^{\perp g}(x_2, b_T^{*2}; \mu_b^2, \mu_b). \end{aligned} \quad (2.30)$$

We see that the b_T^* -prescription that encompasses the b_c -prescription is applied to the perturbative Sudakov factor and the TMDs, while only the b_c -prescription is applied to the nonperturbative Sudakov factor, as the latter is supposedly describing physics beyond $b_{T\max}$. Let us note that since S_{NP} describes intrinsic nonperturbative physics

of the TMDs, it is in general different for different combinations of two TMDs. For example the S_{NP} that may be extracted from $\mathcal{C}[f_1^g f_1^g]$ is expected to be different from the one extracted from $\mathcal{C}[w_A h_1^{\perp g} h_1^{\perp g}]$, although the CSS formalism tells us that part of it should be universal. Usual constraints are that S_{NP} should be zero at small scales where the perturbative computations are valid, and should eventually (smoothly) vanish at large distances in order for the convolutions to converge. In addition to the model chosen, S_{NP} naturally depends on the prescriptions used to separate the perturbative and nonperturbative components inside the convolution.

While quite elaborate fits of S_{NP} are available for quarks [50], no data are available at the moment to realise a proper extraction of gluon TMDs. Although gluon densities are very important in protons at the LHC, there is no process that allows to access the gluon TMDs as easily as the quark ones. In the first place, only a handful of processes exist for which a proof of TMD factorisation could clearly be established that are in majority quark-induced. Therefore one needs to find new processes where TMD factorisation could reasonably be expected to hold, in order to give us access to new observables that would allow in particular to study the gluon TMDs. As we will see in the next chapters, quarkonium production processes could be the way to extract these TMDs, as such reactions can be very promising tools regarding the conditions required for TMD factorisation to be valid.

Chapter 3

Quarkonium production

The era of quarkonium physics starts in 1974, when two groups simultaneously discover a new particle of mass approximately equal to 3.1 GeV: the J/ψ , whose signal was observed in e^+e^- collisions for one team and in p -*nucleus* collisions for the other [52, 53]. This was the so-called "November revolution". A slightly heavier resonance called ψ' was also detected that would be understood to be an excited state of the J/ψ (the former is also named $\psi(2S)$). Their quantum numbers were $J^{PC} = 1^{--}$ so the same as the photon. Their hadronic nature was showed first through the ratio $R = \sigma(e^+e^- \rightarrow \text{hadrons}) / \sigma(e^+e^- \rightarrow \mu^+\mu^-)$ that was higher at the resonance, meaning that these particles were directly decaying into hadrons. Particles with charge conjugation $C \neq -1$ were found later (firstly the χ_c in 1975 [54]) as their production in e^+e^- collisions happened through the decay of a $\psi(3S)$ (or ψ'') state. It became clear that the J/ψ was the lowest-mass $c\bar{c}$ bound state with the quantum numbers of the photon, allowing it to be easily produced in e^+e^- colliders by fragmentation of a virtual photon into a quark pair. The analogy with a bound pair e^+e^- , that is a positronium, had physicists call a $c\bar{c}$ state a *charmonium*. This was a milestone in the confirmation of the existence of quarks as physical entities and not only mathematical objects used to describe symmetries in hadrons. Although the charm in charmonia was hidden, the discovery of D mesons in 1976 [55], that have open charm and undergo P -violating decays where the charm weakly decays, only confirmed further its existence [56]. The years following the November revolution saw the discovery of several heavy hadrons and the proof of existence of the charm quark.

However, more hadrons were to be discovered. The discovery of the Υ meson that is the equivalent of the J/ψ with bottom (or beauty) quarks was made in 1977 [57]. This was again followed by the discovery of excited states of Υ (right after for the $\Upsilon(2S)$ and other bottomonia, as well as open beauty mesons in 1980 [58]). Tables 3.1 and 3.2 summarise the characteristics of the main charmonia and bottomonia that have been observed.

In this chapter we will explore the vast topic that is quarkonium production. We will see how various production mechanisms can (or cannot) be employed to describe the large amount of quarkonium data. Indeed, quarkonia are, in theory, the simplest hadronic

Meson	$n^{2S+1}L_J$	J^{PC}	Mass (GeV)
η_c	1^1S_0	0^{-+}	2.980
J/ψ	1^3S_1	1^{--}	3.097
$\chi_{c0,1,2}$	$1^3P_{0,1,2}$	$0^{++}, 1^{++}, 2^{++}$	3.415, 3.511, 3.556
h_c	1^1P_0	1^{+-}	3.523
$\eta_c(2S)$	2^1S_0	0^{-+}	3.594
$\psi(2S)$	2^3S_1	1^{--}	3.686

Table 3.1: Charmonium states and their characteristics

Meson	$n^{2S+1}L_J$	J^{PC}	Mass (GeV)
η_b	1^1S_0	0^{-+}	9.389
$\Upsilon(1S)$	1^3S_1	1^{--}	9.460
$\chi_{b0,1,2}(1P)$	$1^3P_{0,1,2}$	$0^{++}, 1^{++}, 2^{++}$	9.860, 9.893, 9.913
$\Upsilon(2S)$	2^3S_1	1^{--}	10.023
$\chi_{b0,1,2}(2P)$	$2^3P_{0,1,2}$	$0^{++}, 1^{++}, 2^{++}$	10.232, 10.255, 10.269
$\Upsilon(3S)$	3^3S_1	1^{--}	10.355
$\chi_{b1,2}(3P)$	$3^3P_{1,2}$	$1^{++}, 2^{++}$	10.513, 10.524

Table 3.2: Bottomonium states and their characteristics

bound states that can exist, owing to their nonrelativistic nature as we will see soon. Nevertheless, their production remains very challenging to describe. Much progress has been made but many features of the data are left unexplained. We will first describe the main models used to describe quarkonium production. We will then see how well they can describe data for inclusive quarkonium production. We will finally consider the specific case of polarised quarkonium production, and how the models so far failed to account for the production rates observed in the colliders.

3.1 Production mechanisms

Models attempting to depict quarkonium production in hadronic collisions usually use factorisation to divide the production process into a short-scale partonic scattering, leading to the creation of a $Q\bar{Q}$ pair and computable in perturbative QCD, from the long-scale evolution towards a bound state, that is the quarkonium. The latter can be described by a mechanism specific to the model. The motivation behind the idea of scale separation between the hard scattering and the hadronisation can be found in the study of the charmonium spectroscopy. Indeed, as showed in Tables 3.1 and 3.2, the observed bound states

of $c\bar{c}$, $b\bar{b}$ can be classified using nonrelativistic-quantum-mechanics numbers and their masses can be computed with good agreement with the data using a Coulombic potential completed with a confinement term [59, 60]. The possibility to use a nonrelativistic potential and the fact that the mass of the mesons are close to that of their constituent quarks indicates that the bound state can be represented as a $c\bar{c}$ pair with small relative velocity $v^2 \ll 1$. Moreover, since the coupling constant remains small, any extra colour exchange is α_s -suppressed. One can therefore assume in first approximation that the quark pair does not undergo any additional interaction before binding, and thus has the same quantum number as the charmonium it forms. Originating from these considerations, the Colour-Singlet Model (CSM) is one of the earliest attempts at describing the quarkonium hadronisation process, initially for η_c and χ_c production [61]. It corresponds to an on-shell $Q\bar{Q}$ pair binding without any additional final-state interaction. This implies that the spin and colour of the quark do not change during the process. As the final physical state must be colourless, the pair is required to be created in a colour-singlet state, hence the name of the model. Moreover, quarkonia masses are not much larger than the $Q\bar{Q}$ mass; this means the quarks inside the bound state have a small relative momentum δq and are approximated to be *at rest* in the meson frame, ($\delta q = 0$). The only nonperturbative component entering the computation of the production amplitude is then the Schrödinger wave function at the origin. The amplitude to create the meson can be written as follows:

$$\mathcal{A} = \int \phi(\delta q) \mathcal{M}(\delta q) \delta(\delta q^0) d\delta q \approx \mathcal{M}(\delta q = 0) \psi(\mathbf{x} = 0), \quad (3.1)$$

with δq the relative momentum of the quark in the pair rest frame, $\phi(\delta q)$ contains the Schrödinger wave function and will be defined soon, \mathcal{M} is derived from the partonic scattering amplitude and $\psi(0)$ is the coordinate-space wave function at the origin. Note that this expression is valid for S-waves; in the case of P-waves, $\psi(0)$ is zero and the second term in the Taylor expansion of \mathcal{M} in δq must be taken, featuring $\psi'(0)$. Fortunately the wave function at the origin also appears in the computation of the leptonic decay width of the meson, and can therefore be independently extracted from measurements. This gives to the CSM a great predictive power, as the only non-computable input can be extracted from decay data.

The differential cross section for inclusive single quarkonium production $pp \rightarrow \mathcal{Q} + X$ in the collinear approximation has the form:

$$\frac{d\sigma}{dy dq_T} = \int_0^1 dx_1 dx_2 f_{g/P}(x_1, Q) f_{g/P}(x_2, Q) 2\hat{s} q_T \frac{1}{16\pi\hat{s}^2} \overline{|\mathcal{M}(k_1, k_2; q)|^2}, \quad (3.2)$$

where y is the rapidity of the quarkonium; $f_{g/P}(x, Q)$ is the collinear PDF of a gluon inside a proton, the scale Q is set as the hard scale of the process i.e. $Q = M_T = \sqrt{M^2 + q_T^2}$; the

parton-scattering amplitude \mathcal{M} is averaged over the initial colour states, and summed over the final colour and possible polarisation states if one intends to study unpolarised production. It can be expressed as follows:

$$\mathcal{M}(k_1, k_2; q) = \int \frac{d^4 \delta q}{(2\pi)^4} \text{Tr} [O(k_1, k_2; q, \delta q) \phi(q, \delta q)], \quad (3.3)$$

where O corresponds to the amplitude without the quark spinors involved in the quarkonium bound state. The amplitude can therefore be computed using amputated Feynman diagrams. The spinors are included in the Bethe-Salpeter wave function of the bound state $\phi(q, \delta q)$. Since $|\delta q|$ is small compared to the non-relativistic bound state mass M , one can expand the wave function the following way:

$$\phi(q, \delta q) \simeq 2\pi \delta(\delta q^0) \sum_{L_z, S_z} \psi_{LL_z}(\delta \mathbf{q}) \langle LL_z; SS_z | JJ_z \rangle P_{SS_z}(q, \delta q). \quad (3.4)$$

ψ_{LL_z} is the Schrödinger wave function, and the brackets are the relevant Clebsch-Gordan coefficients. P_{SS_z} is a spin projection operator:

$$\begin{aligned} P_{SS_z}(q, \delta q) &= \sum_{s, \bar{s}} \langle \frac{1}{2} s; \frac{1}{2} \bar{s} | SS_z \rangle u\left(\frac{1}{2} q + \delta q\right) \bar{v}\left(\frac{1}{2} q - \delta q\right) \\ &\simeq \frac{1}{4M^{3/2}} (\not{q} + 2\delta \not{\mathbf{q}} + M) \not{\epsilon}_{S_z}(q) (-\not{q} + 2\delta \not{\mathbf{q}} + M), \end{aligned} \quad (3.5)$$

whose leading term in the $\delta \mathbf{q}$ -expansion is given in the case of a triplet state (γ^5 replaces $\delta \not{\mathbf{q}}$ for a pseudoscalar state) and uses the Feynman slash notation: $\not{a} = a^\mu \gamma_\mu$. The vector ϵ_{S_z} denotes the polarisation vector of a triplet state. One can then fix $\delta q = 0$ inside of $O(k_1, k_2; q, \delta q)$ and $P_{SS_z}(q, \delta q)$, leaving the only dependence on δq in the wave function. Inserting (3.4) in (3.3) allows integrating over the δq^0 variable using the Dirac delta:

$$\begin{aligned} \mathcal{M}(k_1, k_2; q) &= \int \frac{d^3 \delta \mathbf{q}}{(2\pi)^3} \sum_{L_z, S_z} \psi_{LL_z}(\delta \mathbf{q}) \langle LL_z; SS_z | JJ_z \rangle \\ &\times \text{Tr} [O(k_1, k_2; q, 0) P_{SS_z}(q, 0)]. \end{aligned} \quad (3.6)$$

It is then justified to expand the latter expression in powers of $|\delta \mathbf{q}|$ and keep only the first non-vanishing term. For S-waves ($L = 0, S = J$), it is the static approximation $|\delta \mathbf{q}| = 0$. The integral over the three $\delta \mathbf{q}$ components identifies with the Fourier transform of $\psi_{00}(\delta \mathbf{q})$ at the origin:

$$\int \frac{d^3 \delta \mathbf{q}}{(2\pi)^3} \psi_{00}(\delta \mathbf{q}) = \int \frac{d^3 \delta \mathbf{q}}{(2\pi)^3} e^{i\delta \mathbf{q} \cdot \mathbf{r}} \psi_{00}(\delta \mathbf{q}) \Big|_{\mathbf{r}=\mathbf{0}} = \tilde{\psi}_{00}(\mathbf{r} = \mathbf{0}), \quad (3.7)$$

whose modulus is directly proportional to that of the radial S-wave function at the origin in the coordinate space, $|R_0(0)|$:

$$|\tilde{\psi}_{00}(\mathbf{r} = \mathbf{0})| = \frac{1}{\sqrt{4\pi}} |R_0(0)|. \quad (3.8)$$

The amputated hard scattering matrix element O contains the following Clebsch-Gordan coefficients encoding the colour-singlet state of each $q\bar{q}$ pair:

$$\langle 3i; \bar{3}j | 1 \rangle = \frac{\delta_{ij}}{\sqrt{N_c}}. \quad (3.9)$$

The contraction of these Clebsch-Gordan coefficients with the SU(3) generators of the $q\bar{q}g$ vertices from the hard part result in a Kronecker delta δ_{ab} , with a and b the colours of the initial gluons. To summarise, the CSM uses a set of reasonable hypotheses to compute quarkonium-production processes. Although it describes the hadronisation of a quark-antiquark pair that is beyond the validity domain of perturbative QCD, it requires only one parameter that needs to be extracted from data. However, it cannot be applied to compute the P -wave quarkonium decay rates into light hadrons that know an infrared divergence in the CSM [62], hinting at a breaking of factorisation.

While the CSM only considers a $Q\bar{Q}$ pair with quantum numbers identical to that of the bound states it evolves into, it was proposed that higher Fock states, for example containing one gluon in addition to the pair, could cancel this IR divergence. In such a state, the $c\bar{c}$ pair is in a *colour-octet* state, that forms a colour singlet with the complementary gluon. In 1992, an effective field theory was proposed to improve the description of quarkonium production and annihilation. It proposes a systematic expansion of the physical quarkonium state in a sum of all possible Fock states. The terms are organised in the expansion by powers of α_s and the quark velocity $v = \delta q/m_Q$ in order to truncate the expansion at the desired accuracy. This EFT is called NonRelativistic QCD or NRQCD [63, 64, 65]. For example, the expansion of the wave function for a vector S -wave quarkonium state reads:

$$\begin{aligned} |\mathcal{Q}\rangle = & \mathcal{O}(1) |Q\bar{Q} [{}^3S_1^{(1)}]\rangle + \mathcal{O}(v) |Q\bar{Q} [{}^3P_J^{(8)}g]\rangle + \mathcal{O}(v^2) |Q\bar{Q} [{}^1S_0^{(8)}g]\rangle \\ & + \mathcal{O}(v^2) |Q\bar{Q} [{}^3S_1^{(1,8)}gg]\rangle + \mathcal{O}(v^2) |Q\bar{Q} [{}^3D_J^{(1,8)}gg]\rangle + \dots \end{aligned} \quad (3.10)$$

In this expression, the superscript number in parenthesis indicates the colour state of the quark pair, while the $\mathcal{O}(v^n)$ factor is the power in the velocity expansion at which the corresponding Fock state appears. It can be found following the velocity scaling rules of NRQCD. The α_s power of a term is deduced from the Feynman diagrams needed to produce the partons entering a given Fock state. Using this formalism, one can also factorise the cross section of a reaction into a sum of partonic cross sections creating a $Q\bar{Q}$ pair (and possibly other partons entering a Fock state) each multiplied by a Long-Distance Matrix Element (LDME) containing the transition toward the physical quarkonium state:

$$d\sigma(\mathcal{Q} + X) = \sum_Q d\sigma(Q\bar{Q} [{}^{2S+1}L_J^{(1,8)}] + X) \langle \mathcal{O}^{\mathcal{Q}} [{}^{2S+1}L_J^{(1,8)}] \rangle, \quad (3.11)$$

where $d\sigma(Q\bar{Q}[^{2S+1}L_J^{(1,8)}] + X)$ is the partonic cross section and $\langle \mathcal{O}^{2S+1}L_J^{(1,8)} \rangle$ is the LDME. The latter is defined in terms of operators as the creation and annihilation of a quark-antiquark pair in the required state:

$$\begin{aligned} \mathcal{O}^{2S+1}L_J^{(1,8)} &= \phi A \chi^\dagger \left(\sum_X \sum_{J_z} |\mathcal{Q} + X\rangle \langle Q + X| \right) \phi^\dagger A \chi \\ &= \phi A \chi^\dagger (a_{\mathcal{Q}}^\dagger a_{\mathcal{Q}}) \phi^\dagger A \chi, \end{aligned} \quad (3.12)$$

where ϕ and χ are the heavy-quark spinors and the A factors can be retrieved using the Lagrangian of NRQCD. The LDMEs can be visualised as describing the probability that a perturbatively-generated quark pair will evolve into the relevant physical state. The CSM that corresponds to the static approximation $v = 0$ is in fact the leading contribution to NRQCD, provided that this contribution is nonzero for the considered bound state.

NRQCD is a sound approach to take into account corrections to the static approximation in a way that allows one to select the most relevant contributions only. However it lacks the predictive power of the CSM as each term of the expansion is accompanied by a phenomenological factor that requires to be extracted from data and cannot be extracted from decay widths nor computed in lattice studies [66]. This does not mean that NRQCD has no predictive power as the LDMEs are supposed to be universal (in the sense independent from the partonic cross section they factorise) and their values, once measured, can thus be used in all the processes they enter. We will see in the following that there is some tension between this presumed universality and some data.

Another model was introduced in the early years of quarkonium physics in an attempt to describe their production: the Colour Evaporation Model (CEM) [67, 68]. This model does not postulate that the quark-antiquark pair is produced in a colour singlet state that directly hadronises without any additional interaction. The pair is instead assumed to undergo a large number of soft interactions that eventually produce a colour singlet that evolves into the physical bound state. Since these numerous random interactions completely decorrelate the quantum numbers of perturbatively produced partons from that of the pair forming the bound state, even a single gluon can evolve into a physical state, which is not allowed by colour conservation in the CSM. For example, the cross section to produce a charmonium in this picture is:

$$\sigma(\text{charmonium} + X) = \frac{1}{9} \int_{2m_c}^{2m_D} \frac{d\sigma(c\bar{c} + X)}{dm} dm. \quad (3.13)$$

One indeed sums the partonic cross section for the production of a $c\bar{c}$ pair from the threshold $2m_c$ to the production threshold of a pair of D mesons. Since the probability for a pair in a random state to be in a colour-singlet state is $1/9$, the cross section

is weighted by this probability. The model is limited by its simplicity, for example it cannot account for the difference between the production rates of J/ψ and χ_c mesons in photoproduction and hadroproduction.

Quarkonia may also be produced through the decay or de-excitation of heavier states. It was first noted that a significant fraction of ψ mesons could originate from the decay of B mesons [69]. This component of charmonium production is called *non-prompt* and actually encompasses all channels where the charmonium is created from the decay of a meson containing b quarks. Some experimental collaborations manage to isolate non-prompt charmonia by detecting the distance between the B creation vertex and its decay into a charmonium, allowing one to extract the *prompt* component. Within this prompt component, a charmonium may still be created via the decay or de-excitation of a heavier one, for example a J/ψ meson can come from the decay of a χ_c or the de-excitation of a ψ' . The fraction of quarkonia that are directly generated by a hard scattering and not the decay of a higher mass state is called the *direct* component. It is generally not possible to extract the direct component alone. J/ψ mesons created from χ_c decay require the detection of the de-excitation photon in order to be properly identified, which is possible but not systematically done. One must therefore keep in mind that quarkonium production data usually contain a non-direct fraction of events that need to be isolated. The case of bottomonium production is similar to the charmonium case except that all bottomonia are naturally prompt.

Now that we have seen what the main mechanisms considered to describe quarkonium production are, we will give a brief account of their capability to correctly predict various related cross sections, and how progress was made over the decades.

3.2 Explaining inclusive quarkonium production data

The CDF collaboration managed to extract the prompt component of J/ψ and ψ' production at the Tevatron [70]. It was discovered that the CSM predictions (using leading-order in α_s hard-scattering amplitudes) for ψ production were strongly undershooting the data. The ψ' predictions were several orders of magnitude lower than the data; the discrepancy was less pronounced for J/ψ , but this was likely due to the feed-down from χ_c decay that still contributes to prompt production [71]. The failure of the LO CSM to describe the CDF ψ data has triggered a lot of theoretical and experimental effort in order to solve this puzzle.

One of the most plausible explanation was logically contributions from coloured $Q\bar{Q}$ pairs that evolve toward a physical bound state through a different mechanism,

then label Colour-Octet Mechanism (COM). In particular, the fragmentation of a gluon into a $Q\bar{Q}$ pair emitting other gluons before hadronising was showed to be potentially dominant at large transverse momentum, despite being an order higher in α_s [72]. The authors of [73] show that including CO corrections allows them to describe properly the $Y(1,2,3S)$ q_T -differential cross sections from CDF data [74]. However, global fits to world J/ψ data give different values for the LDMEs, and it remains very difficult to describe all data with one set of values [75, 76, 77].

On the other hand, the CDF and ATLAS ψ' transverse-momentum-spectrum data [70, 78, 79] can be reasonably well described within the CSM by adding higher-order corrections in α_s to the LO computation (NNLO^{*}, i.e. NLO + real gluon emissions). We note that a gap between the predictions and the data opens with increasing p_T . NNLO^{*} also significantly reduce the discrepancy between theory and data in the case of Y production [80].

One should then be very careful when assessing which mechanism dominates the production, as it seems to be strongly process-, fit- and kinematics-dependent. Reviews on the topic allow one to grasp the complexity of the topic and the need to treat each process separately [81, 82, 66].

Even though the various quarkonium production mechanisms can usually manage to describe the available cross-section data when adding relevant corrections, they mostly fail in describing the quarkonium polarisation measurements. Let us start with some reminders about polarised production and polarisation measurements. The spin of a final-state particle cannot be directly measured. In the case of an unstable particle, one can infer information about its spin state from the angular distribution of its decay products. This information is in most cases greatly truncated, as it can be strongly correlated with other particles generated in the final state that are not measured. Furthermore, in the case of hadronic collisions, the momenta of the interacting partons are not known and therefore integrated over all possible values, diluting even more the information. In the case of a two-body decay, one can observe the polar angle θ of the aligned momenta of the pair regarding a given axis in the unstable particle rest frame. By using the Spin-Quantisation Axis (SQA) of the unstable particle as reference axis, the distribution becomes directly correlated to the probabilities for the projection of the possible spin states along the axis.

In the case of a vector quarkonium decaying into a pair of leptons, one can compute the trace associated with the process $Q\bar{Q} \rightarrow \gamma^* \rightarrow l^+l^-$ contracted with different polarisations of the initial quarkonium. For a population of exclusively longitudinally polarised quarkonia, the θ -distribution of the dilepton momenta follows $1 - \cos^2 \theta$; while in the case of transversely polarised quarkonia the distribution behaves as $1 + \cos^2 \theta$.

For a chosen spin-quantisation axis X , one requires the polarisation vectors to be orthogonal to the momentum of the quarkonium: $\varepsilon \cdot q = 0$, and to be normalised: $\varepsilon^2 = -1$. Since the longitudinal polarisation 3-vector ε_L is parallel to the SQA, one can build it by projecting X on the plane orthogonal to q and then normalising it [83]:

$$\tilde{X}^\mu = \left(-g^{\mu\nu} + \frac{q^\mu q^\nu}{q^2} \right) X^\nu, \quad \varepsilon_L^\mu = \frac{\tilde{X}^\mu}{\sqrt{-\tilde{X}^2}}. \quad (3.14)$$

The SQA is usually chosen to lie in the plane formed by the momenta of the two initial colliding particles. In the gCM frame, the SQA is the sum of the momenta of the gluons: $X_{gCM}^\mu = k_1^\mu + k_2^\mu$. The projection of the spin of one quarkonium over this axis corresponds to its helicity in the gluons centre-of-mass frame. The resulting longitudinal polarisation 3-vector $\varepsilon_L(q_i)$ is parallel to the momentum q_i in this frame. The hCM frame presents the same properties in the hadrons centre-of-mass frame: the SQA is defined as the sum of the protons momenta $X_{hCM}^\mu = P_1^\mu + P_2^\mu$. The SQA in the Collins-Soper (CS) frame is defined as the bisector between \mathbf{P}_1 and $-\mathbf{P}_2$ in the quarkonium rest frame. The SQA is defined as: $X_{CS}^\mu(q) = \frac{P_1^\mu}{q \cdot P_1} - \frac{P_2^\mu}{q \cdot P_2}$.

In order to compute the unpolarised cross section, one can sum over the quarkonium polarisations and contract the resulting tensor with the squared amplitude:

$$\sum_\lambda \varepsilon_\lambda^\mu(q) \varepsilon_\lambda^\nu(q) = -g^{\mu\nu} + \frac{q^\mu q^\nu}{M^2}. \quad (3.15)$$

The general trend is that, where the theory predicts important polarisation of the produced quarkonium, the experiments measure little to no polarisation. Possible explanations are that the truncations in the double expansion in α_s and ν of the NRQCD factorisation are too restrictive. For example, LO and NLO computations in the CSM predict drastically different polarisations for either J/ψ or Y production [84, 85]. Nevertheless, all of these computations predict strong polarisation of the quarkonium, while the experiment finds values of the polarisation estimator compatible with 0. However, it could also be that factorisation breaks down in some cases where it was primarily expected to hold. Improving the accuracy of predictions for the usual processes also becomes more and more challenging: higher-order in α_s computations may stay out of reach for a long time, and more LDMEs need to be extracted to improve the ν -expansion; worse, LDME values extracted from different processes can be contradictory [86, 87, 88]. Furthermore it seems impossible to make separate polarisation measurements of the direct and non-direct production components, only the prompt one is accessible. The feed-down from heavier states contributes to modify the measured polarisation in

experimental setups.

In this chapter we had an overview of quarkonium production. We described the three main models used to reproduce data, the CSM, the CEM and the COM implemented via the effective theory NRQCD that uses a double expansion in α_s and v . One can factorise the hard scattering from the hadronisation process, allowing the use of an α_s -expansion as well for the former. Describing quarkonium production data has proved to be challenging, as the dominant mechanism is strongly dependent on the process and kinematics under consideration. The ψ' production puzzle found potential answers on the theoretical side with CO and NLO-NNLO corrections. While such corrections can be used to describe specific observables, a global description of the world quarkonium production datasets remains missing. Quarkonium production can be a tool to study other aspects of the strong interaction, provided that the dominant mechanisms for the considered process and kinematics are known. We will see in the next chapter how it can be used to study the gluon TMDs in pp collisions. In addition to single-quarkonium production, we will consider the case of associated production, with a specific focus on quarkonium pair production at the LHC.

Chapter 4

Quarkonia as probes of the gluon TMDs

As can be inferred from Fig. 1.7, reactions inside (anti)proton-proton colliders are initiated by gluon fusion in vast majority. Even processes for which the α_s expansion favours quark-initiated contributions may actually be dominated by higher-order gluon contributions due to the magnitude of the gluon PDF at the considered energies. This is an advantage that can be exploited to study the gluon TMDs inside the proton with negligible quark contributions that would complicate the analysis. The large centre-of-mass energies and luminosities that can be reached in these colliders ensure a large number of events and allow one to study rare processes of interest. The downside is that the large number and variety of produced particles make it hard to isolate the events one is interested in. Lepton collisions are more suited for precision measurements, as the relative simplicity of the electromagnetic interaction implies reactions with lower multiplicity. It also makes processes like DIS, SIDIS or Drell-Yan ideal probes of the proton as the leptons that carry information about the proton structure are not subjected to any additional interactions before or after the hard scattering. Nevertheless, we saw in the previous chapter that quarkonia, which can be considered as the simplest hadrons existing, are an interesting tool for the study of the strong interaction. As said in Chapter 3, their production mechanisms are still subject to debate and a unified description of all the accumulated data remains missing. Yet models are usually able to describe specific datasets related to quarkonium production, at least when considering unpolarised production. Moreover some quarkonia, like the J/ψ , are produced in copious amounts in hadron accelerators. It was then natural that physicists got interested in using them as probes of the proton structure. In this chapter, we will present the main processes that have been considered for the study of the gluon TMDs, mostly at the LHC. We will then focus on quarkonium-pair production and especially J/ψ and Υ production, and will discuss about their potential as probes of the gluon TMDs inside unpolarised protons. We will finally try to draw a picture of the advantages and drawbacks of such processes for this purpose.



Figure 4.1: LO Feynman diagrams for (pseudo)scalar quarkonium production from gluon fusion.

4.1 Processes of interest for the study of the gluon TMDs

The simplest gluon-fusion initiated process one can think of is the creation of a single (pseudo)scalar meson in a $2 \rightarrow 1$ process such as the $\eta_{c,b}$ or the $\chi_{c0,b0}$ ($J^{PC} = 0^{\pm+}$). Such a process is at order α_s^2 at LO as it does not require any extra gluon emission (cf. Fig. 4.1). The kinematics are very simple, NLO corrections are not expected to be large (they can be found for example in [89]). Colour-octet contributions are suppressed by a power of v^4 [90] in the $\eta_{c,b}$ case.

In the case of $\chi_{c,b}$ production, there is a colour-octet contribution of same order in v as the colour-singlet one, but it is suppressed by a $2N_c$ factor. Single vector quarkonium production such as J/ψ , Υ or $\chi_{c1,b1}$ production from on-shell gluon fusion are prohibited at leading order by C -parity in the CSM, they require at least an extra gluon emission. $\chi_{c2,b2}$ production is possible from two gluons. These processes have been studied in the frame of TMD factorisation in [91]. The transverse-momentum spectrum is sensitive to the two first terms of Eq. (2.5) and therefore to both gluon TMDs for unpolarised protons, f_1^g and $h_1^{\perp g}$. The formalism of the CSM developed in Chapter 3 is used to describe the hadronisation process, as in Eq. (3.5). The spin projection operator gives γ^5 instead of $\not{\epsilon}$ for a pseudoscalar meson in the case of $\eta_{c,b}$ production. We recall that in the case of P -wave production, one needs to take the second term of the expansion of the wave function in the relative momentum of the quarks, as the wave function itself is zero at the origin.

The cross sections for $\eta_{c,b}$, $\chi_{c0,b0}$ and $\chi_{c2,b2}$ in the LO CSM using TMD factorisation read [91]:

$$\begin{aligned} \frac{d\sigma(\eta_Q)}{dy d^2\mathbf{q}_T} &= \frac{1}{9} \frac{N_c \pi^2 \alpha_s^2}{M^3 \hat{s}} |R_0(0)|^2 \mathcal{C} [f_1^g(x_1, k_{1T}^2) f_1^g(x_2, k_{2T}^2)] [1 - R(\mathbf{q}_T^2)], \\ \frac{d\sigma(\chi_{Q0})}{dy d^2\mathbf{q}_T} &= 4 \frac{N_c \pi^2 \alpha_s^2}{M^5 \hat{s}} |R'_1(0)|^2 \mathcal{C} [f_1^g(x_1, k_{1T}^2) f_1^g(x_2, k_{2T}^2)] [1 + R(\mathbf{q}_T^2)], \end{aligned}$$

$$\frac{d\sigma(\chi_{Q2})}{dy d^2\mathbf{q}_T} = \frac{16}{3} \frac{N_c \pi^2 \alpha_s^2}{M^5 \hat{s}} |R'_1(0)|^2 \mathcal{C}[f_1^g(x_1, k_{1T}^2) f_1^g(x_2, k_{2T}^2)], \quad (4.1)$$

with the ratio $R = \mathcal{C}[w_2 h_1^{\perp g}(x_1, k_{1T}^2) h_1^{\perp g}(x_2, k_{2T}^2)] / \mathcal{C}[f_1^g(x_1, k_{1T}^2) f_1^g(x_2, k_{2T}^2)]$ where the transverse weight w_2 is defined as in Eq. (2.7). Comparing the features of the different reactions shows that, depending on the parity of the (pseudo)scalar meson under scrutiny, the effect of $h_1^{\perp g}$ on the transverse-momentum spectrum will change sign. Moreover, the case of χ_{Q2} production for which contributions from $h_1^{\perp g}$ are suppressed provides a way to compare the spectrum with and without the influence of $h_1^{\perp g}$. In particular, the $d\sigma(\chi_{Q0})/d\sigma(\chi_{Q2})$ ratio is simply equal to $\frac{3}{4}(1 + R(q_T^2))$, and is free of the uncertainty on f_1^g . In addition, the q_T -differential cross section normalised by the q_T -integrated one cancels out the LDME and the uncertainty affecting it. Let us note that the scalar case is very similar to Higgs production, which was also proposed to study gluon TMDs in a similar fashion (see *e.g.* [92]).

Quarkonium production processes dominated by the LO CSM contribution are good candidates for the application of TMD factorisation. The quarkonia do not recoil against any other particle, therefore their transverse momentum is small and find its origin in the intrinsic transverse momentum of the initial gluons, hinting at small factorisation-breaking corrections of order $\mathcal{O}(q_T/Q)$ where in this case $Q = M_{\eta_Q}$. Moreover, quarkonium production via CS quark pairs could hamper the appearance of other factorisation-breaking effects. Indeed, it was showed that in general, TMD factorisation does not hold for reactions in which the initial and final states of the hard scattering subprocess are coloured [93, 94, 95]. However, quark-antiquark pairs produced in a colour-singlet state and hadronising without further interaction as in the CSM can be seen as very small colour dipoles that could escape factorisation-breaking effects due to soft gluons, although this would require a general proof. A proof of factorisation exists for η_Q production up to NLO, where it is showed that soft gluons do not couple with the leading colour-singlet contribution in the NRQCD expansion [96]. Very recently, a different factorisation proof for η_Q production was proposed [97]. It uses the Soft-Collinear Effective Theory (SCET) in order to check the factorisation hypothesis. It is found that one actually cannot disentangle soft-gluon radiation from the formation of the bound state. Nevertheless, a TMD factorisation theorem is still possible to establish: the cross section is the product of a hard-scattering part with a convolution of the two gluon TMDs, but this convolution contains an extra factor called TMD shape function that needs to be modelled alongside the TMDs. Regarding P -wave production, there is a leading contribution from colour-octet states that breaks factorisation beyond the one-loop level for χ_Q , and at one-loop level for h_Q [98]. A factorisation theorem is derived for χ_Q decay into quarks and their fragmentation into hadrons in [99], which requires the

use of TMD shape functions.

On the experimental side, low-transverse-momentum particles remain challenging to detect due to their proximity to the beam. Moreover, particles like η_Q are not as easy to identify as other quarkonia such as the J/ψ which leptonic decay channel allows a clear identification. It was suggested that detectors with large rapidity acceptance such as LHCb could still be able to study low- q_T (pseudo)scalar quarkonium production at the LHC. However so far, only two studies of η_c production has been realised by LHCb (using the $\eta_c \rightarrow p\bar{p}$ decay channel), for mesons with a transverse momentum of at least 6.5 GeV [100, 101]. This is more than twice the mass of the η_c , placing such events in a kinematical range where TMD factorisation does not apply. It could be possible that a fixed-target experiment would facilitate this study thanks to a lower background [102, 103, 66]. We emphasise that fixed-target setups are complementary to the normal collider mode as they probe distributions at larger values of x . Another possibility would be the study of η_b : its mass (around 9 GeV) could be large enough to put TMD factorisation on firmer grounds, provided that the q_T -threshold could be lowered as LHCb's 6 GeV threshold would remain too high; moreover, NRQCD corrections are reduced for bottomonia as v is smaller. However, it remains out of reach at the LHC owing to its tiny branching to exploitable decay channels. On the other hand, Higgs production is free of any factorisation-breaking effects due to the absence of colour in the final state, and the mass of the boson allows one to extend the validity range of factorisation to transverse momenta large enough to be easily detectable. However, at these energies, evolution effects which we will talk about later strongly suppress the ratio R that is then around the percent level [92].

In addition to the difficulty of detecting low transverse-momentum particles, single-particle final states present the inconvenience of having the hard scale naturally fixed to be the mass of the particle. Since distributions evolve with the scale under consideration, such processes can only probe TMDs at one value of the hard scale. Furthermore, not all of them are sensitive to azimuthal modulations that offer more possibilities to extract the TMDs: the $\mathcal{C}[w_3 f_1^g h_1^{\perp g}]$ convolution appearing in the $\cos(2\phi)$ -asymmetry provides a way to determine the sign of $h_1^{\perp g}$, while $\mathcal{C}[w_4 h_1^{\perp g} h_1^{\perp g}]$ allows one to extract $h_1^{\perp g}$ independently of f_1^g . These limitations disappear when one considers two-particle final states. Indeed, one can have two particles with large individual transverse momenta, with a total transverse momentum remaining small (both particles are approximately back-to-back in the transverse plane). Then even at central rapidities, the pair can have a large invariant mass that is the hard scale of the process, with a small transverse momentum. This invariant mass can be tuned with the individual momenta of the detected particles, allowing one to study the evolution of TMDs with the hard scale.

Finally, the angle one can define between both particles in the transverse plane makes it possible to study azimuthal modulations.

η_Q -pair production at low transverse momentum has been studied in [104] at a centre-of-mass energy of the protons $\sqrt{S} = 7$ TeV. TMD factorisation is expected to hold as well for this process since it is dominated by colour-singlet contributions up to corrections of order $\mathcal{O}(v^4)$. It is the simplest $2 \rightarrow 2$ process involving quarkonia and suffers very low contamination from $q\bar{q}$ channels. Although the mesons can in this case have a large transverse momentum that facilitates their detection, the requirement to observe two at the same time still makes it a rare process, as the number of expected events is taken down twice by the branching to $p\bar{p}$. The observables defined are equivalent to those in Eq. (2.17) integrated over all but the meson rapidity. The process presents the interesting feature to maximise the effect of $h_1^{\perp g}$ in the transverse-momentum spectrum, *i.e.* the hard scattering coefficient F_2 can be equal to F_1 . The author argues that the ϕ -invariant and $\cos(2\phi)$ cross sections could reach values of the order of the femtobarn after application of the squared branching ratio, and may be observable at a high-luminosity LHC (the $\cos(4\phi)$ cross section remains too small). These results are obtained by saturating the positivity bound for $h_1^{\perp g}$, therefore maximising its effects on the cross section.

Another process that has been considered is the production of a J/ψ or Υ meson in association with a photon: $g + g \rightarrow \mathcal{Q} + \gamma$ [105]. The radiation of a photon by one of the quark lines allows the process from gluon fusion, unlike single J/ψ or Υ production. As there is a photon in the final state, it is of order $\alpha_s^2 \alpha^2$ at leading order. It can be showed for this process too that quark-antiquark annihilation is negligible compared to gluon fusion. Colour-octet contributions are generally not dominant [106, 107, 108]. In [105], the authors estimated that in the case of $\Upsilon + \gamma$, the CS contribution is roughly two orders of magnitude above the CO over the whole considered range of invariant masses (between 20 and 40 GeV), while in the $J/\psi + \gamma$ case, the CS dominates for invariant masses up to 20 GeV. Moreover, CO contributions can be additionally suppressed by isolating the quarkonium: at sufficiently large transverse momentum, soft emissions occurring during the hadronisation of the $Q\bar{Q}$ pair become energetic enough to be detected as they get boosted in the lab frame, and such events can then be discarded as colour-octet. The TMD cross section for this process presents an interesting peculiarity: the F_2 coefficient is zero, in total contrast with the double η_Q case. This has as a consequence that the transverse-momentum spectrum is free of any dependence on $h_1^{\perp g}$, allowing for a clean extraction of f_1^g from this observable. In order to make predictions, the authors used various models of Unintegrated Gluon Distributions (UGDs) computed in the small- x limit as ansatz for the TMDs. They define observables equivalent to $\langle \cos(n\phi_{CS}) \rangle$ but

with the convolution $\mathcal{C}[f_1^g f_1^g]$ in the denominator integrated over $\mathbf{P}_{\mathcal{Q}\gamma_T}$. They note that the transverse-momentum spectrum measured in bins of 1 GeV would allow one to determine the shape of $h_1^{\perp g}$, while a measure of the $\langle \cos(2\phi_{CS}) \rangle$ observable integrated over $P_{\mathcal{Q}\gamma_T}$ would prove $h_1^{\perp g}$ to be nonzero. Although F_3 is power-suppressed in $M_{\mathcal{Q}\gamma}$ while F_4 scales like F_1 , the $\cos(4\phi_{CS})$ -asymmetry again appears to be too small to be measurable, while the suppression for the $\cos(2\phi_{CS})$ is not crippling (we recall that TMD evolution is not accounted for in the analysis). One could wonder about the possibility of considering a two-photon final state [109]. We note that while isolation is not necessarily required for the quarkonium, the photon has to be isolated in order to be identified from background, requiring a minimal transverse momentum of about 10 GeV. Each photon needs to be detected which represents a challenge, but there is also much background from π_0 decay, and non-negligible contributions from quark-antiquark annihilation. For these reasons, it appears that photon-pair production is not so suited for the study of the gluon TMDs. Furthermore, the production of a J/ψ or Υ meson in association with a virtual photon or Z^0 boson has been studied in [110]. However in this case, the TMD-related effects are expected to be too small to be accessed in the data.

$\mathcal{Q} + \gamma$ can also be studied at a fixed-target experiment. The lower multiplicity would make photon isolation easier, with lower transverse-momentum thresholds, especially in the backward region accessible by such a setup [66]. Despite the large values of x probed in this configuration ($x \sim 0.65$ for $M_{\mathcal{Q}\gamma} = 10$ GeV and $Y=-2$), gluon fusion remains the dominant mechanism for this process; CS contributions also dominate for $M_{\mathcal{Q}\gamma} < 20$ GeV. Therefore $\mathcal{Q} + \gamma$ presents a very good opportunity to realise a first extraction of the gluon TMDs at large x .

In the next section, we will present the process that we will focus on in this thesis: J/ψ - and Υ -pair production. We will see the advantages of such a process for the study of the gluon TMDs at the LHC and discuss the different contributions, and how well they describe the corresponding data.

4.2 J/ψ - and Υ -pair production

The production of a pair of identical S-wave vector quarkonia in a proton collision is a relatively complex hadronic process. The partonic subprocess indeed involves six partons, the two merging initial-state gluons as well as two pairs of quarks and antiquarks in the final state: $gg \rightarrow Q\bar{Q}Q\bar{Q}$. At leading order in α_s , there are 31 diagrams contributing to the CS component of this subprocess only. The LO is of order α_s^4 , and typical CS diagrams are showed in Fig. 4.2 while typical diagrams for the CO component involve one or two quarkonia being created from a gluon splitting (cf. Fig. 4.3). The total

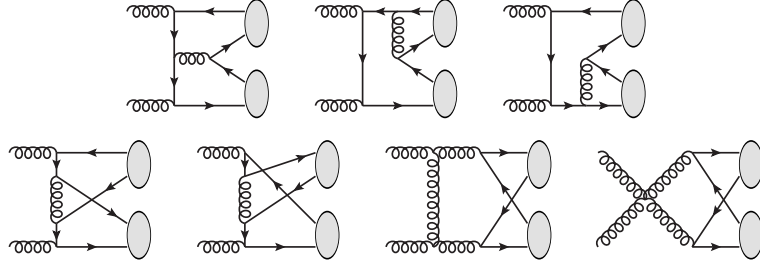


Figure 4.2: Typical LO diagrams for double J/ψ or Υ production in the CSM.

uncontracted amplitude can be found in [111] and is symmetrical under the exchange of the two identical mesons. The corresponding unpolarised squared amplitude matches that given in [112].

Thanks to the ease of detection of J/ψ mesons, J/ψ -pair production has been extensively measured at the Tevatron and the LHC [113, 114, 115, 116, 117]. These studies cover various proton centre-of-mass energies: 1.8, 7 and 13 TeV. Differential cross sections are provided, although no TMD extraction exists so far. An analysis of Υ -pair production was also realised by the CMS collaboration, but the sample only contains some 40 events [118]. A new analysis was published very recently using a sample of about a thousand pairs [119]. It is possible to compare predictions to experimental results already available for J/ψ -pair production, although these studies were not designed to extract gluon TMDs. More double J/ψ data will be available in the high-luminosity phase of the LHC, and a substantial number of Υ pairs are to be detected.

As expected from the large proton-proton centre-of-mass energy, one can safely neglect the $q\bar{q}$ -induced contribution [111, 120]. Mixed contributions from gq and $g\bar{q}$ initial states can be confidently neglected as well. In the case of a two-meson final state, each wave function is independently expanded in terms of Fock states. The terms in the total NRQCD expansion contain products of two LDMEs, so that the powers of v corresponding to each of them also multiply. Therefore the velocity scaling rules of NRQCD give the pair of spectroscopic states $|Q\bar{Q}[^3S_1^{(1)}]\rangle|Q\bar{Q}[^3S_1^{(1)}]\rangle$ as the leading contribution to J/ψ -pair production, that is the CSM contribution. Mixed CSM/COM contributions, where one meson comes from gluon fragmentation: $|Q\bar{Q}[^3S_1^{(1)}]\rangle|Q\bar{Q}[^3S_1^{(8)}]gg\rangle$, are suppressed by a power v^4 with regard to the colour-singlet channel. Spin-singlet S -waves $|Q\bar{Q}[^1S_0^{(8)}]g\rangle$ and spin-triplet P -waves $|Q\bar{Q}[^3P_J^{(8)}]g\rangle$ (with $J = 0, 1, 2$) are respectively suppressed by v^3 and v^4 compared to the colour-singlet $|Q\bar{Q}[^3S_1^{(1)}]\rangle$. The partial exception to this counting is the double gluon-fragmentation channel $|Q\bar{Q}[^3S_1^{(8)}]gg\rangle|Q\bar{Q}[^3S_1^{(8)}]gg\rangle$. Even though it

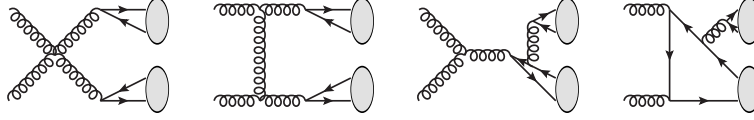


Figure 4.3: Typical LO diagrams for double J/ψ or Y production in the COM.

is suppressed in the velocity expansion by a power v^8 , it also benefits from a kinematic enhancement that could make it the dominant production mechanism at sufficiently large $P_{\mathcal{Q}\mathcal{Q}_T}$ for LO J/ψ -pair production. For these reasons, colour singlet and bi-gluon fragmentation colour octet are considered to be the main channels needed to describe this process, at least for small and large $P_{\mathcal{Q}\mathcal{Q}_T}$ respectively. Mixed production such as $J/\psi + Y$ is also interesting as the colour-singlet channel is absent at leading order, making it a gateway to the study of CO mechanisms [121, 122].

NLO corrections to the hard-scattering amplitude are also important to retrieve the observed differential cross sections. In the case of quarkonium-pair production, a full NLO computation is very challenging. A smart approach used to tackle this difficult problem is to compute only the α_s^5 real-gluon emission corrections. Such computation is referred to as NLO^{*}. Because the loop corrections, like the LO topologies, suffer a $P_{\mathcal{Q}\mathcal{Q}_T}^2$ -suppression with respect to the real gluon-emission diagrams, the NLO^{*} computation becomes a reliable approximation of that of the full NLO at sufficiently large $P_{\mathcal{Q}\mathcal{Q}_T}$. The infrared divergences are regulated by a cut-off; the computation sensitivity to this cut-off vanishes very quickly with growing $P_{\mathcal{Q}\mathcal{Q}_T}$. [120] shows that for J/ψ -pair production, the NLO^{*} contribution should already dominate the production yield in $d\sigma/dP_{\mathcal{Q}\mathcal{Q}_T}$ at $P_{\mathcal{Q}\mathcal{Q}_T} \gtrsim 7$ GeV, for both central and forward rapidities. It also reproduces the CMS data on $d\sigma/d|\Delta y|$ (Δy being the rapidity difference between the two mesons) for $|\Delta y| < 2$, $d\sigma/dM_{\psi\psi}$ for $M_{\psi\psi} < 20$ GeV and $d\sigma/dP_{\psi\psi_T}$ over the entire accessible range [123]. The agreement with the ATLAS data is quite good as well. The main discrepancies that are not connected to small $P_{\psi\psi_T}$ values impairing the NLO^{*} approximation validity are located at large $M_{\psi\psi}$ and Δy . A result for full NLO double J/ψ production was recently published [124]; it does not seem to improve the agreement with the different data where NLO^{*} fails.

When looking at the polarisation of one of the detected J/ψ , one finds that the addition of the NLO^{*} corrections drastically modify it. While it is slightly longitudinal at LO (for $P_{\mathcal{Q}\mathcal{Q}_T} \gtrsim 7$ where the NLO^{*} approximation is valid and a comparison can be made), it becomes significantly transverse at NLO^{*}. This is to be expected owing to the new topologies included in the corrections. Such changes in polarisation between

LO and NLO predictions also occur in single J/ψ or Υ production [66] as mentioned in the previous chapter, as well as in associated production like $\mathcal{Q} + \gamma$ or $\mathcal{Q} + g$ [108]; the exception is $\mathcal{Q} + Z^0$ which sees no change in polarisation of the meson at NLO [125].

CSM and COM contributions to $d\sigma/dP_{\mathcal{Q}\mathcal{Q}_T}$ for J/ψ - and Υ -pair production at the LHC have been estimated in [111, 122, 123, 126, 127]. The authors of [127] review the various differential cross sections provided by the LHC collaborations and compare them with predictions from the CSM at NLO* augmented by a gauge-invariant, infrared-safe subset of loop-induced contributions, and LO COM with various sets of values for the relevant LDMEs. We note that the inclusion of colour-octet contributions is in most cases not necessary to describe the data, or does not significantly reduce the discrepancy. They can enhance the size of theoretical predictions for some ATLAS data at large rapidity gap and invariant mass of the pair, but the latter remain lower than the data points. The relevance of the CO corrections is also varying with the considered values for the LDMEs; as said previously, while the latter should be universal, different extractions give different results that undermine the predictive power of the COM. The CO contributions matter even less in the di- Υ case for which the quark velocity is smaller than inside the J/ψ , making NRQCD corrections negligible.

Despite the large number of experimental studies on J/ψ -pair production, so far none of them provided any doubly differential cross section. This would be of great use for a study oriented toward the extraction of gluon TMDs: indeed, one needs to consider both the transverse momentum of the pair $P_{\psi\psi_T}$ and its invariant mass $M_{\psi\psi}$ in order to make sure an event lies in the range of validity of TMD factorisation. Even a rough binning in $M_{\psi\psi}$ of the transverse-momentum spectra would allow one to select regions where corrections to the factorisation formula remain reasonably small. From the landscape depicted in the previous lines of this section, one can safely assume that CO corrections are negligible in the case of di- J/ψ and di- Υ production: they may only contribute at large rapidity differences where no model can account for the data and factorisation may not hold due to interactions with proton remnants. Regarding higher-order corrections, the most relevant ones are real-gluon emissions at α_s^5 . In such a scenario, the meson pair recoils against the hard gluon and acquires a transverse momentum which is much larger than the intrinsic gluon k_T , which is also outside of the TMD validity range. Therefore requiring the quarkonium pair to have a low transverse momentum naturally selects the LO contribution, which is that we will use in computations. Loop corrections are another order of α_s higher and the ones computed in [127] were showed to not bring significant modifications of the yields.

We have presented some characteristics of the double $J/\psi(\Upsilon)$ production process, in

particular the expected importance of colour-octet and higher-order corrections to the LO CSM, and argued that they have little impact in the phase space relevant for TMD studies. We therefore believe that the large amounts of data already available and to come, as well as the possibility to use the LO CSM with the TMD formalism without the need for large corrections or a serious risk of factorisation breakdown, make J/ψ - and Υ pair production very promising processes for a first extraction of the gluon TMDs inside unpolarised protons at the LHC.

4.3 Double Parton Scattering and feed-down

So far we ignored a hurdle specific to processes with several particles in the final state: Multiple Parton Interactions (MPI). Indeed (we restrict ourselves to the case of two-particle final states), pair production can also originate from two separate scatterings: this process is called Double Parton Scattering (DPS). Two different pairs of gluons from the colliding hadrons scatter and create each a quarkonium, resulting in the same final state as the Single Parton Scattering (SPS), which is what we have discussed so far. The two scatterings can be approximated to be independent. The DPS cross section for pair production can then be factorised as a product of two single quarkonium production cross sections, weighted by the inverse of an effective cross section σ_{eff} . This parameter, supposed to be process- and energy-independent if factorisation holds, describes the effective size of the parton interactions. There is no proof for such a factorisation; actually, factorisation-breaking effects are a way to study correlations between partons. σ_{eff} is a nonperturbative quantity and needs to be experimentally extracted case by case.

Because of the high gluon densities at the LHC energies, DPS can become as substantial a source of pairs of quarkonia as SPS. Depending on which contribution one is focusing on, the other will be a background. It is then of interest to be able to disentangle them. More specifically, J/ψ -pair production has been analysed in several papers as an interesting channel for the study of DPS [123, 128]. In these comparative studies, two methods were used to compute the SPS contribution: one is the regular NLO^{*} computation in collinear factorisation; the other one uses a Monte-Carlo event generator including some nonperturbative effects such as initial-state radiation and an intrinsic transverse momentum for the gluon. Both are globally in good agreement, as can be seen in [129]. SPS cross sections are largest near the pair mass threshold, therefore large momentum differences logically are strongly suppressed, leading to a decrease of the cross section in $M_{\psi\psi}$ and Δy . DPS cross sections do decrease with Δy too, but do not suffer such an important suppression owing to the presumed absence of correlation between the mesons. The ratio $d\sigma_{\text{SPS}}/d\sigma_{\text{DPS}}$ therefore decreases with Δy , and DPS dominates the cross section at large rapidity differences. Adding DPS to the

cross-section predictions allows reducing the discrepancies with the CMS and the ATLAS data at large $M_{\psi\psi}$ and Δy [114, 116], while DPS remains sub-leading compared to SPS in the small range. The situation at LHCb is less contrasted. Since there is no $P_{\psi\psi_T}$ -cut on the J/ψ , small- $P_{\psi\psi_T}$ ranges dominate the cross section, where α_s^5 corrections are not necessarily dominant. DPS contributions can already compete with SPS, even at small $M_{\psi\psi}$ and Δy , in particular in the $d\sigma/dP_{\psi\psi_T}$ spectrum. This feature is expected to be even more pronounced in the LHCb study at 13 TeV. Indeed, the DPS estimate provided in [117] shows that DPS represents a significant fraction of the differential cross sections, including at small $P_{\psi\psi_T}$ or $M_{\psi\psi}$.

The azimuthal angular correlations observable in $d\sigma/d\Delta\phi$ could help disentangling SPS and DPS: the differential cross section should be completely flat for DPS assuming that the two scatterings are really independent, while it peaks at $\Delta\phi = \pi$ (back-to-back configuration) for LO SPS. However, as soon as one considers higher-order corrections or initial-state effects, the distribution can be altered as the pair can recoil on hard gluons. The pair is in a back-to-back configuration in the TMD validity range, provided that the quarkonia have a large transverse momentum. That configuration corresponds to a maximal contribution from the LO SPS. In any case, selecting pairs of relatively central rapidity should limit the impact of DPS over the extraction of the gluon TMDs, although it is not clear yet how much the DPS would alter such an extraction. Data in ATLAS and CMS should be relatively free of DPS at central rapidities (below 10% in the integrated yield [127]). LHCb does not have a threshold on P_{ψ_T} that reduces the number of recorded events, but the contamination from DPS is then too important to be ignored. An accurate estimate of DPS is therefore required in order to isolate the SPS component. LHCb provides an estimate of the DPS contribution to the $P_{\psi\psi_T}$ -spectrum, one can therefore subtract it from the data points to obtain the SPS one, provided that the estimate is accurate.

We finally have a look at the feed-down affecting J/ψ -pair production. The feed-down from χ_c mesons, denoted by $F_{\psi\psi}^{\chi_c}$, is expected to be small. Indeed, $gg \rightarrow J/\psi + \chi_c$ or $gg \rightarrow \psi' + \chi_c$ is forbidden at LO in α_s in the CSM by C-parity. Double χ_c feed-down is also expected to be low because of the squared branching ratio that is then strongly suppressive. For these reasons, $F_{\psi\psi}^{\chi_c}$ should not exceed a few percent [130, 123, 66]. On the other hand, ψ' mesons can be produced in a way identical to J/ψ in gluon fusion reactions. The only difference in the cross section is the value of their wave function at the origin: $|R_{\psi'}(0)|^2 = 0.53 \text{ GeV}^3$ whereas $|R_{J/\psi}(0)|^2 = 0.81 \text{ GeV}^3$. The branching ratio for the de-excitation is $B(\psi' \rightarrow J/\psi) = 55\%$ [131]. As the χ_c feed-down is approximated to be small, one can neglect the $\chi_c + \psi'$ contribution and compute the ratio between direct

production and ψ' feed-down in pair creation:

$$\begin{aligned} \frac{F_{\psi\psi}^{\psi'}}{F_{\psi\psi}^{\text{direct}}} &= 2 \frac{F_{\psi}^{\psi'}}{F_{\psi}^{\text{direct}}} + \left(\frac{F_{\psi}^{\psi'}}{F_{\psi}^{\text{direct}}} \right)^2 \\ &= 2 \frac{|R_{\psi'}(0)|^2 B(\psi' \rightarrow J/\psi)}{|R_{J/\psi}(0)|^2} + \left(\frac{|R_{\psi'}(0)|^2 B(\psi' \rightarrow J/\psi)}{|R_{J/\psi}(0)|^2} \right)^2 \simeq 100\%, \end{aligned} \quad (4.2)$$

giving a value for $F_{\psi\psi}^{\psi'}$ as high as 50%. Because the J/ψ and ψ' respective cross sections only differ by this $(|R_{\psi'}(0)|/|R_{J/\psi}(0)|)^2 \times B(\psi' \rightarrow J/\psi)$ numerical factor, one can simply link the direct and prompt cross sections through a $(1 + F_{\psi\psi}^{\psi'}/F_{\psi\psi}^{\text{direct}})$ scaling factor: $\sigma_{\text{prompt}} = 2 \sigma_{\text{direct}}$.

It is interesting to note that in the DPS case, where both scatterings are considered independent, the situation is quite different. One finds a large χ_c feed-down, $F_{\psi\psi}^{\chi_c} \simeq 50\%$, followed by direct production, $F_{\psi\psi}^{\text{direct}} \simeq 35\%$ and a smaller ψ' component, $F_{\psi\psi}^{\psi'} \simeq 20\%$. In [123, 66], the authors suggested that the measurement of the different feed-down fractions could be a test of DPS or SPS dominance that would be independent of the value of σ_{eff} . Similar reasoning can be made about bottomonium production, although there are more possible excited states than for charmonia, making the feed-down analysis more complex. The feed-down for Υ -pair production was evaluated to be around 30%, coming in majority from the de-excitation of $\Upsilon(2S, 3S)$ states [132]. Regarding the DPS estimate, there are in general tensions between the values of σ_{eff} extracted from different processes. In the central low- $P_{Y\Upsilon_T}$ region, DPS is estimated to contribute for around 5% of the events [127]. For the di- Υ case, the CMS collaboration estimates in its latest study $\sigma_{\text{DPS}}/\sigma_{\text{SPS}} \simeq 25\%$ for $|\Delta y| < 0.5$ [119].

While DPS may actually complicate the interpretation of quarkonium-pair production data, the magnitude and kinematical behaviour of this contribution are currently under scrutiny so that we should be able to better evaluate its impact in the future. Having established the advantages and limitations of J/ψ - and Υ -pair production in the phase space relevant for TMD factorisation, we will in the next chapter include the LO CSM component in the TMD cross section, in order to make predictions for the transverse-momentum spectrum and azimuthal asymmetries. We will focus on J/ψ -pair production, knowing that all the results can be used for Υ by simply changing the numerical values of the meson mass and wave function at the origin. We will see that, in addition to being free of large CO or QCD corrections, the hard-scattering coefficients associated with the process are particularly interesting for the study of the gluon TMDs.

Chapter 5

Predictions for Gaussian TMDs in J/ψ -pair production

In this chapter of the thesis¹, we will show that quarkonium-pair production, and more specifically J/ψ - and Υ -pair production, could provide access to the gluon TMDs inside the unpolarised proton. We will first focus on di- J/ψ production and give some further insight about the hard-scattering coefficients that multiply the various convolutions appearing in the TMD cross section for this process (cf. Eq. (2.5)). The next step will be to use a simple model as an input for both TMDs in order to understand the observables described in the previous chapters and to make predictions for these observables. The unpolarised distribution f_1^g will be modelled using a k_T -Gaussian of width $\langle k_T^2 \rangle$ multiplying the gluon collinear PDF, while two different Gaussian-based models will be used to model $h_1^{\perp g}$. The first model, described in [134] uses an adjustable width while always satisfying the positivity bound defined in Eq. (2.3). The second model simply saturates the positivity bound, allowing for maximal effects of the linearly polarised gluon distribution on the cross section.

The first observable we will look at is the transverse-momentum spectrum of the final-state pair $d\sigma/dP_{\psi\psi_T}$. We will see how in the case of di- J/ψ production, this quantity is quasi-independent of any gluon polarisation-related effect, allowing us to express it as a function of one unknown parameter only, the width $\langle k_T^2 \rangle$ of the Gaussian f_1^g distribution. We will then use this advantage to try and constrain the value $\langle k_T^2 \rangle$ using the 13 TeV J/ψ -pair production LHCb data [133]. We will fit the normalised $P_{\psi\psi_T}$ -differential cross section onto the normalised data, and discuss the possible impact of DPS or NLO contributions over the shape of the LHCb spectrum. In addition, we will consider the impact of the fitting procedure over the extracted value of $\langle k_T^2 \rangle$, and discuss this value.

Following this, we will compute the associated azimuthal asymmetries and detail the role of the hard-scattering coefficients and TMD convolutions play in the obtained results. We will see that the choice of the explored kinematical range conditions the asymmetry sizes to expect and that these are particularly large for quarkonium-pair production, mak-

¹This chapter is largely based on [133].

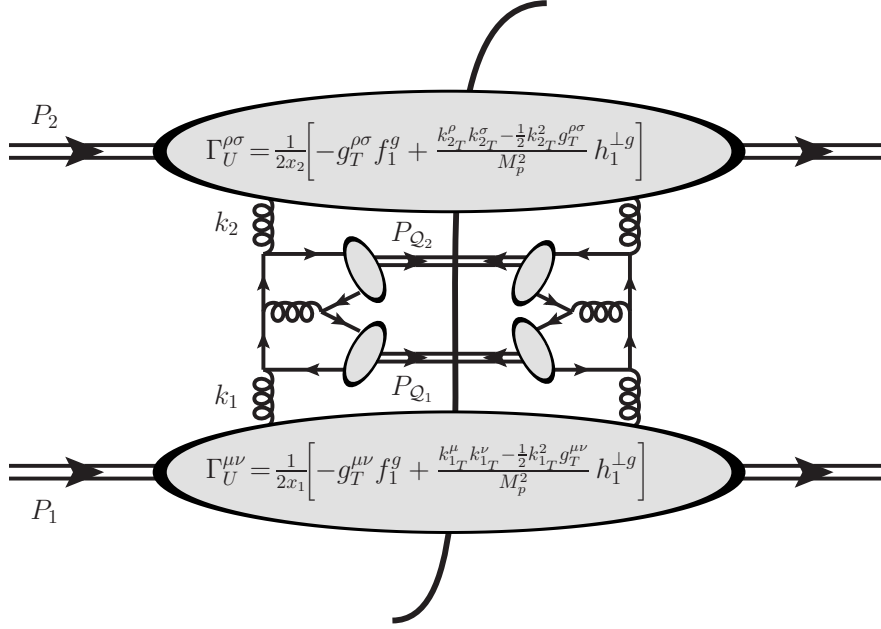


Figure 5.1: Quarkonium-pair production via gluon fusion at LO in the TMD framework

ing it a promising tool for the study of the gluon TMDs.

5.1 Hard-scattering coefficients and TMD models

We have previously explained how quarkonium-pair production at the LHC can be a potential probe of the gluon TMDs inside the unpolarised proton. The large centre-of-mass energy ensures that the main production channel is gluon fusion. The selection of events with a small final-state transverse momentum $P_{\psi\psi_T}$ allows them to be described in the framework of TMD factorisation, looking for the related TMD effects in the transverse-momentum spectrum as well as asymmetries in the azimuthal plane.

As we have seen in Chapter 2, the contraction of the two gluon TMD correlators with the hard-scattering amplitude for quarkonium-pair production generates four terms in the factorised cross section. Each of them is the product of the convolution of two TMD amplitudes and a given transverse weight, from which can arise a $\cos(n\phi_{CS})$ factor, with a hard-scattering coefficient that is a specific sum of helicity amplitudes. The definition of these coefficients denoted $F_{1,2,3,4}^{(\prime)}$, in terms of helicity amplitudes, is universal to

all gluon-fusion-induced processes as it stems from the helicity structure of the gluon correlator (Eq. (2.12)), as does Eq. (2.5). The expressions corresponding to these helicity amplitudes, that can be perturbatively computed, depend on the considered final state.

In the case of di- J/ψ or di- Y production, we use the LO amplitude provided in [111] and contract it with the gluon correlator to obtain the associated hard-scattering coefficients. One can write the coefficients as polynomials in $\cos(\theta_{\text{CS}})$, with θ_{CS} the Collins-Soper angle of the pair [42]:

$$\begin{aligned}
 F_1 &= \frac{\mathcal{N}}{\mathcal{D}M_{\mathcal{Q}}^2} \sum_{n=0}^6 f_{1,n} (\cos(\theta_{\text{CS}}))^{2n}, \\
 F_2 &= \frac{2^4 3 M_{\mathcal{Q}}^2 \mathcal{N}}{\mathcal{D}M_{\mathcal{Q}\mathcal{Q}}^4} \sum_{n=0}^4 f_{2,n} (\cos(\theta_{\text{CS}}))^{2n}, \\
 F_3' = F_3 &= \frac{-2^3 (1 - \alpha^2) \mathcal{N}}{\mathcal{D}M_{\mathcal{Q}\mathcal{Q}}^2} \sum_{n=0}^5 f_{3,n} (\cos(\theta_{\text{CS}}))^{2n}, \\
 F_4 &= \frac{(1 - \alpha^2)^2 \mathcal{N}}{\mathcal{D}M_{\mathcal{Q}}^2} \sum_{n=0}^6 f_{4,n} (\cos(\theta_{\text{CS}}))^{2n}.
 \end{aligned} \tag{5.1}$$

All the coefficients contain a common pre-factor, whose numerator is $\mathcal{N} = 2^{11} 3^{-4} \pi^2 \alpha_s^4 |R_{\mathcal{Q}}(0)|^4$ and denominator is $\mathcal{D} = M_{\mathcal{Q}\mathcal{Q}}^4 (1 - (1 - \alpha^2) \cos(\theta_{\text{CS}})^2)^4$. They contain the radial wave function of the quarkonium at the origin $R_{\mathcal{Q}}(0)$, as well as the coupling α_s which appears at fourth power at LO. The variable $\alpha = 2M_{\mathcal{Q}}/M_{\mathcal{Q}\mathcal{Q}}$ can be tuned to study the variation of the centre-of-mass energy of the system $M_{\mathcal{Q}\mathcal{Q}}$. The large- $M_{\mathcal{Q}\mathcal{Q}}$ limit corresponds to $\alpha \rightarrow 0$, while the threshold limit corresponds to $\alpha \rightarrow 1$. The $f_{i,n}$ coefficients are polynomials in α and can be found in Appendix B.

We observe that for the considered process, the coefficients F_3 and F_3' are equal. This simplification arises from considering two identical particles in the final state, the corresponding amplitude being symmetrical under the exchange of the two quarkonium momenta. When considering the $\cos(2\phi_{\text{CS}})$ asymmetry, the gluon momenta that are each associated to a different TMD, couple the same way to one or the other quarkonium momentum. The corresponding hard-scattering coefficients are therefore equal. We will therefore discuss only F_3 in the following, knowing that everything applies equally to F_3' . Another simplification linked to the identical nature of the final-state particles is the $\theta_{\text{CS}} \leftrightarrow -\theta_{\text{CS}}$ symmetry. As such a transformation amounts to an exchange of the quarkonium momenta in the rest frame of the pair, it also leaves the hard-scattering coefficients unchanged. This symmetry is reflected in Eq. (5.1) with the powers of the $\cos(\theta_{\text{CS}})$ that are always even numbers.

It is then interesting to look at the form the coefficients take for $\alpha \rightarrow 0$ and $\cos(\theta_{\text{CS}}) \rightarrow 0$:

$$F_4 \rightarrow F_1 \rightarrow \frac{256\mathcal{N}}{M_{\mathcal{Q}\mathcal{Q}}^4 M_{\mathcal{Q}}^2}, \quad (5.2)$$

$$F_2 \rightarrow \frac{81M_{\mathcal{Q}}^4 \cos^2(\theta_{\text{CS}})}{2M_{\mathcal{Q}\mathcal{Q}}^4} \times F_1, \quad (5.3)$$

$$F_3 \rightarrow \frac{-24M_{\mathcal{Q}}^2 \cos^2(\theta_{\text{CS}})}{M_{\mathcal{Q}\mathcal{Q}}^2} \times F_1. \quad (5.4)$$

The first observation about (5.2)–(5.4) is that in pair production at central rapidities for $M_{\mathcal{Q}\mathcal{Q}} \gg M_{\mathcal{Q}}$, the coefficient F_4 becomes equal to F_1 and reaches its maximal value. Such a result has important consequences for the experimental search of the gluon polarisation inside the proton. Indeed, the size of the $\cos(4\phi_{\text{CS}})$ asymmetry, which is a direct consequence of the existence of $h_1^{\perp g}$, occurs to be maximal in a region of phase-space studied by CMS and ATLAS and where DPS contamination is expected to be low. Thus, as the asymmetry is maximally sensitive to $h_1^{\perp g}$ in this region covered by experimental setups, gluon polarisation could be detected provided that the magnitude of the polarised distribution is not too low. Moreover, we notice that the other coefficients F_2 and F_3 scale like $1/M_{\mathcal{Q}\mathcal{Q}}^4$ and $1/M_{\mathcal{Q}\mathcal{Q}}^2$ at large $M_{\mathcal{Q}\mathcal{Q}}$. As a consequence, the only $h_1^{\perp g}$ -related effect remaining is the $\cos(4\phi_{\text{CS}})$ asymmetry. While depriving us from additional TMD-related observables in this favourable kinematical regime, this fact also allows a more straightforward interpretation of the detection of any azimuthal asymmetry in quarkonium-pair production data².

Now if one considers the threshold limit $M_{\psi\psi} \rightarrow 2M_{\psi} \Rightarrow \alpha \rightarrow 1$, the same coefficients become:

$$F_1 \rightarrow \frac{787\mathcal{N}}{16M_{\mathcal{Q}}^6}, \quad F_2 \rightarrow \frac{3F_1}{787}, \quad F_{3,4} \rightarrow 0. \quad (5.5)$$

Every gluon polarisation-related effect is strongly suppressed near the reaction threshold. In particular, the coefficient F_2 remains small in the whole phase-space we will consider ($M_{\mathcal{Q}\mathcal{Q}} < 50$ GeV and $|\cos(\theta_{\text{CS}})| < 0.5$). This allows us to safely neglect its impact over the $P_{\mathcal{Q}\mathcal{Q}_T}$ -spectrum and in the denominator of the $\langle \cos(n\phi_{\text{CS}}) \rangle$ observables.

²We will see in the next chapter that the dominance of the $\cos(4\phi_{\text{CS}})$ -asymmetry is weakened by TMD evolution effects.

So far, the gluon TMDs remain to be determined from first principles or extracted from experimental data. To do the latter, one needs to assume a model which free parameters are fitted to data. In the case of f_1^g , one can use a simple Gaussian dependence in \mathbf{k}_T^2 [135]:

$$f_1^g(x, \mathbf{k}_T^2, \mu) = \frac{g(x, \mu)}{\pi \langle k_T^2 \rangle} \exp\left(-\frac{\mathbf{k}_T^2}{\langle k_T^2 \rangle}\right), \quad (5.6)$$

where $g(x, \mu)$ is the collinear gluon PDF and $\langle k_T^2 \rangle$ is the average squared transverse momentum of the gluon. It is implicitly depending on the scale μ and is the only free parameter of the model. The normalisation of the Gaussian is chosen to obtain the collinear PDF when integrating Eq. (5.6) over \mathbf{k}_T^2 . We see that, in addition to the simple \mathbf{k}_T^2 -dependence, the dependence on x and \mathbf{k}_T^2 are completely factorised, the latter being considered independent from the former. One can then completely extract the x -dependence of the TMDs from the convolution, as it is entirely contained in the collinear PDF.

The nature of $h_1^{\perp g}$ being completely unknown, a common practice is to saturate its positivity bound which was described previously. In this case, the polarisation of gluons is maximal and so will be the magnitude of its related effects on the TMD cross section. $h_1^{\perp g}$ then reads:

$$h_1^{\perp g}(x, \mathbf{k}_T^2, \mu) = \frac{2M_p^2}{\mathbf{k}_T^2} f_1^g(x, \mathbf{k}_T^2, \mu). \quad (5.7)$$

Note that Eq. (5.7) fixes the sign of $h_1^{\perp g}$ as positive, but it can very well be negative. The advantages of having such an expression, apart from maximising the estimated TMD effects, is that $h_1^{\perp g}$ is also described by a simple expression that allows one to analytically compute the TMD convolutions. In addition, the x -dependence factorises outside of the convolutions. Moreover, since in such a configuration, both TMDs have exactly the same x -dependence, the latter becomes an overall pre-factor in the cross section which cancels out in all convolution ratios.

Another Gaussian-based model was used to make predictions for scalar and pseudoscalar single quarkonium production, as well as Higgs production [91, 134]. It is adapted from a model derived in [136] used to describe the fragmentation function of polarised Λ in SIDIS. In this model, $h_1^{\perp g}$ reads:

$$h_1^{\perp g}(x, \mathbf{k}_T^2, \mu) = \frac{2M_p^2}{\langle k_T^2 \rangle} \frac{(1-r)}{r} \frac{g(x, \mu)}{\pi \langle k_T^2 \rangle} \exp\left(1 - \frac{\mathbf{k}_T^2}{r \langle k_T^2 \rangle}\right). \quad (5.8)$$

This expression respects the positivity bound for $r < 1$, although it does not saturates it everywhere like the previous model. The usual value taken for r is $2/3$, as it maximises the

second \mathbf{k}_T moment of $h_1^{\perp g}$. Such a choice is motivated by low- x models for the polarised gluon TMD which tend to give large values of $h_1^{\perp g}$ [137, 138]. This trend also justifies the use of the bound-saturating model. The interest in testing two different models is that it gives us an insight of the dependence of the observables on the nature of the TMDs, and more specifically their widths and magnitude. While the bound-saturating model gives us an idea about the feasibility of measuring gluon-polarisation effects in the cross section, the second model provides us with less optimistic predictions and allows us to derive an appropriate uncertainty band for the latter.

Now that we have expressions for the hard-scattering coefficients and the TMDs, one can compute the TMD cross section for quarkonium-pair production and the related observables.

5.2 The transverse-momentum spectrum

The transverse-momentum spectrum is obtained by integrating the TMD cross section over the azimuthal angle ϕ_{CS} , at a given value of $M_{\mathcal{Q}\mathcal{Q}}$ and $Y_{\mathcal{Q}\mathcal{Q}}$, and only depends on the first two terms of Eq. (2.5). Therefore even though it is not sensitive to azimuthal modulations, it remains affected by $h_1^{\perp g}$. However we have seen that, in the case of quarkonium-pair production, the hard-scattering coefficient F_2 associated with the convolution $\mathcal{C}[w_2 h_1^{\perp g} h_1^{\perp g}]$ remains of negligible size over the whole phase space, with a ratio F_2/F_1 smaller than the percent level. One consequently can consider the effects of gluon polarisation on the transverse-momentum spectrum of di-quarkonium production to be negligible. The $P_{\mathcal{Q}\mathcal{Q}T}$ -spectrum $d\sigma/dP_{\mathcal{Q}\mathcal{Q}T} \propto P_{\mathcal{Q}\mathcal{Q}T} \mathcal{C}[f_1^g f_1^g]$ then becomes a tool to study f_1^g without any form of contamination from the second gluon TMD. When computed using the model of Eq. (5.6), the convolution reads:

$$\mathcal{C}[f_1^g f_1^g] = \frac{g(x_1, \mu)g(x_2, \mu)}{2\pi\langle k_T^2 \rangle} \exp\left(-\frac{P_{\mathcal{Q}\mathcal{Q}T}^2}{2\langle k_T^2 \rangle}\right). \quad (5.9)$$

We omit the \mathbf{k}_T - and x -dependence of the TMDs inside the convolution for brevity. Even when using a Gaussian model for f_1^g , many variables still enter the transverse-momentum spectrum, like the gluon PDFs, the pair rapidity in the kinematical pre-factor, the hard-scattering coefficient F_1 ... All of these factors do not affect the shape of the $P_{\mathcal{Q}\mathcal{Q}T}$ -spectrum but will affect its normalisation. Moreover, if one wishes to compare the predictions of the model to data, one must be able to reproduce the normalisation of the spectrum, that could be modified by virtual corrections to the LO scattering amplitude. DPS could also modify both the normalisation and shape of the spectrum. Nevertheless, working with the normalised spectrum is sufficient to study the width of f_1^g . Such an

observable reads as follows:

$$\frac{d\sigma/dP_{\mathcal{Q}\mathcal{Q}_T}}{\int_0^{M_{\mathcal{Q}\mathcal{Q}}/2} d\sigma/dP_{\mathcal{Q}\mathcal{Q}_T} dP_{\mathcal{Q}\mathcal{Q}_T}} = \frac{P_{\mathcal{Q}\mathcal{Q}_T} \exp(-\frac{P_{\mathcal{Q}\mathcal{Q}_T}^2}{2\langle k_T^2 \rangle})}{1 - \exp(-\frac{M_{\mathcal{Q}\mathcal{Q}}^2}{8\langle k_T^2 \rangle})}. \quad (5.10)$$

The normalised spectrum cancels all the $P_{\mathcal{Q}\mathcal{Q}_T}$ -independent pre-factors: the cross-section kinematical pre-factor, the hard scattering coefficient F_1 as well as the collinear gluon PDFs. The spectrum is normalised over a $P_{\mathcal{Q}\mathcal{Q}_T}$ -range extending from 0 to $M_{\mathcal{Q}\mathcal{Q}}/2$, as we consider it to be the limit of the validity range to apply the TMD formalism. The normalised spectrum therefore conserves an explicit dependence on $M_{\mathcal{Q}\mathcal{Q}}$, in addition to the implicit $M_{\mathcal{Q}\mathcal{Q}}$ -dependence of the width $\langle k_T^2 \rangle$.

In [133], we fitted the width of the Gaussian f_1^g to the di- J/ψ production transverse-momentum spectrum released by the LHCb collaboration [117] at 13 TeV. The fit is obtained using the least squares method and the data points are weighted by the inverse square of their error. The weighting of the errors does not strongly affect the fit as the errorbars are of comparable size. The reduced χ^2 is about 0.41. This low value, characteristic of an overfit despite the simplicity of the model, is due to the fact that we only have four data points to use with relatively large uncertainties. It is however sufficient to give us an order of magnitude for $\langle k_T^2 \rangle$. The data are provided in bins of 1 GeV, starting at $P_{\psi\psi_T}=0$. As the data are not doubly differential, the value of $M_{\psi\psi}$ inside of each bin is not known. We therefore considered the $M_{\psi\psi}$ -spectrum and assumed the average value to be approximately $\langle M_{\psi\psi} \rangle = 8$ GeV. We therefore considered the first four points of the $P_{\psi\psi_T}$ -spectrum to be in the TMD regime. The associated spectrum was normalised by dividing each point value by the sum of the four.

If one uses Eq. (5.10) to fit $\langle k_T^2 \rangle$ on the normalised LHCb data, the resulting value is 5.12 ± 0.72 GeV² (cf. Fig. 5.2). Our first observation is that the resulting value of $\langle k_T^2 \rangle$ is remarkably high, since one would expect the intrinsic momentum of partons inside a proton to be in the sub-GeV range. This Gaussian model does not explicitly account for any perturbative contributions to the intrinsic average transverse momentum of the initial-state gluons. Such pre-scattering interactions enhance the initially low transverse momentum of the gluon. In addition, gluons entering the hard scattering with a large momentum are likely to be the product of a large number of initial-state radiations. $\langle k_T^2 \rangle$ thus becomes larger with an increasing value of the gluons centre-of-mass energy, which coincides with $M_{\psi\psi}$ at LO. It is then natural that we find a large value of $\langle k_T^2 \rangle$ from the data, as it is an effective one that runs with $M_{\psi\psi}$. In order to study the intrinsic transverse momentum of the gluons, one needs to consider the evolution of the TMDs with the hard scale. This will be the subject of the next chapter.

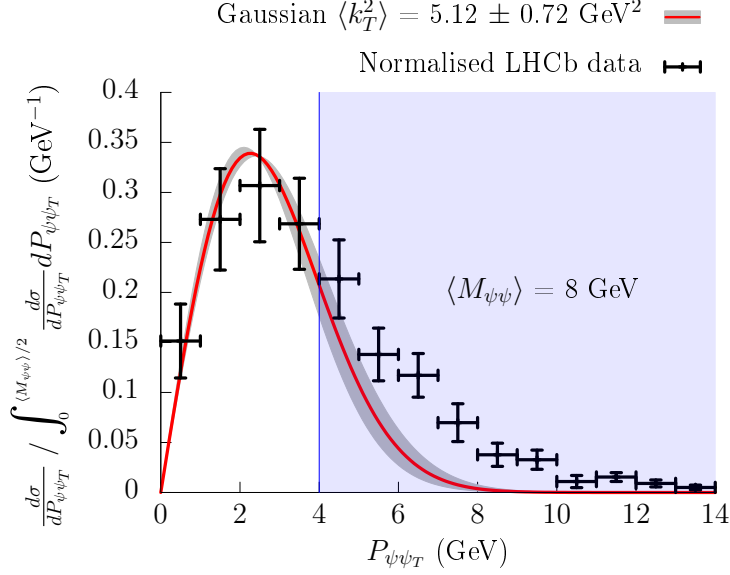


Figure 5.2: Fit of the width $\langle k_T^2 \rangle$ of the Gaussian-model TMD f_1^g to LHCb normalised data for $d\sigma/dP_{\psi\psi_T}$ in di- J/ψ production. The data and cross-section expression used are normalised over the range of validity for TMD factorisation $[0; \langle M_{\psi\psi} \rangle/2]$ (delimited by the blue line), and the fit is realised using the data points located within this range. The grey band depicts the uncertainty in the value of $\langle k_T^2 \rangle$.

We also remark that when plotted past the four points used to extract the width $\langle k_T^2 \rangle$, the fitted model with a Gaussian fall-off progressively undershoots the data. Indeed, high transverse momenta for the J/ψ pair are characteristic of real-gluon emissions where the pair recoils against a hard gluon. Such contributions become dominant at large $P_{\psi\psi_T}$. NLO contributions to the partonic cross section are necessary to describe this sector and the TMD formalism is not valid anymore (corrections in $P_{\psi\psi_T}/M_{\mathcal{Q}\mathcal{Q}}$ become large), while the collinear formalism is expected to work. One needs to implement a matching procedure in order to describe the transition between the two regimes [29].

A remaining concern for such an analysis is the DPS in the data [66, 128, 123, 126, 139]. Indeed in this kinematical regime, the DPS is expected to be non-negligible. The associated $P_{\psi\psi_T}$ -spectrum alters the shape of the spectrum and therefore complicates the extraction of a relevant value of $\langle k_T^2 \rangle$. It was argued that DPS represents a significant part of events in di- J/ψ production. In D0, it was reported that nearly 50% of the events were

to be attributed to DPS [115]. The proportion of DPS events in the LHCb data is probably of the same order, and therefore cannot be neglected (cf. Section 4.3). It is however complicated to extract this component, as values of σ_{eff} coming from different extractions are significantly different. Extractions made from quarkonium-related observables seem to favour smaller values of σ_{eff} than jet ones, meaning larger DPS contributions. However in this case, the DPS when combined with the known SPS channels seem to overshoot the data.

If we subtract the DPS contribution as estimated by LHCb from the $P_{\psi\psi_T}$ -spectrum, the resulting fitted value of $\langle k_T^2 \rangle$ is significantly reduced as can be seen in Fig. 5.3, meaning that the DPS component has a wider $P_{\psi\psi_T}$ -spectrum than the SPS one. However, such a statement depends strongly on the accuracy of the DPS estimate. One can also see in Fig. 5.4 that realising a fit in bins of 1 GeV slightly modifies the fit result but the new value remains well within the uncertainty band of the previous one.

Let us emphasise that even if the DPS transverse-momentum spectrum is uncertain and can make an extraction of a precise value of $\langle k_T^2 \rangle$ delicate, its order of magnitude does not change and remains well above what is expected for the intrinsic transverse momentum of partons inside a proton. This is a clear sign of TMD evolution from the di- J/ψ production data.

Having obtained a first estimate of the value of $\langle k_T^2 \rangle$ using the LHCb data, one can use it in the Gaussian-based models for f_1^g and $h_1^{\perp g}$ in order to make predictions for the TMD convolutions and the corresponding azimuthal asymmetries in J/ψ -pair production.

5.3 Azimuthal asymmetries

As we have seen in Eq. (5.9), one can analytically compute the TMD convolutions using a k_T -Gaussian for f_1^g . With the Gaussian-like and positivity bound-saturating models provided for $h_1^{\perp g}$ in the previous section, one can also give analytical expressions for the other convolutions. Using the Gaussian-like model from [134], one gets the following results:

$$\begin{aligned} \mathcal{C}[w_2 h_1^{\perp g} h_1^{\perp g}] &= \frac{\left(P_{\mathcal{Q}\mathcal{Q}_T}^4 - 8P_{\mathcal{Q}\mathcal{Q}_T}^2 r \langle k_T^2 \rangle + 8r^2 \langle k_T^2 \rangle^2 \right) (r-1)^2}{32\pi \langle k_T^2 \rangle^3} \frac{1}{r} e^{-\frac{P_{\mathcal{Q}\mathcal{Q}_T}^2}{2r \langle k_T^2 \rangle}}, \\ \mathcal{C}[w_3 f_1^g h_1^{\perp g}] &= \frac{P_{\mathcal{Q}\mathcal{Q}_T}^2}{\pi \langle k_T^2 \rangle^2} \frac{(r-1)r^2}{(r+1)^3} e^{-\frac{P_{\mathcal{Q}\mathcal{Q}_T}^2}{(r+1) \langle k_T^2 \rangle}}, \end{aligned}$$

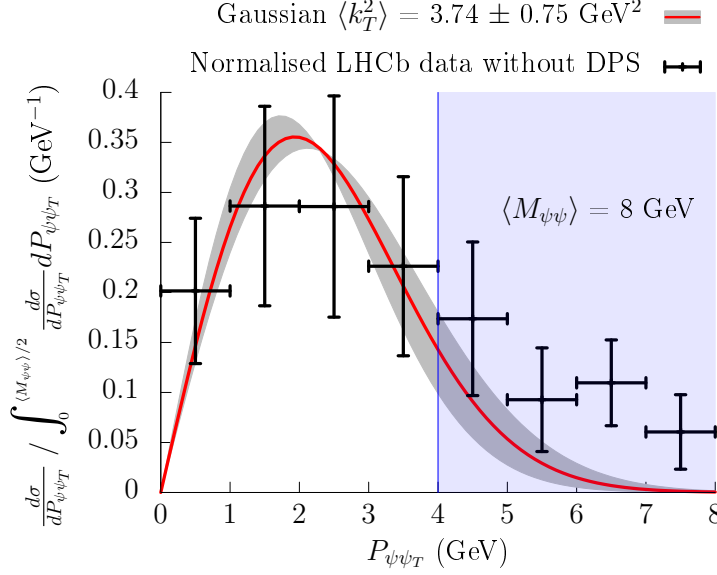


Figure 5.3: Fit of the width $\langle k_T^2 \rangle$ of the Gaussian-model TMD f_1^g to LHCb normalised data *with DPS subtracted* for $d\sigma/dP_{\psi\psi_T}$ in di- J/ψ production.

$$\mathcal{C}[w_4 h_1^{\perp g} h_1^{\perp g}] = \frac{P_{\mathcal{Q}\mathcal{Q}_T}^4}{32\pi \langle k_T^2 \rangle^3} \frac{(r-1)^2}{r} e^{-\frac{P_{\mathcal{Q}\mathcal{Q}_T}^2}{2r \langle k_T^2 \rangle}}. \quad (5.11)$$

The integrals can be computed either in momentum (k_T) or position (b_T) space. The latter is more straightforward and gives a particular insight on the structure of the convolutions. Indeed when realising the integration in b_T space, one can see that the transverse weights w_i present inside the different convolutions modify the angular component in characteristic ways. The angular integral inside $\mathcal{C}[f_1^g f_1^g]$ and $\mathcal{C}[w_2 h_1^{\perp g} h_1^{\perp g}]$ will generate a Bessel function $J_0(b_T P_{\mathcal{Q}\mathcal{Q}_T})$, whereas the one inside $\mathcal{C}[w_3 f_1^g h_1^{\perp g}]$ generates $J_2(b_T P_{\mathcal{Q}\mathcal{Q}_T})$ and the one inside $\mathcal{C}[w_4 h_1^{\perp g} h_1^{\perp g}]$ generates $J_4(b_T P_{\mathcal{Q}\mathcal{Q}_T})$. At $P_{\mathcal{Q}\mathcal{Q}_T} = 0$, one gets $J_0(0) = 1$ versus $J_{2,4}(0) = 0$. The consequence is that at $P_{\mathcal{Q}\mathcal{Q}_T} = 0$, only the azimuthally-invariant convolutions are potentially nonzero. This makes sense when defining ϕ_{CS} using the pair transverse momentum vector, as ϕ_{CS} cannot be defined when $P_{\mathcal{Q}\mathcal{Q}_T} = 0$. In the large $P_{\mathcal{Q}\mathcal{Q}_T}$ limit, all the convolutions become 0 due to their Gaussian nature. Since the asymmetries are proportional to ratios of the convolutions involving $h_1^{\perp g}$ and $\mathcal{C}[f_1^g f_1^g]$, it is instructive to consider how these ratios behave with $P_{\mathcal{Q}\mathcal{Q}_T}$. As said previously, the only possible nonzero ratio at $P_{\mathcal{Q}\mathcal{Q}_T} = 0$ is $\mathcal{C}[w_2 h_1^{\perp g} h_1^{\perp g}] / \mathcal{C}[f_1^g f_1^g] = e^2 / 27 \approx 0.27$ for $r = 2/3$. In the large- $P_{\mathcal{Q}\mathcal{Q}_T}$ limit, the ratios all

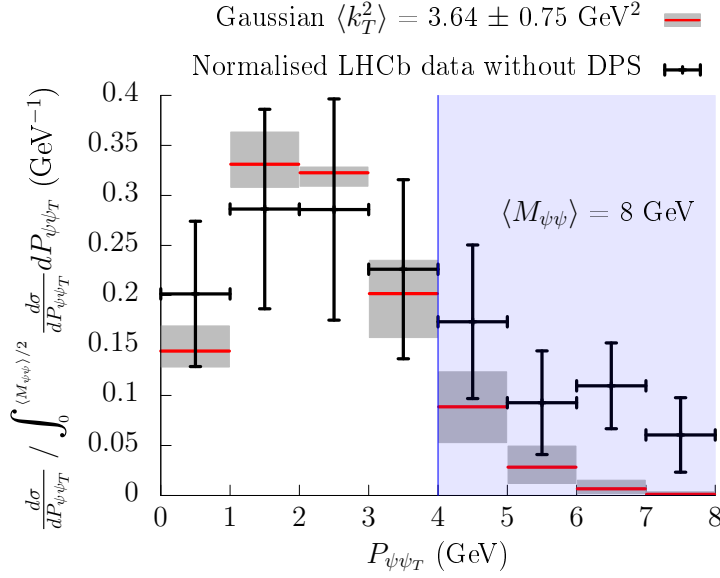


Figure 5.4: Fit of the width $\langle k_T^2 \rangle$ of the Gaussian-model TMD f_1^g to LHCb normalised data *with DPS subtracted* for $d\sigma/dP_{\psi\psi_T}$ in di- J/ψ production using 1 GeV bins.

tend toward 0 as the Gaussians in $\mathcal{C}[w_2 h_1^{\perp g} h_1^{\perp g}]$, $\mathcal{C}[w_3 f_1^g h_1^{\perp g}]$ and $\mathcal{C}[w_4 h_1^{\perp g} h_1^{\perp g}]$ are all steeper than that in $\mathcal{C}[f_1^g f_1^g]$. This is a consequence of the presence of the factor $1/r$ (that is larger than 1) in the argument of the k_T -exponential inside $h_1^{\perp g}$.

Using the bound-saturating definition of $h_1^{\perp g}$, one gets:

$$\begin{aligned} \mathcal{C}[w_3 f_1^g h_1^{\perp g}] &= -\frac{\left(P_{\mathcal{Q}\mathcal{Q}_T}^2 - 2\langle k_T^2 \rangle\right) e^{\frac{P_{\mathcal{Q}\mathcal{Q}_T}^2}{2\langle k_T^2 \rangle}} + 2\langle k_T^2 \rangle}{2\pi P_{\mathcal{Q}\mathcal{Q}_T}^2 \langle k_T^2 \rangle} e^{-\frac{P_{\mathcal{Q}\mathcal{Q}_T}^2}{\langle k_T^2 \rangle}}, \\ \mathcal{C}[w_4 h_1^{\perp g} h_1^{\perp g}] &= \frac{4\langle k_T^2 \rangle \left(P_{\mathcal{Q}\mathcal{Q}_T}^2 + 2\langle k_T^2 \rangle\right) + \left(P_{\mathcal{Q}\mathcal{Q}_T}^4 - 8\langle k_T^2 \rangle^2\right) e^{\frac{P_{\mathcal{Q}\mathcal{Q}_T}^2}{2\langle k_T^2 \rangle}}}{2\pi P_{\mathcal{Q}\mathcal{Q}_T}^4 \langle k_T^2 \rangle} e^{-\frac{P_{\mathcal{Q}\mathcal{Q}_T}^2}{\langle k_T^2 \rangle}}. \end{aligned} \quad (5.12)$$

In the high- $P_{\mathcal{Q}\mathcal{Q}_T}$ limit, in contrast to the previous model, the $P_{\mathcal{Q}\mathcal{Q}_T}$ -Gaussians in the $\mathcal{C}[w_3 f_1^g h_1^{\perp g}]$ and $\mathcal{C}[w_4 h_1^{\perp g} h_1^{\perp g}]$ convolutions are as wide as the one in $\mathcal{C}[f_1^g f_1^g]$. They actually all become identical (up to a minus sign for $\mathcal{C}[w_3 f_1^g h_1^{\perp g}]$), making their ratio equal to 1 (or -1). Having $h_1^{\perp g}$ saturating the positivity bound therefore makes the related convolutions as large as $\mathcal{C}[f_1^g f_1^g]$, ensuring a maximal size for the azimuthal asymme-

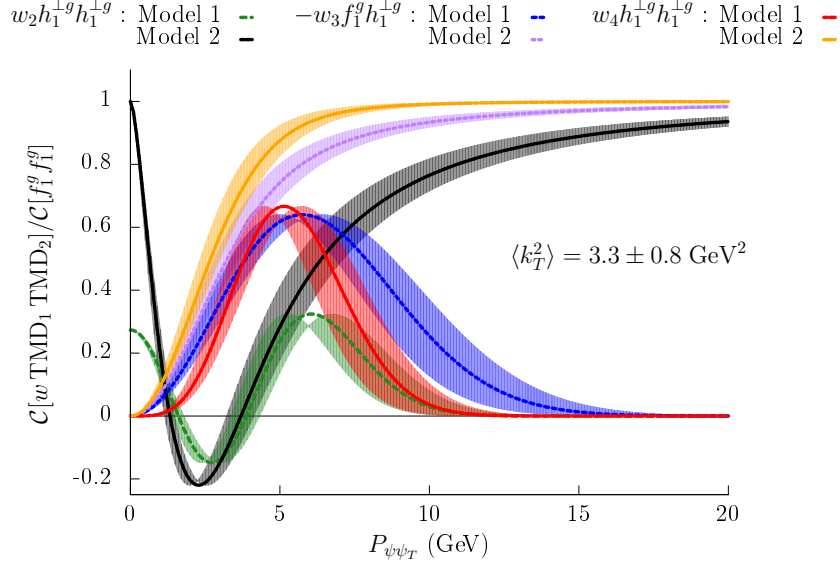


Figure 5.5: The ratios between $\mathcal{C}[w_2 h_1^{\perp g} h_1^{\perp g}]$, $-\mathcal{C}[w_3 f_1^g h_1^{\perp g}]$, $\mathcal{C}[w_4 h_1^{\perp g} h_1^{\perp g}]$ and $\mathcal{C}[f_1^g f_1^g]$ as functions of $P_{\psi\psi_T}$ for $\langle k_T^2 \rangle = 3.3 \pm 0.8 \text{ GeV}^2$. Both $h_1^{\perp g}$ models are included: model 1 is the Gaussian-based model from [134], model 2 is the bound-saturating model.

tries. In particular, this implies that the $\langle \cos(4\phi_{CS}) \rangle$ -asymmetry can reach a size of 100% in the high-energy limit at central rapidities, as the hard-scattering coefficient F_4 becomes equal to F_1 in this limit.

Although we did not have an analytical expression for $\mathcal{C}[w_2 h_1^{\perp g} h_1^{\perp g}]$ at our disposal in the bound-saturating model, one can easily compute it numerically and show that it also saturates the bound, both in the large and small transverse momentum limits. However, this will not be sufficient to affect the $P_{\mathcal{Q}\mathcal{Q}_T}$ -spectrum in a visible way as the hard-scattering coefficient F_2 remains too small and will suppress the contribution. The convolution ratios are shown in Fig. 5.5 for $\langle k_T^2 \rangle = 3.3 \pm 0.8 \text{ GeV}^2$ for both models. We observe that increasing (decreasing) $\langle k_T^2 \rangle$ within this range increases (decreases) the width of the convolution ratios. This shifts the value at which the ratios from Model 1 peak, while it makes the ratios from Model 2 slower to reach their maximal value. For the considered range, the induced variation is minor.

The second element that will determine the size and shape of the azimuthal asymmetries is the ratio of the hard-scattering coefficients associated with a given TMD convolution. Indeed since the F_2 component makes the second term in the denominator of

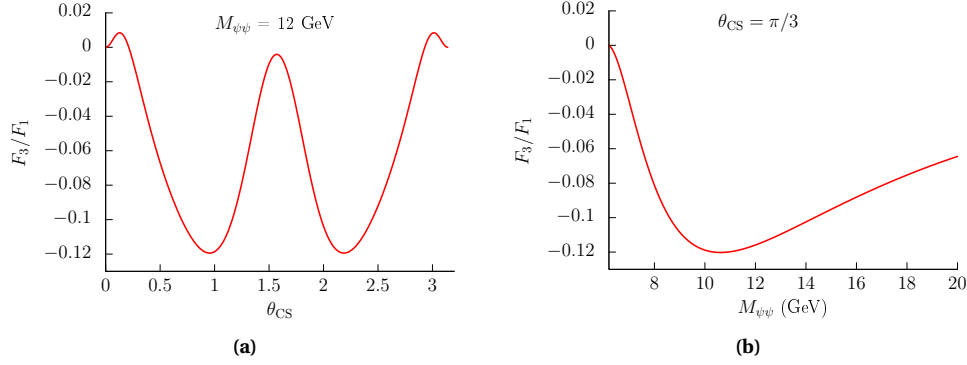


Figure 5.6: Hard-scattering-coefficient ratio F_3/F_1 as a function of θ_{CS} at $M_{\psi\psi} = 12$ GeV (5.6a) and as a function of $M_{\psi\psi}$ at $\theta_{CS} = \pi/3$ (5.6b)

$\langle \cos(n\phi_{CS}) \rangle$ negligible, the only remaining term is $F_1 \mathcal{C}[f_1^g f_1^g]$. The disappearance of this sum in the denominator of $\langle \cos(n\phi_{CS}) \rangle$ means that the observable can be factored into a product of the convolutions ratio and the hard-scattering coefficients ratio, as demonstrated in Eq. (5.13):

$$\begin{aligned} \langle \cos(2\phi_{CS}) \rangle &= \frac{1}{2} \frac{F_3 \mathcal{C}[w_3 f_1^g h_1^{\perp g}] + F_3' \mathcal{C}[w_3' h_1^{\perp g} f_1^g]}{F_1 \mathcal{C}[f_1^g f_1^g] + F_2 \mathcal{C}[w_2 h_1^{\perp g} h_1^{\perp g}]} \simeq \frac{F_3}{F_1} \frac{\mathcal{C}[w_3 f_1^g h_1^{\perp g}]}{\mathcal{C}[f_1^g f_1^g]}, \\ \langle \cos(4\phi_{CS}) \rangle &= \frac{1}{2} \frac{F_4 \mathcal{C}[w_4 h_1^{\perp g} h_1^{\perp g}]}{F_1 \mathcal{C}[f_1^g f_1^g] + F_2 \mathcal{C}[w_2 h_1^{\perp g} h_1^{\perp g}]} \simeq \frac{1}{2} \frac{F_4}{F_1} \frac{\mathcal{C}[w_4 h_1^{\perp g} h_1^{\perp g}]}{\mathcal{C}[f_1^g f_1^g]}. \end{aligned} \quad (5.13)$$

The hard-scattering coefficients give the explicit dependence of the asymmetry in $M_{\psi\psi}$ and θ_{CS} . As previously mentioned for the TM spectrum, taking ratios cancels the dependence on x and $Y_{\mathcal{Q}\mathcal{Q}}$. The former is described by the collinear gluon PDF that factors out in the Gaussian models used here to model the TMDs, while the latter only appears in the overall kinematical factor of the cross section and is therefore simplified in the ratio. If we plot F_3/F_1 as a function of θ_{CS} (Fig. 5.6a), we see that the ratio peaks at $\theta_{CS} = \pi/3$ and cancels at $\theta_{CS} = \pi/2$. The consequence is that in the case of di- J/ψ production, the $\cos(2\phi_{CS})$ -asymmetry will not be maximal at central ($\theta_{CS} = \pi/2$) but rather forward rapidities. Regarding the $M_{\mathcal{Q}\mathcal{Q}}$ -dependence, one can see that the ratio value peaks at roughly 12% for $M_{\mathcal{Q}\mathcal{Q}} \simeq 10 - 12$ GeV, and then fall down as anticipated from Eq. (5.4).

The case of the $\cos(4\phi_{CS})$ -asymmetry is rather different. One can see on Fig. 5.7a that the ratio peaks at $\theta_{CS} = \pi/2$ which corresponds to central rapidity production, and then

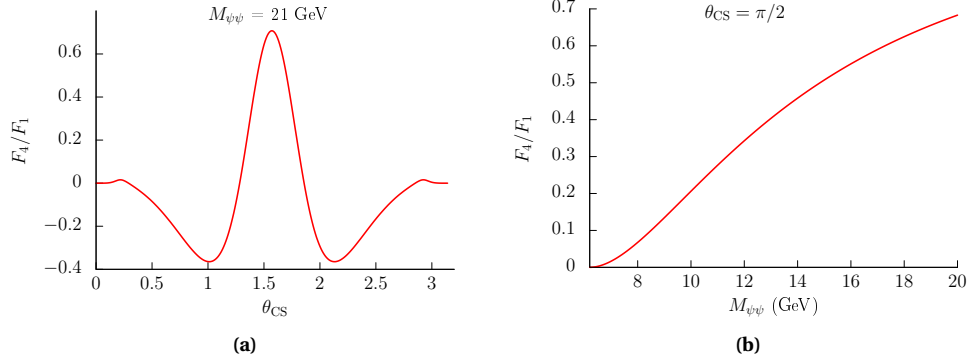


Figure 5.7: Hard-scattering-coefficient ratio F_4/F_1 as a function of θ_{CS} at $M_{\psi\psi} = 21 \text{ GeV}$ (5.7a) and as a function of $M_{\psi\psi}$ at $\theta_{CS} = \pi/2$ (5.7b)

falls down and changes sign, with a new peak in the forward region. The consequence of this sign change is that one should not simply integrate over the whole θ_{CS} -range in order to collect the largest number of events, hoping to get the largest signal. This would result in a cancellation between the central and forward regions, making the resulting asymmetry smaller. It is therefore recommended to split the range in two bins: a central one covering the $|\cos(\theta_{CS})| < 0.25$ values (which roughly corresponds to a rapidity difference range $|\Delta y| < 1$), and a forward one covering the $0.25 < |\cos(\theta_{CS})| < 0.5$ values (which corresponds to a range $1 < |\Delta y| < 2$). We will do so when presenting our results for the azimuthal asymmetries, for both the $\cos(2\phi_{CS})$ and the $\cos(4\phi_{CS})$. Applying these cuts for both asymmetries allows one to compare them in the same kinematical configurations. One can provide predictions for two regions that should be differently affected by the DPS contribution, which is more important in the forward region. Let us note that the ends of the θ_{CS} -range of Figs. 5.6a and 5.7a are out of experimental reach as they correspond to pairs of J/ψ with an extremely large rapidity difference, which grows exponentially with the polar angle. As shown in Eq. (5.2), the ratio F_4/F_1 tends toward 1 with increasing $M_{\psi\psi}$, making the resulting asymmetry larger and larger at high $M_{\psi\psi}$. The ratio peaks at 70% for $M_{\psi\psi} = 21 \text{ GeV}$ which is a representative value for the ATLAS data.

The plots for the azimuthal asymmetries are shown in Fig. 5.8. The asymmetries are computed as function of $P_{\psi\psi_T}$ for $M_{\psi\psi} = 8, 12$ and 21 GeV which are respectively relevant for the LHCb [117], CMS [114] and ATLAS [116] kinematics. The data are plotted up to $M_{\psi\psi}/2$ in order to stay within a reasonable range for TMD factorisation to be valid. Each asymmetry is computed in the previously discussed central and forward rapidity

bins, with the two models used to describe $h_1^{\perp g}$ forming the uncertainty band of the plot with a width $\langle k_T^2 \rangle = 3.3 \text{ GeV}^2$. The plots represent $2\langle \cos(n\phi_{CS}) \rangle$ as the asymmetries are proportional to the bare products of ratios $F_i/F_1 \times \mathcal{C}[w_i \text{TMD}_1 \text{TMD}_2] / \mathcal{C}[f_1^g f_1^g]$, while the $\langle \cos(n\phi_{CS}) \rangle$ observable contains an extra factor 1/2 in its definition³. The vertical axis range is left unchanged between two plots of the same asymmetry in different rapidity bins for comparison purposes.

In line with previous observations, we see that the $\cos(2\phi_{CS})$ asymmetry is larger in the forward region, where it can reach 16% at $M_{\psi\psi} = 12 \text{ GeV}$. It also remains sizeable at higher and lower energies and when using Model 1. In the central region, the asymmetries are significantly smaller in connection with the reduction of the hard-scattering coefficient F_3 around $\theta_{CS} = \pi/2$, with a maximal value of 4%. While the maximal value would be near 24% at $M_{\psi\psi} = 12 \text{ GeV}$ and $\theta_{CS} = \pi/3$, the average value over the θ_{CS} -bin is naturally lower. One would need doubly differential data in both variables to measure an asymmetry approaching the theoretical maximum.

Because of the large size of the F_4 coefficient at large $M_{\psi\psi}$ for $\theta_{CS} \approx \pi$, we obtain as expected large $\cos(4\phi_{CS})$ asymmetries in Fig. 5.8c, reaching 45% at $M_{\psi\psi} = 21 \text{ GeV}$ in the bound-saturating model. The asymmetry remains large at 12 GeV, reaching 20%. Fig. 5.8b displays the expected sign change of the asymmetry as a consequence of the sign change of F_4 between the central and forward region. It remains of reasonable size at 12 and 21 GeV with respective magnitudes of 8 and 20%. Note that the asymmetry remains positive at $M_{\psi\psi} = 8 \text{ GeV}$, although it barely reaches the percent level.

In view of the computed magnitude for various asymmetries in the kinematical ranges explored by LHCb, ATLAS and CMS, we think that an experimental extraction of these asymmetries should be possible from di- J/ψ production data. Such an extraction could also be possible at a fixed-target experiment at the LHC, as well as at RHIC. The High-Luminosity phase to come at the LHC will, in addition to providing many more J/ψ -pair production events, give us enough Υ pairs to study the same asymmetries and TM spectrum in a different mass range. Indeed, although using Gaussian models for the TMDs that factor out the x - and $M_{\mathcal{Q}\mathcal{Q}}$ -dependence already helps us understanding the new observables associated with the TMD formalism and making predictions, our fit of the LHCb data clearly shows that gluons with large TM are needed to describe such data even near the reaction threshold. Such large momenta cannot be intrinsic and call for the inclusion of evolution effects in our modelling of the gluon TMDs describing how the latter evolves with the mass of the observed system. Implementing TMD evolution is therefore the topic of the next chapter, where we will show how the formalism derived in Chapter 2 modi-

³We recall that integrating $\langle \cos(n\phi_{CS}) \rangle$ over some variables corresponds to integrating the numerator and denominator separately.

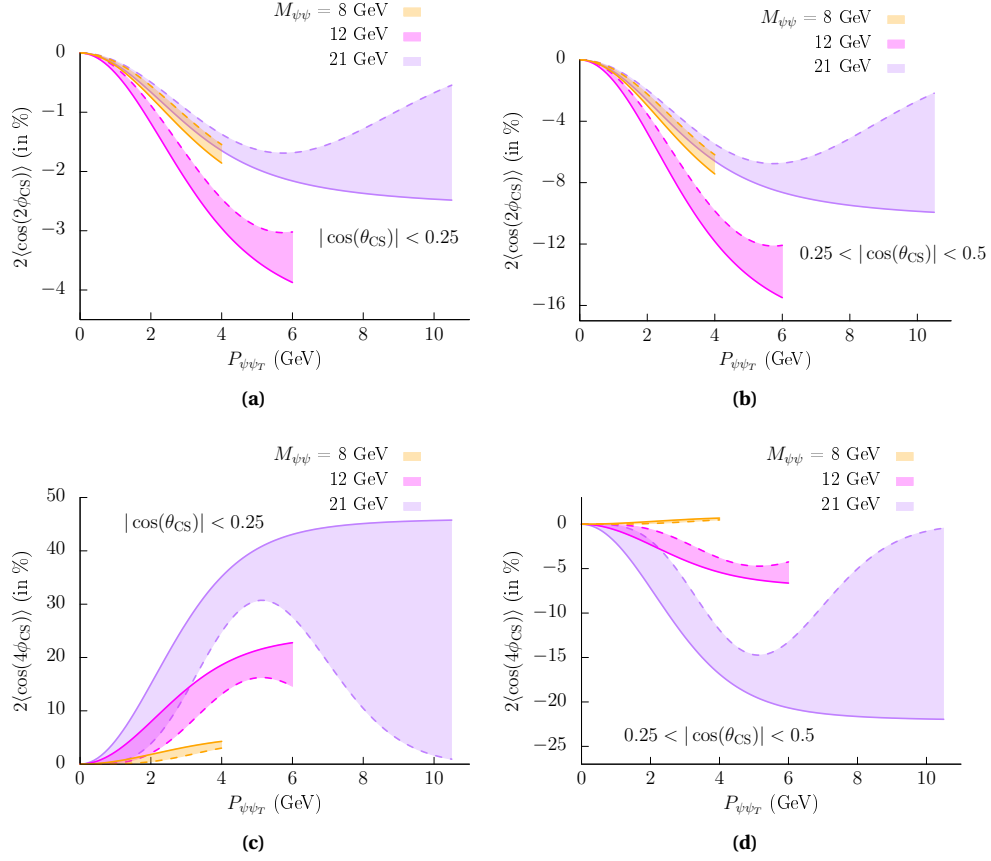


Figure 5.8: $2\langle\cos(n\phi_{CS})\rangle$ for $n = 2,4$ computed for $|\cos(\theta_{CS})| < 0.25$ and for $0.25 < \cos(\theta_{CS}) < 0.5$ for $\langle k_T^2 \rangle = 3.3 \text{ GeV}^2$ for 3 values of $M_{\mathcal{Q}\mathcal{Q}}$ (8, 12 and 21 GeV). The spectra are plotted up to $M_{\mathcal{Q}\mathcal{Q}}/2$. The uncertainty bands result from the use of both models of $h_1^{\perp g}$. The solid line, which shows the largest asymmetries corresponds to the Model 2 (saturation of the positivity bound) and the dashed line to Model 1.

ties the observables studied in this chapter and what can we learn from them in this new context. We will also compute the asymmetries for Y -pair production.

Chapter 6

Predictions for evolved TMDs in J/ψ - and Υ -pair production

In this chapter¹, we will use the formalism detailed in 2.3 in order to improve our model describing the gluon TMDs as well as our theoretical predictions for J/ψ - and Υ -pair production at the LHC. Using the renormalisation group equations as well as the Collins-Soper equation, one can describe the evolution of the gluon TMDs with its factorisation scale μ and its rapidity scale ζ . Indeed, the renormalisation scale used to evaluate the hard-scattering coefficients F_i should be of the order of the hard scale of the process $\mu \sim M_{\mathcal{Q}\mathcal{Q}}$ in order to avoid large logarithms of $\mu/M_{\mathcal{Q}\mathcal{Q}}$. On the other hand, the TMD should be evaluated at its natural scale $\mu \sim \sqrt{\zeta} \sim b_0/b_T$ in order to avoid large logarithms of μb_T and ζb_T^2 , with $b_0 = 2e^{-\gamma_E}$ and b_T the impact parameter conjugate to the transverse momentum of the gluons k_T . It can then be evolved to the hard scale $M_{\mathcal{Q}\mathcal{Q}}$ by solving the mentioned evolution equations. As we have already seen, this introduces a Sudakov factor S_A in the definition of the TMD in impact parameter space. At small scales where the coupling α_s is small enough, it is possible to compute the perturbative Sudakov factor as well as the TMD inputs perturbatively. This reduces the theoretical uncertainties associated with the unknown nature of the gluon TMDs by allowing one to partially compute them from perturbative QCD principles. What is left is the nonperturbative component, which remains to be modelled and extracted from data. In Chapter 2, we introduced some prescriptions in order to keep the perturbative description of the TMDs restricted to its domain of validity and introduced a nonperturbative Sudakov factor S_{NP} which aims at correcting the deviation between the perturbative estimate and the actual behaviour of the TMD.

In the first section, we will introduce a Gaussian model for S_{NP} that will allow us to have a simple picture of the TMD and to connect our results with those of the previous chapter. In the second section, we will examine how each component of the evolution formalism contributes to the different TMD convolutions and how such modifications affect the observables we are interested in. In the last section, we will present our improved predictions for the TM spectrum and azimuthal asymmetries, which then include

¹This chapter is largely based on [140].

the dependence on the hard scale $M_{\mathcal{Q}\mathcal{Q}}$ that does not trivially factorise out of the TMDs anymore. We will compare those predictions with that made using the Gaussian-based models in Chapter 5 and discuss the prospects for future measurements and experimental extractions of information about the gluon TMDs.

6.1 Exploring the nonperturbative component of TMDs with a Gaussian input

As seen in Eq. (2.30), each convolution contains two TMDs perturbatively evaluated at a scale $\mu_b = b_0/b_T^*(b_c(b_T))$ that is bounded between $b_0/b_{T_{\max}}$ and $M_{\mathcal{Q}\mathcal{Q}}$, convoluted with a perturbative Sudakov factor $S_A(b_T^*(b_c(b_T)))$ describing the evolution between the TMD scale μ_b and the hard scale $M_{\mathcal{Q}\mathcal{Q}}$. The remaining ingredient needed is the nonperturbative Sudakov factor $S_{\text{NP}}(b_c(b_T))$ which corrects the perturbative expression at large b_T . It appears inside an exponential $e^{-S_{\text{NP}}}$ and the nonperturbative input for one TMD is $e^{-S_{\text{NP}}/2}$. In contrast with the quark case where some advanced fit have been realised using SIDIS, Drell-Yan and Z^0 production, there is no information available about the nonperturbative component of gluon TMDs. Consequently, any model used can only be an educated guess. A possibility is then to consider the nonperturbative Sudakov factor derived from quark data and re-scale it by a colour factor C_A/C_F . This is a reasonable choice, albeit not very useful to investigate the role of S_{NP} in the TMD observables as it is a finely tuned input.

We rather prefer to use a simple model for S_{NP} that allows for a straightforward study of its impact and that of possible variations over the TM spectrum and azimuthal asymmetries. Some reasonable conditions can be put on the expected behaviour of S_{NP} . First of all, the nonperturbative Sudakov factor should tend toward 0 at small values of b_T . Indeed, the perturbative expression of the TMDs is valid at small scales and should not need corrections to be applied. On the other hand, S_{NP} should be growing larger with increasing b_T in order to make the TMD vanish at infinity and allow the convolutions to converge. In addition, one expects the vanishing of the TMDs to occur within the confinement distance that would be the proton radius. It is usual to take a b_T^2 dependence for the nonperturbative Sudakov factor which respects the conditions cited above. The resulting exponential $e^{-S_{\text{NP}}}$ is then a Gaussian whose width can be tuned in a range extending between $b_{T_{\max}}$ and the proton diameter. One can in addition choose an expression that encapsulates the expected logarithmic dependence of S_{NP} on the scale [141]. Since our natural scale is $M_{\mathcal{Q}\mathcal{Q}}$, the resulting formula we will use reads as follows:

$$S_{\text{NP}}(b_c(b_T)) = A \ln \left(\frac{M_{\mathcal{Q}\mathcal{Q}}}{Q_{\text{NP}}} \right) b_c^2(b_T), \quad Q_{\text{NP}} = 1 \text{ GeV}. \quad (6.1)$$

Q_{NP} is a constant nonperturbative scale. If the renormalisation scale μ is equal to this scale, there is no evolution: S_{NP} cancels and $e^{-S_{\text{NP}}}$ has no effect. Varying A for a fixed scale allows us to vary the width of the Gaussian.

We recall that if one considers a Gaussian f_1^g as in Eq. (5.6), its Fourier transform reads $\tilde{f}_1^g = e^{-\langle k_T^2 \rangle b_T^2 / 4} g(x)$. If we identify the width of the b_T Gaussian with $S_{\text{NP}}/2$, we obtain the relation between A and $\langle k_T^2 \rangle$, which reads: $\langle k_T^2 \rangle = 2A \ln(M_{\mathcal{Q}\mathcal{Q}}/Q_{\text{NP}})$. In this case, the parameter $\langle k_T^2 \rangle$ considered is more intrinsic than the one in the previous chapter, as it excludes the enhancement due to perturbative contributions that we believe to be the reason the value fitted over LHCb data was so large. However it would be too ambitious to consider an extraction of the intrinsic value of $\langle k_T^2 \rangle$ using the formalism developed here as many assumptions need to be made, especially regarding the modelling of S_{NP} . We consider this more of a toy model to test what is to be expected in the observables using reasonable assumptions. As b_T represents the transverse distance between the two gluon fields in the correlator, it is interesting to consider the distance at which the correlation vanishes, *i.e.* when the nonperturbative Sudakov factor becomes approximately zero. We call this limit distance $b_{T_{\text{lim}}}$ such that S_{NP} approximately falls down to 10^{-3} and will use it as a visual indication of the Gaussian width. We will use three different values for the parameter A that are 0.64, 0.16 and 0.04 GeV^2 . The corresponding values of $\langle k_T^2 \rangle$, $b_{T_{\text{lim}}}$ and the radius r in femtometers are reported in Table 6.1 for $M_{\mathcal{Q}\mathcal{Q}} = 12 \text{ GeV}$.

A (GeV^2)	$\langle k_T^2 \rangle$ (GeV^2)	$b_{T_{\text{lim}}}$ (GeV^{-1})	r (fm)
0.64	3.18	2	0.2
0.16	0.80	4	0.4
0.04	0.20	8	0.8

Table 6.1: Values of the parameter A used in Eq. (6.1) for the nonperturbative Sudakov factor, along with the corresponding $b_{T_{\text{lim}}}$, $\langle k_T^2 \rangle$ and r at $M_{\mathcal{Q}\mathcal{Q}} = 12 \text{ GeV}$

The narrowest nonperturbative Sudakov factor we consider is that using $A = 0.64 \text{ GeV}^2$ with a $b_{T_{\text{lim}}}$ of 2 GeV^{-1} . This configuration is very close to the S_{NP} fitted by Aybat and Rogers [50] with a corrected colour factor for gluons. On the other side, the widest S_{NP} we considered is for $A = 0.04 \text{ GeV}^2$ and corresponds to a value of $b_{T_{\text{lim}}}$ equal to 8 GeV^{-1} , which approximately corresponds to the diameter of the proton. We therefore consider this case as an indicative upper limit of the width S_{NP} can reach in a Gaussian model. Fig. 6.1 depicts $e^{-S_{\text{NP}}}$ as a function of b_T . The function is plotted for the three values of A displayed in Table 6.1 with bands corresponding to values of $M_{\mathcal{Q}\mathcal{Q}}$ between 12 and 30 GeV .

Let us note that replacing $e^{S_{\text{NP}}(b_T)}$ by $e^{S_{\text{NP}}(b_c(b_T))}$ has little impact on this figure, one can however see that the exponential does not exactly reach 1 at $b_T = 0$ as $b_c(b_T)$ has a

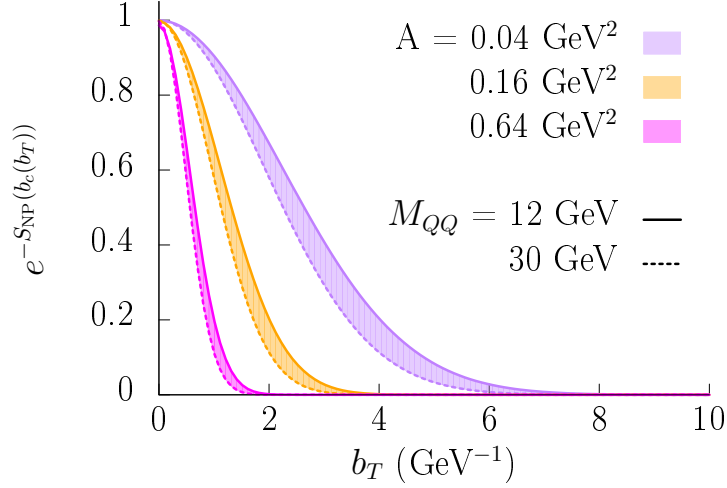


Figure 6.1: $e^{-S_{\text{NP}}}$ from Eq. (6.1) vs b_T for $A = 0.04$ (purple), 0.16 (orange) and 0.64 (magenta) GeV^2 , for values of $M_{Q\bar{Q}}$ ranging from 12 to 30 GeV . The boundaries around the bands depict the exponential at $M_{Q\bar{Q}}=12$ GeV (solid line) and at $M_{Q\bar{Q}}=30$ GeV (dotted line).

lower bound of $b_0/M_{Q\bar{Q}}$.

One could consider a narrower $e^{-S_{\text{NP}}}$, although it should in principle not become too suppressing for b_T values lower than $b_{T_{\text{max}}}$ as the perturbative estimate is supposed to be approximately valid below this limit. If we take $b_{T_{\text{max}}} = 1.5 \text{ GeV}^{-1}$, the nonperturbative Sudakov factor with $b_{T_{\text{lim}}} = 2 \text{ GeV}^{-1}$ is already of order 10^{-2} at $b_{T_{\text{max}}}$. In addition, even though the $M_{Q\bar{Q}}$ -dependence is supposedly universal, f_1^g and $h_1^{\perp g}$ are expected to have different behaviours in the nonperturbative regime. Therefore each may have a different expression for S_{NP} in the most general case. When using the Gaussian S_{NP} model described above, each TMD gives a nonperturbative contribution $e^{-S_{\text{NP}}/2}$ to the integrand of the convolution. These two exponentials therefore combine to give one nonperturbative Sudakov factor whose width is the average of the two individual widths $e^{-(S_{\text{NP}1}+S_{\text{NP}2})/2}$. Considering that we vary the width of S_{NP} within the same range for f_1^g and $h_1^{\perp g}$, the average width is then also included within this range for all convolutions.

In the following section, we will look at the different TMD convolutions in b_T and analyse how each component affects the integrand, and how this affects the total value of the convolution. This will allow us to understand the impact of the different ingredients

of the evolution formalism on the observables.

6.2 TMD convolutions in the evolution formalism

As we have seen in the previous chapter, analysing the TMD convolutions using purely Gaussian TMDs is rather straightforward, allowing us to obtain analytical solutions thanks to the factorisation of the $P_{\mathcal{Q}\mathcal{Q}_T}$ -, $M_{\mathcal{Q}\mathcal{Q}}$ -, x -dependences and the simplicity of the involved functions. When using the formulae for TMDs developed within the evolution formalism, all of these factorisations are lost. The b_c -prescription which ensures that the scale μ_b at which the TMDs are evaluated does not exceed the hard scale, entangles the b_T - and $M_{\mathcal{Q}\mathcal{Q}}$ -dependences inside all of the components of the TMDs. Moreover, the perturbative and nonperturbative Sudakov factors are dependent on the hard scale by definition. The factorisation of the x -dependence is lost because the gluon PDFs, as input of the TMDs, are also evaluated at the scale μ_b . Because of the complexity of the integrand and the presence inside of it of PDFs that cannot be evaluated numerically, all computations need to be done numerically. However this does not prevent us to analyse the role of each factor in the integral.

As can be seen in Eq. (2.20), the first difference in b_T -space between the integrands of the various convolutions is the Bessel function they contain. We will see that such a difference will generate very distinct behaviours of the integrands and associated convolutions. Let us start by studying the convolution of two unpolarised gluon TMDs $\mathcal{C}[f_1^g f_1^g]$. It contains the Bessel function $J_0(b_T P_{\mathcal{Q}\mathcal{Q}_T})$ that is equal to one at $b_T = 0$ and then oscillates progressively towards 0 with increasing b_T . A larger value of $P_{\mathcal{Q}\mathcal{Q}_T}$ will increase the frequency of the oscillations. While the integral from 0 to infinity of $J_0(b_T P_{\mathcal{Q}\mathcal{Q}_T})$ converges toward $1/P_{\mathcal{Q}\mathcal{Q}_T}$, the integral of $b_T J_0(b_T P_{\mathcal{Q}\mathcal{Q}_T})$ does not as the additional b_T amplifies the oscillations in an uncontrolled way. However, several factors can contribute to dampen the large- b_T contribution and make the integral convergent. Moreover, narrowing the integrand in b_T will typically broaden the integral as a function of its conjugate variable $P_{\mathcal{Q}\mathcal{Q}_T}$.

Let us first consider \tilde{f}_1^g . The leading coefficient of its perturbative expansion is the gluon collinear PDF $g(x, \mu)$. In the previous chapter, we evaluated the PDF at the hard scale $M_{\mathcal{Q}\mathcal{Q}}$ without any dependence on any transverse momenta, the latter was additionally factorising out of the convolutions. Now the PDF, as leading-order term describing the gluon TMD, needs to be evaluated at μ_b . As b_T increases, μ_b falls down from its maximal value $M_{\mathcal{Q}\mathcal{Q}}$ toward its minimum $b_0/b_{T_{\max}}$. The PDF follows this trend and therefore falls down with increasing b_T until reaching a minimal value plateau around $b_T = 2 \text{ GeV}^{-1}$. This will contribute to partially dampen the increasing

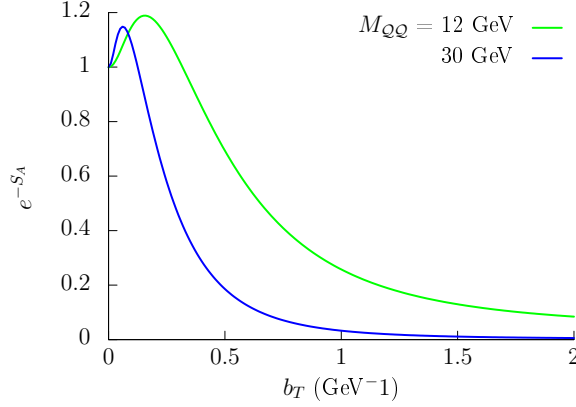


Figure 6.2: The perturbative Sudakov factor e^{-S_A} at NLLA as a function of b_T for $M_{Q\bar{Q}} = 12$ and 30 GeV.

oscillations of $b_T J_0(b_T P_{Q\bar{Q}T})$, and is actually enough to tame them and make the integral convergent. Indeed, although the oscillations resume growing in amplitude past some minimum, they also quickly become centred around 0, making their contribution to the integral less relevant. If we compare $g(x, \mu_b)$ with a Gaussian $g(x, M_{Q\bar{Q}})e^{-(k_T^2)\langle k_T^2 \rangle^{-1} b_T^2/4}$ of width $\langle k_T^2 \rangle = 3.3 \text{ GeV}^2$, we see that the former is narrower in b_T . As mentioned previously, the consequence of this stronger large- b_T suppression is that the integral (and therefore $\mathcal{C}[f_1^g f_1^g]$) will be broader as a function of $P_{Q\bar{Q}T}$, as depicted in Fig. 6.5. The spectrum consequently develops a tail.

We now add the perturbative Sudakov factor S_A in the analysis. As is visible in Fig. 6.2, S_A can quickly suppress large- b_T values but this effect is strongly dependent of the hard scale of the process. At low scales, it is wide and will not contribute much to the widening of the $P_{Q\bar{Q}T}$ -spectrum. On the opposite, S_A will be strongly suppressive at large scales and be the main source of the spectrum widening. Let us note that the slight bump $e^{-S_A} > 1$ at small b_T technically contributes to the $P_{Q\bar{Q}T}$ -widening by enhancing small b_T values, but this is a minor effect. We note that using the NLLA expression for S_A (*i.e.* that includes $\mathcal{O}(\ln(\zeta/\bar{\mu}^2))$ terms in Eq. (2.25)) does not significantly modify the size or shape of TMD observables in comparison with an LLA expression in the cases studied here.

Finally, we investigate the effect the presence of S_{NP} has on the spectrum. At the largest width considered $b_{T_{\text{lim}}} = 8 \text{ GeV}^{-1}$, this effect is rather weak except at very low scales. One can see on Fig. 6.5 that the end of the purple band, that is the narrowest in

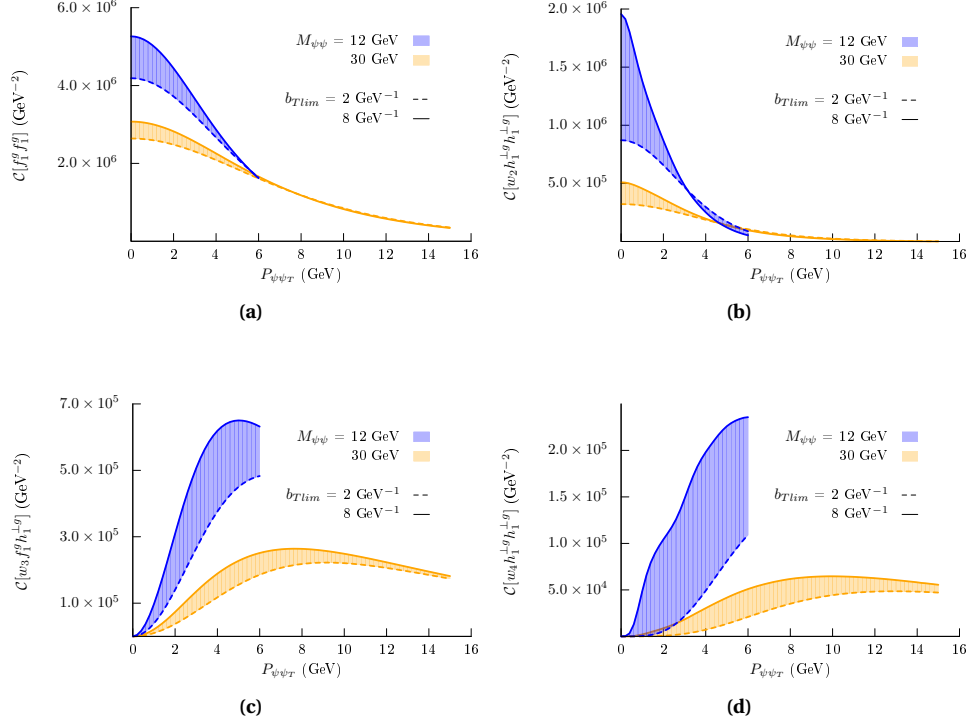


Figure 6.3: The four different TMD convolutions as functions of $P_{\mathcal{Q}\mathcal{Q}_T}$ for centre-of-mass energies $M_{\mathcal{Q}\mathcal{Q}} = 12, 30$ GeV and S_{NP} -widths $b_{T\text{lim}} \in [2; 8]$ GeV $^{-1}$.

$P_{\mathcal{Q}\mathcal{Q}_T}$ (corresponding to the widest $e^{-S_{\text{NP}}}$ in b_T -space), is entirely overlapping with the orange curve computed without any nonperturbative Sudakov factor, showing that the latter already has no effect at $M_{\mathcal{Q}\mathcal{Q}} = 12$ GeV. The other end of the band that corresponds to $b_{T\text{lim}} = 2$ GeV $^{-1}$ is slightly wider in $P_{\mathcal{Q}\mathcal{Q}_T}$, demonstrating a small suppression of large b_T values by S_{NP} . Overall, unless considering very low scales, the nonperturbative Sudakov factor will have a weak influence on $\mathcal{C}[f_1^g f_1^g]$ and therefore on the transverse-momentum spectrum. The convolution $\mathcal{C}[f_1^g f_1^g]$ as a function of $P_{\mathcal{Q}\mathcal{Q}_T}$ is displayed for $M_{\mathcal{Q}\mathcal{Q}} = 12$ and 30 GeV and $b_{T\text{lim}} \in [2; 8]$ GeV $^{-1}$ in Fig. 6.3a.

Regarding the $M_{\mathcal{Q}\mathcal{Q}}$ -dependence, we have already seen that the perturbative Sudakov factor is strongly varying with the hard scale, so it is expected to be the main actor in the variation of $\mathcal{C}[f_1^g f_1^g]$ with $M_{\mathcal{Q}\mathcal{Q}}$. Since the impact of S_{NP} on this convolution is very

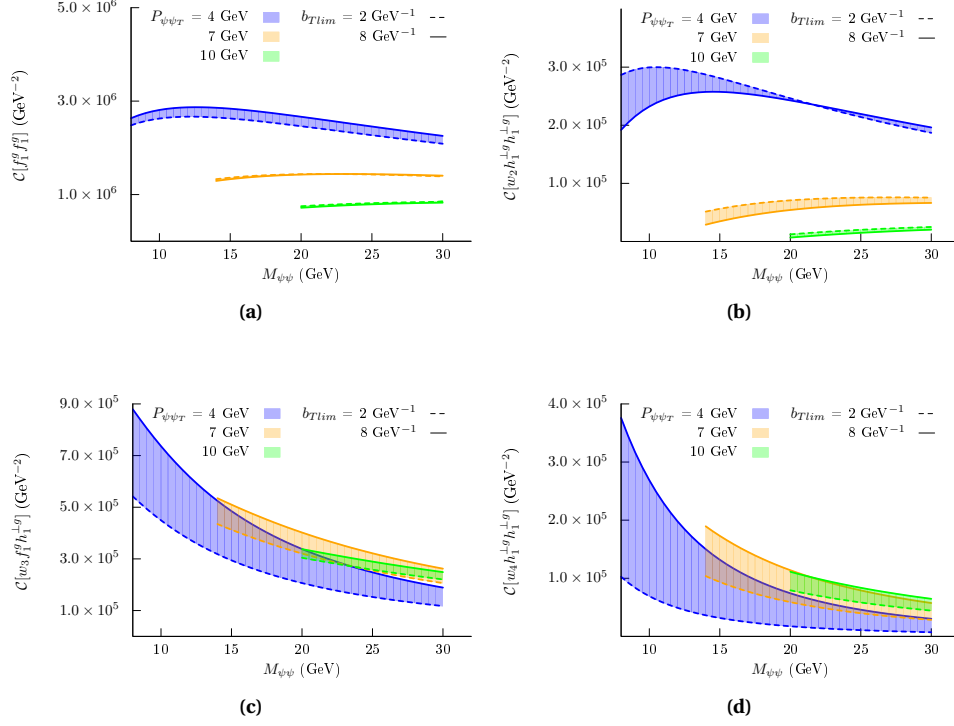


Figure 6.4: The four different TMD convolutions as functions of $M_{\psi\psi}$ for values of the pair transverse momentum $P_{\psi\psi_T} = 4, 7, 10 \text{ GeV}$ and S_{NP} -widths $b_{T_{\text{lim}}} \in [2; 8] \text{ GeV}^{-1}$.

limited and its own variation with $M_{\psi\psi}$ moderate, it will not be a relevant factor in this case. The remaining factor that depends on the hard scale is the gluon collinear PDF. However, since its dependence on the former is also weak, one can safely approximate that the perturbative Sudakov factor is the only element that effectively governs the $M_{\psi\psi}$ -dependence of $\mathcal{C}[f_1^g f_1^g]$. We recall that e^{-S_A} narrows down in b_T with increasing $M_{\psi\psi}$, meaning that the $P_{\psi\psi_T}$ -spectrum will be wider at larger values of $M_{\psi\psi}$. If one considers $\mathcal{C}[f_1^g f_1^g]$ as a function of the hard scale at fixed $P_{\psi\psi_T}$, the convolution will eventually fall down, since a wider transverse-momentum spectrum is also lower in magnitude. This can be seen in Fig. 6.6 where the transverse-momentum spectrum is plotted for $M_{\psi\psi} = 12, 20$ and 30 GeV . The bare convolution as a function of $M_{\psi\psi}$ for fixed $P_{\psi\psi_T} = 4, 7$ and 10 GeV and the considered $b_{T_{\text{lim}}}$ -range is showed in Fig. 6.4a.

Finally, we observe in Fig. 6.7 that the shape of the convolution is almost not affected

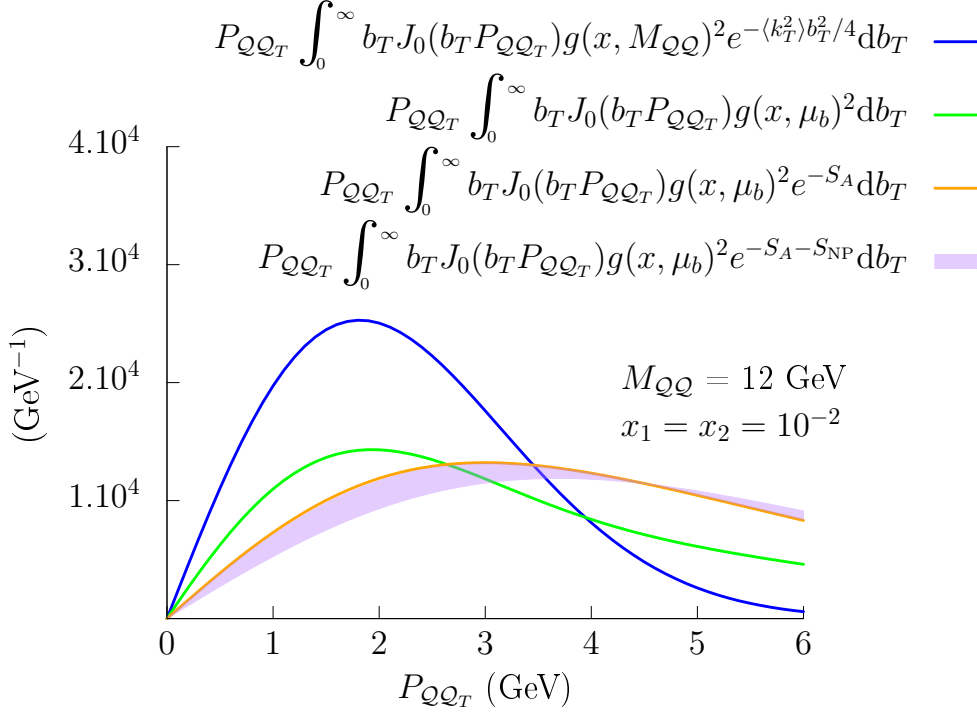


Figure 6.5: Comparison of the transverse-momentum spectrum obtained with the (Fourier-transformed) Gaussian model for f_1^g used in Chapter 5 with $\langle k_T^2 \rangle = 3.3 \text{ GeV}^2$ (blue), the one obtained when replacing \tilde{f}_1^g by its perturbative expression evaluated at μ_b according to Eq. (2.26) (green), when adding the perturbative Sudakov factor S_A (orange), and finally when including S_{NP} with a width $b_{T_{\text{lim}}} \in [2; 8] \text{ GeV}^{-1}$ (purple band).

by variations of the momentum fractions $x_{1,2}$ in the ranges relevant for quarkonium-pair production (typically 10^{-2} – 10^{-3}). The only component depending on them is the gluon PDE. However, only its normalisation is affected by variations of x , not its shape as a function of μ_b . This fact is interesting from an experimental point of view, as it means there is no need for a binning in x of the data in order to look for the trends predicted for the spectrum.

The convolution $\mathcal{C}[w_2 h_1^{\perp g} h_1^{\perp g}]$ only differs from $\mathcal{C}[f_1^g f_1^g]$ by the b_T -space gluon TMDs it contains, namely $\tilde{h}_1^{\perp g}$ instead of \tilde{f}_1^g : indeed, the TMD weight disappears in the b_T -space expression (cf. Eq. (2.20)). The Bessel function that enters the integrand remains J_0 . The variations in behaviour between these two convolutions are therefore

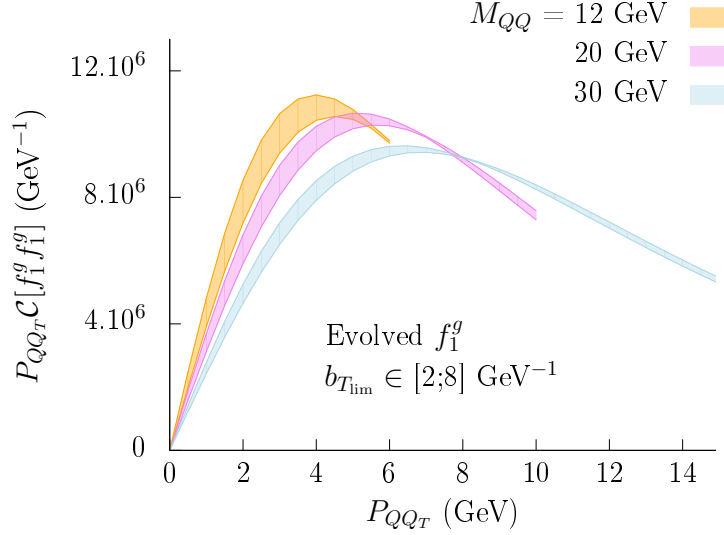


Figure 6.6: The $P_{\mathcal{Q}\mathcal{Q}_T}$ -spectrum using evolved gluon TMDs at $M_{\mathcal{Q}\mathcal{Q}} = 12, 20$ and 30 GeV and $x_1 = x_2 = 10^{-3}$.

solely induced by the difference between the perturbative expressions of both TMDs. We remind from Eq. (2.27) that $\tilde{h}_1^{\perp g}$ emerges as a higher-order in α_s effect where the gluon originates from the splitting of another quark or gluon. It is therefore constructed as the sum of splitting functions, one for each type of parton with the appropriate colour factor. Since $\tilde{h}_1^{\perp g}$ is not a leading-order term in the perturbative expansion, one naturally expects it to be suppressed as well as the associated convolutions. Moreover, since $\alpha_s(\mu_b)$ falls down with increasing scales, it will be a growing function of b_T . This impact on the b_T integrand is limited as the bounds on μ_b consequently set bounds on the variation of α_s . Nevertheless, the presence of α_s leads to a double suppression, first on the overall normalisation of $\tilde{h}_1^{\perp g}$ and second by steepening the downward $P_{\mathcal{Q}\mathcal{Q}_T}$ slope of the convolution that contains it. In addition to this, the splitting function when compared to the bare PDF also contributes to enhance the large b_T values. On the other side, since $\tilde{h}_1^{\perp g}$ receives contributions from all partons and not only gluons, it sees its normalisation typically increased by 20% at $x = 10^{-3}$. However this only partly counters the suppression due to the size of α_s which value is around 0.4 in average over the b_T -range.

In order to assess the influence of each component of $\tilde{h}_1^{\perp g}$ inside $\mathcal{C}[w_2 h_1^{\perp g} h_1^{\perp g}]$, we successively plot in Fig. 6.8 the different components of $\tilde{h}_1^{\perp g}(x_1, b_T) \tilde{h}_1^{\perp g}(x_2, b_T)$ for $x_{1,2} = 10^{-3}$.

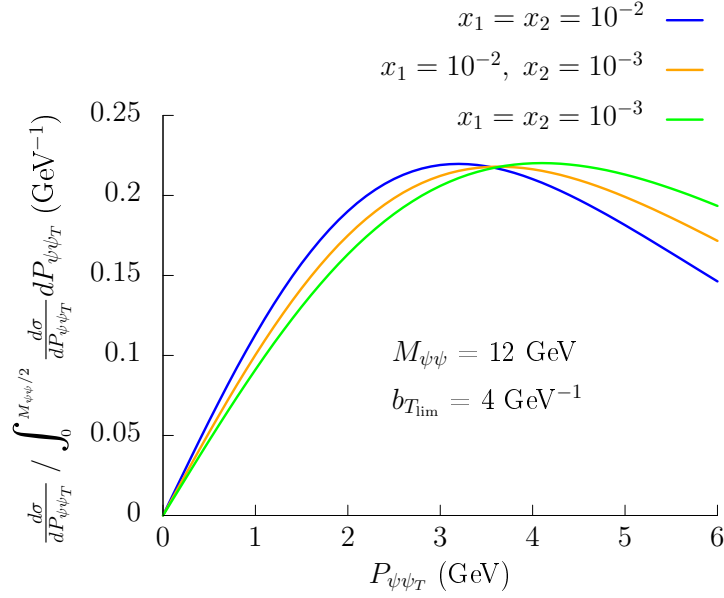


Figure 6.7: The normalised $P_{\mathcal{Q}\mathcal{Q}_T}$ -spectrum for J/ψ -pair production at $M_{\psi\psi} = 12$ GeV and $b_{T\text{lim}} = 4$ GeV $^{-1}$ with $x_{1,2} = 10^{-2}$ or 10^{-3} .

The purple curve depicts the simple product of the two collinear gluon PDFs which corresponds to the input for \tilde{f}_1^g in the $\mathcal{C}[f_1^g f_1^g]$ convolution. As discussed earlier, this product falls as a function of b_T before stabilising when the scale μ_b approaches its boundary limit. Then the blue curve shows the same PDFs inside a splitting function necessary to describe the polarised gluons as emissions from other partons. The curve is now falling much slower with b_T , suppressing large $P_{\mathcal{Q}\mathcal{Q}_T}$ values for the convolution. The addition of the squared coupling constant (pink curve) naturally lowers the normalisation of the function, but also suppresses small b_T values, reinforcing the $P_{\mathcal{Q}\mathcal{Q}_T}$ -narrowing of $\mathcal{C}[w_2 h_1^{\perp g} h_1^{\perp g}]$. Finally, adding the quark contributions to the distribution slightly increases the whole normalisation of the function, as can be seen from the gap between the pink and orange curves. Because of this extra factor of b_T -widening, $\mathcal{C}[w_2 h_1^{\perp g} h_1^{\perp g}]$ will fall faster with $P_{\mathcal{Q}\mathcal{Q}_T}$ than $\mathcal{C}[f_1^g f_1^g]$. It is also more sensitive to the influence of S_{NP} , and will fall faster for a large value of $b_{T\text{lim}}$. The convolution as a function of $P_{\mathcal{Q}\mathcal{Q}_T}$ is shown in Fig. 6.3b.

In a similar way to $\mathcal{C}[f_1^g f_1^g]$, the convolution $\mathcal{C}[w_2 h_1^{\perp g} h_1^{\perp g}]$ as a function of $P_{\mathcal{Q}\mathcal{Q}_T}$ will widen with increasing $M_{\mathcal{Q}\mathcal{Q}}$, due to the narrowing of the perturbative Sudakov factor in b_T -space. The behaviour of $\tilde{h}_1^{\perp g}$ is weakly dependent on $M_{\psi\psi}$ for the ranges con-

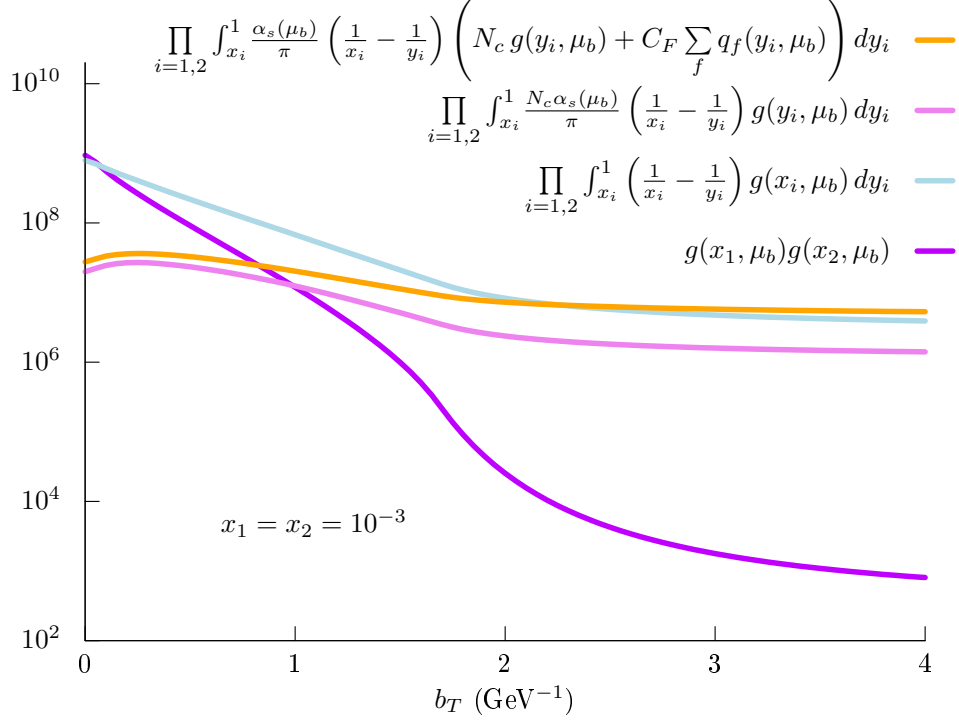


Figure 6.8: The various contributions to the product of the two linearly polarised gluons distributions $\tilde{h}_1^{\perp g}(x_1, \mu_b) \tilde{h}_1^{\perp g}(x_2, \mu_b)$ as a function of b_T for $x_{1,2} = 10^{-3}$.

sidered here, as can be seen in Fig. 6.4b. As for $\mathcal{C}[f_1^g f_1^g]$, the $M_{\mathcal{Q}\mathcal{Q}}$ -dependence mostly comes from the perturbative Sudakov factor in the convolution. Therefore the $M_{\mathcal{Q}\mathcal{Q}}$ -dependence of both convolutions is very similar, making their ratio as a function of $M_{\mathcal{Q}\mathcal{Q}}$ mostly flat. The x -dependence of $\tilde{h}_1^{\perp g}$ is more significant than that of \tilde{f}_1^g : the low b_T values are even more suppressed at $x \sim 10^{-2}$ than at $x \sim 10^{-3}$. However, this dependence does not visibly affect the shape of any observable and only slightly modifies their amplitudes, meaning one can still safely make computations without bothering about x -binning. The results on Fig. 6.8 are also relevant for $\mathcal{C}[w_4 h_1^{\perp g} h_1^{\perp g}]$, although we will see that the different Bessel function entering the convolution changes the way the convolution responds to modulations of the b_T -integrand. We present in Fig. 6.9 the results for $\mathcal{C}[w_3 f_1^g h_1^{\perp g}]$, where one TMD is \tilde{f}_1^g described by the gluon PDF, and the other one is $\tilde{h}_1^{\perp g}$ described by the splitting function. Naturally, the b_T -widening and α_s -suppression appear to be more moderate than for a double occurrence of $\tilde{h}_1^{\perp g}$.

As anticipated, a crucial difference between these two convolutions and $\mathcal{C}[w_3 f_1^g h_1^{\perp g}]$

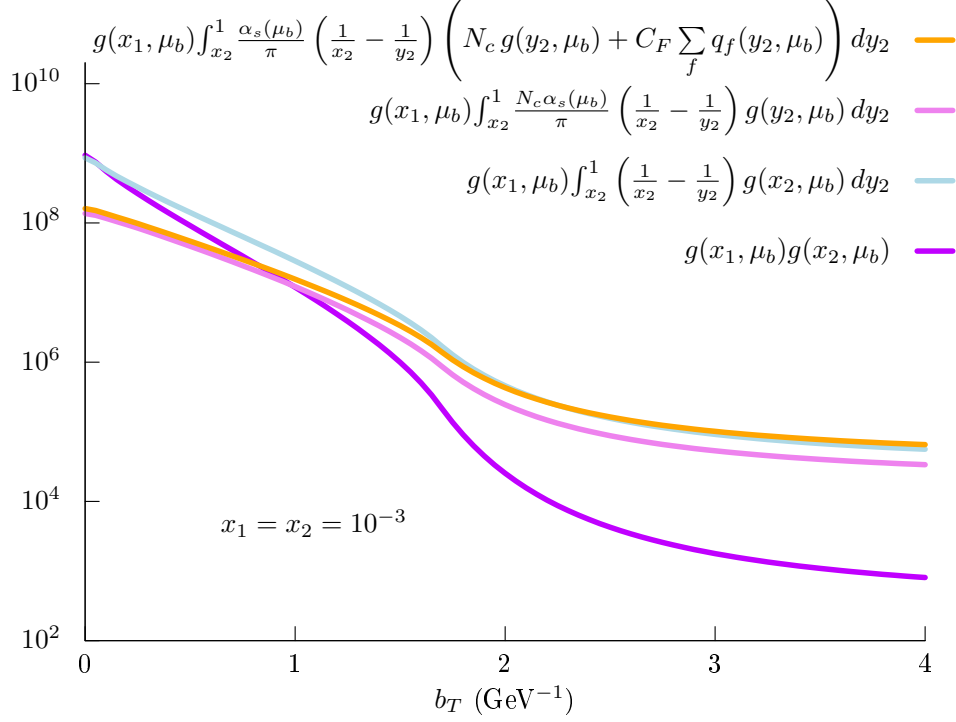


Figure 6.9: The various contributions to the product of the two gluons distributions $\tilde{f}_1^g(x_1, \mu_b) \tilde{h}_1^{\perp g}(x_2, \mu_b)$ as a function of b_T for $x_{1,2} = 10^{-3}$.

is the Bessel function they contain. Instead of J_0 , the b_T -integrand inside $\mathcal{C}[w_3 f_1^g h_1^{\perp g}]$ contains J_2 . This function is not equal to 1 but 0 at $b_T = 0 \text{ GeV}^{-1}$. It then oscillates with a lower frequency than J_0 for a fixed value of $P_{\perp \perp T}$. The consequence is that the b_T -integral will not necessarily profit from the smallest b_T values like it was the case for $\mathcal{C}[f_1^g f_1^g]$ and $\mathcal{C}[w_2 h_1^{\perp g} h_1^{\perp g}]$, but from larger ones instead. Thus the various factors entering the integral will have a different impact on it when compared to the cases studied previously. Indeed, the shape of this convolution as a function of $P_{\perp \perp T}$ is different from that of $\mathcal{C}[f_1^g f_1^g]$ and $\mathcal{C}[w_2 h_1^{\perp g} h_1^{\perp g}]$ that are maximal at $P_{\perp \perp T} = 0$ and then fall down with increasing transverse momentum of the final state. Instead, at low $P_{\perp \perp T}$, the first oscillation in b_T -space of J_2 will be so wide that it will not have time to grow enough before being suppressed by the other elements of the integrand. At larger values of $P_{\perp \perp T}$, the frequency of the oscillations is higher, the latter can consequently contribute maximally to the integral, allowing the value of the convolution to grow up to a maximum. Then, at larger $P_{\perp \perp T}$, an increasing number of oscillations whose central

value progressively tends toward 0 are contributing to the non-suppressed b_T -range, making the convolution tend toward 0 as well, in a way similar to that of $\mathcal{C}[f_1^g f_1^g]$ and $\mathcal{C}[w_2 h_1^{\perp g} h_1^{\perp g}]$. Therefore $\mathcal{C}[w_3 f_1^g h_1^{\perp g}]$ as a function of $P_{\mathcal{Q}\mathcal{Q}T}$ will grow up a maximum before decreasing again and tend toward 0, as displayed in Fig. 6.3c. It is important to note that, at equal value of $P_{\mathcal{Q}\mathcal{Q}T}$, oscillations in the b_T -integrand of $\mathcal{C}[w_3 f_1^g h_1^{\perp g}]$ are of lower frequency than that inside convolutions containing J_0 . Therefore, even though the convolution does decrease at large $P_{\mathcal{Q}\mathcal{Q}T}$, its fall will be slower than that of $\mathcal{C}[f_1^g f_1^g]$ and $\mathcal{C}[w_2 h_1^{\perp g} h_1^{\perp g}]$. The logical consequence is that the ratio $\mathcal{C}[w_3 f_1^g h_1^{\perp g}]/\mathcal{C}[f_1^g f_1^g]$ that enters the definition of the $\cos(2\phi)$ -asymmetry is always a growing function of $P_{\mathcal{Q}\mathcal{Q}T}$, and so is the asymmetry. This does not mean that the asymmetry can eventually become larger than 100%, as too large values of $P_{\mathcal{Q}\mathcal{Q}T}$ for a given value of $M_{\mathcal{Q}\mathcal{Q}}$ would reach the limit of validity for a TMD formalism. We notice that since the convolution is sensitive to larger b_T -values even at higher $P_{\mathcal{Q}\mathcal{Q}T}$, the uncertainty band associated with the varying width of S_{NP} is wider than that of $\mathcal{C}[f_1^g f_1^g]$ and does not shrink as fast as it does for $\mathcal{C}[w_2 h_1^{\perp g} h_1^{\perp g}]$.

Regarding the $M_{\mathcal{Q}\mathcal{Q}}$ -dependence of the convolution, we know that the main factor of the evolution is the perturbative Sudakov factor that becomes narrower in b_T when increasing $M_{\mathcal{Q}\mathcal{Q}}$. As the main contribution to $\mathcal{C}[f_1^g f_1^g]$ comes from the lowest b_T values that are the least affected by the large- b_T suppression of S_A , we observe that it is almost unaffected by variations of $M_{\mathcal{Q}\mathcal{Q}}$ at fixed $P_{\mathcal{Q}\mathcal{Q}T}$. On the other hand, because the main contribution to $\mathcal{C}[w_3 f_1^g h_1^{\perp g}]$ comes from larger values of b_T than $\mathcal{C}[f_1^g f_1^g]$, the former will therefore decrease as $M_{\mathcal{Q}\mathcal{Q}}$ increases due to the effect of the perturbative Sudakov factor (cf. Fig. 6.4c). The ratio of the two convolutions will then decrease as well. However, the $M_{\mathcal{Q}\mathcal{Q}}$ dynamics of $\cos(2\phi)$ are also influenced by the hard-scattering coefficient F_3 that is varying with $M_{\mathcal{Q}\mathcal{Q}}$. While the $P_{\mathcal{Q}\mathcal{Q}T}$ dependence of the asymmetry can be assessed from the convolutions only, its $M_{\mathcal{Q}\mathcal{Q}}$ dependence is defined by both the convolution and hard-scattering coefficient ratios.

We finally investigate the behaviour of the last convolution $\mathcal{C}[w_4 h_1^{\perp g} h_1^{\perp g}]$. This convolution contains the Bessel function J_4 , that oscillates in a similar way to J_2 but with a lower frequency. For this reason and the fact that $\mathcal{C}[w_4 h_1^{\perp g} h_1^{\perp g}]$ contains $\tilde{h}_1^{\perp g}$ twice in its integrand, the value of the integral stems from even larger b_T values. Therefore most of the trends observed in $\mathcal{C}[w_3 f_1^g h_1^{\perp g}]$ apply in a more pronounced way to $\mathcal{C}[w_4 h_1^{\perp g} h_1^{\perp g}]$. It is wider in $P_{\mathcal{Q}\mathcal{Q}T}$, meaning that the $\cos(4\phi)$ asymmetry will also grow with increasing transverse momentum, albeit slower than the $\cos(2\phi)$ one since the growth of the $\mathcal{C}[w_4 h_1^{\perp g} h_1^{\perp g}]$ convolution is slower than that of $\mathcal{C}[w_3 f_1^g h_1^{\perp g}]$. The uncertainty band associated with the width of S_{NP} is also wider than that of the other convolutions. Its fall with $M_{\mathcal{Q}\mathcal{Q}}$ is more pronounced due to an increased sensitivity of the integrand to

the large- b_T suppression by S_A . Its overall magnitude also suffers from the double α_s suppression of both polarised gluon TMDs. The convolution as a function of $P_{\mathcal{Q}\mathcal{Q}_T}$ and $M_{\mathcal{Q}\mathcal{Q}}$ is showed in Fig. 6.3d and 6.4d respectively.

Let us note that since both gluon TMDs may also behave differently in the nonperturbative region, one should allow for a different width of the nonperturbative Sudakov factor for each of them. The consequence would be that, when computing an asymmetry, the convolution in the numerator of the ratio and the $\mathcal{C}[f_1^g f_1^g]$ convolution in the denominator should be allowed to have a different width for S_{NP} . One would then expect to obtain an increased uncertainty band due to the additional variable width in the ratio. In practice, we observe that $\mathcal{C}[f_1^g f_1^g]$ varies little with the width of S_{NP} (cf. Fig. 6.3a). The only area of phase space where $\mathcal{C}[f_1^g f_1^g]$ varies significantly with A is at low $M_{\mathcal{Q}\mathcal{Q}}$ and low $P_{\mathcal{Q}\mathcal{Q}_T}$ where large b_T values are the most relevant for this convolution. However, since $\mathcal{C}[w_3 f_1^g h_1^{\perp g}]$ and $\mathcal{C}[w_4 h_1^{\perp g} h_1^{\perp g}]$ are growing functions of $P_{\mathcal{Q}\mathcal{Q}_T}$ starting at 0, they remain rather small in this area. The widening of the uncertainty band due to this extra varying width can therefore be neglected. We emphasise that if one were to consider modifications of the $P_{\mathcal{Q}\mathcal{Q}_T}$ -spectrum generated by $\mathcal{C}[w_2 h_1^{\perp g} h_1^{\perp g}]^2$, it would be necessary to use different widths for the two convolutions. Indeed, $\mathcal{C}[w_2 h_1^{\perp g} h_1^{\perp g}]$ behaves in a way similar to $\mathcal{C}[f_1^g f_1^g]$; its largest magnitude and the S_{NP} -related variation are found at low $P_{\mathcal{Q}\mathcal{Q}_T}$. Thus the uncertainty of the $\mathcal{C}[w_2 h_1^{\perp g} h_1^{\perp g}]/\mathcal{C}[f_1^g f_1^g]$ ratio would be much larger than when applying identical values of A to both convolutions and the latter method would significantly underestimate the uncertainty. Such a remark is relevant for a process like low-energy single quarkonium production where the transverse momentum of the detected particle is small and the F_2 coefficient is sizeable.

Now that we understand how the different elements of the TMD evolution formalism influence the magnitude and behaviour of the convolutions, we can combine the latter with their respective hard-scattering coefficients, computed as explained in Chapter 2, and provide improved predictions for the transverse-momentum spectrum as well as the azimuthal asymmetries. In addition to J/ψ -pair production, we will also provide plots for Υ -pair production, as a sufficient number of events could be recorded in the future high-luminosity phase of the LHC.

6.3 Improved predictions for the TMD observables

Now that we have computed the various TMD convolutions entering the quarkonium-pair production cross section, we are able to evaluate the observables considered in Chap-

²here we do not since the associated hard coefficient F_2 is very small

ter 5 using the Gaussian TMD model, but with evolution effects taken into account in the estimations. We remind that one also needs to make several assumptions, especially about the nonperturbative component of the TMDs that remains unknown, and that other sources of uncertainty would need to be accounted for in a more complete calculation. The interest of this procedure is to minimise the uncertainty due to our lack of knowledge of nonperturbative QCD by evaluating perturbatively the TMDs in the relevant validity range of distance/momentum. Although the model can be refined, it is already interesting to analyse how the inclusion of evolution effects modifies our previous predictions.

6.3.1 The transverse-momentum spectrum in J/ψ -pair production

We will first consider the normalised transverse-momentum spectrum ($P_{\mathcal{Q}\mathcal{Q}_T}$) for di- J/ψ production in the LHCb setup previously used to fit an effective value of $\langle k_T^2 \rangle$ using the experimental data. In Fig. 6.10, we compare the normalised spectrum obtained when using the Gaussian TMD model with a width $\langle k_T^2 \rangle = 3.3 \pm 0.8 \text{ GeV}^2$ and the evolved TMD model with $b_{T_{\text{lim}}} \in [2; 8] \text{ GeV}^{-1}$. We superpose the normalised LHCb data for di- J/ψ production from which the estimated DPS contribution has been subtracted. For an estimated average $M_{\mathcal{Q}\mathcal{Q}}$ of 8 GeV, the plots and data are shown for $P_{\psi\psi_T}$ up to $M_{\psi\psi}/2$.

One can see that the uncertainty band associated with the width of S_{NP} is rather narrow when considering the normalised spectrum, yet it does reasonably fit the data points. Since the range of widths covered by the band correspond to intrinsic values of $\langle k_T^2 \rangle$ ranging from the sub-GeV to the GeV region, we note that it is not possible to constraint the value of the intrinsic $\langle k_T^2 \rangle$ in S_{NP} of the improved model using these data. One would need to considerably reduce the uncertainty on the data in order to be able to fit the width of S_{NP} , and take into account all the theoretical uncertainties as well. In this case, the interest in comparing the model to the data is to show that one can now provide a curve that fits the points using a realistic sub-GeV value of $\langle k_T^2 \rangle$. This was not possible with the Gaussian model which was *de facto* encapsulating perturbative contributions, hence the large extracted $\langle k_T^2 \rangle$. Moreover, we see that regardless of the S_{NP} width, the transverse-momentum spectrum is wider when using evolved TMDs, as it develops a perturbative tail at large $P_{\psi\psi_T}$. We further note that larger values of $b_{T_{\text{lim}}}$ generate narrower $P_{\mathcal{Q}\mathcal{Q}_T}$ -spectra.

6.3.2 Azimuthal asymmetries

In this last section, we discuss the computations of the TMD convolutions in the evolution formalism. Now, as we did in the previous chapter with the Gaussian model, we can combine them with their respective hard-scattering coefficients in order to evaluate the

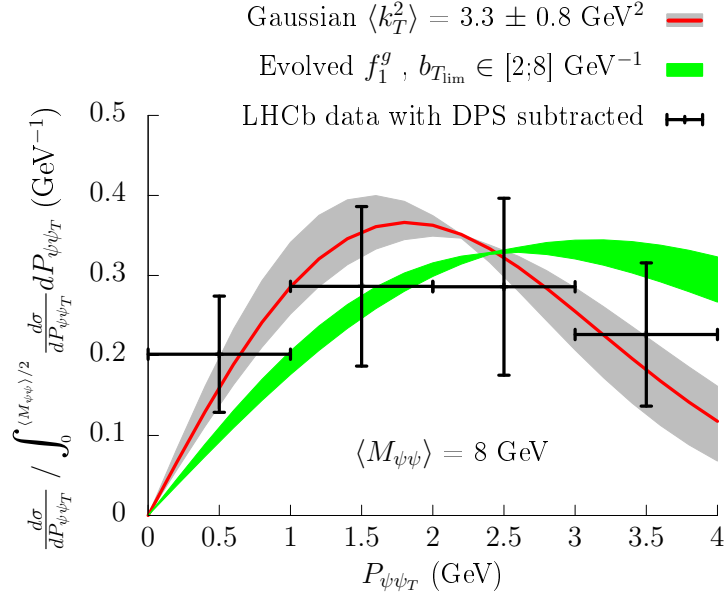


Figure 6.10: The *normalised* $P_{\mathcal{Q}\mathcal{Q}_T}$ -spectrum for J/ψ -pair production at $M_{\psi\psi} = 8 \text{ GeV}$ using two models of the gluon TMDs. The first curve is the Gaussian Ansatz with $\langle k_T^2 \rangle = 3.3 \pm 0.8 \text{ GeV}^2$ fitted to the LHCb data [133] (the red curve shows the central value and the gray band the associated uncertainty). The second curve is the result of our computation using TMD evolution. The green band results from the uncertainty on the b_T width of the nonperturbative Sudakov factor S_{NP} . The estimated DPS contribution has been subtracted from the LHCb data (black crosses) which were also normalised over the interval after subtraction.

magnitude and shape of the $\langle \cos(2, 4\phi_{\text{CS}}) \rangle$ observables. While the convolution ratios in the Gaussian model using a positivity bound-saturating $h_1^{\perp g}$ were approaching 100%, we will see that this is not the case when considering evolution.

As expected, the asymmetries undergo a suppression in comparison to the previous idealistic model. In particular, the b_T -space polarised gluon TMD $\tilde{h}_1^{\perp g}$ is α_s -suppressed in its perturbative region, which particularly affects the $\cos(4\phi)$ -asymmetry. On the other side, we have seen that the $\mathcal{C}[w_3 f_1^g h_1^{\perp g}]$ and $\mathcal{C}[w_4 h_1^{\perp g} h_1^{\perp g}]$ convolutions, by the nature of the TMD weights they contain in k_T -space, encapsulate Bessel functions that make them grow and then fall slower with $P_{\mathcal{Q}\mathcal{Q}_T}$ than $\mathcal{C}[f_1^g f_1^g]$. This $P_{\mathcal{Q}\mathcal{Q}_T}$ widening renders the ratio in the definition of the asymmetries a continuously growing function of $P_{\mathcal{Q}\mathcal{Q}_T}$. As the whole $P_{\mathcal{Q}\mathcal{Q}_T}$ dependence of the asymmetries comes from the convolutions, the

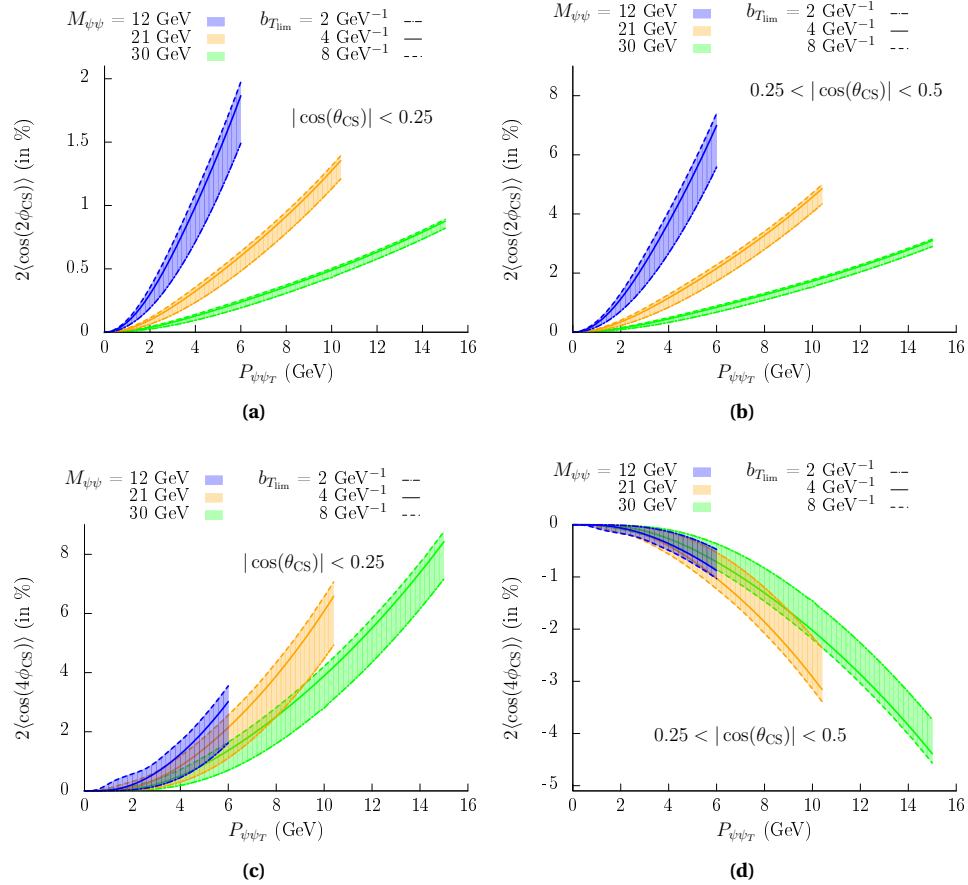


Figure 6.11: The azimuthal asymmetries for di- J/ψ production as functions of $P_{\mathcal{Q}\mathcal{Q}_T}$. The different plots show $2\langle\cos(2\phi_{CS})\rangle$ (a,b) and $2\langle\cos(4\phi_{CS})\rangle$ (c,d), at $|\cos(\theta_{CS})| < 0.25$ (a,c) and at $0.25 < |\cos(\theta_{CS})| < 0.5$ (b,d). Results are presented for $M_{\psi\psi} = 12, 21$ and 30 GeV, and for $b_{Tlim} = 2, 4$ and 8 GeV^{-1} .

hard-scattering coefficients will only affect the normalisation of these asymmetries. We present in Fig. 6.11 the computed asymmetries for J/ψ -pair production as function of $P_{\psi\psi_T}$ in the central and forward/backward rapidity ranges (in a similar fashion as in Fig. 5.8) for $M_{\psi\psi} = 12, 21$ and 30 GeV with the usual S_{NP} -related uncertainty band.

We see that the size of the asymmetries is considerably reduced, with maximal values around 8% for $2\langle\cos(2\phi_{CS})\rangle$ in the forward range and $2\langle\cos(4\phi_{CS})\rangle$ in the cen-

tral range. In comparison, these asymmetries were reaching around 16% and 45% in the Gaussian bound-saturating model. The double $\tilde{h}_1^{\perp g}$ -suppression which impacts $\mathcal{C}[w_4 h_1^{\perp g} h_1^{\perp g}]$ then makes $\langle \cos(4\phi_{CS}) \rangle$ comparable to $\langle \cos(2\phi_{CS}) \rangle$, as the dominance of the hard-scattering coefficient F_4 is compensated by the $\tilde{h}_1^{\perp g}$ -suppression. We nonetheless emphasise that these magnitudes remain sizeable and maintain the hope of measuring asymmetries in the di- J/ψ data. The inclusion of the quark component inside the perturbative expansion of $\tilde{h}_1^{\perp g}$ significantly enhances the size of the asymmetries, in particular $\langle \cos(4\phi_{CS}) \rangle$ which would be several units lower if this contribution was neglected. We notice that the results at $b_{T\text{lim}} = 4 \text{ GeV}^{-1}$ are quite close to those at $b_{T\text{lim}} = 8 \text{ GeV}^{-1}$, showing that extending the b_T -range of S_{NP} does not bring any significant modification to the computed asymmetries, even at low $M_{\psi\psi}$. Since the $\mathcal{C}[w_3 f_1^g h_1^{\perp g}]$ convolution reaches higher magnitudes at low $M_{\psi\psi}$ and since the F_3 coefficient peaks around 12 GeV, the curve at $M_{\psi\psi} = 12 \text{ GeV}$ naturally reaches the highest value. While the $\mathcal{C}[w_4 h_1^{\perp g} h_1^{\perp g}]$ convolution also substantially decreases with $M_{\psi\psi}$, we know that its associated hard-scattering coefficient F_4 conversely grows with $M_{\psi\psi}$, up to the limit $F_4/F_1 = 1$. One can see that $\langle \cos(4\phi_{CS}) \rangle$ seems to be slightly lower for higher values of $M_{\psi\psi}$, as the fall of the convolution is mostly balanced by the rise of the hard-scattering coefficient. However, because considering higher scales allows one to compute TMD convolutions over an extended $P_{\mathcal{Q}\mathcal{Q}T}$ -range, and since the asymmetry only grows with the transverse momentum, it is at higher masses that we obtain the largest magnitude for the asymmetry.

These trends are clearly visible in Fig. 6.12, where the $\langle \cos(2\phi_{CS}) \rangle$ observable depicted in Fig. 6.12a and 6.12b quickly falls with $M_{\psi\psi}$ while $\langle \cos(4\phi_{CS}) \rangle$ showed in Fig. 6.12c and 6.12d exhibits a much weaker slope.

We finally present the asymmetries computed for Υ -pair production. The main difference in the computations for this process when compared with di- J/ψ production is the mass of the final state meson $M_\Upsilon \simeq 9.46 \text{ GeV}$ since we approximate the b -quark mass to be $m_b = M_\Upsilon/2$. The nonrelativistic wave function at the origin also differs in value, but it cancels in the ratios considered here. This reaction typically occurs at higher scale, the threshold being around 19 GeV. In Fig. 6.13, the asymmetries as functions of $P_{\Upsilon\Upsilon T}$ are depicted in a similar fashion as the previous ones but for higher $M_{\mathcal{Q}\mathcal{Q}}$, namely $M_{\Upsilon\Upsilon} = 30, 40$ and 50 GeV .

The first observation we make is that the uncertainty band from varying the width of S_{NP} are thinner than in the J/ψ case. This is an expected consequence of the higher scales considered that strengthen the large- b_T suppressive power of the perturbative Sudakov factor. This makes S_{NP} less relevant for the value of the convolutions. We also see that the plots corresponding to different values of $M_{\Upsilon\Upsilon}$ are closer to each other than

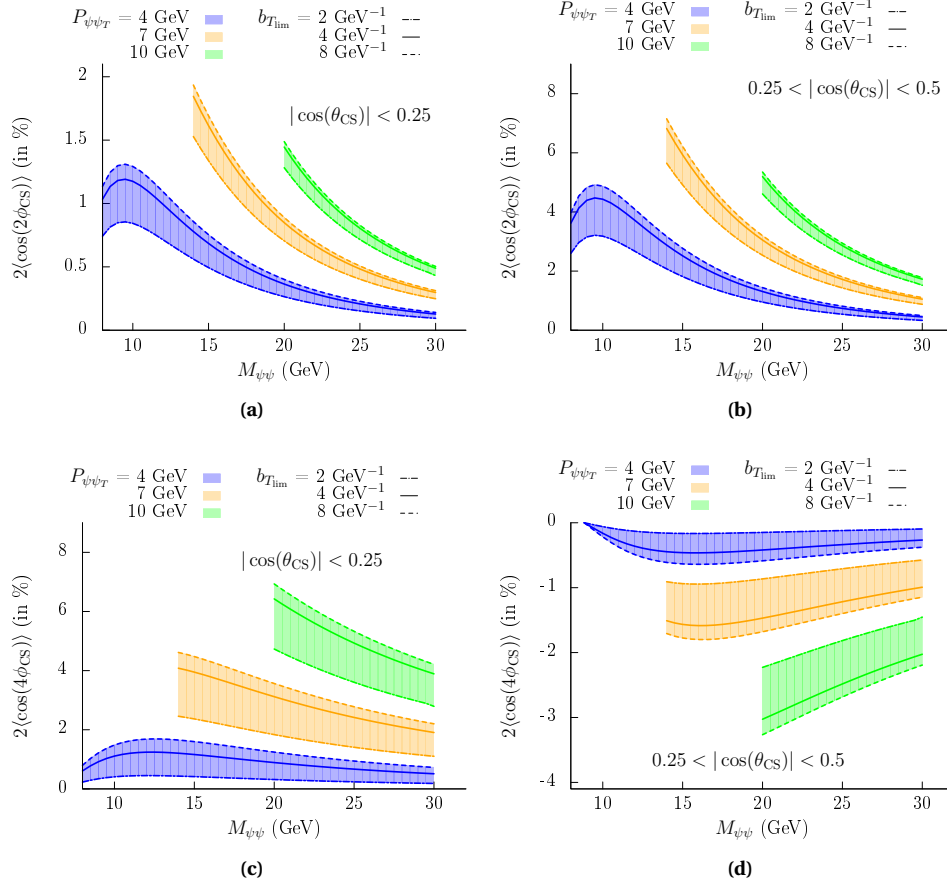


Figure 6.12: The azimuthal asymmetries for di- J/ψ production as functions of $M_{\psi\psi}$. The different plots show $2\langle\cos(2\phi_{CS})\rangle$ (a,b) and $2\langle\cos(4\phi_{CS})\rangle$ (c,d), at $|\cos(\theta_{CS})| < 0.25$ (a,c) and at $0.25 < |\cos(\theta_{CS})| < 0.5$ (b,d). Results are presented for $P_{\mathcal{Q}\mathcal{Q}_T} = 4, 7$ and 10 GeV, and for $b_{Tlim} = 2, 4$ and 8 GeV $^{-1}$.

in the di- J/ψ case, despite the gap between the considered values being relatively larger. The main reason is that the convolutions fall slower at large $M_{\mathcal{Q}\mathcal{Q}}$, a trend which is visible in Fig. 6.4. Moreover, the hard-scattering coefficients for quarkonium-pair production vary slower with $M_{\mathcal{Q}\mathcal{Q}}$ because of the greater size of $M_{\mathcal{Q}}$. This effect profits the size of $\langle\cos(2\phi_{CS})\rangle$ at large $M_{\Upsilon\Upsilon}$, as the coefficient F_3 does not rise and fall as fast as in J/ψ -pair production after reaching its peak value, in this case around 40 GeV. Due to the higher scale under consideration, one can extend the TMD validity range further, up to $P_{\Upsilon\Upsilon_T}$

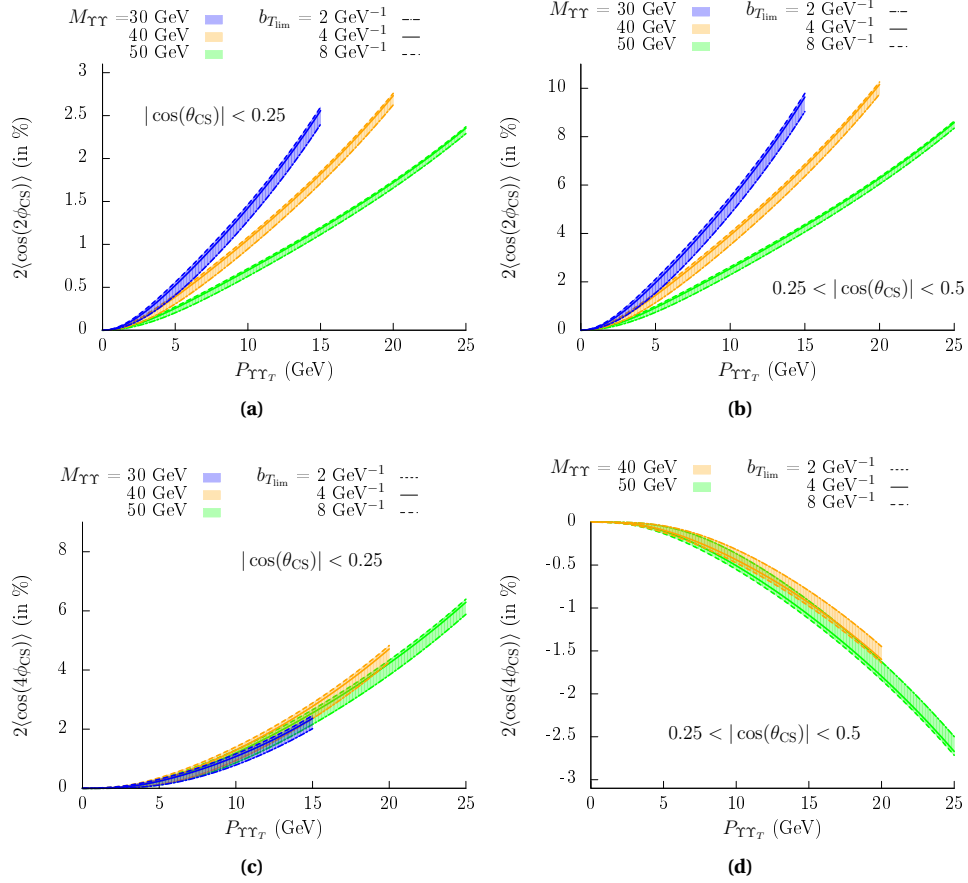


Figure 6.13: The azimuthal asymmetries for di- Υ production as functions of $P_{\mathcal{Q}\mathcal{Q}T}$. The different plots show $2\langle\cos(2\phi_{CS})\rangle$ (top) and $2\langle\cos(4\phi_{CS})\rangle$ (bottom), at $|\cos(\theta_{CS})| < 0.25$ (left) and at $0.25 < |\cos(\theta_{CS})| < 0.5$ (right). Results are presented for $M_{\Upsilon\Upsilon} = 30, 40$ and 50 GeV, and for $b_{T_{lim}} = 2, 4$ and 8 GeV $^{-1}$. Results for $M_{\Upsilon\Upsilon} = 30$ GeV are not included in (d) as they are below percent level.

$= 25$ GeV, allowing the asymmetry to grow further. This allows the $\cos(2\phi)$ -asymmetry to reach slightly larger values than in the J/ψ case, exceeding 10 % at forward θ_{CS} as can be seen in Fig. 6.13b. On the other hand, the slower growth of the hard-scattering coefficients with $M_{\Upsilon\Upsilon}$ reduces the size of $\langle\cos(4\phi_{CS})\rangle$ which was taking advantage of the increase of F_4 with the energy. One sees that the curves in Fig. 6.13c and 6.13d are mostly overlapping, the slower growth of F_4 being compensated by the slower fall of

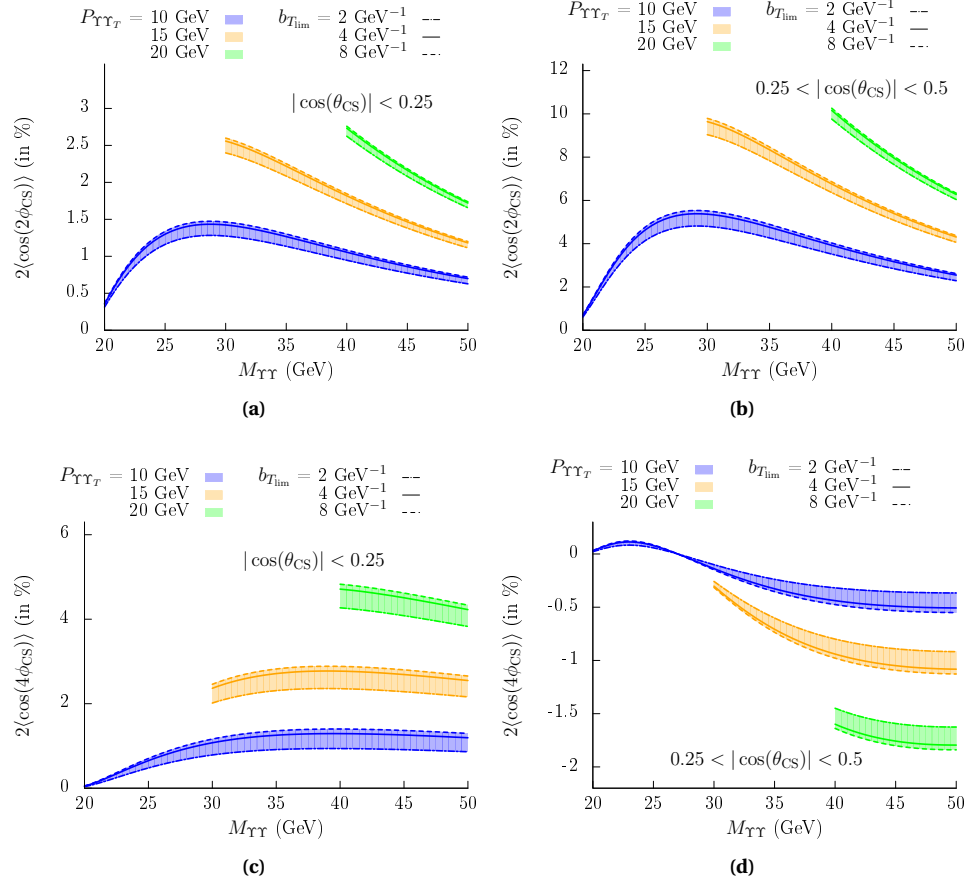


Figure 6.14: The azimuthal asymmetries for di- Υ production as functions of $M_{\psi\psi}$. The different plots show $2\langle\cos(2\phi_{CS})\rangle$ (a,b) and $2\langle\cos(4\phi_{CS})\rangle$ (c,d), at $|\cos(\theta_{CS})| < 0.25$ (a,c) and at $0.25 < |\cos(\theta_{CS})| < 0.5$ (b,d). Results are presented for $P_{\mathcal{Q}\mathcal{Q}_T} = 10, 15$ and 20 GeV, and for $b_{Tlim} = 2, 4$ and 8 GeV $^{-1}$.

$\mathcal{E}[w_4 h_1^{\perp g} h_1^{\perp g}]$. Therefore, while the asymmetry appears a bit smaller in the Υ case, it remains quite sizeable, reaching 6 % at $M_{\Upsilon\Upsilon} = 50$ GeV.

When plotting the asymmetries as functions of $M_{\Upsilon\Upsilon}$ (cf. Fig. 6.14), we indeed observe that the slopes of the curves are much weaker than in the J/ψ case. One can even notice the progressive sign change of $\langle\cos(4\phi_{CS})\rangle$ at low transverse momentum and forward rapidities, as the covered phase space sees the hard-scattering coefficient change sign

with growing $M_{\Upsilon\Upsilon}$.

In conclusion of this chapter, we have analysed in detail the way the gluon TMD-evolution formalism, which we introduced in Chapter 2, impacts the TMD observables in quarkonium-pair production. We have implemented a Gaussian nonperturbative Sudakov factor with a varying width between reasonable bounds in order to understand how the nonperturbative component of TMDs affects the various convolutions. We have also investigated the role of the perturbative elements inside each convolution. We have finally presented our improved results and compared them with those of Chapter 5, in order to assess the effect of evolution on the observables. The conclusions of the analysis using Gaussian TMDs drawn in the previous chapter are modified by TMD evolution. The transverse-momentum spectrum is widened and the asymmetries grow with $P_{\mathcal{Q}\mathcal{Q}_T}$. The asymmetries are significantly smaller as h_1^{1g} is α_s suppressed, and the $\cos(2\phi_{CS})$ and $\cos(4\phi_{CS})$ asymmetries become comparable in size as the latter is doubly suppressed. Finally, we have added results for Υ -pair production as such a process presents interesting advantages on the theoretical side and more data is expected to be recorded in the future high-luminosity phase at the LHC. In addition, we saw that the impact of S_{NP} was logically more important at low scale; a proper extraction of S_{NP} would therefore require low-mass data.

In the next chapter, we will focus on the hard-scattering coefficients in *polarised* quarkonium-pair production. In particular, we will present results in the high-mass and threshold limits in the helicity frame, and see how this helps us shed some light on the behaviour of the hard-scattering coefficients.

Chapter 7

Polarised quarkonium-pair production

We have seen, through an analysis of the helicity structure of the gluon TMD correlator, that the polarised gluon TMD $h_1^{\perp g}$ flips the helicity of an initial-state gluon between the scattering amplitude and its complex conjugate. Such a property allows one to decompose the hard-scattering coefficients of the different TMD convolutions in sums of helicity amplitudes. The cross section therefore presents a richer structure in terms of helicity amplitudes than in the collinear case, where helicity flips do not occur. In this chapter, we will see how decomposing the different coefficients in terms of helicity amplitudes allows to better understand their behaviour across the phase space and how they make quarkonium-pair production a process of great interest for TMD study. We will inter alia be able to use the amplitudes obtained for J/ψ -pair production in the context of Central Exclusive Production (CEP) that present interesting expressions in the high-energy and threshold limit.

Working with helicity amplitudes also implies studying the polarisation states of the outgoing quarkonia. Given the difficulties one faces when trying to explain polarised quarkonium production data, it is interesting to find new ways to explore this topic. As quarkonium-pair production within the TMD framework presents a richer helicity structure, it could offer new ways to study polarised production. We will study polarised pair production within the Gluon Centre-of-Mass (gCM) frame. We will compare these helicity amplitudes to the hard-scattering coefficients derived in Chapter 5, and in particular in the high-mass and threshold limits.

7.1 Helicity amplitudes in the high-mass limit

The gCM frame is the frame where the initial-state gluons have opposite momenta, so that the pair is at rest. It is usually not accessible experimentally. However, at LO in α_s , there are no gluons attached to the quark line. Due to momentum conservation, the rest frame of the final-state quarkonia coincides with that of the gluons. The partonic sub-process is then identical to that of CEP. The spin-quantisation axis (SQA) in this frame simply reads $X_{gCM}^\mu = k_1^\mu + k_2^\mu$. The projection of the spin of a quarkonium onto

this axis corresponds to its helicity in the gCM. We remind that in the case of a final state with identical particles as in quarkonium-pair production, the amplitude is symmetrical under the exchange of the quarkonium momenta. This implies that the polarised cross sections are also identical under polarisation state exchange, provided that the SQA itself is invariant under exchange of the momenta of the two gluons in its definition. Therefore one finds that $\sigma_{TL} = \sigma_{LT}$ (and $\sigma_{UL} = \sigma_{LU}$) in the gCM frame. Similarly, cross-section ratios of the different polarised contributions in the gCM frame are invariant under a boost of the CM of the pair. In such a frame where the dynamics do not depend on the partonic momentum fractions $x_{1,2}$, one can factorise the rapidity of the pair y_{pair} out of the polarised squared amplitude; the latter then depends only on the rapidity gap between the quarkonia Δy . This pre-factor cancels in the cross-section ratios.

Meson-pair production has been studied by computing the helicity amplitudes associated with the process in the frame of Central Exclusive Production (CEP) in [142], while [143] specifically focused on J/ψ pair production. As exclusive production does not allow any final-state gluon emission, the hard-scattering amplitude corresponds to that used in inclusive production in the CS channel at LO. The helicity amplitudes are denoted:

$$\mathcal{M}_{\lambda_{k_1}\lambda_{k_2};\lambda_{q_1}\lambda_{q_2}} = \mathcal{M}^{\mu\nu\rho\sigma} \varepsilon_{\lambda_{k_1}}^\rho(k_1) \varepsilon_{\lambda_{k_2}}^\sigma(k_2) \left(\varepsilon_{\lambda_{q_1}}^\mu(q_1) \right)^* \left(\varepsilon_{\lambda_{q_2}}^\nu(q_2) \right)^*, \quad (7.1)$$

where k_1 and k_2 are the momenta of the two initial gluons while q_1 and q_2 are the momenta of the outgoing J/ψ mesons, and the ε are their respective polarisation vectors of helicity λ contracting the bare amplitude. In [143], the helicity amplitudes were computed in the high-mass limit where $M_{\mathcal{Q}\mathcal{Q}} \rightarrow \infty$. One can write the amplitude as a function of $\alpha = 2M_\psi/M_{\psi\psi}$ and $\cos(\theta_{CS})$. Therefore the high-mass limit corresponds to $\alpha \rightarrow 0$, which is equivalent to quarks and mesons being massless in the hard scattering. The various helicity amplitudes happen to have very simple forms in the high-mass limit, despite the bare amplitude being a complex tensor resulting from the contributions of 31 distinct Feynman diagrams. Amplitudes with transversely polarised mesons in the final states (TT states in the gCM frame) correspond to helicities $\lambda_{q_1,q_2} = \pm 1$ and read as follows:

$$\mathcal{M}_{\lambda_{k_1}\lambda_{k_2};++} = \mathcal{M}_{\lambda_{k_1}\lambda_{k_2};--} = 0, \quad (7.2)$$

$$\mathcal{M}_{++;+-} = \mathcal{M}_{++;-+} = \mathcal{M}_{--;+-} = \mathcal{M}_{--;-+} = 0, \quad (7.3)$$

$$\mathcal{M}_{+-;+-} = \mathcal{M}_{-+;-+} = -16C\alpha^2 \cos(\theta_{CS}) (1 + \cos(\theta_{CS})), \quad (7.4)$$

$$\mathcal{M}_{+-;-+} = \mathcal{M}_{-+;+-} = 16C\alpha^2 \cos(\theta_{CS}) (1 - \cos(\theta_{CS})), \quad (7.5)$$

where $C = 2\pi|R_0(0)|^2\alpha_s^2/M_{\mathcal{Q}}^3$ is a constant. The azimuthal phase ϕ_{CS} is left out of these expressions, but amplitudes with two gluons having opposite helicities contain a phase factor $e^{\pm 2i\phi_{CS}}$, independently of the final state polarisation. One can see from Eq. (7.2)

that amplitudes with a final-state helicity of 2 do not contribute. Indeed in the high-mass limit where quarks become massless, helicity conservation along the quark propagator is restored. Moreover, in the nonrelativistic limit, the helicity of the J/ψ is given by the sum of the helicities of its constituent quark and antiquark. The latter must therefore add up in order to have $\lambda \neq 0$. Since Feynman diagrams for di- J/ψ production at leading order in α_s contain two quark lines whose helicities are constrained by the required helicity of the produced quarkonia, it is easy to see that final states with helicity $\lambda_{\psi_1+\psi_2} = 2$ (*i.e.* ++ and – states) would not respect helicity conservation. In addition to this, Eq. (7.3) shows that amplitudes with one particle whose helicity differs from others also cancel. Such a suppression can be demonstrated for scattering amplitudes of n massless partons (in our case $n = 6$) [144]. The only non-zero amplitudes, given in Eq. (7.4) and (7.5), present indeed a very simple form despite being the product of many diagrams.

It should be noted that all amplitudes vanish in the high-mass limit as the total cross section falls with growing $M_{\psi\psi}$, even though some are written to be zero and some other are not, where the α^2 factor (corresponding to a scaling in $1/M_{\psi\psi}^2$) is kept in the expression. Such values correspond to the leading-power terms of the Taylor expansion of the amplitudes in α . When one amplitude is written to be equal to 0, it is to be understood that this amplitude is sub-leading in the high-energy limit and is therefore neglected. The amplitudes with one transverse and one longitudinal meson (LT states) or two longitudinal mesons (LL states) are:

$$\mathcal{M}_{\lambda_{k_1} \lambda_{k_2}; 0\pm} = \mathcal{M}_{\lambda_{k_1} \lambda_{k_2}; \pm 0} = 0, \quad (7.6)$$

$$\mathcal{M}_{++; 00} = \mathcal{M}_{--; 00} = 0, \quad (7.7)$$

$$\mathcal{M}_{+-; 00} = \mathcal{M}_{-+; 00} = -16C\alpha^2 \left(\cos^2(\theta_{CS}) - \frac{C_F}{N_c} \right). \quad (7.8)$$

Again Eq. (7.6) ensues from helicity conservation for massless quark lines. Therefore the mixed polarisation (LT states) amplitudes are all zero for $M_{\mathcal{Q}\mathcal{Q}} \rightarrow 0$, meaning the two mesons are either both longitudinally or transversally polarised. It occurs that $(\pm\pm; 00)$ states also do not contribute in the high-energy limit, as seen in Eq. (7.7). Part of the gluon fusion diagrams involved in meson-pair production have similar expressions to photon fusion diagrams, where the only difference in the structure of the Feynman diagram is the coupling in the vector boson - quark - antiquark vertex. It was shown for $\gamma\gamma \rightarrow \pi^0\pi^0$ that a diagram with same-helicity photons are proportional to an $(e_1 - e_2)$ factor, where e_1 and e_2 are the absolute value charges of the quarks forming the final-state scalar meson. Therefore in the case of flavour-singlet scalar mesons, the amplitude vanishes. This is logically applicable to the diagrams of J/ψ - and Υ -pair production where gluons can be substituted to initial-state photons, provided that the final state quarkonia have helicities equal to zero. However, more diagrams contribute to CS quarkonium-pair production

due to the existence of the three-gluon and four-gluon vertices. These diagrams also happen to cancel in the high-mass limit, effectively making the $(\pm\pm;00)$ amplitudes null. Therefore, the only contribution to LL final states will come from gluons with opposite helicities.

It appears from Eq. (7.8) that the LL final state has an amplitude zero at $\cos(\theta_{CS}) = \sqrt{C_F/N_c} = 2/3$. Such an effect, also labelled a 'radiation zero' and present in all theories with massless bosons, may occur in QCD but is usually washed out by the sum over colours associated with the hadronisation process or by higher-order corrections. The position of the zero results from an interplay between the parameters of the theory (in this case, colour factors) and the kinematics of the reaction (the angle θ_{CS} of the pair). It was already noted in [143] that J/ψ -pair production presents an interesting opportunity to observe a QCD radiation zero. Indeed, because only the $(\pm\mp;00)$ amplitudes contribute to the LL final state, it is technically possible to detect the radiation zero by studying the angular distribution of longitudinal pairs of mesons. Furthermore, the fact that LT -state amplitudes also cancel at high mass means that only one J/ψ meson needs to be measured in a longitudinal polarisation state in order to ensure the pair is in an LL state, and so subject to the amplitude zero ($\sigma_{LT} = 0 \Rightarrow \sigma_{LU} = \sigma_{LL}$). Equivalently, if one detects transversely polarised mesons, a peak to 100% transverse polarisation should be observed at $\cos(\theta_{CS}) = 2/3$. However, it is likely that higher-order corrections will neutralise this peak in most cases: this includes mass corrections due to $M_{\psi\psi}$ being actually finite, but also diagrams with higher powers of α_s as well as CO contributions (those are subleading but could dampen the zero). Studying the radiation zero in the TMD formalism is of great interest, as the formalism is valid in a regime where one avoids real-gluon emissions that could potentially wash out the radiation zero.

As aforementioned, the helicity amplitudes in Eq. (7.2)-(7.8) that have two gluons with opposite helicities lack a phase factor $e^{\pm 2i\phi_{CS}}$. Such a phase is not relevant in the collinear approximation where no helicity flip is possible. In such a case, the product of an amplitude with its complex conjugate cancels the phase out. The situation is different in the TMD framework. For example, the helicity cross sections in the $F_3^{(1)}$ term each multiply a helicity amplitude with no phase with a helicity amplitude with a phase $e^{\pm 2i\phi_{CS}}$. One can therefore extract a factor $e^{2i\phi_{CS}} + e^{-2i\phi_{CS}} \sim \cos(2\phi_{CS})$ from the sum, meaning the azimuthal modulation actually comes from the hard-scattering coefficient. For the F_4 term, one gets that two amplitudes describing the same final state but with inverted gluon helicities have opposite phases, namely $\mathcal{M}_{+-; \lambda_{q_1} \lambda_{q_2}} = (\mathcal{M}_{-+; \lambda_{q_1} \lambda_{q_2}})^*$. The products encountered in the helicity cross sections then add the phases up, allowing one to extract a factor $e^{4i\phi_{CS}} + e^{-4i\phi_{CS}} \sim \cos(4\phi_{CS})$ from F_4 . In the high-mass limit, one can use equations (7.2)-(7.8) and (2.13), (2.14) to evaluate the different hard-scattering coefficients

of the TMD cross section for (un)polarised J/ψ pair production. Their expressions read as follows:

$$\begin{aligned}
F_1^{LLg} &= 2\mathcal{M}_{+-;00}^2 \\
&= 512 C^2 \alpha^4 \left(\cos^2(\theta_{CS}) - \frac{C_F}{N_c} \right)^2, \\
F_1^{LTg} &= 0, \\
F_1^{TTg} &= 2(\mathcal{M}_{+-;+-}^2 + \mathcal{M}_{+-;-+}^2) \\
&= 1024 C^2 \alpha^4 \cos^2(\theta_{CS}) (\cos^2(\theta_{CS}) + 1), \\
F_4^{LLg} &= F_1^{LLg}, \\
F_4^{LTg} &= 0, \\
F_4^{TTg} &= 4\mathcal{M}_{+-;+-}\mathcal{M}_{+-;-+} \\
&= 1024 C^2 \alpha^4 \cos^2(\theta_{CS}) (\cos^2(\theta_{CS}) - 1), \\
F_2^{all} &= F_3^{(l)all} = 0.
\end{aligned} \tag{7.9}$$

We emphasise that all amplitudes are real. The amplitude products contributing to F_2 always contain amplitudes of the type $(\lambda\lambda; \lambda_{q_1} \lambda_{q_2})$ or $(-\lambda\lambda; \lambda\lambda)$ that are all sub-leading in the high-mass limit, making it zero as previously mentioned in Chapter 7. These suppressions find their origin in both helicity conservation in the massless limit and in identities applied to this specific case of 6-parton scatterings, as well as the suppression of the photon-fusion-like diagrams for a flavour-singlet state. F_2 is therefore negligible for all final-state polarisations at high masses. The $F_3^{(l)}$ coefficients also become subleading for all polarisations as their amplitude products contain the same types of amplitudes.

F_1 receives contributions of all kinds of amplitudes, and thus from the few that are leading at high masses: $(+-;+-)$, $(+-;-+)$, $(+-;00)$ plus the amplitudes obtained after exchange of the two mesons. Again, we see that LT states do not appear at high energies in any hard-scattering coefficient (see Eq. (7.6)) as a consequence of helicity conservation along the massless quark lines. The LL state experiences the radiation zero at $\cos^2(\theta_{CS}) = C_F/N_c$ as the amplitudes containing the zero are the only leading ones contributing. F_4 contains products of amplitudes that are either of the type $(+-;++)(-+;++)$ or $(+-;+-)(+-;-+)$ for the TT state, and $(+-;00)(-+;00) = (+-;00)^2$ for the LL state. The first type of products are subleading, but not the second nor the third that only combine leading amplitudes. Indeed as a consequence of its definition, this coefficient only contains amplitudes with opposite-helicity gluons. Moreover, since there is no helicity flips between the amplitude and its conjugate for the final-state quarkonia, the leading and sub-leading amplitudes will not mix together as it occurs for $F_{2,3}^{(l)}$, making

F_4 of the same order in α as F_1 . Furthermore, one finds that F_4^{LLg} is exactly equal to F_1^{LLg} , as they must use combinations of amplitudes that happen to be invariant under the double helicity flip associated with $h_1^{\perp g}$, and are therefore equal. For TT final states, although both coefficients combine the leading amplitudes differently, they appear to be similar: the ratio F_4^{TTg}/F_1^{TTg} is equal to $(\cos^2(\theta_{CS}) - 1)/(\cos^2(\theta_{CS}) + 1)$. This explains why, in the central production case where $\cos(\theta_{CS}) = 0$ and the ratio is equal to one, both coefficients are strictly equal even for unpolarised production.

The radiation zero from the high-mass limit, already found out for double J/ψ CEP, also appears in TMD factorisation that introduces additional terms to the cross section. Indeed, the F_2 coefficient is sub-leading in this limit and remains moreover negligible away from the threshold. On the other hand, the helicity amplitudes and their combinations appearing in the different hard-scattering coefficients of the TMD formalism allow the F_4 coefficient to be comparable with F_1 (and incidentally to inherit the radiation zero in its longitudinal component). At the same time, the remaining coefficients are suppressed, creating this unique configuration that could allow to extract the $\cos(4\phi_{CS})$ -asymmetry from quarkonium-pair production data. We have seen that the suppression of such a large number of helicity amplitudes finds its origin in different mechanisms: helicity conservation in the massless limit associated with the transposition of the $Q\bar{Q}$ pair quantum numbers to its parent meson in the nonrelativistic limit, the cancellation of specific diagrams for pairs of flavour-singlet mesons, as well as identities for 6-parton scatterings. Because of all these requirements, it seems that such a configuration of the TMD hard-scattering coefficients would be hard to find in another process than di- J/ψ or di- Y production, that also occurs to be accessible experimentally.

We provide in Appendix B the full expressions for the unpolarised hard-scattering coefficients as well as in the LL and LU polarisation states in the gCM, *i.e.* without requiring the high-mass limit. From these three states, one can obtain the LT and TT states by subtraction. Using the full expressions for the hard-scattering coefficients in the gCM frame, one can check how the amplitude zero survives the mass corrections for a J/ψ pair in an LU polarisation state. Fig. 7.1 presents the coefficients $F_{1,4}^{LUg}$ as functions of $\cos(\theta_{CS})$ for increasing values of $M_{\psi\psi}$:

Near the mass threshold, the mass corrections are too important and no specific cancellation pattern is seen. Yet slightly above, at $M_{\psi\psi} = 10$ GeV, one can see that the F_1 coefficient already shows signs of the amplitude zero, although its position in $\cos(\theta_{CS})$ is shifted away from the expected value of $2/3$. This is interesting as α is not so small yet, around 0.62, but expected since the leading amplitudes are still of order α^4 which is then about 0.15. The consequence is that the LL amplitude quickly approaches its high-mass

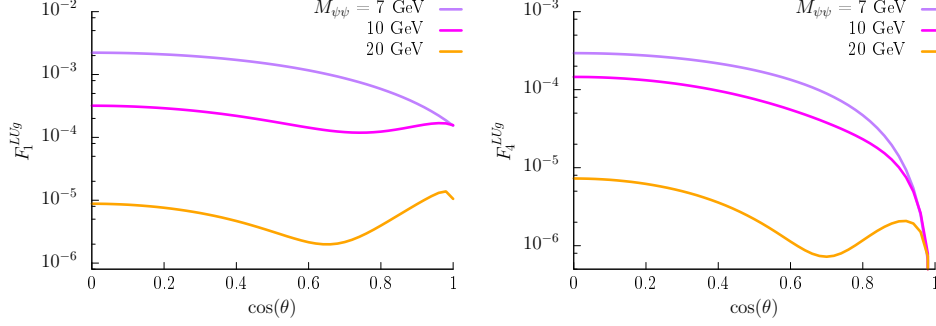


Figure 7.1: The F_1 and F_4 coefficients for a J/ψ pair produced in a LU polarisation state, as functions of $\cos(\theta_{CS})$ for different values of $M_{\mathcal{Q}\mathcal{Q}}$

limit while the LT amplitudes (that are nonzero in the general case) do not excessively attenuate the suppression around $\cos(\theta_{CS}) = 2/3$. It may therefore be possible to detect a partial cancellation of the $\cos(\theta_{CS})$ -differential cross section in J/ψ pairs with at least one longitudinally polarised meson. The F_4 term also presents the characteristic zero despite mass corrections, although it requires higher values of $M_{\mathcal{Q}\mathcal{Q}}$ in order to be visible. Moreover, the zero in this case would be very challenging to detect as it would require to extract the TMD $\cos(4\phi_{CS})$ -modulations in addition to the measurement of one J/ψ polarisation.

7.2 Helicity amplitudes in the threshold limit

We will now consider the same helicity amplitudes in the threshold limit, *i.e.* when $M_{\mathcal{Q}\mathcal{Q}} \rightarrow 2M_{\mathcal{Q}}$ which corresponds to $\alpha \rightarrow 1$. When computed, these also take simple forms:

$$\begin{aligned}
\mathcal{M}_{\lambda_{k_1}\lambda_{k_2};\lambda_{q_1}\lambda_{q_2}} &= \frac{C}{9} (15(\lambda_{k_1}\lambda_{k_2} - 1) + 2 + \lambda_{q_1}\lambda_{q_2}(1 + \lambda_{k_1}\lambda_{k_2}) \\
&\quad - 14(\lambda_{k_1} - \lambda_{k_2})(\lambda_{q_1} - \lambda_{q_2})\cos(\theta_{CS}) + 14\lambda_{q_1}\lambda_{q_2}(1 - \lambda_{k_1}\lambda_{k_2})\cos^2(\theta_{CS})), \\
\mathcal{M}_{\lambda_{k_1}\lambda_{k_2};\lambda_{q_1}0} &= \frac{28C}{9\sqrt{2}} \sin(\theta_{CS}) ((\lambda_{k_2} - \lambda_{k_1}) - \lambda_{q_1}(1 - \lambda_{k_1}\lambda_{k_2})\cos(\theta_{CS})), \\
\mathcal{M}_{\lambda_{k_1}\lambda_{k_2};0\lambda_{q_2}} &= -\frac{28C}{9\sqrt{2}} \sin(\theta_{CS}) ((\lambda_{k_2} - \lambda_{k_1}) + \lambda_{q_2}(1 - \lambda_{k_1}\lambda_{k_2})\cos(\theta_{CS})), \\
\mathcal{M}_{\lambda_{k_1}\lambda_{k_2};00} &= \frac{2C}{9} (15 - 13\lambda_{k_1}\lambda_{k_2} - 14(1 - \lambda_{k_1}\lambda_{k_2})\cos^2(\theta_{CS})), \tag{7.10}
\end{aligned}$$

where it is understood that helicities λ that are not written as zero are equal to plus or minus one. The computation of the transverse helicity amplitudes therefore gives:

$$\begin{aligned}
\mathcal{M}_{\pm\pm;\pm\pm} &= \mathcal{M}_{\pm\pm;\mp\mp} = \frac{4C}{9}, \\
\mathcal{M}_{\pm\pm;\mp\pm} &= \mathcal{M}_{\pm\pm;\pm\mp} = 0, \\
\mathcal{M}_{\pm\mp;\pm\pm} &= \mathcal{M}_{\mp\pm;\pm\pm} = \frac{28C}{9}(\cos^2(\theta_{CS}) - 1), \\
\mathcal{M}_{\pm\mp;\mp\pm} &= -\frac{28C}{9}(\cos^2(\theta_{CS}) - 1), \\
\mathcal{M}_{\pm\mp;\pm\mp} &= -\frac{28C}{9}(\cos^2(\theta_{CS}) + 1),
\end{aligned} \tag{7.11}$$

while LT amplitudes are:

$$\mathcal{M}_{\pm\pm;0\pm} = \mathcal{M}_{\pm\pm;0\mp} = 0, \tag{7.12}$$

$$\mathcal{M}_{\pm\mp;0\pm} = \mp \frac{28\sqrt{2}C}{9}(\cos(\theta_{CS}) - 1)\sqrt{1 - \cos^2(\theta_{CS})}, \tag{7.13}$$

$$\mathcal{M}_{\pm\mp;0\mp} = \pm \frac{28\sqrt{2}C}{9}(\cos(\theta_{CS}) + 1)\sqrt{1 - \cos^2(\theta_{CS})}, \tag{7.14}$$

and we recall that the final state being symmetric under the exchange of the two mesons, LT amplitudes are equal to those. Finally the LL amplitudes read:

$$\mathcal{M}_{\pm\pm;00} = \frac{4C}{9}, \tag{7.15}$$

$$\mathcal{M}_{\pm\mp;00} = -\frac{56C}{9}(\cos^2(\theta_{CS}) - 1) \tag{7.16}$$

We observe that amplitudes with gluons in the same helicity state that correspond to spin projection $J_z = 0$ still tend to be suppressed at threshold when compared with opposite-helicity ones, although they are not all subleading as in the high-mass limit. The suppression is a factor 7 at least (hence 49 in the squared amplitude). This feature appears to be specific to the process: it is for example not observed in $\gamma\gamma \rightarrow W^+W^-$ [145]. We also see that gluon pairs in a $J_z = 0$ state generate amplitudes with no θ_{CS} -dependence, while $J_z = 2$ amplitudes always contain a $\cos(\theta_{CS})$. This is also the case in the high-mass limit, although it was not as clear as all $J_z = 0$ amplitudes are subleading in this limit. The cancellation in the second line of Eq. (7.11), that we also see at high masses (cf. Eq. (7.3)), actually appears to hold for any value of the centre-of-mass energy and is found in many other processes such as $\gamma\gamma \rightarrow W^+W^-$, $\gamma\gamma \rightarrow q\bar{q}$ and $gg \rightarrow q\bar{q}$. The hard-scattering coefficients in the threshold limit reduce to:

$$F_1^{LLg} = 2(\mathcal{M}_{++;00}^2 + \mathcal{M}_{+-;00}^2)$$

$$\begin{aligned}
&= \frac{32 C^2}{81} (1 + 196(\cos^2(\theta_{CS}) - 1)^2), \\
F_1^{LTg} &= 2(\mathcal{M}_{+-;0+}^2 + \mathcal{M}_{+-;0-}^2) \\
&= \frac{6272 C^2}{81} (-\cos^6(\theta_{CS}) + \cos^4(\theta_{CS}) - \cos^2(\theta_{CS}) + 1), \\
F_1^{TTg} &= 2(2(\mathcal{M}_{++;++}^2 + \mathcal{M}_{+-;++}^2) + \mathcal{M}_{+-;+-}^2 + \mathcal{M}_{+-;-+}^2) \\
&= \frac{64 C^2}{81} (1 + 98(\cos^4(\theta_{CS}) - \cos^2(\theta_{CS}) + 1)), \\
F_2^{LLg} &= 2\mathcal{M}_{++;00}^2 \\
&= \frac{32 C^2}{81}, \\
F_2^{LTg} &= 0, \\
F_2^{TTg} &= 4\mathcal{M}_{++;++}^2 \\
&= \frac{64 C^2}{81}, \\
F_3^{LLg} &= 4\mathcal{M}_{++;00}\mathcal{M}_{+-;00} \\
&= -\frac{896 C^2}{81} (\cos^2(\theta_{CS}) - 1), \\
F_3^{LTg} &= 0, \\
F_3^{TTg} &= 8\mathcal{M}_{++;++}\mathcal{M}_{+-;++} \\
&= \frac{896 C^2}{81} (\cos^2(\theta_{CS}) - 1), \\
F_4^{LLg} &= 2\mathcal{M}_{+-;00}^2 \\
&= \frac{6272 C^2}{81} (\cos^2(\theta_{CS}) - 1)^2, \\
F_4^{LTg} &= 4\mathcal{M}_{+-;0+}\mathcal{M}_{-+;0+} \\
&= -\frac{6272 C^2}{81} (\cos^2(\theta_{CS}) - 1)^2, \\
F_4^{TTg} &= 4(\mathcal{M}_{+-;++}^2 + \mathcal{M}_{+-;+-}\mathcal{M}_{+-;-+}) \\
&= \frac{6272 C^2}{81} \cos^2(\theta_{CS})(\cos^2(\theta_{CS}) - 1). \tag{7.17}
\end{aligned}$$

When compared with the unpolarised coefficients at threshold presented in Eq. (5.5), one first notices that the polarised F_3 and F_4 coefficients generally do not vanish, while the unpolarised ones do. Summing the polarised coefficients together (counting the LT contribution twice as it is equal to the TL one) shows that an exact cancellation

between different polarisation states occurs for both coefficients. Moreover, in the central production configuration $\cos(\theta_{CS}) = 0$, we retrieve the ratio $F_2^{UU}/F_1^{UU} = 3/787$, showing that the F_2 coefficient is also small enough at low masses to neglect its effect on the TM spectrum. Interestingly, F_1^{LLg} becomes equal to F_2^{LLg} in the forward limit $\cos(\theta_{CS}) = 1$ (F_2 itself is θ_{CS} -invariant as it only combines same-gluon-helicity states). However in this region of the phase-space, factorisation cannot be trusted because of numerous interactions of the mesons with proton remnants [142].

In conclusion, we have seen that working with the helicity amplitudes for quarkonium pair production allows us to shed light on this process and its interest for the study of the gluon TMDs. The many simplifications appearing in the high-mass and threshold limits make the analysis of the reaction at LO relatively simple considering the number of partons involved in the process. Such a situation, that allows in particular the F_4 coefficient to become comparable to F_1 at high masses and even equal to it for $\theta_{CS} = \pi/2$, is probably unique to J/ψ and Υ pair production. Since the former are abundantly produced and the process is likely free of radiations, it can also allow us to detect a QCD radiation zero in longitudinal vector quarkonium production. Indeed, the zero remains present in the TMD cross section. This is interesting since the applicability of TMD factorisation requires the absence of gluon emissions that also erase the amplitude zero. Its detectability is therefore maximal in the TMD validity range. We showed in Fig. 7.1 that the zero survives at reasonably low masses for pairs with at least one longitudinal meson.

Conclusions

In this thesis, we have studied the possibility to access the gluon TMDs inside unpolarised protons in collisions at the LHC, which could also be studied at RHIC and using Tevatron data. We have first introduced the notions of factorisation of hadronic cross sections in terms of hard-scattering amplitudes at the partonic level and correlators that describe the extraction of a parton from its parent hadron. We have seen that these correlators containing the information about the hadron structure could be parametrised in terms of functions which have a probability density interpretation: the PDFs.

We have then extended factorisation to take into account the intrinsic transverse momentum of the partons. The new correlators are parametrised in terms of transverse momentum-dependent PDFs, also called TMDs. We have seen in particular that the gluon correlator for an unpolarised proton can be written using two different TMDs denoted f_1^g and $h_1^{\perp g}$. We have then provided the expression for the cross section describing a gluon-fusion-induced process with a two-particle final state in the TMD formalism. We have shown that such a cross section could be separated in four terms containing various convolutions of two gluon TMDs, each convolution being multiplied by a hard-scattering coefficient as a result of factorisation. This expression is valid for all inclusive $gg \rightarrow X_1 X_2$, only its hard-scattering coefficients vary with the observed final state. The convolutions, denoted $\mathcal{C}[f_1^g f_1^g]$, $\mathcal{C}[w_2 h_1^{\perp g} h_1^{\perp g}]$, $\mathcal{C}[w_3 f_1^g h_1^{\perp g}]$ and $\mathcal{C}[w_4 h_1^{\perp g} h_1^{\perp g}]$, are associated with different dependences in the azimuthal angle ϕ_{CS} defined by the two particles in the final state. While the terms containing $\mathcal{C}[f_1^g f_1^g]$ and $\mathcal{C}[w_2 h_1^{\perp g} h_1^{\perp g}]$ are azimuthally invariant, the one containing $\mathcal{C}[w_3 f_1^g h_1^{\perp g}]$ with $\mathcal{C}[w_3' h_1^{\perp g} f_1^g]$ and that containing $\mathcal{C}[w_4 h_1^{\perp g} h_1^{\perp g}]$ respectively generate $\cos(2\phi_{CS})$ and $\cos(4\phi_{CS})$ asymmetries. The azimuthally invariant terms affect the transverse-momentum spectrum of the cross section. In addition, we have shown that the helicity structure of the gluon correlator combines f_1^g and $h_1^{\perp g}$ with different products of helicity amplitudes. f_1^g is associated with products of amplitudes

with no gluon helicity flip, while $h_1^{\perp g}$ multiplies products of amplitudes with a helicity flip.

We have then presented a formalism to account for the evolution of TMDs with the scale of the process in order to account for a class of QCD corrections for TMD observables previously defined. Such a procedure is realised in the coordinate space in order to simplify the computations. We have then provided in Eq. (2.30) the expressions for the convolutions accompanied by the relevant modifications brought by the evolution formalism.

We have then discussed the mechanisms at work in quarkonium production in colliders, in particular the Colour-Singlet Model and Colour-Octet Mechanism embedded in the effective theory NRQCD. We have also briefly presented some of the successes and remaining challenges, before giving an overview of the opportunities of (associated) quarkonium production for the study of the gluon TMDs. We have argued that associated or pair production was a more viable option in order to be able to observe particles with large transverse momenta within the TMD validity range. It also allows one to study TMD evolution by tuning the hard scale, which is impossible in single quarkonium production. We have then presented the processes that have been considered in the literature, before turning toward J/ψ - and Υ -pair production, which is a promising tool for gluon TMD study. In particular, we have argued about the dominance of CS contributions at LO, a necessary (although not sufficient) condition for TMD factorisation to hold in such a process. We have discussed about the ease to observe J/ψ pairs in colliders as the number of already existing studies can attest. We have also emphasised the possibility that contributions to quarkonium-pair production from double parton scatterings and feed-down from heavier states may account for a significant fraction of the data. The consequence is that these contributions must be properly modelled in order to extract the direct component of quarkonium-pair production that we are interested in.

In Chapter 5, we have used in first place a simple Gaussian-based model for the gluon TMDs in order to make predictions of the magnitude of TMD observables in J/ψ -pair production. In particular, we have observed that the contribution of the term $F_2 \mathcal{C}[w_2 h_1^{\perp g} h_1^{\perp g}]$ to the cross section was negligible because of the small size of F_2 . This makes f_1^g the only TMD necessary to describe the $P_{\psi\psi_T}$ spectrum of J/ψ pairs. We have also shown that, in the high-mass limit at central rapidities, the coefficient F_4 was becoming equal to F_1 , maximising the size of the $\cos(4\phi_{CS})$ asymmetry. On the other hand, the other contributions were falling down, which represents a great opportunity for the measurement of the $\langle \cos(4\phi_{CS}) \rangle$ asymmetry. Using a Gaussian expression for f_1^g , we have fitted the LHCb $P_{\psi\psi_T}$ spectrum in the region where TMD factorisation should apply, in order to extract the width of f_1^g . We have found it to be of the order of 3 GeV.

Such a value is larger than the mass of the proton and it indicates that the TM of the gluons entering the hard scattering is inflated by the effect of evolution. Using this width as parameter for f_1^g and, using two different models for $h_1^{\perp g}$, we have computed the azimuthal asymmetries for different masses and rapidity differences of the pair. We found that, when using a saturation model, those could reach impressively large values (up to 50%), which we have explained to be a consequence of the favourable hard-scattering coefficients of the process.

We have then improved our study by including TMD evolution into the computations. This allows us to consider a class of QCD corrections. To do so, we have used the b_T -space expressions for the convolutions previously derived which contain the required perturbative and nonperturbative Sudakov factors, S_A and S_{NP} . While S_A can be evaluated perturbatively, S_{NP} needs to be modelled as it contains the information about the nonperturbative behaviour of the gluons. We have used for this component a simple b_T Gaussian with a width depending logarithmically on the hard scale. We have varied this width between the perturbative limit and the size of the proton which we considered to be the widest reasonable bounds one can take. This has allowed us to observe how the variation influences the cross section. We also have provided a detailed account of the influence of each component inside the convolutions over the final observables. We have then observed in particular a widening of the $P_{\mathcal{Q}\mathcal{Q}_T}$ spectrum as compared with the Gaussian model. Yet we have noted that the LHCb data are not sufficient to provide constraints on the width of S_{NP} .

Regarding the azimuthal asymmetries, we have noticed the expected suppression due to the perturbative expansion of $h_1^{\perp g}$ that suppresses it by one order in α_s compared to f_1^g . We have found the asymmetries remain sizeable, reaching up to 8% in the di- $J\psi$ case and 10% in the di- Υ case. Finally, we have found the asymmetries to be consistently growing with $P_{\mathcal{Q}\mathcal{Q}_T}$. This behaviour is a consequence of the angular structure of the $\mathcal{E}[w_3 f_1^g h_1^{\perp g}]$ and $\mathcal{E}[w_4 h_1^{\perp g} h_1^{\perp g}]$ convolutions in the evolution formalism that, to our knowledge, went unnoticed until now.

We have finally pushed further the analysis of the hard-scattering coefficients for di- J/ψ and di- Υ production in the helicity formalism. To do so, we have studied the helicity structure of the correlators and therefore that of the hard-scattering coefficients in terms of helicity amplitudes. We have found that the amplitudes contributing to F_2 were all subleading at high masses, which explains its suppression in the process. We have also noted that in this high-mass limit, the helicity amplitudes contributing to F_1 and F_4 were comparable, explaining the important size of the $\cos(4\phi_{CS})$ -asymmetry.

Considering the amplitudes at threshold also allowed us to explain the behaviour of the cross section in this regime. In particular, we have seen that the suppression of the unpolarised F_3 and F_4 coefficients near the threshold results from a cancellation between their polarised components which are generally nonzero. We have also found that the amplitude zero existing at high masses in CEP for longitudinally-polarised-pair production was preserved in the TMD limit. Polarised-quarkonium production is notoriously difficult to describe theoretically. Finding new observables, such as azimuthal asymmetries, could allow us to test our models of polarised production in different ways and therefore bring some new insight on the question.

A TMD convolutions in b_T -space

In this appendix, we demonstrate how one obtains the $\mathcal{C}[w_4 h_1^{\perp g} h_1^{\perp g}]$ convolution expressed in impact-parameter space presented in Eq. (2.20) as a function of $\tilde{h}_1^{\perp g}$ defined in Eq. (2.19), starting from the momentum-space definition. Using the definition from Eq. (2.6) with the appropriate TMD weight (cf. Eq. (2.7)), it reads:

$$\begin{aligned} \mathcal{C}[w_4 h_1^{\perp g} h_1^{\perp g}] &= \int d^2 \mathbf{k}_{1T} d^2 \mathbf{k}_{2T} \delta^{(2)}(\mathbf{k}_{1T} + \mathbf{k}_{2T} - \mathbf{q}_T) \left(2 \left(\frac{\mathbf{k}_{1T} \cdot \mathbf{k}_{2T}}{2M_p^2} \right. \right. \\ &\quad \left. \left. - \frac{(\mathbf{k}_{1T} \cdot \mathbf{q}_T)(\mathbf{k}_{2T} \cdot \mathbf{q}_T)}{M_p^2 \mathbf{q}_T^2} \right) - \frac{\mathbf{k}_{1T}^2 \mathbf{k}_{2T}^2}{4M_p^4} \right) h_1^{\perp g}(\mathbf{k}_{1T}^2) h_1^{\perp g}(\mathbf{k}_{2T}^2), \end{aligned} \quad (\text{A.1})$$

where \mathbf{q}_T refers to the total transverse momentum of the system and is used here for brevity. We use the Dirac delta to switch to \mathbf{b}_T -space and put all the terms in the transverse weight over the common denominator $4M_p^4 \mathbf{q}_T^4$:

$$\begin{aligned} \mathcal{C}[w_4 h_1^{\perp g} h_1^{\perp g}] &= \frac{1}{(2\pi)^2} \frac{1}{4M_p^4 \mathbf{q}_T^4} \int d^2 \mathbf{b}_T e^{-i\mathbf{b}_T \cdot \mathbf{q}_T} \int d^2 \mathbf{k}_{1T} e^{i\mathbf{b}_T \cdot \mathbf{k}_{1T}} h_1^{\perp g}(\mathbf{k}_{1T}^2) \\ &\quad \times \int d^2 \mathbf{k}_{2T} e^{i\mathbf{b}_T \cdot \mathbf{k}_{2T}} h_1^{\perp g}(\mathbf{k}_{2T}^2) (2(\mathbf{k}_{1T} \cdot \mathbf{k}_{2T})^2 \mathbf{q}_T^4 + 8(\mathbf{k}_{1T} \cdot \mathbf{q}_T)^2 (\mathbf{k}_{2T} \cdot \mathbf{q}_T)^2 \\ &\quad - 8(\mathbf{k}_{1T} \cdot \mathbf{k}_{2T})(\mathbf{k}_{1T} \cdot \mathbf{q}_T)(\mathbf{k}_{2T} \cdot \mathbf{q}_T) \mathbf{q}_T^2 - \mathbf{k}_{1T}^2 \mathbf{k}_{2T}^2 \mathbf{q}_T^4) \\ &= \frac{1}{16\pi^2 M_p^4 \mathbf{q}_T^4} q_T^a q_T^b q_T^c q_T^d \int d^2 \mathbf{b}_T e^{-i\mathbf{b}_T \cdot \mathbf{q}_T} \left(\int d^2 \mathbf{k}_{1T} e^{i\mathbf{b}_T \cdot \mathbf{k}_{1T}} h_1^{\perp g}(\mathbf{k}_{1T}^2) k_{1T}^i k_{1T}^j \right) \\ &\quad \times \left(\int d^2 \mathbf{k}_{2T} e^{i\mathbf{b}_T \cdot \mathbf{k}_{2T}} h_1^{\perp g}(\mathbf{k}_{2T}^2) k_{2T}^l k_{2T}^m \right) (2\delta_{il} \delta_{jm} \delta_{ab} \delta_{cd} + 8\delta_{ia} \delta_{jb} \delta_{lc} \delta_{md} \\ &\quad - 8\delta_{il} \delta_{ja} \delta_{mb} \delta_{cd} - \delta_{ij} \delta_{lm} \delta_{ab} \delta_{cd}). \end{aligned} \quad (\text{A.2})$$

One can express the transverse-momentum integrals as functions of the impact-parameter components instead of the momentum ones:

$$\int d^2 \mathbf{k}_T e^{i\mathbf{b}_T \cdot \mathbf{k}_T} h_1^{\perp g}(\mathbf{k}_T^2) k_T^i k_T^j = A \delta^{ij} + B \left(b_T^i b_T^j - \frac{\mathbf{b}_T^2}{2} \delta^{ij} \right), \quad (\text{A.3})$$

Contracting Eq. (A.2) by δ^{ij} and $\left(b_T^i b_T^j - \frac{\mathbf{b}_T^2}{2} \delta^{ij}\right)$ yields the solutions:

$$\begin{aligned} A &= \frac{1}{2} \int d^2 \mathbf{k}_T e^{i \mathbf{b}_T \cdot \mathbf{k}_T} h_1^{\perp g}(\mathbf{k}_T^2) \mathbf{k}_T^2, \\ B &= \frac{2}{\mathbf{b}_T^4} \int d^2 \mathbf{k}_T e^{i \mathbf{b}_T \cdot \mathbf{k}_T} h_1^{\perp g}(\mathbf{k}_T^2) \left((\mathbf{k}_T \cdot \mathbf{b}_T)^2 - \frac{\mathbf{k}_T^2 \mathbf{b}_T^2}{2} \right). \end{aligned} \quad (\text{A.4})$$

If one changes the Cartesian variables (k_T^x, k_T^y) to polar ones (k_T, θ) , the angular integrals can be expressed in terms of Bessel functions of the first kind:

$$\begin{aligned} A &= \frac{1}{2} \int_0^\infty dk_T k_T^3 h_1^{\perp g}(k_T^2) \int_{-\pi}^\pi d\theta e^{-i b_T k_T \sin(\theta)} \\ &= \pi \int_0^\infty dk_T k_T^3 J_0(b_T k_T) h(k_T^2), \\ B &= -\frac{1}{2b_T^2} \int_0^\infty dk_T k_T^3 h_1^{\perp g}(k_T^2) \int_{-\pi}^\pi d\theta \left(e^{i(2\theta - b_T k_T \sin(\theta))} + e^{i(-2\theta - b_T k_T \sin(\theta))} \right) \\ &= -\frac{2\pi}{b_T^2} \int_0^\infty dk_T k_T^3 J_2(b_T k_T) h(k_T^2). \end{aligned} \quad (\text{A.5})$$

We then use this result inside Eq. (A.3), which is itself used for each transverse-momentum integral inside Eq. (A.2). After contracting all the indices together, the convolution becomes:

$$\begin{aligned} \mathcal{E}[w_4 h_1^{\perp g} h_1^{\perp g}] &= \frac{1}{16M_p^4 q_T^4} \int d^2 \mathbf{b}_T e^{-i \mathbf{b}_T \cdot \mathbf{q}_T} 4 \left(q_T^4 + 8 \left(\frac{(\mathbf{b}_T \cdot \mathbf{q}_T)^4}{\mathbf{b}_T^4} - \frac{q_T^2 (\mathbf{b}_T \cdot \mathbf{q}_T)^2}{\mathbf{b}_T^2} \right) \right) \\ &\quad \times \int_0^\infty dk_{1T} k_{1T}^3 J_2(b_T k_{1T}) h(k_{1T}^2) \int_0^\infty dk_{2T} k_{2T}^3 J_2(b_T k_{2T}) h(k_{2T}^2). \end{aligned} \quad (\text{A.6})$$

We notice that only the product of integrals containing $J_2(b_T k_{1T}) J_2(b_T k_{2T})$ survives, while terms containing $J_0(b_T k_{1T}) J_0(b_T k_{2T})$ or $J_0(b_T k_{1,2T}) J_2(b_T k_{2,1T})$ vanish. The remaining integrals are proportional to the second b_T^2 -derivative of the Fourier-transformed TMD:

$$\begin{aligned} \tilde{h}_1^{\perp g(2)}(x, b_T^2) &= 2 \left(-\frac{2}{M_p^2} \frac{\partial}{\partial b_T^2} \right)^2 \tilde{h}_1^{\perp g}(x, b_T^2) \\ &= \frac{2}{M_p^4} \int_0^\infty dk_T \frac{k_T^3}{b_T^2} J_2(b_T k_T) h_1^{\perp g}(x, k_T^2). \end{aligned} \quad (\text{A.7})$$

We can then replace the k_T -integrals of $h_1^{\perp g}$ by the Fourier-transformed distributions and compute the angular integral in terms of Bessel functions:

$$\mathcal{E}[w_4 h_1^{\perp g} h_1^{\perp g}] = \frac{M_p^4}{16q_T^4} \int_0^\infty db_T b_T^5 q_T^4 \tilde{h}_1^{\perp g(2)}(x_1, b_T^2) \tilde{h}_1^{\perp g(2)}(x_2, b_T^2) \int_0^{2\pi} d\theta e^{-i b_T q_T \cos(\theta)}$$

$$\begin{aligned} & \times (1 + 8 \cos^2(\theta)(\cos^2(\theta) - 1)) \\ & = \frac{\pi M_p^4}{8} \int_0^\infty db_T b_T^5 J_4(b_T q_T) \tilde{h}_1^{\perp g(2)}(x_1, b_T^2) \tilde{h}_1^{\perp g(2)}(x_2, b_T^2). \end{aligned} \quad (\text{A.8})$$

The separation between the radial and angular components of the integral allow to simplify the q_T^4 factor in the numerator and denominator. We notice how the angular integral simply results in a Bessel function $J_4(b_T q_T)$ which therefore encodes the whole q_T -dependence of the convolution. Finally, one can replace $\tilde{h}_1^{\perp g(2)}$ by the function defined in Eq. (2.19), called $\tilde{h}_1^{\perp g}$ for brevity. We therefore re-define $\tilde{h}_1^{\perp g}$, and the correspondence between the two is as follows:

$$\tilde{h}_1^{\perp g}(x, b_T^2) = -\pi \int_0^\infty dk_T \frac{k_T^3}{M_p^2} J_2(b_T k_T) h_1^{\perp g}(x, k_T^2) = -\frac{\pi M_p^2 b_T^2}{2} \tilde{h}_1^{\perp g(2)}(x, b_T^2). \quad (\text{A.9})$$

Using this equality, one retrieves the expression for $\mathcal{C}[w_4 h_1^{\perp g} h_1^{\perp g}]$ in Eq. (2.20):

$$\mathcal{C}[w_4 h_1^{\perp g} h_1^{\perp g}] = \int_0^\infty \frac{db_T}{2\pi} b_T J_4(b_T q_T) \tilde{h}_1^{\perp g}(x_1, b_T^2) \tilde{h}_1^{\perp g}(x_2, b_T^2). \quad (\text{A.10})$$

The computational steps are analogous for the other convolutions in order to retrieve all the expressions of Eq. (2.20).

B $gg \rightarrow \mathcal{Q}\mathcal{Q}$ hard-scattering coefficients

B.1 The full expressions of the $f_{i,n}$ for unpolarised J/ψ -pair production

The factors $f_{i,n}$ in Eq. (5.1) multiplying the $\cos(\theta_{\text{CS}})$ -polynomials in the hard-scattering coefficients describing unpolarised J/ψ - and Υ -pair production are polynomials in α themselves, and we recall $\alpha = 2M_{\mathcal{Q}}/M_{\mathcal{Q}\mathcal{Q}}$:

$$\begin{aligned} f_{1,0} &= 6\alpha^8 - 38\alpha^6 + 83\alpha^4 + 480\alpha^2 + 256, \\ f_{1,1} &= 2(1 - \alpha^2)(6\alpha^8 + 159\alpha^6 - 2532\alpha^4 + 884\alpha^2 + 208), \\ f_{1,2} &= 2(1 - \alpha^2)^2(3\alpha^8 + 19\alpha^6 + 7283\alpha^4 - 8448\alpha^2 - 168), \\ f_{1,3} &= -2(1 - \alpha^2)^3(159\alpha^6 + 6944\alpha^4 - 17064\alpha^2 + 3968), \\ f_{1,4} &= (1 - \alpha^2)^4(4431\alpha^4 - 27040\alpha^2 + 17824), \\ f_{1,5} &= 504(1 - \alpha^2)^5(15\alpha^2 - 28), \\ f_{1,6} &= 3888(1 - \alpha^2)^6, \end{aligned} \quad (\text{A.11})$$

$$f_{2,0} = \alpha^4,$$

$$\begin{aligned}
f_{2,1} &= -2(\alpha^6 + 17\alpha^4 - 126\alpha^2 + 108), \\
f_{2,2} &= (1 - \alpha^2)^2(\alpha^4 + 756), \\
f_{2,3} &= -36(1 - \alpha^2)^3(\alpha^2 + 24), \\
f_{2,4} &= 324(1 - \alpha^2)^4,
\end{aligned} \tag{A.12}$$

$$\begin{aligned}
f_{3,0} &= \alpha^2(16 - 3\alpha^2), \\
f_{3,1} &= 6\alpha^6 + 159\alpha^4 - 1762\alpha^2 + 1584, \\
f_{3,2} &= (1 - \alpha^2)(3\alpha^6 + 19\alpha^4 + 5258\alpha^2 - 6696), \\
f_{3,3} &= -(1 - \alpha^2)^2(159\alpha^4 + 5294\alpha^2 - 10584), \\
f_{3,4} &= 18(1 - \alpha^2)^3(99\alpha^2 - 412), \\
f_{3,5} &= 1944(1 - \alpha^2)^4,
\end{aligned} \tag{A.13}$$

$$\begin{aligned}
f_{4,0} &= 3\alpha^4 - 32\alpha^2 + 256, \\
f_{4,1} &= -(6(\alpha^4 + 36\alpha^2 - 756)\alpha^2 + 4768), \\
f_{4,2} &= 3\alpha^8 + 38\alpha^6 + 11994\alpha^4 - 32208\alpha^2 + 20400, \\
f_{4,3} &= -2(1 - \alpha^2)(105\alpha^6 + 5512\alpha^4 - 23120\alpha^2 + 19520), \\
f_{4,4} &= (1 - \alpha^2)^2(3459\alpha^4 - 30352\alpha^2 + 38560), \\
f_{4,5} &= 72(1 - \alpha^2)^3(105\alpha^2 - 268), \\
f_{4,6} &= 3888(1 - \alpha^2)^4.
\end{aligned} \tag{A.14}$$

B.2 The hard-scattering coefficients for polarised J/ψ -pair production in the gluon helicity frame

The coefficients for a polarised pair in the gCM frame read:

$$\begin{aligned}
F_1^{LLg} &= \frac{\mathcal{N}}{\mathcal{D}} \left[2\alpha^8 + 2\alpha^6 - 31\alpha^4 - 32\alpha^2 + 1296(\alpha^2 - 1)^4(\alpha^2 + 1)^2 c\theta^{12} \right. \\
&\quad - 72(\alpha^2 - 1)^3(\alpha^2 + 1)(5\alpha^2 - 11)(7\alpha^2 + 8)c\theta^{10} + (\alpha^2 - 1)^2 \\
&\quad \times (1477\alpha^8 - 5974\alpha^6 - 8283\alpha^4 + 10256\alpha^2 + 12640)c\theta^8 + 2(\alpha - 1) \\
&\quad \times (\alpha + 1)(53\alpha^{10} + 1582\alpha^8 - 1491\alpha^6 - 6516\alpha^4 + 1072\alpha^2 + 6560)c\theta^6 \\
&\quad + 2(\alpha^{12} + \alpha^{10} + 900\alpha^8 + 883\alpha^6 - 3415\alpha^4 - 1992\alpha^2 + 3720)c\theta^4 \\
&\quad \left. - 2(2\alpha^{10} + 55\alpha^8 + 19\alpha^6 - 644\alpha^4 - 324\alpha^2 + 1088)c\theta^2 + 256 \right],
\end{aligned} \tag{A.15}$$

$$F_2^{LLg} = \frac{\mathcal{N}}{\mathcal{D}} \left[\alpha^4(\alpha^2 - (\alpha^2 - 1)c\theta^2(\alpha^2 + 18(\alpha^2 - 1)c\theta^2 + 18))^2 \right], \tag{A.16}$$

$$F_3^{LLg} = \frac{\mathcal{N}}{\mathcal{D}} \left[-2\alpha^2 (c\theta - 1)(c\theta + 1) \left(-\alpha^2 (\alpha^2 + 1) + 36(\alpha^2 - 1)^2 (\alpha^2 + 1) c\theta^4 \right. \right. \\ \left. \left. + (\alpha^6 + 36\alpha^4 + 15\alpha^2 - 52) c\theta^2 + 16 \right) ((\alpha - 1)(\alpha + 1) c\theta^2 (\alpha^2 \right. \\ \left. + 18(\alpha^2 - 1) c\theta^2 + 18) - \alpha^2 \right], \quad (\text{A.17})$$

$$F_4^{LLg} = \frac{\mathcal{N}}{\mathcal{D}} \left[(c\theta^2 - 1)^2 (\alpha^4 + \alpha^2 - 36(\alpha^2 - 1)^2 (\alpha^2 + 1) c\theta^4 \right. \\ \left. - (\alpha^6 + 36\alpha^4 + 15\alpha^2 - 52) c\theta^2 - 16 \right)^2 \right], \quad (\text{A.18})$$

$$F_1^{LUG} = \frac{\mathcal{N}}{\mathcal{D}} \left[2\alpha^8 + 6\alpha^6 - 95\alpha^4 + 224\alpha^2 + 1296(\alpha^2 - 1)^6 c\theta^{12} - 72(\alpha^2 - 1)^4 \right. \\ \times (35\alpha^4 - 89\alpha^2 + 88) c\theta^{10} + (\alpha^2 - 1)^3 (1477\alpha^6 - 9721\alpha^4 + 13432\alpha^2 \\ - 12640) c\theta^8 + 2(\alpha^2 - 1)^2 (53\alpha^8 + 2445\alpha^6 - 7142\alpha^4 + 7420\alpha^2 - 6560) \\ \times c\theta^6 + 2(\alpha - 1)(\alpha + 1) (\alpha^{10} + 4\alpha^8 + 2552\alpha^6 - 4583\alpha^4 + 4284\alpha^2 \\ - 3720) c\theta^4 - 2(2\alpha^{10} + 59\alpha^8 - 795\alpha^6 + 882\alpha^4 - 1040\alpha^2 + 1088) c\theta^2 \\ \left. + 256 \right], \quad (\text{A.19})$$

$$F_2^{LUG} = \frac{\mathcal{N}}{\mathcal{D}} \left[\alpha^4 (\alpha^4 + 324(\alpha^2 - 2)(\alpha^2 - 1)^3 c\theta^8 + 36(\alpha^2 - 1)^2 (\alpha^4 \right. \\ \left. + 26\alpha^2 - 45) c\theta^6 + (\alpha - 1)(\alpha + 1) (\alpha^6 - \alpha^4 + 972\alpha^2 - 1296) c\theta^4 \right. \\ \left. - 2(\alpha^6 + 17\alpha^4 - 180\alpha^2 + 162) c\theta^2 \right], \quad (\text{A.20})$$

$$F_3^{LUG} = \frac{\mathcal{N}}{\mathcal{D}} \left[-2\alpha^2 (c\theta^2 - 1) (\alpha^6 + \alpha^4 - 16\alpha^2 + 648(\alpha^2 - 1)^5 c\theta^8 - 648 \right. \\ \times (1 - \alpha^2)^{7/2} c\theta^7 + 18(\alpha^2 - 1)^3 (3\alpha^4 + 109\alpha^2 - 108) c\theta^6 + 36(1 \\ - \alpha^2)^{5/2} (\alpha^2 + 44) c\theta^5 + (\alpha^2 - 1)^2 (\alpha^6 + \alpha^4 + 1960\alpha^2 - 1944) c\theta^4 \\ - 1224(1 - \alpha^2)^{3/2} c\theta^3 - 2(\alpha - 1)(\alpha + 1) (\alpha^6 + 28\alpha^4 - 315\alpha^2 + 324) c\theta^2 \\ \left. - 36\sqrt{1 - \alpha^2} (\alpha^2 - 8) c\theta \right], \quad (\text{A.21})$$

$$F_4^{LUG} = \frac{\mathcal{N}}{\mathcal{D}} \left[(\alpha^2 - 1) (c\theta^2 - 1)^2 (32(\alpha^2 - 8) + (\alpha^2 - 1) (\alpha^4 + 1296(\alpha^2 - 1)^4 \right. \\ \times c\theta^8 + 72(\alpha^2 - 1)^2 (\alpha^4 + 53\alpha^2 - 52) c\theta^6 + (\alpha^2 - 1)^2 (\alpha^4 + 3856) c\theta^4 \\ \left. - 2(\alpha^6 + 35\alpha^4 - 684\alpha^2 + 832) c\theta^2) \right], \quad (\text{A.22})$$

where $c\theta = \cos(\theta_{CS})$.

Lay summary

The strong nuclear force was first theorised in order to explain how the atomic nucleus was bound together in spite of the protons mutual electromagnetic repulsion. It is an attractive force acting upon protons and neutrons (also called nucleons). It was later understood that protons and neutrons were not elementary particles but made up of constituent particles called quarks. Their interactions are described by Quantum ChromoDynamics (QCD). Quarks carry a “colour” charge (in addition to an electric charge) which can be red, green or blue. Quarks with different charges attract each other and their interactions are mediated by a gauge boson called gluon. The strong nuclear force that binds nucleons together is actually a residuum of the strong interaction between quarks.

A crucial difference between the strong and electromagnetic interactions is that the gluon carries a colour charge, while the photon is electrically neutral. A consequence is that gluons can interact with each other in addition to their interactions with quarks. One quark and gluon can radiate many low-energy gluons, which can themselves interact with other quarks and gluons. The result is that the strong coupling α_s is actually larger at low energies than high energies, which correspond to small scales (since wavelength is decreasing with increasing energy). This phenomenon is called the running of the coupling and also happens for the electromagnetic coupling α , but the opposite way. It even tends toward zero at infinitely large energy, meaning quarks and gluons are almost blind to each other at these energy scales: this behaviour is called asymptotic freedom. On the other side, the coupling becomes infinite for a sufficiently low (yet finite) energy scale at which perturbative QCD breaks down and cannot be trusted.

Particles composed of quarks and gluons are called hadrons. Two mains types of hadrons exist: mesons are made up of a quark-antiquark pair, while (anti)baryons

contain three (anti)quarks. Other types of hadrons have been discovered since, such as tetraquarks and pentaquarks. The existence of other exotic hadrons predicted by QCD, such as glueballs or exotic mesons, remains to be proven. Neither quarks nor gluons have ever been directly observed. In addition, all hadrons are colour-neutral. This means that colour remains *confined* inside hadrons at all times. The quarks inside a baryon each carry a different colour, that cancel the total charge of the hadron. A meson contains a quark of a given colour and an antiquark of the corresponding anticolour. Confinement is believed to be a consequence of the divergent growth of α_s with increasing length scales, although a complete mathematical demonstration of confinement remains to be established.

This decomposition of hadrons into a small number of quarks and gluons is called the valence structure. It reproduces the quantum numbers of hadrons and their classification, but does not describe the structure of hadrons in collisions. Deeply Inelastic Scattering (DIS) was the first process used to probe the structure of the proton in colliders. It occurs when an electron collides with a proton with a large momentum transfer Q . Their interaction can be described using perturbative Quantum ElectroDynamics (QED), in which the interaction is mediated by a virtual photon. The proton is destroyed in the process while the scattered electron momentum is compared with the incident one in order to get information about the proton. The photon therefore acts as some kind of microscope: the larger Q is, the smaller scales are explored. At the fundamental level, the photon scatters with one quark.

One can separate the DIS cross section in two parts. On one side, the small-scale photon-quark scattering, also called hard scattering, that is characterised by a large momentum transfer and can be computed using perturbative techniques: in this case an expansion of the transition matrix in powers of α that is sufficiently small. The corresponding leading contribution in terms of Feynman diagrams is the virtual photon exchange between the electron and the quark. On the other side, the “extraction” of a quark from the large-scale proton state cannot be described using perturbative QCD as the strong coupling is also large. However, one can factorise the small- and large-scale components of the reaction, and the second one can be parametrised using Parton Distribution Functions (PDFs). These functions are probability densities of finding a quark or gluon carrying a fraction x of the proton momentum (hence the name parton now assimilated to quarks and gluons), for a given value of Q . The PDFs therefore describe the structure of the proton at various scales and cannot be computed using perturbative QCD. Instead they need to be extracted from experimental data. However, their presumed universality (the distribution supposedly is an intrinsic characteristic of the proton, not the way it is studied) allows one to predict cross sections for all kinds of

hadronic reactions, as the parton-level scattering can be computed using perturbative QCD. Naturally, the PDFs evolve with the probed scale as a side effect of the running of α_s , meaning that electrons probing different scales will “see” different populations of partons inside the proton. The factorisation of the short- and large-scale components of a hadronic process is complicated to justify as partons entering the hard scattering can exchange low-energy gluons with their environment, but has been rigorously proven for PDFs. In this picture, the only component of the parton momentum that is not integrated out is the one that is *collinear* to the parent proton momentum.

Transverse momentum-dependent factorisation is used to describe hadronic collisions while taking into account the intrinsic transverse momentum of partons inside hadrons. This requires the use of Transverse Momentum-Dependent Parton Distribution Functions (TMDPDFs or simply TMDs) in order to parametrise the parton correlator. Such distributions need to be extracted from experimental data. Quark TMDs are relatively well known thanks to processes such as semi-inclusive deep inelastic scattering (SIDIS) and Drell-Yan for which numerous data exist. Gluon TMDs remain poorly known, since there is no ideal process to probe them in the operating colliders. The future Electron-Ion Collider (EIC) will offer a much better access to them, but its first run remains at least 10 years from now. Moreover, it is important to study TMDs in various kinds of processes in order to check their universality which is not as trivial as that of collinear PDFs.

We propose to use quarkonium-pair production to study the two leading-twist gluon TMDs needed to describe unpolarised proton collisions at the Large Hadron Collider (LHC). Quarkonia are mesons, i.e. bound states of a quark-antiquark pair. In the case of a quarkonium, the pair is made of heavy flavours: charmonia combine a charm with an anticharm, while bottomonia combine a bottom with an antibottom. J/ψ mesons are the fundamental state of vector charmonia and are produced in large amounts at the LHC. J/ψ pairs originate from gluon fusion in vast majority, which is important in order to focus on gluon TMDs. Studying two-particle final states also allows to tune the hard scale of the process that is the pair mass, which in turn allows to study TMD evolution.

We first use a simple model of Gaussian-based TMDs to compute observables in J/ψ -pair production that are sensitive to the TMDs. These observables are the transverse-momentum spectrum of the pair, mostly sensitive to the unpolarised gluon TMD, and azimuthal asymmetries, which existence requires the linearly-polarised gluon TMD. We see that J/ψ pair production is an ideal process to probe the linearly-polarised gluon distribution through one azimuthal asymmetry that is maximal at large hard scales. We also use the LHCb data on the J/ψ pair transverse momentum to fit the average gluon

transverse momentum using our Gaussian-based model. The large value that is obtained is interpreted as a consequence of TMD evolution that perturbatively enhances the intrinsic transverse momentum of the gluon at such large hard scales.

We then improve our predictions by including TMD evolution in the formalism used to describe the gluon TMDs in our calculations. In this picture, the unpolarised gluon distribution is a leading contribution in an expansion of the strong coupling, while the linearly-polarised distribution is subleading. The remaining nonperturbative component is modelled using a Gaussian. We observe that the computed magnitude of the azimuthal asymmetries in J/ψ -pair production are lower than when using the purely Gaussian model. However, we observe that these asymmetries remain sizeable and could be detected at the LHC. We also provide predictions for Υ -pair production (the Υ is the bottomonium equivalent of the J/ψ).

We finally study the helicity structure of the quarkonium-pair production amplitude. Indeed, it can be written as a sum of sub-amplitudes corresponding to various helicity states of the initial-state gluons and final-state quarkonia. In the high-mass limit of the pair, the amplitudes greatly simplify and explain how the hard-scattering coefficients of J/ψ -pair production maximise the size of one azimuthal asymmetry, as previously observed. Moreover, it is shown that the amplitude zero for longitudinally polarised pairs predicted at leading order in the collinear regime exists as well in TMD factorisation. It should survive for intermediate masses as hard gluon emissions are suppressed in the TMD regime.

Samenvatting

De sterke kernkracht werd oorspronkelijk bedacht om te verklaren hoe atoomkernen bij elkaar kunnen blijven, ondanks de afstotende elektromagnetische kracht tussen de protonen. Het is een aantrekkende kracht die werkt op protonen en neutronen (ook wel nucleonen genoemd). Later kwam men erachter dat protonen en neutronen geen elementaire deeltjes zijn, maar dat ze bestaan uit quarks. Interacties tussen quarks worden beschreven door Quantum ChromoDynamica (QCD). Quarks hebben een kleurlading (naast een elektrische lading), die rood, groen of blauw kan zijn. Quarks met verschillende ladingen trekken elkaar aan en hun interacties worden uitgewisseld door ijkbosonen die gluonen heten. De sterke kernkracht die de nucleonen bij elkaar houdt is een overblijfsel van de interactie tussen quarks.

Een cruciaal verschil tussen de sterke en elektromagnetische interacties is dat gluonen zelf een kleurlading hebben, terwijl fotonen elektrisch neutraal zijn. Een gevolg hiervan is dat gluonen interacties met elkaar kunnen hebben naast hun interacties met quarks. Een quark of gluon kan veel laag-energetische gluonen uitstralen, die weer interacties kunnen hebben met andere quarks en gluonen. Het gevolg hiervan is dat de sterke koppeling α_s groter is op lage energie dan op hoge energie, wat overeenkomt met kleine schalen (omdat golflengte afneemt met toenemende energie). Dit fenomeen wordt de running van de koppeling genoemd en dit vindt ook plaats voor de elektromagnetische koppeling α , maar dan andersom. De sterke interactie wordt zelfs willekeurig zwak voor oneindig hoge energieën, wat betekent dat quarks en gluonen op deze schalen geen interacties meer hebben. Dit gedrag wordt asymptotische vrijheid genoemd. Aan de andere kant wordt de koppeling groter dan 1 voor een energie die laag genoeg is, waardoor perturbatieve QCD dan dus niet meer vertrouwd kan worden.

Deeltjes die bestaan uit quarks en gluonen worden hadronen genoemd. Er bestaan

twee belangrijke typen hadronen: mesonen die uit quark-antiquark paren bestaan, en (anti)baryonen die uit drie (anti)quarks bestaan. Andere typen hadronen, zoals pentaquarks, zijn later ook ontdekt. Het bestaan van andere exotische hadronen die door QCD zijn voorspeld, zoals glueballs of exotische mesonen, is nog niet vastgesteld. Quarks en gluonen zijn beide nog nooit direct geobserveerd. Daarnaast zijn alle hadronen kleur-neutraal. Dit betekent dat kleur altijd *confined* blijft binnen hadronen. De quarks in een baryon hebben elk een verschillende kleur, zodat de totale kleurlading neutraal is. Een meson bevat een quark met een bepaalde kleur, en een antiquark met de bijbehorende anti-kleur. Er is geen wiskundige verklaring voor confinement in QCD.

De ontleding van hadronen in een klein aantal quarks wordt de valentiestructuur genoemd, maar deze beschrijft niet volledig de structuur van hadronen in botsingen. *Deeply Inelastic Scattering* (DIS) was het eerste proces dat gebruikt werd om de structuur van het proton in botsingsexperimenten te bestuderen. Het vindt plaats als een lepton met een proton botst met een grote momentumoverdracht Q . Hun interactie kan beschreven worden met perturbatieve Quantum ElectroDynamica (QED), waarbij de interactie wordt overgedragen door een virtueel foton. Het proton wordt hierbij vernietigd, maar de impuls van het verstrooide lepton kan worden vergeleken met de waarde voor verstrooiing om informatie te krijgen over het proton. Het foton wordt dus gebruikt als microscoop: hoe groter Q , des te kleiner de schaal die bestudeerd kan worden.

De DIS botsingsdoorsnede kan in twee delen worden gescheiden. Aan de ene kant is er op kleine schaal de lepton-quark interactie, ook wel harde interactie genoemd, die gekarakteriseerd wordt door een grote momentumoverdracht en die met perturbatieve technieken berekend kan worden: in dit geval een expansie van de overgangsmatrix in machten van α die klein genoeg is. Het bijbehorende Feynman diagram met de grootste bijdrage is de uitwisseling van een virtueel foton tussen lepton en quark. Aan de andere kant kan de onttrekking van een quark aan het proton op grote schaal niet met perturbatieve QCD worden berekend omdat de sterke koppeling dan groot is. Maar men kan de componenten van de interactie op kleine en grote schaal factoriseren, en de laatste kan met Parton Distributie Functies (PDFs) geparametriseerd worden. Deze functies zijn waarschijnlijkheidsverdelingen voor het vinden van een quark of gluon met een fractie x van het momentum van het proton, voor een bepaalde waarde van Q (de naam parton wordt gebruikt om quarks en gluonen aan te geven). De PDFs beschrijven dus de structuur van het proton op verschillende schalen en kunnen niet met perturbatieve QCD berekend worden. In plaats daarvan moeten ze uit experimentele data gehaald worden. Maar omdat verondersteld wordt dat deze universeel zijn (de verdeling is vermoedelijk een intrinsieke eigenschap van het proton, onafhankelijk van hoe het wordt bestudeerd), is het mogelijk botsingsdoorsnedes te voorspellen voor allerlei hadronische processen,

waarbij de verstrooiing op het niveau van het parton met perturbatieve QCD kan worden berekend. Omdat de PDFs veranderen afhankelijk van de schaal die wordt bestudeerd, zullen leptonen op verschillende schaal ook een andere verdeling van partonen in het proton zien. De factorisatie van de componenten op kleine en grote schaal voor een bepaald proces moet rigoureus bewezen worden, omdat partonen die onderdeel zijn van de harde verstrooiing laag-energetische gluonen kunnen uitwisselen met de omgeving, en zo factorisatie kunnen belemmeren. Voor DIS is factorisatie bewezen. Hierbij is de enige component van het parton momentum die niet uitgeïntegreerd wordt degene die collineair is aan het momentum van het oorspronkelijke proton.

Transversaal-momentum-afhankelijke factorisatie wordt gebruikt om hadronische botsingen te beschrijven waarbij rekening wordt gehouden met het intrinsieke transversale momentum van de partonen in de hadronen. Het gebruik van Transversaal-Momentum-afhankelijke Parton Distributie Functies (in het Engels afgekort tot TMD-PDFs of simpelweg TMDs) is nodig om de parton correlator te parametriseren. Zulke distributies moeten uit experimentele data gehaald worden. Quark TMDs zijn vrij goed bekend dankzij processen als semi-inclusieve deep inelastic scattering (SIDIS) en Drell-Yann waarvoor talrijke data beschikbaar zijn. Gluon TMDs zijn nog steeds slecht bekend, omdat er geen ideaal proces is om deze in huidige botsingsexperimenten te onderzoeken. De toekomstige Electron-Ion Collider (EIC) biedt veel beter toegang tot deze TMDs, maar het duurt nog minstens 10 jaar tot de eerste run. Daarnaast is het belangrijk om TMDs te onderzoeken in verschillende soorten processen om hun universaliteit te checken, omdat deze niet zo triviaal is als die van collineaire PDFs.

Wij stellen voor om quarkonium paarproductie te gebruiken voor onderzoek naar de twee leading-twist gluon TMDs die te onderzoeken zijn met botsingen van ongepolariseerde protonen in de Large Hadron Collider (LHC). Quarkonia zijn mesonen, gebonden toestanden van een quark-antiquark paar. In het geval van quarkonia bestaat het paar uit quarks van dezelfde zware smaak: charmonia bestaat uit een charm en een anticharm, bottomonia bestaat uit een bottom en een antibottom. J/ψ mesonen zijn de laagst gelegen vector-toestanden van charmonia en worden in grote hoeveelheden geproduceerd in de LHC. J/ψ paren worden voornamelijk geproduceerd door gluonfusie, wat een belangrijk proces is om gluon TMD te onderzoeken. Het bestuderen van eindtoestanden met twee deeltjes maakt het mogelijk om het proces op verschillende harde schalen te bestuderen, wat het mogelijk maakt om onderzoek te doen naar de TMD evolutie.

We gebruiken eerst een simpel model van Gaussian-based TMDs om observabelen in J/ψ paarproductie te berekenen die gevoelig zijn voor de TMDs. Deze observabelen

zijn het transversaal-momentum spectrum van het paar, vooral gevoelig voor de TMD van het ongepolariseerde gluon, en azimuthale asymmetrieën, die alleen aanwezig zijn als er een lineair gepolariseerde gluon TMD is. We zien dat J/ψ paarproductie een ideaal proces is om lineair gepolariseerde gluon verdelingen te onderzoeken via het gebruik van een azimuthale symmetrie die maximaal is als de harde schaal groot is. Ook gebruiken we LHCb data van het transversale momentum van de J/ψ paren om het gemiddelde transversale momentum van het gluon te fitten met ons Gaussian-based model. De grote waarde die verkregen wordt, wordt geïnterpreteerd als een gevolg van de TMD evolutie die perturbatief het intrinsieke transversale momentum van het gluon op grote harde schaal versterkt.

We verbeteren onze voorspellingen daarna door TMD evolutie toe te voegen aan het formalisme dat we gebruiken om de gluon TMDs te beschrijven. Deze modellen kunnen het LHCb transversaal-momentum spectrum beschrijven met een intrinsiek transversaal momentum van het gluon in de sub-GeV regio. Hierbij is de verdeling van het ongepolariseerde gluon de belangrijkste bijdrage in een expansie in de sterke koppeling, terwijl de lineair gepolariseerde verdeling een kleiner effect heeft. De niet-perturbatieve component die overblijft wordt met een Gaussische verdeling beschreven. We zien dat de berekende grootte van de azimuthale asymmetrieën in J/ψ productie lager is dan wanneer het volledig Gaussische model gebruikt wordt. Maar we zien ook dat deze asymmetrieën groot genoeg blijven om te worden waargenomen in de LHC. We doen ook voorspellingen voor Υ paarproductie (de Υ is de bottomonium equivalent van de J/ψ).

Tenslotte bestuderen we de heliceit-structuur van de quarkonium paarproductie amplitude. Deze kan worden geschreven als een som van subamplitudes van de verschillende heliceit toestanden van de gluonen in de begintoestand en quarkonia in de eindtoestand. In de limiet waarbij het paar een grote massa heeft, versimpelen de amplitudes sterk en verklaren ze hoe de harde verstrooiingscoëfficiënten van J/ψ paarproductie de grootte van een azimuthale asymmetrie maximaliseren, zoals is waargenomen. Daarnaast laten we zien dat een amplitude van nul voor longitudinaal gepolariseerde paren, zoals voorspeld op eerste orde in het collineaire regime, ook in TMD factorisatie bestaat. Het zou voor tussenliggende massa's ook moeten blijven gelden omdat harde gluon emissies onderdrukt zijn in het TMD regime.

Résumé

La factorisation dépendante de l'impulsion transverse est utilisée pour décrire les collisions hadroniques en incluant l'impulsion transverse intrinsèque des partons à l'intérieur des hadrons. Cela requiert l'usage de distributions dépendantes de l'impulsion transverse (Transverse Momentum-Dependent distributions en anglais ou TMDs). De telles distributions doivent être extraites de données expérimentales. Les TMDs de quarks sont relativement connues grâce à des processus pour lesquels de nombreuses données sont disponibles. Les TMDs de gluons restent peu connues car il n'existe pas de processus idéal pour les étudier dans les accélérateurs en fonctionnement. Le futur Electron-Ion Collider (EIC) permettra leur étude de façon beaucoup plus complète, mais sa mise en fonctionnement n'est pas prévue avant au moins 10 ans. De plus, il est important d'étudier les TMDs à l'aide de divers processus afin de tester leur universalité qui n'est pas aussi triviale que celle des distributions colinéaires.

Nous proposons d'utiliser la production de paire de quarkonia pour étudier les deux TMDs de gluon accessibles dans les collisions de protons non polarisés au LHC. Les quarkonia sont des mésons, c'est-à-dire des états liés de paires quark-antiquark. Dans le cas d'un quarkonium, la paire est faite de quarks de la même saveur lourde : les charmonia combinent un charm et un anticharm, tandis que les bottomonia combinent un bottom et un antibottom. Les mésons J/ψ sont des charmonia de spin 1 et sont produits en grandes quantités au LHC. Les paires de J/ψ sont en grande majorité produites via des fusions de gluons, ce qui est important pour l'étude spécifique des TMDs de gluons. L'étude d'états finaux à deux particules permet également de sélectionner diverses valeurs de l'échelle dure du processus, qui dans ce cas est de l'ordre de la masse de la paire, ce qui permet de plus d'étudier l'évolution des TMDs.

Nous utilisons d'abord un modèle simple de TMDs gaussiennes pour calculer des

observables de la production de paires de J/ψ qui sont sensibles au TMDs. Ces observables sont le spectre de l'impulsion transverse de la paire, principalement sensible à la TMD de gluon non polarisés, et les asymétries azimutales, dont l'existence requiert la TMD de gluons linéairement polarisés. Nous utilisons également les données LHCb sur la production de paires de J/ψ pour extraire l'impulsion transverse moyenne des gluons dans notre modèle gaussien. L'importante valeur obtenue est interprétée comme une conséquence de l'évolution des TMDs qui augmente l'impulsion transverse intrinsèque du gluon via des contributions perturbatives présentes aux grandes échelles dures.

Nous améliorons par la suite nos prédictions en incluant l'évolution des TMDs dans le formalisme utilisé pour décrire les TMDs de gluons dans nos calculs. Dans ce modèle, la distribution des gluons non polarisés est une contribution dominante, tandis que la distribution de gluons linéairement polarisés est sous-dominante. La composante non-perturbative restante est modélisée à l'aide d'une gaussienne. Nous observons que la magnitude des asymétries calculées pour la production de paires de J/ψ est plus petite que celle calculée à l'aide du modèle purement gaussien. Cependant, nous observons également que ces asymétries restent de taille raisonnable et pourraient être détectées au LHC. Nous fournissons également des prédictions pour la production de paires de Υ (le Υ est l'équivalent bottomonium du J/ψ).

Enfin, nous étudions la structure en termes d'hélicité de l'amplitude de production de paires de quarkonia. En effet, elle peut être décomposée en une somme de sous-amplitudes correspondant à divers états d'hélicités des gluons incidents et des quarkonia produits. Dans la limite de grande masse de la paire, ces amplitudes se simplifient grandement et expliquent comment la production de paires de J/ψ optimise l'amplitude d'une asymétrie.

Acknowledgments

Completing a thesis is a task that requires the help and support of many people.

First of all, I would like to thank my supervisors, Jean-Philippe Lansberg and Daniël Boer. Both of you worked together to give me the chance to realise this dream and supported me all along the way. Jean-Philippe, you enrolled me as an intern when I was starting to lose hope, then you made the PhD happen. You gave me the opportunity to travel across the world, meet the scientific community and present our results on many different occasions. With your inexhaustible energy, you always pushed me to find new ways, to think differently and to overcome problems. Always busy yet always available, your door was never closed for me. Daniël, you kindly welcomed me in the north, in a city I have only seen once then. You helped me with everything you could in order for me to settle, become a part of the institute and travel to workshops and conferences. In spite of all your responsibilities, you took the time to explain me all the concepts I was struggling with, you patiently answered all the questions I was constantly asking you. Your knowledge and understanding of physics always impressed me, and so did your sense of rigour and organisation. Both of you managed together to set up this international cooperation between two universities without me having to worry about anything else than my research. I cannot emphasise how grateful I am for this unique opportunity. I would like to extend my gratitude to the people of the assessment committee who took the time to read this manuscript, and to those of the examining committee for making my defence possible.

In this section as in others, I try to conciliate the french and dutch ways to write a thesis. I will try to stay concise and serious, but there are some people and words that I still think deserve a place here.

I want to thank the people I worked with the most or whom often offered me advices and help: Cristian, Marc, Miguel, but also Hua-Sheng, Jakub, Pieter, Thomas and many others, you taught me a lot along the years.

IPN has been a second home for more than two years. In this home, I met people who greatly helped me: Elias and David, as directors of the doctoral school, Laure-Amélie

as my Linux mentor, Géraldine and all of her colleagues feeding us day after day, and of course Pascale who sometimes seems to run this institute. I also want to thank all of my own colleagues of the theory group and others with whom I got to share meals, coffees and stories. In this home, I had many brothers and sisters with whom I shared more than just a lot of time: Alice, Anastasia, Antoine, Clément, Jana, Marc, Melih, Noël, Olivier, to cite just some of them.

VSI is the place where most of this manuscript was written. Special thanks to Annelien, Hilde and Iris who took care of any issue I ever had with administration and were always so kind to me, and to all my colleagues who were always nice. Although I spent more time alone than I wished, I still got to meet great people that made my days more cheerful: Alba, Alexander, Ceyda, Chalis, Femke, Evgenii, Gideon, Jan, Johannes, Marco, Perseas, Pi, Simone, Ubbi, Yangyang, Yongliao, and many others. I also met great people thanks to the great work of our PhD student associations.

I particularly thank the two great persons who would have been my paranymphs if not for the circumstances of this year. Ruud, you were the one who welcomed and helped me even before I arrived to the Netherlands, and a good friend as well. Henrique, where to start? From the cold padel fields of Groningen to the hot springs of the Caribbean, your friendship means a lot to me. And with Anna, Casey, Rosa and Thomas, we will always be the pony house that brought me so much joy.

Je continue maintenant en français pour les personnes dont l'anglais est aussi bon que mon néerlandais. Je tiens tout d'abord à remercier mes parents, qui les premiers m'ont encouragé dans ma passion pour la nature et les sciences, et n'ont jamais cessé de le faire. Merci également à mes grands-parents, ma soeur, mon beau-frère, mon charmant neveu et sa soeur, pour le soutien et la joie qu'ils m'apportent tous les jours. Merci à Karine, Fiona et Claude qui agrandissent cette petite famille pour le meilleur. Je remercie également tous les professeurs grâce à qui je suis ici aujourd'hui. En particulier, mille mercis à M. Ghirardi pour m'avoir transmis non moins que la passion de la physique. À Annick, Benoit, Camille, Charlène, Clémence, JP, Juliette, Matthieu, Nicolas, Valentin, Xavier, mes meilleurs amis depuis plus de dix ans déjà, merci pour tous les bons moments passés et à venir. À mes comparses de master: Samir, Xavier et les autres, merci d'avoir rendu ces débuts dans le monde académique aussi mémorables. Je finis ce grand tour par la coloc d'Orsay, où de nombreuses grandes amitiés sont nées. À Annabelle, Antoine, Emilie, Karol, Laetitia, Marion, Thibault, Romain et tous les autres. À Adeline, qui a transformé ma vie au détour de la Seine et sans qui cette thèse n'aurait pas la même signification. À tous ceux que je n'ai pas la place d'évoquer mais qui ont contribué d'une façon ou d'une autre à ce projet.

Merci.

Wait, did I mention Petar?

Bibliography

- [1] M. Gell-Mann, “The Eightfold Way: A Theory of strong interaction symmetry,” Cited on p. 1.
- [2] V. E. Barnes and Others, “Observation of a Hyperon with Strangeness Minus Three,” *Phys. Rev. Lett.* **12** (1964) 204–206. Cited on p. 1.
- [3] E. Tkachov, “A Contribution to the history of quarks: Boris Struminsky’s 1965 JINR publication,” [arXiv:0904.0343](https://arxiv.org/abs/0904.0343) [[physics.hist-ph](https://arxiv.org/abs/0904.0343)]. Cited on p. 1.
- [4] O. W. Greenberg, “Spin and Unitary Spin Independence in a Paraquark Model of Baryons and Mesons,” *Phys. Rev. Lett.* **13** (1964) 598–602. Cited on p. 1.
- [5] M. Y. Han and Y. Nambu, “Three Triplet Model with Double SU(3) Symmetry,” *Phys. Rev.* **139** (1965) B1006–B1010. Cited on p. 1.
- [6] H. Fritzsch, M. Gell-Mann, and H. Leutwyler, “Advantages of the Color Octet Gluon Picture,” *Phys. Lett.* **47B** (1973) 365–368. Cited on p. 2.
- [7] C.-N. Yang and R. L. Mills, “Conservation of Isotopic Spin and Isotopic Gauge Invariance,” *Phys. Rev.* **96** (1954) 191–195. Cited on p. 2.
- [8] B. R. Stella and H.-J. Meyer, “Y(9.46 GeV) and the gluon discovery (a critical recollection of PLUTO results),” *Eur. Phys. J.* **H36** (2011) 203–243, [arXiv:1008.1869](https://arxiv.org/abs/1008.1869) [[hep-ex](https://arxiv.org/abs/1008.1869)]. Cited on p. 3.
- [9] P. Soding, “On the discovery of the gluon,” *Eur. Phys. J.* **H35** (2010) 3–28. Cited on p. 3.
- [10] J. Collins, “Foundations of perturbative QCD,” *Camb. Monogr. Part. Phys. Nucl. Phys. Cosmol.* **32** (2011) 1–624. Cited on p. 8.

- [11] K. G. Wilson, “Nonlagrangian models of current algebra,” *Phys. Rev.* **179** (1969) 1499–1512. Cited on p. 12.
- [12] R. L. Jaffe, “Spin, twist and hadron structure in deep inelastic processes,” in *The spin structure of the nucleon. Proceedings, International School of Nucleon Structure, 1st Course, Erice, Italy, August 3-10, 1995*, pp. 42–129. 1996. [arXiv:hep-ph/9602236](https://arxiv.org/abs/hep-ph/9602236) [hep-ph]. Cited on p. 12.
- [13] H. D. Politzer, “Power Corrections at Short Distances,” *Nucl. Phys.* **B172** (1980) 349–382. Cited on p. 12.
- [14] T. Muta, “Foundations of quantum chromodynamics: An Introduction to perturbative methods in gauge theories,” *World Sci. Lect. Notes Phys.* **5** (1987) 1–409. Cited on p. 13.
- [15] M. G. A. Buffing, *Color and TMD Universality in Hadronic Interactions*. PhD thesis, NIKHEF, Amsterdam. http://www.nikhef.nl/pub/services/biblio/theses_pdf/thesis_M_Buffing.pdf. Cited on p. 15.
- [16] A. Bacchetta and P. J. Mulders, “Deep inelastic leptonproduction of spin-one hadrons,” *Phys. Rev.* **D62** (2000) 114004, [arXiv:hep-ph/0007120](https://arxiv.org/abs/hep-ph/0007120) [hep-ph]. Cited on p. 16.
- [17] W. den Dunnen, *Polarization effects in proton-proton collisions within the Standard Model and beyond*. PhD thesis, Vrije Universiteit Amsterdam, 2013. Cited on p. 16.
- [18] R. K. Ellis, W. J. Stirling, and B. R. Webber, “QCD and collider physics,” *Camb. Monogr. Part. Phys. Nucl. Phys. Cosmol.* **8** (1996) 1–435. Cited on p. 17.
- [19] M. Tanabashi et al., “Review of Particle Physics,” *Phys. Rev. D* **98** no. 3, (2018) 30001. <https://link.aps.org/doi/10.1103/PhysRevD.98.030001>. Cited on p. 17.
- [20] V. N. Gribov and L. N. Lipatov, “Deep inelastic e p scattering in perturbation theory,” *Sov. J. Nucl. Phys.* **15** (1972) 438–450. Cited on p. 19.
- [21] G. Altarelli and G. Parisi, “Asymptotic Freedom in Parton Language,” *Nucl. Phys.* **B126** (1977) 298–318. Cited on p. 19.
- [22] Y. L. Dokshitzer, “Calculation of the Structure Functions for Deep Inelastic Scattering and e+ e- Annihilation by Perturbation Theory in Quantum Chromodynamics.,” *Sov. Phys. JETP* **46** (1977) 641–653. Cited on p. 19.
- [23] R. D. Ball and Others, “Parton distributions from high-precision collider data,” *Eur. Phys. J.* **C77** no. 10, (2017) 663, [arXiv:1706.00428](https://arxiv.org/abs/1706.00428) [hep-ph]. Cited on p. 20.

- [24] J. C. Collins, D. E. Soper, and G. F. Sterman, “Factorization of Hard Processes in QCD,” *Adv. Ser. Direct. High Energy Phys.* **5** (1989) 1–91, [arXiv:hep-ph/0409313 \[hep-ph\]](#). Cited on p. 23.
- [25] R. Brock and Others, “Handbook of perturbative QCD: Version 1.0,” *Rev. Mod. Phys.* **67** (1995) 157–248. Cited on p. 23.
- [26] J. P. Ralston and D. E. Soper, “Production of Dimuons from High-Energy Polarized Proton Proton Collisions,” *Nucl. Phys.* **B152** (1979) 109. Cited on p. 23.
- [27] D. W. Sivers, “Single Spin Production Asymmetries from the Hard Scattering of Point-Like Constituents,” *Phys. Rev.* **D41** (1990) 83. Cited on p. 23.
- [28] R. D. Tangerman and P. J. Mulders, “Intrinsic transverse momentum and the polarized Drell-Yan process,” *Phys. Rev.* **D51** (1995) 3357–3372, [arXiv:hep-ph/9403227 \[hep-ph\]](#). Cited on p. 23.
- [29] J. Collins, L. Gamberg, A. Prokudin, T. C. Rogers, N. Sato, and B. Wang, “Relating Transverse Momentum Dependent and Collinear Factorization Theorems in a Generalized Formalism,” *Phys. Rev.* **D94** no. 3, (2016) 34014, [arXiv:1605.00671 \[hep-ph\]](#). Cited on pp. 24, 29, 37, and 68.
- [30] M. Diehl, “Introduction to GPDs and TMDs,” *Eur. Phys. J.* **A52** no. 6, (2016) 149, [arXiv:1512.01328 \[hep-ph\]](#). Cited on p. 24.
- [31] D. Boer, P. J. Mulders, and F. Pijlman, “Universality of T odd effects in single spin and azimuthal asymmetries,” *Nucl. Phys.* **B667** (2003) 201–241, [arXiv:hep-ph/0303034 \[hep-ph\]](#). Cited on p. 26.
- [32] J. C. Collins, “Leading twist single transverse-spin asymmetries: Drell-Yan and deep inelastic scattering,” *Phys. Lett.* **B536** (2002) 43–48, [arXiv:hep-ph/0204004 \[hep-ph\]](#). Cited on p. 27.
- [33] X.-d. Ji and F. Yuan, “Parton distributions in light cone gauge: Where are the final state interactions?,” *Phys. Lett.* **B543** (2002) 66–72, [arXiv:hep-ph/0206057 \[hep-ph\]](#). Cited on p. 27.
- [34] A. V. Belitsky, X. Ji, and F. Yuan, “Final state interactions and gauge invariant parton distributions,” *Nucl. Phys.* **B656** (2003) 165–198, [arXiv:hep-ph/0208038 \[hep-ph\]](#). Cited on p. 27.
- [35] M. G. A. Buffing, A. Mukherjee, and P. J. Mulders, “Generalized Universality of Definite Rank Gluon Transverse Momentum Dependent Correlators,” *Phys. Rev. D* **88** (2013) 54027, [arXiv:1306.5897 \[hep-ph\]](#). Cited on p. 27.

- [36] M. Aghasyan and Others, “First measurement of transverse-spin-dependent azimuthal asymmetries in the Drell-Yan process,” *Phys. Rev. Lett.* **119** no. 11, (2017) 112002, [arXiv:1704.00488 \[hep-ex\]](#). Cited on p. 28.
- [37] P. J. Mulders and J. Rodrigues, “Transverse momentum dependence in gluon distribution and fragmentation functions,” *Phys. Rev.* **D63** (2001) 94021, [arXiv:hep-ph/0009343 \[hep-ph\]](#). Cited on p. 28.
- [38] D. Boer, S. Cotogno, T. van Daal, P. J. Mulders, A. Signori, and Y.-J. Zhou, “Gluon and Wilson loop TMDs for hadrons of spin ≤ 1 ,” *JHEP* **10** (2016) 13, [arXiv:1607.01654 \[hep-ph\]](#). Cited on p. 28.
- [39] P. Sun and F. Yuan, “Transverse momentum dependent evolution: Matching semi-inclusive deep inelastic scattering processes to Drell-Yan and W/Z boson production,” *Phys. Rev.* **D88** no. 11, (2013) 114012, [arXiv:1308.5003 \[hep-ph\]](#). Cited on p. 29.
- [40] M. Boglione, J. O. Gonzalez Hernandez, S. Melis, and A. Prokudin, “A study on the interplay between perturbative QCD and CSS/TMD formalism in SIDIS processes,” *JHEP* **02** (2015) 95, [arXiv:1412.1383 \[hep-ph\]](#). Cited on p. 29.
- [41] M. G. Echevarria, T. Kasemets, J.-P. Lansberg, C. Pisano, and A. Signori, “Matching factorization theorems with an inverse-error weighting,” *Phys. Lett.* **B781** (2018) 161–168, [arXiv:1801.01480 \[hep-ph\]](#). Cited on p. 29.
- [42] J. C. Collins and D. E. Soper, “Angular Distribution of Dileptons in High-Energy Hadron Collisions,” *Phys. Rev.* **D16** (1977) 2219. Cited on pp. 29 and 63.
- [43] J. C. Collins and D. E. Soper, “Parton Distribution and Decay Functions,” *Nucl. Phys.* **B194** (1982) 445–492. Cited on p. 33.
- [44] X. Ji, J. P. Ma, and F. Yuan, “QCD factorization for semi-inclusive deep-inelastic scattering at low transverse momentum,” *Physical Review D - Particles, Fields, Gravitation and Cosmology* **71** no. 3, (2005) 1–28, [arXiv:0404183v1 \[arXiv:hep-ph\]](#). Cited on p. 34.
- [45] J. Collins, “New definition of TMD parton densities,” *Int. J. Mod. Phys. Conf. Ser.* **4** (2011) 85–96, [arXiv:1107.4123 \[hep-ph\]](#). Cited on p. 35.
- [46] P. Sun, B.-W. Xiao, and F. Yuan, “Gluon Distribution Functions and Higgs Boson Production at Moderate Transverse Momentum,” *Phys. Rev.* **D84** (2011) 94005, [arXiv:1109.1354 \[hep-ph\]](#). Cited on p. 36.

- [47] J. Collins and T. Rogers, “Understanding the large-distance behavior of transverse-momentum-dependent parton densities and the Collins-Soper evolution kernel,” *Physical Review D - Particles, Fields, Gravitation and Cosmology* **91** no. 7, (2015) 1–38, [arXiv:1412.3820](#). Cited on pp. 36 and 37.
- [48] F. Landry, R. Brock, P. M. Nadolsky, and C. P. Yuan, “Tevatron Run-1 Z boson data and Collins-Soper-Sterman resummation formalism,” *Phys. Rev.* **D67** (2003) 73016, [arXiv:hep-ph/0212159](#) [hep-ph]. Cited on p. 37.
- [49] A. V. Konychev and P. M. Nadolsky, “Universality of the Collins-Soper-Sterman nonperturbative function in gauge boson production,” *Phys. Lett.* **B633** (2006) 710–714, [arXiv:hep-ph/0506225](#) [hep-ph]. Cited on p. 37.
- [50] S. M. Aybat and T. C. Rogers, “Transverse momentum dependent parton distribution and fragmentation functions with QCD evolution,” *Physical Review D - Particles, Fields, Gravitation and Cosmology* **83** no. 11, (2011) 1–22, [arXiv:1101.5057](#). Cited on pp. 37, 38, and 79.
- [51] U. D’Alesio, M. G. Echevarria, S. Melis, and I. Scimemi, “Non-perturbative QCD effects in q_T spectra of Drell-Yan and Z -boson production,” *JHEP* **11** (2014) 98, [arXiv:1407.3311](#) [hep-ph]. Cited on p. 37.
- [52] J. J. Aubert and Others, “Experimental Observation of a Heavy Particle J ,” *Phys. Rev. Lett.* **33** (1974) 1404–1406. Cited on p. 39.
- [53] J. E. Augustin and Others, “Discovery of a Narrow Resonance in e^+e^- Annihilation,” *Phys. Rev. Lett.* **33** (1974) 1406–1408. Cited on p. 39.
- [54] W. Braunschweig and Others, “Observation of the Two Photon Cascade $3.7\text{-GeV} \rightarrow 3.1\text{-GeV} + \gamma\gamma$ via an Intermediate State $\psi - \text{Charm}$,” *Phys. Lett.* **57B** (1975) 407–412. Cited on p. 39.
- [55] G. Goldhaber, “Observation of a Narrow State at $1865\text{-MeV}/c^2$ Decaying Into $K\pi$ and $K\pi\pi\pi$ Produced in e^+e^- Annihilation,” in *IPP International Summer School - Experimental Status & Theoretical Approaches in Physics at High Energy Accelerators Montreal, Quebec, Canada, June 21-26, 1976*, pp. 241–271. 1976. Cited on p. 39.
- [56] J. Wiss and Others, “Evidence for Parity Violation in the Decays of the Narrow States Near $1.87\text{-GeV}/c^2$,” *Phys. Rev. Lett.* **37** (1976) 1531–1534. Cited on p. 39.
- [57] S. W. Herb and Others, “Observation of a Dimuon Resonance at 9.5-GeV in 400-GeV Proton-Nucleus Collisions,” *Phys. Rev. Lett.* **39** (1977) 252–255. Cited on p. 39.

- [58] C. Bebek and Others, “Evidence for New Flavor Production at the Upsilon (4S),” *Phys. Rev. Lett.* **46** (1981) 84. Cited on p. 39.
- [59] T. Appelquist, A. De Rujula, H. D. Politzer, and S. L. Glashow, “Charmonium Spectroscopy,” *Phys. Rev. Lett.* **34** (1975) 365. Cited on p. 41.
- [60] E. Eichten, K. Gottfried, T. Kinoshita, J. B. Kogut, K. D. Lane, and T.-M. Yan, “The Spectrum of Charmonium,” *Phys. Rev. Lett.* **34** (1975) 369–372. Cited on p. 41.
- [61] M. B. Einhorn and S. D. Ellis, “Hadronic Production of the New Resonances: Probing Gluon Distributions,” *Phys. Rev.* **D12** (1975) 2007. Cited on p. 41.
- [62] R. Barbieri, R. Gatto, and E. Remiddi, “Singular Binding Dependence in the Hadronic Widths of 1^{++} and 1^{+-} Heavy Quark anti-Quark Bound States,” *Phys. Lett.* **61B** (1976) 465–468. Cited on p. 43.
- [63] W. E. Caswell and G. P. Lepage, “Effective Lagrangians for Bound State Problems in QED, QCD, and Other Field Theories,” *Phys. Lett.* **167B** (1986) 437–442. Cited on p. 43.
- [64] B. A. Thacker and G. P. Lepage, “Heavy quark bound states in lattice QCD,” *Phys. Rev.* **D43** (1991) 196–208. Cited on p. 43.
- [65] G. T. Bodwin, E. Braaten, and G. P. Lepage, “Rigorous QCD analysis of inclusive annihilation and production of heavy quarkonium,” *Phys. Rev.* **D51** (1995) 1125–1171, [arXiv:hep-ph/9407339](https://arxiv.org/abs/hep-ph/9407339) [hep-ph]. Cited on p. 43.
- [66] J.-P. Lansberg, “New Observables in Inclusive Production of Quarkonia,” *arXiv:hep-ph/1903.09185* (2019), [arXiv:1903.09185](https://arxiv.org/abs/1903.09185) [hep-ph]. Cited on pp. 44, 46, 52, 54, 57, 59, 60, and 68.
- [67] H. Fritzsche, “Producing Heavy Quark Flavors in Hadronic Collisions: A Test of Quantum Chromodynamics,” *Phys. Lett.* **67B** (1977) 217–221. Cited on p. 44.
- [68] F. Halzen, “Cvc for Gluons and Hadroproduction of Quark Flavors,” *Phys. Lett.* **69B** (1977) 105–108. Cited on p. 44.
- [69] F. Halzen, F. Herzog, E. W. N. Glover, and A. D. Martin, “The J/ψ as a Trigger in $p\bar{p}$ Collisions,” *Phys. Rev.* **D30** (1984) 700. Cited on p. 45.
- [70] F. Abe and Others, “ J/ψ and $\psi(2S)$ production in $p\bar{p}$ collisions at $\sqrt{s} = 1.8$ TeV,” *Phys. Rev. Lett.* **79** (1997) 572–577. Cited on pp. 45 and 46.
- [71] F. Abe and Others, “Production of J/ψ mesons from χ_c meson decays in $p\bar{p}$ collisions at $\sqrt{s} = 1.8$ TeV,” *Phys. Rev. Lett.* **79** (1997) 578–583. Cited on p. 45.

- [72] E. Braaten and T. C. Yuan, “Gluon fragmentation into heavy quarkonium,” *Phys. Rev. Lett.* **71** (1993) 1673–1676, [arXiv:hep-ph/9303205 \[hep-ph\]](#). Cited on p. 46.
- [73] A. K. Leibovich, “Nonrelativistic QCD analysis of bottomonium production at the Fermilab Tevatron,” *Physical Review D - Particles, Fields, Gravitation and Cosmology* **63** no. 9, (2001) 12, [arXiv:0008091 \[hep-ph\]](#). Cited on p. 46.
- [74] D. Acosta and Others, “ Υ Production and Polarization in $p\bar{p}$ Collisions at $\sqrt{s} = 1.8$ -TeV,” *Phys. Rev. Lett.* **88** (2002) 161802. Cited on p. 46.
- [75] M. Butenschoen and B. A. Kniehl, “ J/ψ polarization at Tevatron and LHC: Nonrelativistic-QCD factorization at the crossroads,” *Phys. Rev. Lett.* **108** (2012) 172002, [arXiv:1201.1872 \[hep-ph\]](#). Cited on p. 46.
- [76] B. Gong, L.-P. Wan, J.-X. Wang, and H.-F. Zhang, “Polarization for Prompt J/ψ and $\psi(2s)$ Production at the Tevatron and LHC,” *Phys. Rev. Lett.* **110** no. 4, (2013) 42002, [arXiv:1205.6682 \[hep-ph\]](#). Cited on p. 46.
- [77] K.-T. Chao, Y.-Q. Ma, H.-S. Shao, K. Wang, and Y.-J. Zhang, “ J/ψ Polarization at Hadron Colliders in Nonrelativistic QCD,” *Phys. Rev. Lett.* **108** (2012) 242004, [arXiv:1201.2675 \[hep-ph\]](#). Cited on p. 46.
- [78] T. Aaltonen and Others, “Production of $\psi(2S)$ Mesons in p anti- p Collisions at 1.96-TeV,” *Phys. Rev.* **D80** (2009) 31103, [arXiv:0905.1982 \[hep-ex\]](#). Cited on p. 46.
- [79] G. Aad and Others, “Measurement of the production cross-section of $\psi(2S) \rightarrow J/\psi(\rightarrow \mu^+ \mu^-) \pi^+ \pi^-$ in pp collisions at $\sqrt{s} = 7$ TeV at ATLAS,” *JHEP* **09** (2014) 79, [arXiv:1407.5532 \[hep-ex\]](#). Cited on p. 46.
- [80] G. Aad and Others, “Measurement of Upsilon production in 7 TeV pp collisions at ATLAS,” *Phys. Rev.* **D87** no. 5, (2013) 52004, [arXiv:1211.7255 \[hep-ex\]](#). Cited on p. 46.
- [81] N. Brambilla and Others, “Heavy quarkonium physics,” [arXiv:hep-ph/0412158 \[hep-ph\]](#). Cited on p. 46.
- [82] J. P. Lansberg, “ J/ψ , ψ' and ν production at hadron colliders: A Review,” *Int. J. Mod. Phys.* **A21** (2006) 3857–3916, [arXiv:hep-ph/0602091 \[hep-ph\]](#). Cited on p. 46.
- [83] E. Braaten, D. Kang, J. Lee, and C. Yu, “Optimal spin quantization axes for quarkonium with large transverse momentum,” *Phys. Rev.* **D79** (2009) 54013, [arXiv:0812.3727 \[hep-ph\]](#). Cited on p. 47.

- [84] B. Gong and J.-X. Wang, “Next-to-leading-order QCD corrections to J/ψ polarization at Tevatron and Large-Hadron-Collider energies,” *Phys. Rev. Lett.* **100** (2008) 232001, [arXiv:0802.3727 \[hep-ph\]](#). Cited on p. 47.
- [85] P. Artoisenet, J. Campbell, J. P. Lansberg, F. Maltoni, and F. Tramontano, “ Υ Production at Fermilab Tevatron and LHC energies,” *Physical Review Letters* **101** no. 15, (2008) 152001, [arXiv:0806.3282](#). Cited on p. 47.
- [86] Y.-Q. Ma, K. Wang, and K.-T. Chao, “ $J/\psi(\psi')$ production at the Tevatron and LHC at $\mathcal{O}(\alpha_s^4 v^4)$ in nonrelativistic QCD,” *Phys. Rev. Lett.* **106** (2011) 42002, [arXiv:1009.3655 \[hep-ph\]](#). Cited on p. 47.
- [87] M. Butenschön and B. A. Kniehl, “Reconciling J/ψ production at HERA, RHIC, tevatron, and LHC with nonrelativistic QCD factorization at next-to-leading order,” *Physical Review Letters* **106** no. 2, (2011) 22003, [arXiv:1009.5662](#). Cited on p. 47.
- [88] Y. Feng, B. Gong, C.-H. Chang, and J.-X. Wang, “Remaining parts of the long-standing J/ψ polarization puzzle,” *Phys. Rev.* **D99** no. 1, (2019) 14044, [arXiv:1810.08989 \[hep-ph\]](#). Cited on p. 47.
- [89] A. Petrelli, M. Cacciari, M. Greco, F. Maltoni, and M. L. Mangano, “NLO production and decay of quarkonium,” *Nucl. Phys.* **B514** (1998) 245–309, [arXiv:hep-ph/9707223 \[hep-ph\]](#). Cited on p. 50.
- [90] F. Maltoni and A. D. Polosa, “Observation potential for eta(b) at the Tevatron,” *Phys. Rev.* **D70** (2004) 54014, [arXiv:hep-ph/0405082 \[hep-ph\]](#). Cited on p. 50.
- [91] D. Boer and C. Pisano, “Polarized gluon studies with charmonium and bottomonium at LHCb and after,” *Physical Review D - Particles, Fields, Gravitation and Cosmology* **86** no. 9, (2012) 1–12, [arXiv:1208.3642](#). Cited on pp. 50 and 65.
- [92] D. Boer and W. J. den Dunnen, “TMD evolution and the Higgs transverse momentum distribution,” *Nuclear Physics B* **886** (2014) 421–435, [arXiv:1404.6753](#). Cited on pp. 51 and 52.
- [93] J. Collins and J.-W. Qiu, “ k_T factorization is violated in production of high-transverse-momentum particles in hadron-hadron collisions,” *Phys. Rev.* **D75** (2007) 114014, [arXiv:0705.2141 \[hep-ph\]](#). Cited on p. 51.
- [94] D. Boer, P. J. Mulders, and C. Pisano, “Dijet imbalance in hadronic collisions,” *Phys. Rev.* **D80** (2009) 94017, [arXiv:0909.4652 \[hep-ph\]](#). Cited on p. 51.

- [95] T. C. Rogers and P. J. Mulders, “No Generalized TMD-Factorization in Hadro-Production of High Transverse Momentum Hadrons,” *Phys. Rev.* **D81** (2010) 94006, [arXiv:1001.2977 \[hep-ph\]](#). Cited on p. 51.
- [96] J. P. Ma, J. X. Wang, and S. Zhao, “Transverse momentum dependent factorization for quarkonium production at low transverse momentum,” *Phys. Rev.* **D88** no. 1, (2013) 14027, [arXiv:1211.7144 \[hep-ph\]](#). Cited on p. 51.
- [97] M. G. Echevarria, “Proper TMD factorization for quarkonia production: $pp \rightarrow \eta_c$ as a study case,” [arXiv:1907.06494 \[hep-ph\]](#). Cited on p. 51.
- [98] J. P. Ma, J. X. Wang, and S. Zhao, “Breakdown of QCD Factorization for P-Wave Quarkonium Production at Low Transverse Momentum,” *Phys. Lett.* **B737** (2014) 103–108, [arXiv:1405.3373 \[hep-ph\]](#). Cited on p. 51.
- [99] S. Fleming, Y. Makris, and T. Mehen, “An effective field theory approach to quarkonium at small transverse momentum,” [arXiv:1910.03586 \[hep-ph\]](#). Cited on p. 51.
- [100] R. Aaij and Others, “Measurement of the $\eta_c(1S)$ production cross-section in proton-proton collisions via the decay $\eta_c(1S) \rightarrow p\bar{p}$,” *Eur. Phys. J.* **C75** no. 7, (2015) 311, [arXiv:1409.3612 \[hep-ex\]](#). Cited on p. 52.
- [101] R. Aaij and Others, “Measurement of the $\eta_c(1S)$ production cross-section in pp collisions at $\sqrt{s} = 13$ TeV,” [arXiv:1911.03326 \[hep-ex\]](#). Cited on p. 52.
- [102] J. P. Lansberg, S. J. Brodsky, F. Fleuret, and C. Hadjidakis, “Quarkonium Physics at a Fixed-Target Experiment using the LHC Beams,” *Few Body Syst.* **53** (2012) 11–25, [arXiv:1204.5793 \[hep-ph\]](#). Cited on p. 52.
- [103] S. J. Brodsky, F. Fleuret, C. Hadjidakis, and J. P. Lansberg, “Physics Opportunities of a Fixed-Target Experiment using the LHC Beams,” *Phys. Rept.* **522** (2013) 239–255, [arXiv:1202.6585 \[hep-ph\]](#). Cited on p. 52.
- [104] G. P. Zhang, “Probing transverse momentum dependent gluon distribution functions from hadronic quarkonium pair production,” *Physical Review D - Particles, Fields, Gravitation and Cosmology* **90** no. 9, (2014), [arXiv:1406.5476](#). Cited on p. 53.
- [105] W. J. Den Dunnen, J. P. Lansberg, C. Pisano, and M. Schlegel, “Accessing the transverse dynamics and polarization of gluons inside the proton at the LHC,” *Physical Review Letters* **112** no. 21, (2014) 212001, [arXiv:1401.7611 \[hep-ph\]](#). Cited on p. 53.

- [106] J. P. Lansberg, “Real next-to-next-to-leading-order QCD corrections to J/ψ and Upsilon hadroproduction in association with a photon,” *Phys. Lett.* **B679** (2009) 340–346, [arXiv:0901.4777 \[hep-ph\]](#). Cited on p. 53.
- [107] C. S. Kim, J. Lee, and H. S. Song, “Color octet contributions in the associate $J/\psi + \gamma$ hadroproduction,” *Phys. Rev.* **D55** (1997) 5429–5436, [arXiv:hep-ph/9610294 \[hep-ph\]](#). Cited on p. 53.
- [108] R. Li and J.-X. Wang, “Next-to-Leading-Order QCD corrections to $J/\psi(v) + \gamma$ production at the LHC,” *Phys. Lett.* **B672** (2009) 51–55, [arXiv:0811.0963 \[hep-ph\]](#). Cited on pp. 53 and 57.
- [109] J. W. Qiu, M. Schlegel, and W. Vogelsang, “Probing gluonic spin-orbit correlations in photon pair production,” *Physical Review Letters* **107** no. 6, (2011) 1–5, [arXiv:1103.3861](#). Cited on p. 54.
- [110] J. P. Lansberg, C. Pisano, and M. Schlegel, “Associated production of a dilepton and a $\Upsilon(J/\psi)$ at the LHC as a probe of gluon transverse momentum dependent distributions,” *Nuclear Physics B* **920** (2017) 192–210, [arXiv:1702.00305](#). Cited on p. 54.
- [111] C. F. Qiao, L. P. Sun, and P. Sun, “Testing charmonium production mechanism via the polarized J/ψ pair production at the LHC,” *Journal of Physics G: Nuclear and Particle Physics* **37** no. 7, (2010), [arXiv:arXiv:0903.0954v4](#). Cited on pp. 55, 57, and 63.
- [112] R. Li, Y.-J. Zhang, and K.-T. Chao, “Pair Production of Heavy Quarkonium and $B(c)^*$ Mesons at Hadron Colliders,” *Phys. Rev.* **D80** (2009) 14020, [arXiv:0903.2250 \[hep-ph\]](#). Cited on p. 55.
- [113] R. Aaij and Others, “Observation of J/ψ pair production in pp collisions at $\sqrt{s} = 7\text{TeV}$,” *Phys. Lett.* **B707** (2012) 52–59, [arXiv:1109.0963 \[hep-ex\]](#). Cited on p. 55.
- [114] V. Khachatryan and Others, “Measurement of prompt J/ψ pair production in pp collisions at $s = 7\text{TeV}$,” *Journal of High Energy Physics* no. 9, (2014) 94, [arXiv:1406.0484 \[hep-ex\]](#). Cited on pp. 55, 59, and 74.
- [115] V. M. Abazov and Others, “Observation and studies of double J/ψ production at the Tevatron,” *Phys. Rev.* **D90** no. 11, (2014) 111101, [arXiv:1406.2380 \[hep-ex\]](#). Cited on pp. 55 and 69.

- [116] M. Aaboud, G. Aad, and Others, “Measurement of the prompt J/ψ pair production cross-section in pp collisions at $\sqrt{s} = 8$ TeV with the ATLAS detector,” *The European Physical Journal C* **77** no. 2, (2017) . Cited on pp. 55, 59, and 74.
- [117] G. Wormser, M. Cattaneo, D. Fazzini, and Others, “Measurement of the J/ψ pair production cross-section in pp collisions at $\sqrt{s} = 13$ TeV,” *Journal of High Energy Physics* **6** (2017) 47, [arXiv:1612.07451](#). Cited on pp. 55, 59, 67, and 74.
- [118] V. Khachatryan and Others, “Observation of $\Upsilon(1S)$ pair production in proton-proton collisions at $\sqrt{s} = 8$ TeV,” *JHEP* **05** (2017) 13, [arXiv:1610.07095 \[hep-ex\]](#). Cited on p. 55.
- [119] A. M. Sirunyan and Others, “Measurement of the $\Upsilon(1S)$ pair production cross section and search for resonances decaying to $\Upsilon(1S)\mu^+\mu^-$ in proton-proton collisions at $\sqrt{s} = 13$ TeV,” [arXiv:2002.06393 \[hep-ex\]](#). Cited on pp. 55 and 60.
- [120] J. P. Lansberg and H. S. Shao, “Production of $J/\psi+\eta c$ versus $J/\psi+J/\psi$ at the LHC: Importance of Real α_s^5 Corrections,” *Physical Review Letters* **111** no. 12, (Sep, 2013) . Cited on pp. 55 and 56.
- [121] A. K. Likhoded, A. V. Luchinsky, and S. V. Poslavsky, “Simultaneous production of charmonium and bottomonium mesons at the LHC,” *Phys. Rev.* **D91** no. 11, (2015) 114016, [arXiv:1503.00246 \[hep-ph\]](#). Cited on p. 56.
- [122] P. Ko, J. Lee, and C. Yu, “Inclusive double-quarkonium production at the Large Hadron Collider,” *Journal of High Energy Physics* no. 01, (2011) 70, [arXiv:1007.3095](#). Cited on pp. 56 and 57.
- [123] J. P. Lansberg and H. S. Shao, “ J/ψ -pair production at large momenta: Indications for double parton scatterings and large α_s^5 contributions,” *Physics Letters B* **751** (2015) 479–486, [arXiv:1410.8822](#). Cited on pp. 56, 57, 58, 59, 60, and 68.
- [124] L.-P. Sun, H. Han, and K.-T. Chao, “Impact of J/ψ pair production at the LHC and predictions in nonrelativistic QCD,” *Phys. Rev.* **D94** no. 7, (2016) 74033, [arXiv:1404.4042 \[hep-ph\]](#). Cited on p. 56.
- [125] B. Gong, J.-P. Lansberg, C. Lorce, and J. Wang, “Next-to-leading-order QCD corrections to the yields and polarisations of J/Ψ and Upsilon directly produced in association with a Z boson at the LHC,” *JHEP* **03** (2013) 115, [arXiv:1210.2430 \[hep-ph\]](#). Cited on p. 57.
- [126] Z.-G. He and B. A. Kniehl, “Complete Nonrelativistic-QCD Prediction for Prompt Double J/ψ Hadroproduction,” *Phys. Rev. Lett.* **115** no. 2, (2015) 22002, [arXiv:1609.02786 \[hep-ph\]](#). Cited on pp. 57 and 68.

- [127] J.-P. Lansberg, H.-S. Shao, N. Yamanaka, and Y.-J. Zhang, “Prompt J/ψ -pair production at the LHC: impact of loop-induced contributions and of the colour-octet mechanism,” [arXiv:1906.10049 \[hep-ph\]](#). Cited on pp. 57, 59, and 60.
- [128] C. H. Kom, A. Kulesza, and W. J. Stirling, “Pair production of J/ψ as a probe of double parton scattering at LHCb,” *Physical Review Letters* **107** no. 8, (2011) 82002, [arXiv:1105.4186](#). Cited on pp. 58 and 68.
- [129] C. Borschensky and A. Kulesza, “Double parton scattering in pair production of J/ψ mesons at the LHC revisited,” *Physical Review D* **95** no. 3, (2017) 34029, [arXiv:1610.00666](#). Cited on p. 58.
- [130] A. V. Berezhnoy, A. K. Likhoded, A. V. Luchinsky, and A. A. Novoselov, “Production of J/ψ -meson pairs and $4c$ tetraquark at the LHC,” *Physical Review D - Particles, Fields, Gravitation and Cosmology* **84** no. 9, (2011) 94023, [arXiv:1101.5881 \[hep-ph\]](#). Cited on p. 59.
- [131] M. Tanabashi, K. Hagiwara, and Others, “Review of Particle Physics,” *Phys. Rev. D* **98** no. 3, (2018) 30001. <https://link.aps.org/doi/10.1103/PhysRevD.98.030001>. Cited on p. 59.
- [132] A. V. Berezhnoy, A. K. Likhoded, and A. A. Novoselov, “ Υ -meson pair production at LHC,” [arXiv:1210.5754](#). Cited on p. 60.
- [133] J.-P. Lansberg, C. Pisano, F. Scarpa, and M. Schlegel, “Pinning down the linearly-polarised gluons inside unpolarised protons using quarkonium-pair production at the LHC,” *Physics Letters B* **784** (Sep, 2018) 217–222, [arXiv:1710.01684](#). Cited on pp. 61, 67, and 93.
- [134] D. Boer, W. J. den Dunnen, C. Pisano, M. Schlegel, and W. Vogelsang, “Linearly Polarized Gluons and the Higgs Transverse Momentum Distribution,” *Phys. Rev. Lett.* **108** (2012) 32002, [arXiv:1109.1444 \[hep-ph\]](#). Cited on pp. 61, 65, 69, and 72.
- [135] P. Schweitzer, T. Teckentrup, and A. Metz, “Intrinsic transverse parton momenta in deeply inelastic reactions,” *Phys. Rev.* **D81** (2010) 94019, [arXiv:1003.2190 \[hep-ph\]](#). Cited on p. 65.
- [136] M. Anselmino, D. Boer, U. D’Alesio, and F. Murgia, “Transverse lambda polarization in semiinclusive DIS,” *Phys. Rev.* **D65** (2002) 114014, [arXiv:hep-ph/0109186 \[hep-ph\]](#). Cited on p. 65.

- [137] A. Dumitru, T. Lappi, and V. Skokov, “Distribution of Linearly Polarized Gluons and Elliptic Azimuthal Anisotropy in Deep Inelastic Scattering Dijet Production at High Energy,” *Phys. Rev. Lett.* **115** no. 25, (2015) 252301, [arXiv:1508.04438 \[hep-ph\]](#). Cited on p. 66.
- [138] A. Metz and J. Zhou, “Distribution of linearly polarized gluons inside a large nucleus,” *Phys. Rev.* **D84** (2011) 51503, [arXiv:1105.1991 \[hep-ph\]](#). Cited on p. 66.
- [139] S. P. Baranov and A. H. Rezaeian, “Prompt double J/ψ production in proton-proton collisions at the LHC,” *Phys. Rev.* **D93** no. 11, (2016) 114011, [arXiv:1511.04089 \[hep-ph\]](#). Cited on p. 68.
- [140] F. Scarpa, D. Boer, M. G. Echevarria, J.-P. Lansberg, C. Pisano, and M. Schlegel, “Studies of gluon TMDs and their evolution using quarkonium-pair production at the LHC,” *Eur. Phys. J.* **C80** no. 2, (2020) 87, [arXiv:1909.05769 \[hep-ph\]](#). Cited on p. 77.
- [141] J. C. Collins and D. E. Soper, “Back-To-Back Jets: Fourier Transform from B to K-Transverse,” *Nucl. Phys.* **B197** (1982) 446–476. Cited on p. 78.
- [142] L. A. Harland-Lang, V. A. Khoze, M. G. Ryskin, and W. J. Stirling, “Central exclusive meson pair production in the perturbative regime at hadron colliders,” *Eur. Phys. J.* **C71** (2011) 1714, [arXiv:1105.1626 \[hep-ph\]](#). Cited on pp. 102 and 110.
- [143] L. A. Harland-Lang, V. A. Khoze, and M. G. Ryskin, “Exclusive production of double J/ψ mesons in hadronic collisions,” *J. Phys.* **G42** no. 5, (2015) 55001, [arXiv:1409.4785 \[hep-ph\]](#). Cited on pp. 102 and 104.
- [144] M. L. Mangano and S. J. Parke, “Multiparton amplitudes in gauge theories,” *Phys. Rept.* **200** (1991) 301–367, [arXiv:hep-th/0509223 \[hep-th\]](#). Cited on p. 103.
- [145] G. Belanger and F. Boudjema, “ $\gamma\gamma \rightarrow W^+W^-$ and $\gamma\gamma \rightarrow ZZ$ as tests of novel quartic couplings,” *Phys. Lett.* **B288** (1992) 210–220. Cited on p. 108.

Titre: Étude des distributions dépendantes de l'impulsion transverse des gluons à l'intérieur du proton à l'aide de la production de paires de quarkonia au LHC

Mots clés: TMD, gluon, quarkonium, LHC

Résumé: La factorisation dépendante de l'impulsion transverse est utilisée pour décrire les collisions hadroniques en incluant l'impulsion transverse intrinsèque des partons à l'intérieur des hadrons. Cela requiert l'usage de distributions dépendantes de l'impulsion transverse (Transverse Momentum-Dependent distributions en anglais ou TMDs). De telles distributions doivent être extraites de données expérimentales. Les TMDs de quarks sont relativement connues grâce à des processus pour lesquels de nombreuses données sont disponibles. Les TMDs de gluons restent peu connues car il n'existe pas de processus idéal pour les étudier dans les accélérateurs en fonctionnement. Le futur Electron-Ion Collider (EIC) permettra leur étude de façon beaucoup plus complète, mais sa mise en fonctionnement n'est pas prévue avant au moins 10 ans. De plus, il est important d'étudier les TMDs à l'aide de divers processus afin de tester leur universalité qui n'est pas aussi triviale que celle des distributions colinéaires.

Nous proposons d'utiliser la production de paire de quarkonia pour étudier les deux TMDs de gluon accessibles dans les collisions de protons non polarisés au LHC. Les quarkonia sont des mésons, c'est-à-dire des états liés de paires quark-antiquark. Dans le cas d'un quarkonium, la paire est faite de quarks de la même saveur lourde : les charmonia combinent un charm et un anticharm, tandis que les bottomonia combinent un bottom et un antibottom. Les mésons J/ψ sont des charmonia de spin 1 et sont produits en grandes quantités au LHC. Les paires de J/ψ sont en grande majorité produites via des fusions de gluons, ce qui est important pour l'étude spécifique des TMDs de gluons. L'étude d'états finaux à deux particules permet également de sélectionner diverses valeurs de l'échelle dure du processus, qui dans ce cas est de l'ordre de la masse de la paire, ce qui permet de plus d'étudier l'évolution des TMDs.

Nous utilisons d'abord un modèle simple de

TMDs gaussiennes pour calculer des observables de la production de paires de J/ψ qui sont sensibles au TMDs. Ces observables sont le spectre de l'impulsion transverse de la paire, principalement sensible à la TMD de gluon non polarisés, et les asymétries azimutales, dont l'existence requiert la TMD de gluons linéairement polarisés. Nous utilisons également les données LHCb sur la production de paires de J/ψ pour extraire l'impulsion transverse moyenne des gluons dans notre modèle gaussien. L'importante valeur obtenue est interprétée comme une conséquence de l'évolution des TMDs qui augmente l'impulsion transverse intrinsèque du gluon via des contributions perturbatives présentes aux grandes échelles dures.

Nous améliorons par la suite nos prédictions en incluant l'évolution des TMDs dans le formalisme utilisé pour décrire les TMDs de gluons dans nos calculs. Dans ce modèle, la distribution des gluons non polarisés est une contribution dominante, tandis que la distribution de gluons linéairement polarisés est sous-dominante. La composante non-perturbative restante est modélisée à l'aide d'une gaussienne. Nous observons que la magnitude des asymétries calculées pour la production de paires de J/ψ est plus petite que celle calculée à l'aide du modèle purement gaussien. Cependant, nous observons également que ces asymétries restent de taille raisonnable et pourraient être détectées au LHC. Nous fournissons également des prédictions pour la production de paires de Υ (le Υ est l'équivalent bottomonium du J/ψ).

Enfin, nous étudions la structure en termes d'hélicité de l'amplitude de production de paires de quarkonia. En effet, elle peut être décomposée en une somme de sous-amplitudes correspondant à divers états d'hélicités des gluons incidents et des quarkonia produits. Dans la limite de grande masse de la paire, ces amplitudes se simplifient grandement et expliquent comment la production de paires de J/ψ optimise l'amplitude d'une asymétrie.

Title: Probing the gluon Transverse Momentum-Dependent distributions inside the proton through quarkonium-pair production at the LHC

Keywords: TMD, gluon, quarkonium, LHC

Abstract: Transverse momentum-dependent factorisation is used to describe hadronic collisions while taking into account the intrinsic transverse momentum of partons inside hadrons. This requires the use of Transverse Momentum-Dependent Parton Distribution Functions (TMDPDFs or simply TMDs) in order to parametrise the parton correlator. Such distributions need to be extracted from experimental data. Quark TMDs are relatively well known thanks to processes such as semi-inclusive deep inelastic scattering (SIDIS) and Drell-Yan for which numerous data exist. Gluon TMDs remain poorly known, since there is no ideal process to probe them in the operating colliders. The future Electron-Ion Collider (EIC) will offer a much better access to them, but its first run remains at least 10 years from now. It is also important to study TMDs in various kinds of processes in order to check their universality which is not as trivial as that of collinear PDFs.

We propose to use quarkonium-pair production to study the two leading-twist gluon TMDs accessible through unpolarised proton collisions at the Large Hadron Collider (LHC). Quarkonia are mesons, i.e. bound states of a quark-antiquark pair. In the case of a quarkonium, the pair is made of heavy flavours: charmonia combine a charm with an anticharm, while bottomonia combine a bottom with an antibottom. J/ψ mesons are the lowest lying vector state of charmonia and are produced in large amounts at the LHC. J/ψ pairs originate from gluon fusion in vast majority, which is important in order to focus on gluon TMDs. Studying two-particle final states also allows one to tune the hard scale of the process commensurate to the pair mass, which in turn allows one to study TMD evolution.

We first use a model of Gaussian-based TMDs to compute observables in J/ψ -pair production that are sensitive to the TMDs. These observables are the transverse-momentum spectrum of the pair, mostly sensitive to the unpolarised gluon TMD, and azimuthal asymmetries,

whose existence requires the linearly-polarised gluon TMD. We see that J/ψ pair production is an ideal process to probe the linearly-polarised gluon distribution through one azimuthal asymmetry that is maximal at large hard scales. We also use the LHCb data on the J/ψ pair transverse momentum to fit the average gluon transverse momentum using our Gaussian-based model. The large value that is obtained is interpreted as a consequence of TMD evolution that perturbatively enhances the intrinsic transverse momentum of the gluon at such large hard scales.

We then improve our predictions by including TMD evolution in the formalism used to describe the gluon TMDs in our calculations. In this picture, the unpolarised gluon distribution is a leading contribution in an expansion of the strong coupling, while the linearly-polarised distribution is subleading. The remaining nonperturbative component is modelled using a Gaussian. We observe that the computed magnitude of the azimuthal asymmetries in J/ψ -pair production are lower than when using the purely Gaussian model. However, we observe that these asymmetries remain sizeable and could be detected at the LHC. We also provide predictions for Υ -pair production (the Υ is the bottomonium equivalent of the J/ψ).

We finally study the helicity structure of the quarkonium-pair production amplitude. It can be written as a sum of sub-amplitudes corresponding to various helicity states of the initial-state gluons and final-state quarkonia. In the high-mass limit of the pair, the amplitudes greatly simplify and explain how the hard-scattering coefficients of J/ψ -pair production maximise the size of one azimuthal asymmetry, as previously observed. Moreover, it is shown that the amplitude zero for longitudinally polarised pairs predicted at leading order in the collinear regime exists as well in TMD factorisation. It should survive for intermediate masses as hard gluon emissions are suppressed in the TMD regime.